

10-5-2017

Rotaxane Ligands for Incorporation into Metal-Organic Framework Materials

Ghazale Gholami
University of Windsor

Follow this and additional works at: <https://scholar.uwindsor.ca/etd>

Recommended Citation

Gholami, Ghazale, "Rotaxane Ligands for Incorporation into Metal-Organic Framework Materials" (2017). *Electronic Theses and Dissertations*. 7261.
<https://scholar.uwindsor.ca/etd/7261>

This online database contains the full-text of PhD dissertations and Masters' theses of University of Windsor students from 1954 forward. These documents are made available for personal study and research purposes only, in accordance with the Canadian Copyright Act and the Creative Commons license—CC BY-NC-ND (Attribution, Non-Commercial, No Derivative Works). Under this license, works must always be attributed to the copyright holder (original author), cannot be used for any commercial purposes, and may not be altered. Any other use would require the permission of the copyright holder. Students may inquire about withdrawing their dissertation and/or thesis from this database. For additional inquiries, please contact the repository administrator via email (scholarship@uwindsor.ca) or by telephone at 519-253-3000ext. 3208.

Rotaxane Ligands for Incorporation into Metal-Organic Framework Materials

By

Ghazale Gholami

A Dissertation

Submitted to the Faculty of Graduate Studies
Through the Department of Chemistry and Biochemistry
In Partial Fulfillment of the Requirements for
The Degree of Doctor of Philosophy at the
University of Windsor

Windsor, Ontario, Canada

2017

© 2017 Ghazale Gholami

Rotaxane Ligands for Incorporation into Metal-Organic Framework Materials

by

Ghazale Gholami

APPROVED BY:

D. Leznoff, External Examiner
Simon Fraser University

R. Caron
Department of Mathematics and Statistics

J. Green
Department of Chemistry and Biochemistry

J. Rawson
Department of Chemistry and Biochemistry

S. Loeb, Advisor
Department of Chemistry and Biochemistry

September 15, 2017

DECLARATION OF CO-AUTHORSHIP / PREVIOUS PUBLICATIONS

I. Co-Authorship Declaration

I hereby declare that this dissertation incorporates material that is a result of joint research, as follows: Chapter two (2) contains results published in the article (G. Gholami, K. Zhu, J. S. Ward, P. E. Kruger, and S. J. Loeb, "Formation of a Polythreaded, Metal–Organic Framework Utilizing an Interlocked Hexadentate, Carboxylate Linker". *Eur. J. Inorg. Chem.*, **2016**, 4524.). I performed the synthetic experiments with assistance from K. Zhu. I collected and analyzed the PXRD and single-crystal X-ray diffraction (SCXRD) data with assistance from K. Zhu, S.J. Loeb, J. S. Ward and P. E. Kruger. I have permission from the publishing company to use this work in my dissertation. Chapter three (3) contains results published in the article (G. Gholami, G. Baggi, K. Zhu and S. J. Loeb, "Metal–organic frameworks utilising an interlocked, hexadentate linker containing a tetra-carboxylate axle and a bis(pyridine) wheel", *Dalton Trans.*, **2017**, 46, 2462.). I performed the synthetic experiments with assistance from K. Zhu. I collected and analyzed the PXRD and single-crystal X-ray diffraction (SCXRD) data with assistance from S.J. Loeb, K. Zhu and G. Baggi. Chapter four (4) contains results submitted to the article (K. Zhu, Paula Yu, Giorgio Baggi, Eduardo Schott, Ximena Zarate and S.J. Loeb, "Influence of axle length on the rate and mechanism of shuttling in rigid H-shaped [2]rotaxanes". *Chem. Sci.*, **2017**). I performed the synthetic experiments and all NMR studies for rate calculations with assistance from K. Zhu and Paula Yu. S.J. Loeb and G. Baggi solved the crystal structures. It contains joint research with Eduardo Schott and Ximena Zarate who performed DFT calculations. Chapter five (5) is unpublished; it contains joint research with K. Zhu, C.A. O'Keefe, R.W. Schurko and S.J. Loeb. I performed the synthetic experiments with assistance from K. Zhu. I performed VT-NMR exchange experiments, SEM and NMR with significant assistance from K. Zhu. C.A. O'Keefe collected and analyzed the SSNMR data. R.W. Schurko supervised all SSNMR data collection, analysis, and interpretation. Chapter six (6) is unpublished; it contains joint research with K. Zhu, C.A. O'Keefe, R.W. Schurko and S.J. Loeb. I performed the synthetic experiments with assistance from K. Zhu. I collected and analyzed the PXRD and NMR data with assistance from S.J. Loeb. C.A. O'Keefe collected and analyzed the SSNMR data. R.W. Schurko supervised all SSNMR data collection, analysis, and interpretation.

I am aware of the University of Windsor Senate Policy on Authorship, and I certify that I have properly acknowledged the contribution of other researchers to my dissertation and have obtained written permission from each of the co-author(s) to include the above material(s) in my dissertation.

I certify that, with the above qualification, this dissertation, and the research to which it refers, is the product of my own work.

II. Declaration of Previous Publication

This dissertation includes 2 original papers that have been previously published in peer reviewed journals and 1 paper that is accepted, as follows:

Dissertation Chapter	Publication title/full citation	Publication status
Chapter 2	“Formation of a Polythreaded, Metal–Organic Framework Utilizing an Interlocked Hexadentate, Carboxylate Linker”, (G. Gholami, K. Zhu, J. S. Ward, P. E. Kruger, and S. J. Loeb, <i>Eur. J. Inorg. Chem.</i> , 2016 , 4524.).	<i>Published</i>
Chapter 3	“Metal–organic frameworks utilising an interlocked, hexadentate linker containing a tetra-carboxylate axle and a bis(pyridine) wheel” (G. Gholami, G. Baggi, K. Zhu and S. J. Loeb) , <i>Dalton Trans.</i> , 2017 , 46, 2462.).	<i>Published</i>
Chapter 4	“Influence of axle length on the rate and mechanism of shuttling in rigid H-shaped [2]rotaxanes” (G. Gholami, K. Zhu, Paula Yu, Giorgio Baggi, Eduardo Schott, Ximena Zarate and S.J. Loeb, <i>Chem. Sci.</i> , 2017)	<i>Accepted</i>

I certify that I have obtained written permission from the copyright owner(s) to include the above published material(s) in my dissertation. I certify that the above material describes work completed during my registration as a graduate student at the University of Windsor.

I declare that, to the best of my knowledge, my dissertation does not infringe upon anyone’s copyright nor violate any proprietary rights, and that any ideas, techniques, quotations, or any other material from the work of other people included in my dissertation,

published or otherwise, are fully acknowledged in accordance with the standard referencing practices. Furthermore, to the extent that I have included copyrighted material that surpasses the bounds of fair dealing within the meaning of the Canada Copyright Act, I certify that I have obtained written permission from the copyright owner(s) to include such material(s) in my dissertation.

I declare that this is a true copy of my dissertation, including any final revisions, as approved by my dissertation committee and the Graduate Studies office, and that this dissertation has not been submitted for a higher degree to any other University or Institution.

ABSTRACT

This dissertation focuses on studies of mechanically interlocked molecules (MIMs) specifically [2]rotaxanes in three principle areas: (1) creating [2]rotaxane linkers to incorporate into metal-organic frameworks (MOFs); (2) studying the rate of shuttling motion in solution and finally (3) investigating the shuttling motion inside the MOF. **Chapter 1** provides a brief introduction to MIMs, rotaxanes, MOFs and all previous studies on dynamic motions of MIMs in MOFs.

Chapter 2 describes a [2]rotaxane linker with donor atoms attached to both the axle and the wheel. The linker contains four carboxylate groups attached to a rigid, H-shaped axle and two carboxylate units appended to a crown ether wheel. In the resulting Zn-based MOF, three independent 3-periodic frameworks (threefold interpenetration) are interconnected only by virtue of the threading of their individual components in the rotaxane linker.

In **Chapter 3**, a [2]rotaxane linker was synthesized which combines an H-shaped axle containing four 3-carboxyphenyl groups and a macrocyclic wheel with two 4-pyridyl groups. The synthesized Zn and Cu MOFs showed two independent lattices threaded together by interlocking of the linker.

In **Chapter 4**, a series of [2]rotaxane molecular shuttles was synthesized with varying track lengths between recognition sites. The rates of shuttling of the macrocycle along the rigid track were measured by variable temperature ^1H NMR spectroscopy for the neutral compounds and EXSY experiments for the dicationic species. It was determined that the length of the axle does not affect the shuttling rate.

In **Chapter 5**, molecular shuttling inside Zr-based MOFs under acid-base conditions was studied. ^{13}C SSNMR studies on the first MOF, **UWDM-6** (University of Windsor Dynamic Material) consisting of two linkers 2',3',5',6'-tetramethylterphenyl-4,4'' dicarboxylic acid (**H₄TTTP**) and [2]rotaxane demonstrated no shuttling because of steric hindrance of methyl groups of **H₄TTTP** linker. This steric hindrance limitation was eliminated for **UWDM-7** by changing the linear ligand to terphenyl dicarboxylate (**TPDC**).

In **Chapter 6**, a bistable [2]rotaxane molecular shuttle inside a Zr-based MOFs was studied. The synthesized MOF, **UWDM-8** consisted of [2]rotaxane with two non-equivalent recognition sites and linear linker **H₄TTTP**. Switching was driven by the addition of acid or lithium ions and monitored by ^{15}N SSNMR spectroscopy.

DEDICATION

This work is dedicated to my mother

ACKNOWLEDGEMENTS

First and foremost I want to thank my advisor Prof. Stephen J. Loeb for all his professional guidance, tremendous support, extensive knowledge and endless patience. Steve, you are a real mentor and person. Besides my advisor, I would like to thank Ginny Loeb for all of her kindness and caring. Steve and Ginny, thank you so much for supporting me during these 4 years. Thank you for everything.

I gratefully thank Dr. Kelong Zhu for all his guidance and help in all my projects. Kelong, thank you so much for answering my questions patiently. I could never have completed my PhD without your help.

I would like to thank Dr. James R. Green and Dr. Jeremy Rawson for being on my committee and for their support over the years, as well as Dr. Richard Caron and my external examiner, Dr. Daniel B. Leznoff.

I would also like to thank, Dr. Rob Schurko and his PhD student Chris O'Keefe for all their help in the collection and analysis of all solid state NMR data.

Many thanks to Dr. Giorgio Baggi for his help with X-ray diffraction studies.

I thank Dr. Matt Revington for all of his help with NMR spectroscopy, and Dr. Janeen Auld for all her help with mass spectrometry.

Big thanks to all my friends in LRG group and in chemistry and biochemistry department for helping me and having unforgettable moments.

And last but not least, a special thanks to my mother and brother for all their support and encouragement.

TABLE OF CONTENTS

DECLARATION OF CO-AUTHORSHIP/PREVIOUS PUBLICATIONS.....	iii
ABSTRACT	vi
DEDICATION	viii
ACKNOWLEDGEMENTS.....	ix
LIST OF TABLES	xvii
LIST OF FIGURES.....	xvii
LIST OF SCHEMES.....	xxvii
LIST OF ABBREVIATIONS/SYMBOLS.....	xxixx
CHAPTER 1.....	1
1.1 Mechanically Interlocked Molecules.....	1
1.1.1 Introduction.....	1
1.1.2 Molecular machines.....	1
1.1.3 Molecular shuttles	5
1.2 H-Shaped [2]Rotaxanes	10
1.2.1 T-shaped [2]pseudorotaxane template based on benzimidazolium axles	10
1.2.2 H-shaped [2]rotaxane molecular shuttles based on bis(benzimidazolium) axles	12
1.3 Mechanically interlocked molecules as ligands.....	17
1.3.1 Introduction.....	17
1.3.2 Metal-Organic Rotaxane Frameworks (MORFs).....	18
1.4 Dynamic and controlled motion in the solid state.....	22

Table of Contents

1.4.1 Introduction.....	22
1.4.2 Rotational motion in the solid state.....	22
1.4.3 Translational motion in the solid state.....	26
1.5 Conclusion/Scope of Dissertation.....	31
1.6 References.....	34
CHAPTER 2.....	38
2.1 Formation of Polythreaded, Metal-Organic Framework Utilizing an Interlocked Hexadentate, Carboxylate Linker.....	38
2.1.1 Introduction.....	38
2.1.2 Results and discussion.....	39
2.1.3 Conclusion.....	47
2.2 Experimental.....	48
2.2.2 General comments.....	48
2.2.2 Synthesis of 2.4	48
2.2.3 Synthesis of 2.5	49
2.2.4 Synthesis of MOF $[\text{NH}_2\text{Me}_2]_2[\text{Zn}_2(\text{H}_2\text{O})_2(\mathbf{2.5})]$	50
2.2.5 Single-Crystal X-ray diffraction experiments.....	51
2.2.6 Single-crystal X-ray structure of Ligand, 5.4	51
2.2.7 Single-crystal X-ray structure of MOF, $[\text{NH}_2\text{Me}_2]_2[\text{Zn}_2(\text{H}_2\text{O})_2(\mathbf{5.4})]$	52
2.2.8 Decomposition and analysis of MOF $\{[\text{NH}_2\text{Me}_2]_2[\text{Zn}_2(\text{H}_2\text{O})_2(\mathbf{2.5})]\}$ by ^1H NMR Spectroscopy.....	53
2.3 References.....	55
CHAPTER 3.....	59

Table of Contents

3.1 Metal–Organic Frameworks Utilising an Interlocked, Hexadentate Linker Containing a Tetra-carboxylate Axle and a Bis(pyridine) Wheel.....	59
3.1.1 Introduction.....	59
3.1.2 Results and Discussion.....	60
3.1.3 Conclusion.....	69
3.2. Experimental.....	70
3.2.1 General comments.....	70
3.2.2 Synthesis of 3.1	70
3.2.3 Synthesis of 3.2	71
3.2.4 Synthesis of [3.2-H][BF ₄].....	72
3.2.5 Synthesis of 3.3b	72
3.2.6 Synthesis of 3.4	73
3.2.7 Synthesis of 3.5a	73
3.2.8 Synthesis of 3.6a	74
3.2.9 Synthesis of 3.5b	74
3.2.10 Synthesis of 3.5c	75
3.2.11 Synthesis of 3.6c	76
3.2.12 Synthesis of MOF Zn- 3.6a	76
3.2.13 Synthesis of MOF Zn- 3.6c	77
3.2.14 Synthesis of MOF Cu- 3.6c	77
3.2.15 Single-crystal X-ray diffraction experiments.....	77
3.2.16 X-ray structure of Linker 3.6a	78

Table of Contents

3.2.17 X-ray structure of MOF Zn- 3.6a	78
3.2.18 X-ray structure of MOF Zn- 3.6c	79
3.2.19 X-ray structure of MOF Cu- 3.6c	80
3.2.20 Powder X-ray diffraction experiments.....	81
3.3 References.....	84
CHAPTER 4.....	89
4.1 Influence of Axle Length on the Rate and Mechanism of Shuttling in Rigid H-shaped [2]Rotaxanes.....	89
4.1.1 Introduction.....	89
4.1.2 Results and Discussion.....	91
4.1.2.1 Preparation and characterisation of molecular shuttles.....	91
4.1.2.2 Measurement of shuttling rates	95
4.1.2.3 DFT calculations.....	97
4.1.2.4 Further experimental evidence: a transition state “snap-shot”.....	99
4.1.3 Conclusion.....	101
4.2. Experimental.....	102
4.2.1 General comments.....	102
4.2.2 Synthesis of 4.6	102
4.2.3 Synthesis of 4.7	103
4.2.4 Synthesis of [4.7-H][BF ₄].....	104
4.2.5 Synthesis of 4.2	105
4.2.6 Synthesis of [4.2-H₂][BF ₄] ₂	106
4.2.7 Synthesis of 4.8	106

Table of Contents

4.2.8 Synthesis of [4.8-H][BF₄]	107
4.2.9 Synthesis of 4.3	108
4.2.10 Synthesis of [4.3-H₂][BF₄]₂	109
4.2.11 Synthesis of 4.9	110
4.2.12 Synthesis of 4.10	111
4.2.13 Synthesis of [4.10-H][BF₄]	111
4.2.14 Synthesis of 4.4	112
4.2.15 Synthesis of [4.4-H₂][BF₄]₂	113
4.2.16 Synthesis of 4.11	114
4.2.17 Synthesis of [4.11-H][BF₄]	115
4.2.18 Synthesis of 4.5	116
4.2.19 Synthesis of [4.5-H₂][BF₄]₂	117
4.2.20 Determination of the rate of shuttling for neutral [2]Rotaxanes.....	118
4.2.21 Shuttling rates for series of neutral [2]rotaxanes.....	123
4.2.22 Determination of the rate of shuttling for dicationic [2]Rotaxanes.....	124
4.2.23 Shuttling rates for series of dicationic [2]rotaxanes.....	126
4.2.24 Details of single X-ray crystal structure determinations.....	126
4.2.25 X-ray structure of [2]Rotaxane 4.5	127
4.2.26 X-ray structure of [2]Rotaxane [4.5-H₂][BF₄]₂	127
4.2.27 X-ray structure of [2]Rotaxane 4.2 from THF.....	128
4.2.28 X-ray structure of [2]Rotaxane 4.1-Br	128
4.2.29 Methods and computational details.....	130
4.3 References.....	134
CHAPTER 5.....	138

Table of Contents

5.1 pH-Control of Molecular Shuttling inside Zr-based MOFs.....	138
5.1.1 Introduction.....	138
5.1.2 Results and discussion.....	140
5.1.3 Conclusions.....	147
5.2. Experimental.....	149
5.2.1 General comments.....	149
5.2.2 Synthesis of 4-bromobenzaldehyde- ¹³ C.....	142
5.2.3 Synthesis of 5.2	150
5.2.4 Synthesis of 5.3	151
5.2.5 Synthesis of [5.3-H][BF ₄].....	152
5.2.6 Synthesis of 5.4	152
5.2.7 Synthesis of 5.5	153
5.2.8 ¹ H NMR spectrum of 5.4 with resonance assignments labeling.....	154
5.2.9 Determination of the rates of shuttling for 5.4 , [5.4-H] ⁺ , [5.4-H ₂] ²⁺ in solution.....	155
5.2.10 Analysis of MOFs: UWDM-6 and UWDM-7 by ¹ H NMR Spectroscopy.....	160
5.2.11 Comparing the ¹³ C SSNMR of [UWDM-6-H][TFA] and PCN-57	161
5.2.12 Comparing optical microscope images of microcrystals of UWDM-6 (three states) and 5.5 (three states) in solution under UV irradiation.....	162
5.2.13 Variable Temperature PXRD data for UWDM-6	164
5.2.14 ¹³ C SSNMR of [UWDM-6-H][TFA], UWDM-6 and [UWDM-6-H ₂][OTf] ₂	165
5.3. References.....	166
CHAPTER 6.....	168
6.1 A Bistable Molecular Shuttle that Switches Inside a Zr-MOF.....	168
6.1.1 Introduction.....	168

Table of Contents

6.1.2 Results and discussion.....	170
6.1.3 Conclusions.....	175
6.2 Experimental.....	176
6.2.1 General comments.....	176
6.2.2 Synthesis of 6.5a	176
6.2.3 Synthesis of 6.5b	177
6.2.4 Synthesis of 6.5c	178
6.2.5 Synthesis of 6.5d	178
6.2.6 Synthesis of 6.5e	179
6.2.7 Synthesis of 6.5	179
6.2.8 Synthesis of 6.2	180
6.2.9 Synthesis of [6.2-H][BF ₄].....	181
6.2.10 Synthesis of 6.3	182
6.2.11 Synthesis of 6.4	183
6.2.12 Analysis of UWDM-8 by ¹ H NMR Spectroscopy.....	184
6.2.13 ¹ H- ¹⁵ N SSNMR of UWDM-8 and [UWDM-8-H][TFA].....	185
6.3. References.....	186
CHAPTER 7.....	188
7.1 Summary and Future Work.....	188
7.2 References.....	193
APPENDIX.....	194
A1: Copyright Permissions.....	194
VITA AUCTORIS.....	210

LIST OF TABLES

Table 2.1 – X-ray diffraction data collection, solution, and refinement details.....	52
Table 3.1 – single-crystal X-ray data collection, solution and refinement details for 3.6a and MOFs Zn- 3.6a	78
Table 3.2 – single-crystal X-ray data collection, solution and refinement details for Zn- 3.6c and Cu- 3.6c	80
Table 4.1 – shuttling data from ¹ H NMR experiments for neutral (4.1–4.5) and dicationic ([4.1-H₂] ²⁺ –[4.5-H₂] ²⁺) [2]rotaxanes.	96
Table 4.2 – summary of shuttling rates for neutral [2]rotaxane molecular shuttles.....	123
Table 4.3 – summary of shuttling rates for dicationic [2]rotaxane molecular shuttles.	126
Table 4.4 – single-crystal X-ray data collection, solution and refinement details for 4.5 and [4.5-H₂][BF ₄] ₂	129
Table 4.5 – single-crystal X-ray data collection, solution and refinement details for 4.2 and 4.1-Br	130
Table 4.6 – Calculated thermochemistry values and energy barriers for 4.1 – 4.4 and [4.1-H₂] ²⁺ – [4.4-H₂] ²⁺	132
Table 4.7 – Calculated TS structures for 4.1 – 4.4 and [4.1-H₂] ²⁺ – [4.4-H₂] ²⁺	133
Table 5.1 – kinetic parameters for shuttling process of [5.4-H₂] ²⁺ (no shuttling was observed at 268 K).....	159

LIST OF FIGURES

Figure 1.1.1 – cartoon representation of MIMs: [2]catenane (left), [2]rotaxane (right).....	1
Figure 1.1.2 – a) rotation around a single bond, b) azobenzene isomerization, c) shuttling motion in a [2]rotaxane, d) motion in a [2]catenane.	2

List of Figures

Figure 1.1.3 – positional change of the macrocycle in rotaxane (top), photo-responsive surface based on switchable fluorinated molecular shuttles (bottom).....3

Figure 1.1.4 – light-driven, directional transport of a diiodomethane drop on mica (left), light-driven, directional transport of a diiodomethane drop on mica up a 12° incline against gravity (right).....4

Figure 1.1.5 – synthesis of the [2]catenane from the cyclophane ExBox⁴⁺ and the porphyrin followed by addition of acid (TFA) to protonate the porphyrin ring and the subsequent relative circumrotation of the catenated components positions the porphyrin ring outside the cavity of the cyclophane.5

Figure 1.1.6 – energy diagram in degenerate molecular shuttles..6

Figure 1.1.7 – structures of degenerate [2]rotaxanes containing flexible (left) and rigid spacers (right).7

Figure 1.1.8 – representation of axle length and energy barrier (a), The structure of degenerate [2]rotaxane (b).8

Figure 1.1.9 – pH driven molecular shuttle and equilibrium distribution in [2]rotaxane9

Figure 1.1.10 – chloride-switchable molecular shuttle in [2]rotaxane.....10

Figure 1.2.1 – variation in templating for a range of imidazolium and benzimidazolium axles in the formation of [2]pseudorotaxanes with the 24-membered crown ether **DB24C8**11

Figure 1.2.2 – a) T-shaped templating motif with various substitutions and salts, b) single-crystal X-ray structure of T-shaped axle with **24C8**, c) single-crystal X-ray structure of T-shaped axle with **DB24C8**.....11

Figure 1.2.3 – four states of H-shaped [2]rotaxane by addition and removal of protons and lithium ions (left), ¹H NMR spectra of neutral, monocation and dication (right).14

Figure 1.2.4 – interconversion of the co-conformations of the di-protonated [2]rotaxane molecular shuttle (top), acid–base switching of a bistable [2]rotaxane molecular shuttle between the neutral and dicationic versions (bottom)..15

Figure 1.2.5 – no shuttling of the ring (left), the shuttling of the **DB24C8** in protonated [2]rotaxane (right)16

List of Figures

Figure 1.2.6 – shuttling of the **DB24C8** in [3]rotaxane.....17

Figure 1.3.1 – the protonated diaminoalkane axles and cucurbituril wheel (left), linear one-periodic coordination polymers (right).....18

Figure 1.3.2 – the X-ray crystal structure of a 1D MORF with Co(II) ion (left), the X-ray crystal structure of a 2D MORF with Cd(II) ion (middle), and the X-ray crystal structure of a 3D MORF with Sm(III) ion (right).19

Figure 1.3.3 – the [2]rotaxane ligands used as the linker(**1.4**).....20

Figure 1.3.4 – representation of The two-periodic coordination polymer consisting of $[\text{Cd}_2\text{Cl}_4(\text{H}_2\text{O})_4]$ nodes and **1.4** rotaxane linkers.....20

Figure 1.3.5 – multidentate [2]rotaxane ligands with six S-donor atoms (top), space-filling representations of the X-ray structure of MORF (bottom-left), schematic of the full X-ray structure network (bottom-right).....21

Figure 1.4.1 – neutral [2]rotaxane **1.5** (left), Ball-and-stick representation of a single unit of the **UWDM-1** (middle), linking polyhedral creating narrow channels along the c-axis (right).....23

Figure 1.4.2 – a) ^{13}C SSNMR spectra of **UWDM-1**, b) experimental variable temperature ^2H SSNMR spectra of activated **d₂-UWDM-1**, c) simulated ^2H SSNMR spectra of activated **d₂-UWDM-1**, d) schematic representations of the dynamic motion.....24

Figure 1.4.3 – rotaxane linker **1.6** with deuterium ($\text{D} = ^2\text{H}$) labels (left), X-ray structure of the rotaxane (middle), X-ray structure of MOF **UWDM-5** showing the basic repeating unit (right).....25

Figure 1.4.4 – neutral [2]rotaxane linker **1.7** enriched with ^{13}C shown with asterisks (left), single unit of the linker **1.7** coordinated to four Zn_4O clusters (middle), view of the open channels in the lattice down the c axis with macrocycles (right).....26

Figure 1.4.5 – ^1H - ^{13}C CP/MAS NMR spectra (experimental, simulation) of a ^{13}C enriched sample of **UWDM-4** (a), Eyring plot created from the VT NMR data (b), ^{13}C 2D EXSY SSNMR spectrum of **UWDM-4** (c).....28

Figure 1.4.6 – top: Zr-based MOF with trihexagonal channels based on tetratopic 4,4',4'',4'''-(pyrene 1,3,6,8-tetrayl)tetrabenzoate linker (**PyTBA**) with a molecular formula of $\text{Zr}_6(\mu_3-$

List of Figures

$O)_4(\mu_3-OH)_4(-OH)_4(-OH_2)_4(PyTBA)_2$ (NU-1000), bottom: Incorporating the rotaxanes inside the channels of NU-1000 MOF.....30

Figure 1.5.1 – cartoon representation of [2]rotaxane linker with donor atoms attached to both the axle and the wheel.....31

Figure 1.5.2 – cartoon representation of [2]rotaxane and energy diagram in degenerate molecular shuttles.32

Figure 1.5.3 – representation of shuttling motion inside Zr-based MOF.....32

Figure 1.5.4 – representation of bistable shuttling motion inside Zr-based MOF.....33

Figure 2.1 – 1H NMR spectrum of hexaester **2.4** with resonance assignments corresponding to the labeling shown in Scheme 2.1.....41

Figure 2.2 – crystal structure of **2.5**.(DMSO) $_7$. view of the H-shaped axle and orientation of the four COOH groups (left), view emphasizing the crown ether wheel and positions of two other COOH groups (right), color key: C black, N blue, O red, H white, axle gold, wheel silver, H-bonds dashed lines, DMSO and H atoms not involved in H-bonding are omitted for clarity, only one of the molecules in the asymmetric unit is shown.....42

Figure 2.3 – crystal structure of MOF $\{[NH_2Me_2]_2[Zn_2(H_2O)_2(\mathbf{2.5})]\}$, (a) the interlocked core of the MOF showing all bonds to Zn^{II}; coordinated H₂O not shown, (b) the core unit emphasizing the rotation of the wheel relative to the axle, (c) the coordination spheres of the two unique ZnII ions. A = axle, W = wheel, color key: C black, N blue, O red, Zn1 teal, Zn2 cyan, axle gold, wheel silver, cations, solvent, and hydrogen atoms are omitted for clarity..44

Figure 2.4 – crystal structure of the MOF $\{[NH_2Me_2]_2[Zn_2(H_2O)_2(\mathbf{2.5})]\}$, a) a single 2-periodic, framework (red) with alternating axles and wheels, b) two of the frameworks (red and blue) interpenetrated through the linker, c) three of the frameworks (red, blue and green) interpenetrated through the linker, d) a space-filling model of the three interpenetrated frameworks, color key: frameworks red, blue, green, Zn dark blue, for a), b), and c) hydrogen atoms have been omitted for clarity.....46

Figure 2.5 – VT-PXRD data for the MOF $\{[NH_2Me_2]_2[Zn_2(H_2O)_2(\mathbf{2.5})]\}$ (simulated pattern created by using Diamond 4.0 computer software47

Figure 2.6 – image of crystals of MOF $\{[NH_2Me_2]_2[Zn_2(H_2O)_2(\mathbf{2.5})](H_2O)_{1.25}\}$50

List of Figures

- Figure 2.7** – ^1H NMR Spectrum of MOF $\{[\text{NH}_2\text{Me}_2]_2[\text{Zn}_2(\text{H}_2\text{O})_2(\mathbf{2.5})](\text{H}_2\text{O})_3\}$ after dissolution.....54
- Figure 3.1** – ^1H NMR spectra, (a) tetra ester **3.5a** (R = H), * = acetone and (b) tetra ester **3.5c** (R = 4-pyridine), * = EtOAc. Resonance assignments correspond to the labelling shown in Scheme 3.1 (note: m = para-H for **3.5a**).63
- Figure 3.2** – ball-and-stick representations of **3.6a** (DMF)₂, (a) the [2]rotaxane linker depicting the relative orientation and intramolecular interactions between the axle and the wheel, colour key: C = black, N = blue, O = red; H = white; centroid = orange; axle = gold bonds, wheel = silver bonds; H-bonds = dotted lines, (b) three molecules making up a portion of a 1D ribbon formed by hydrogen-bonding of the four axle COOH groups, colour key: axles = blue, wheels = red, DMF molecules and H-atoms not involved in H-bonding have been omitted for clarity.....64
- Figure 3.3** – ball-and-stick representations of MOF Zn-**3.6a**, (a) the interlocked core of the MOF showing bonds to Zn(II), (b) the SBU coordination sphere, colour key: C = black, N = blue, O = red, Zn = teal; axle = gold bonds, wheel = silver bonds, (c) a 2D sheet of interlocked ligands linked by Zn(II) ions, colour key: axles = blue, wheels = red; Zn = teal, solvent and hydrogen atoms not involved in H-bonds have been omitted for clarity.....66
- Figure 3.4** – ball-and-stick representations of MOF Zn-**3.6c**, (a) the interlocked core of the MOF showing bonds to Zn(II), (b) the SBU coordination sphere, colour key: C = black, N = blue, O = red, Zn = teal; axle = gold bonds, wheel = silver bonds, (c) the 2D sheet of interlocked ligands linked by Zn(II) ions, colour key: axles = blue, wheels = red; Zn = teal, solvent and hydrogen atoms not involved in H-bonds have been omitted for clarity.....68
- Figure 3.5** – ball-and-stick representations of MOF Cu-**3.6c**, (a) the interlocked core of the MOF showing bonds to Cu(II), (b) the coordination sphere of the Cu(II) ions, colour key: C = black, N = blue, O = red, Cu = brown; axle = gold bonds, wheel = silver bonds, (c) two sets of independent 3D lattices (orange axles linked to red wheels and blue axles linked to green wheels) that are interpenetrated (blue < red and orange < green) solely by virtue of the interlocked nature of the linker, Solvent and hydrogen atoms not involved in H-bonds have been omitted for clarity.....69
- Figure 3.6** – a) comparison of PXRD of MOF Zn-**3.6a** (in red) and simulated from the single crystal X-ray structures (in black); b) comparison of PXRD of MOF Zn-**3.6c** (in red) and

List of Figures

simulated from the single crystal X-ray structures (in black); c) comparison of PXRD of MOF Cu-**3.6c** (in red) and simulated from the single crystal X-ray structures (in black).....83

Figure 4.1 – Hirose and co-worker’s degenerate molecular shuttle with alkyl ammonium recognition sites and phenylene spacers ($n = 1-4$).....90

Figure 4.2 – a) ^1H NMR spectra (500 MHz, CD_2Cl_2 , 298 K) of naked axle of **4.5** (top) and neutral [2]rotaxane **4.5** (bottom), b) ^1H NMR spectra (500 MHz, CD_3CN , 298 K) of naked axle of [**4.5**- H_2] $^{2+}$ (top) and dicationic [2]rotaxane [**4.5**- H_2] $^{2+}$ (bottom). The change in chemical shifts due to threading of the DB24C8 wheel on the axle are highlighted. Colour key: blue = [2]rotaxane axle, red = crown ether wheel, black = naked axle. H-atom labels are as shown in Scheme 4.1.....94

Figure 4.3 – ball-and-stick representations of the X-ray structures of [2]rotaxanes: a) **4.5** ($n = \text{Np}$) and b) [**4.5**- H_2][BF_4] $_2$ ($n = \text{Np}$). Only H-atoms involved in hydrogen bonds are shown for clarity. Color key: red = O; blue = N, black = C; white = H; gold bonds = axle; silver bonds = wheel.....95

Figure 4.4 – plots of the energy barrier to translational motion in the molecular shuttles versus the distance between N-atoms on opposite ends of the track. Dotted lines are for visualisation purposes only. (n = number of phenyl rings, Np = naphthyl).....97

Figure 4.5 – structural representations of the transition states for molecular shuttling as determined by DFT calculations. left, **4.1** and right, [**4.1**- H_2] $^{2+}$. $\text{NH}\dots\text{O}$ interactions are shown as dotted lines.....98

Figure 4.6 – ball-and-stick representation of the single-crystal X-ray structure of the [2]rotaxane molecular shuttle **4.2** ($n = 2$) crystallized from THF (crystal formula **4.2**. $(\text{THF})_4$). Only H-atoms involved in hydrogen bonds are shown for clarity. Color key: red = O; blue = N, black = C; white = H; gold bonds = axle; silver bonds = wheel.....99

Figure 4.7 – ball-and-stick representation of the single-crystal X-ray structure of the [2]rotaxane molecular shuttle **4.1-Br** ($n = 1$). Only H atoms involved in hydrogen bonds are

List of Figures

shown for clarity. Color key: teal = bromine, red = O; blue = N, black = C; white = H; gold bonds = axle; silver bonds = wheel.....	101
Figure 4.8 – variable temperature ^1H NMR of 4.2 (500 MHz, CD_2Cl_2).....	119
Figure 4.9 – comparison of the experimental and simulation ^1H NMR data (left) and Eyring plot generated from the simulated data (right) for 4.2	120
Figure 4.10 – variable temperature ^1H NMR of 4.3 (500 MHz, CD_2Cl_2).....	120
Figure 4.11 – comparison of the experimental and simulation ^1H NMR data (left) and Eyring plot generated from the simulated data (right) for 4.3	120
Figure 4.12 – variable temperature ^1H NMR of 4.4 (500 MHz, CD_2Cl_2).....	121
Figure 4.13 – comparison of the experimental and simulation ^1H NMR data (left) and Eyring plot generated from the simulated data (right) for 4.4	121
Figure 4.14 – variable temperature ^1H NMR of 4.5 (500 MHz, CD_2Cl_2).....	122
Figure 4.15 – comparison of the experimental and simulation ^1H NMR data (left) and Eyring plot generated from the simulated data (right) for 4.5	122
Figure 4.16 – partial 2D ^1H - ^1H EXSY (300 MHz, 294K, CD_3CN) spectrum of [4.2 - H_2][BF_4] $_2$	124
Figure 4.17 – partial 2D ^1H - ^1H EXSY (300 MHz, 294K, CD_3CN) spectrum of [4.3 - H_2][BF_4] $_2$	124
Figure 4.18 – partial 2D ^1H - ^1H EXSY (300 MHz, 294K, CD_3CN) spectrum of [4.4 - H_2][BF_4] $_2$	125
Figure 4.19 – partial 2D ^1H - ^1H EXSY (300 MHz, 294K, CD_3CN) spectrum of [4.5 - H_2][BF_4] $_2$	125
Figure 5.1 – tetrahedral and octahedral cages in PCN-57 and a $\text{Zr}_6\text{O}_4(\text{OH})_4(\text{CO}_2)_{12}$ cluster.	139

List of Figures

Figure 5.2 – designing UWDM-6 with the same tetrahedral cavity as PCN-57 , the [2]rotaxane linker was designed as a linear ligand to span the same distance between the centroids of linking terphenyl groups (shown with \bullet).....	142
Figure 5.3 – synthetic route for making UWDM-6 and UWDM-7 (TFA: trifluoroacetic acid). Structures of UWDM-6 and UWDM-7 shown were generated from the X-ray structure of PCN-57 using Material Studio.....	143
Figure 5.4 – PXRD (bottom to top) simulated from the single crystal X-ray structure of PCN-57 , simulated from Material Studio software of UiO-68 , as-synthesized [UWDM-6-H][TFA] and as-synthesized [UWDM-7-H][TFA].....	144
Figure 5.5 – partial ^{13}C SSNMR spectra of neutral UWDM-6 and UWDM-7 (acquired at 9.4 T), (* = occupied site, \bullet = unoccupied site).....	145
Figure 5.6 – a) PXRD of as-synthesized [UWDM-6-H][TFA], UWDM-6 and [UWDM-6-H] $_{2}$ [OTf] $_{2}$, b) SEM of [UWDM-6-H] $_{2}$ [OTf] $_{2}$, UWDM-6 and [UWDM-6-H][TFA] from top to bottom.....	147
Figure 5.7 – ^1H NMR spectrum of 5.4	154
Figure 5.8 – solution ^{13}C NMR spectra (125 MHz, CD_2Cl_2 , 298 K) of 5.4 non-enriched (top) and a ^{13}C -enriched 5.4 (bottom), (* = ^{13}C -enriched atoms).....	155
Figure 5.9 – partial ^{13}C NMR solution spectra (125 MHz, CD_2Cl_2 , 298K) of a) 5.4 (neutral rotaxane linker), b) [5.4-H] $^{+}$ (+1 charged rotaxane linker) the sites are different and resolved, one is charged and occupied the other is neutral and unoccupied, c) [5.4-H] $_{2}^{2+}$ (+2 charged rotaxane linker).....	156
Figure 5.10 – partial ^1H NMR solution spectra (500 MHz, CD_2Cl_2 , 298 K) of a) 5.4 (neutral rotaxane linker), b) [5.4-H] $^{+}$ (+1 charged rotaxane linker) the sites are different and resolved– one is charged and occupied the other is neutral and unoccupied, c) [5.4-H] $_{2}^{2+}$ (+2 charged rotaxane linker).....	156
Figure 5.11 – variable temperature ^{13}C NMR spectra of neutral 5.4 in toluene- d_8 (* = ^{13}C -enriched atoms, (toluene- d_8 was chosen as a solvent since it has very low melting point and polarity).	157

List of Figures

Figure 5.12 – comparison of the experimental and simulation ^{13}C NMR data (left) for the ^{13}C -enriched carbon of neutral **5.4**, Eyring plot (right) for the shuttling of neutral **5.4** generated from the simulated data. 158

Figure 5.13 – partial 2D EXSY ^{13}C NMR (500 MHz, 320 K, CD_3CN with $\tau_m = 500$ ms) spectrum of $[\mathbf{5.4-H}_2]^{2+}$ 159

Figure 5.14 – ^1H NMR of **UWDM-6** after digestion (500 MHz, DMSO-d_6), the integration shows the ratio of **H₄TTTP** to **5.5** is about 4:1. 160

Figure 5.15 – ^1H NMR of **UWDM-7** after digestion (500 MHz, DMSO-d_6), the integration shows the ratio of **TPDC** to **5.5** is about 4:1. 161

Figure 5.16 – ^{13}C SSNMR of $[\mathbf{UWDM-6-H}][\text{TFA}]$ and **PCN-57** (* = carboxylic acid group). 162

Figure 5.17 – optical microscope images of three states of **5.4** linkers in CD_2Cl_2 and microcrystals of **UWDM-6** under UV irradiation. 163

Figure 5.18 – variable temperature PXRD analysis of **UWDM-6**. 164

Figure 5.19 – partial ^{13}C SSNMR of the three states of **UWDM-6** (neutral, 1+, 2+). 165

Figure 6.1 – representations of a degenerate molecular shuttle, a bistable molecular switch and reversing the thermodynamic preference by using external perturbation (top), thermodynamic distribution for the presence of macrocycle between the two recognition sites (bottom). 168

Figure 6.2 – representation of the new design of a bistable molecular switch and the macrocycles translation in response to an external perturbation. 169

Figure 6.3 – relocating of **24C8** as a result of adding chemical perturbation (top), partial ^1H NMR of **6.3**, $[\mathbf{6.3-H}]^+$ and $[\mathbf{6.3.Li}]^+$ in CDCl_3 with resonance assignments (bottom). 172

Figure 6.4 – synthetic route for making **UWDM-8** (TFA: trifluoroacetic acid). A structure of **UWDM-8** shown was generated from the X-ray structure of **PCN-57** using Material Studio 173

Figure 6.5 – PXRD (bottom to top) simulated from the single crystal X-ray structure of **PCN-57**, as-synthesized $[\mathbf{UWDM-8-H}][\text{TFA}]$ and **UWDM-8**. 175

List of Figures

Figure 6.6 – ^1H NMR spectrum of UWDM-8 after digestion (500 MHz, DMSO-d_6), the integration shows the ratio of H₄TTTP to 6.4 is approximately 5:1.....	184
Figure 6.7 – ^1H - ^{15}N SSNMR spectrum of UWDM-8	185
Figure 6.8 – ^1H - ^{15}N SSNMR spectrum of [UWDM-8-H][TFA].....	185
Figure 7.1 – redesigning the non_degenerate [2]rotaxane (on the top) and the proposed synthesis procedure (on the bottom) ,(the synthesis method for making 7.1 is outlined in Chapter 6, experimental 6.2).....	192

LIST OF SCHEMES

Scheme 1.2.1 – synthesis of H-shaped [2]rotaxane with a variety of macrocyclic crown ether.....	12
Scheme 2.1 – synthesis of interlocked, hexadentate carboxylic acid ligand 2.5 . Labels are assignments for the resonances observed in the ^1H NMR spectrum shown in Fig 2.1.....	40
Scheme 3.1 – synthesis of mechanically interlocked [2]rotaxane linkers 3.6a (R = H) and 3.6c (R = 4 pyridine) from [2]pseudorotaxane precursors using a threading followed by a stoppering methodology, ^1H NMR resonances are labelled according to the numbering shown for 3.5c	61
Scheme 4.1 – preparation of rigid, H-shaped [2]rotaxane molecular shuttles containing 2, 3 and 4 phenyl rings or a naphthyl group along the track. Preparation of various aldehyde precursors (n = 2–4, Np) are described in the experimental 4.2.2. The n = 1 analogue was previously prepared as described in ref. H-atom labels are for NMR spectral assignments shown in Fig. 4.2.....	92
Scheme 4.2 – synthesis of 4.6	103
Scheme 4.3 – synthesis of 4.7	104
Scheme 4.4 – synthesis of [4.7-H][BF_4].....	104
Scheme 4.5 – synthesis of 4.2	105
Scheme 4.6 – synthesis of [4.2-H₂][BF_4] ₂	106

List of Schemes

Scheme 4.7 – synthesis of 4.8	107
Scheme 4.8 – synthesis of [4.8-H][BF₄]	108
Scheme 4.9 – synthesis of 4.3	109
Scheme 4.10 – synthesis of [4.3-H₂][BF₄]₂	110
Scheme 4.11 – synthesis of 4.9	110
Scheme 4.12 – synthesis of 4.10	111
Scheme 4.13 – synthesis of [4.10-H][BF₄]	112
Scheme 4.14 – synthesis of 4.4	113
Scheme 4.15 – synthesis of [4.4-H₂][BF₄]₂	114
Scheme 4.16 – synthesis of 4.11	115
Scheme 4.17 – synthesis of [4.11-H][BF₄]	115
Scheme 4.18 – synthesis of 4.5	116
Scheme 4.19 – synthesis of [4.5-H₂][BF₄]₂	117
Scheme 5.1 – a) major steps in the synthesis of a molecular shuttle MOF linker 5.4 (see experimental 5.2.1-5.2.7 for full synthetic details), b) the synthetic route used to enrich the MOF linker with ¹³ C to aid in characterization of the shuttling motion by ¹ H- ¹³ C CP/MAS SSNMR.....	141
Scheme 5.2 – synthesis of 4-bromobenzaldehyde- ¹³ C.....	150
Scheme 5.3 – synthesis of 5.2	150
Scheme 5.4 – synthesis of 5.3	151
Scheme 5.5 – synthesis of [5.3-H][BF₄]	152
Scheme 5.6 – synthesis of 5.4	153
Scheme 5.7 – synthesis of 5.5	154
Scheme 6.1 – major steps in the synthesis of a molecular shuttle linker (see experimental 6.2 for full synthetic details).....	171

List of Schemes

Scheme 6.2 – synthesis of 6.5a	177
Scheme 6.3 – synthesis of 6.5b	177
Scheme 6.4 – synthesis of 6.5c	178
Scheme 6.5 – synthesis of 6.5d	179
Scheme 6.6 – synthesis of 6.5e	179
Scheme 6.7 – synthesis of 6.5	180
Scheme 6.8 – synthesis of 6.2	181
Scheme 6.9 – synthesis of [6.2-H][BF₄]	182
Scheme 6.10 – synthesis of 6.3	183
Scheme 6.11 – synthesis of 6.4	183

LIST OF ABBREVIATIONS/SYMBOLS

24C6	[24]crown-6
Å	Angstrom
B24C6	Benzo[24]crown-6
BMP26C8	Bis-meta-phenylene-[26]crown-8
CHCl₃	Chloroform
COSY	Correlation Spectroscopy
CP	Coordination polymers
D₂O	Deuterated water
DB24C8	DiBenzo[24]crown-8
DB30C10	DiBenzo[30]crown-10
DCM	Dichloromethane
DCM-d₂	Deuterated methylenechloride
DEF	Diethylformamide
DMB24C6	DimethoxyBenzo[24]crown-6
DMF	Dimethylformamide
DMF-d₇	Deuterated dimethylformamide
DMSO	Dimethylsulfoxide
DMSO-d₆	Deuterated dimethylsulfoxide
DNA	Deoxyribonucleic acid
DN24C8	Dinaphtho[24]crown-8
EtOAc	Ethyl acetate
EtOH	Ethanol
EXSY	Exchange Spectroscopy
HMBC	Heteronuclear Multiple Bond Correlation

HR-MS	High resolution mass spectrometry
H₄TTTP	2',3',5',6'-tetramethylterphenyl-4,4'' dicarboxylic acid
Hz	Hertz
ICP-MS	Inductively coupled plasma mass spectrometry
K	Kelvins
kJ/mol	Kilojoules per mole
MeCN	Acetonitrile
MeCN-d₃	Deuterated acetonitrile
MeNO₂	Nitromethane
MeOH	Methanol
MIM	Mechanically Interlocked Molecule
MOF	Metal-organic Framework
MORF	Metal-organic rotaxane framework
MP	Melting point
NOESY	Nuclear Overhauser effect spectroscopy
Np	Naphthyl ring
NU	Northwestern University
OTf	Trifluoromethanesulfonate
PCN	Porous Coordination Network
ppm	Parts per million
PRF	Polyrotaxane framework
PXRD	Powder X-ray diffraction
PyTBA	tetratopic 4,4',4'',4'''-(pyrene 1,3,6,8-tetrayl)tetrabenzoate
RCM	ring-closing metathesis
RCP	Rotaxane coordination polymer

SALI	Solvent-Assisted Ligand Incorporation
SAM	self-assembled monolayer
SCXRD	Single crystal X-ray diffraction
SBU	Secondary building unit
SEM	Scanning electron microscopy
SSNMR	Solid State Nuclear Magnetic Resonance
TCP	Tetra(4-carboxy)-phenyl-porphyrin
TFA	trifluoroacetic acid
THF	Tetrahydrofuran
TLC	Thin layer chromatography
TPDC	terphenyl dicarboxylates
TTTP	2',3',5',6'-tetramethylterphenyl-4,4'' dicarboxylate
UiO	University of Oslo
UV-VIS	Ultraviolet-visible spectroscopy
UWCM	University of Windsor Crystalline Material
UWDM	University of Windsor Dynamic Material
VT	Variable Temperature

CHAPTER 1

1.1 Mechanically Interlocked Molecules

1.1.1 Introduction

Mechanically interlocked molecules (MIMs) are molecules consisting of two or more components that are not connected covalently but a covalent bond must be broken to separate the components. Catenanes and rotaxanes are the two most common types of MIMs (Fig 1.1.1). [n]Catenanes are molecules with n interlocked rings and [n]rotaxanes consist of a dumbbell-shaped molecule and a threaded ring with n total components. Noncovalent bonding interactions between the components of MIMs allow control over the assembly's mechanical motion. This intramolecular motion provides a mechanism for interconversion between different co-conformational states, stabilities and physical properties.^[1]

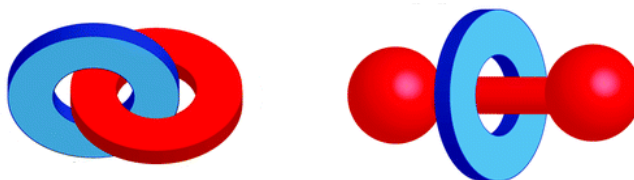


Fig 1.1.1 – cartoon representation of MIMs: [2]catenane (left), [2]rotaxane (right).

1.1.2 Molecular machines

From a macroscopic aspect, machines are groups of components designed to perform specific functions, for example an automobile or food blender. When it comes to the molecular level, molecular machines can display changes in the positions of their components as a result of some external stimulus.^[2] The energy that is needed to make

them “work” can be provided by a photon, a chemical reagent or simply adding/subtracting an electron. Molecular machines have been produced by Nature as well; some examples are ribosomes (synthesizing proteins), helicases (separating strands of DNA) and kinesin (transporting cargo about a cell).^[3] For artificial molecular machines, some possible modes of movement are: a) rotation about a single bond, b) bending as a consequence of double-bond isomerization in azobenzene, c) translational motion of a ring along the dumbbell of a rotaxane or d) rotary movement as a result of the circumrotation of one ring relative to another in a catenane.^[4,5] (Fig 1.1.2).

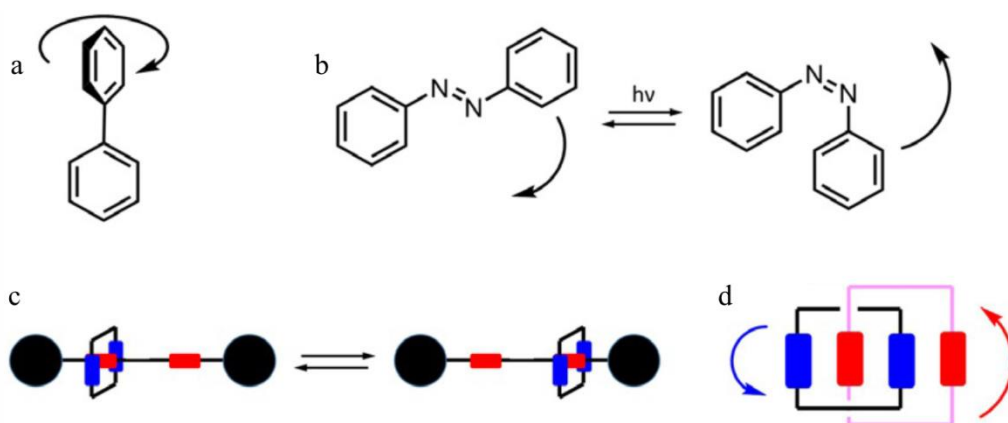


Fig 1.1.2 – a) rotation around a single bond, b) azobenzene isomerization, c) shuttling motion in a [2]rotaxane, d) motion in a [2]catenane. Reprinted with permission from ref^[4].

An artificial molecular machine was reported by Leigh and co-workers that transports a drop of liquid on a photo-responsive surface.^[6] In this report, light-switchable rotaxanes contain a fumaramide station and a tetrafluorosuccinamide station. The macrocycle is translocated from one station to the other when the fumaramide group converts to the maleamide group in the presence of light. Pyridine groups on the rotaxane interact with a self-assembled monolayer (SAM) of 11-mercaptoundecanoic acid ($\text{HO}_2\text{C}(\text{CH}_2)_{10}\text{SH}$) on Au(111) which was deposited on glass or mica (Fig 1.1.3). When the surface is irradiated

with ultraviolet light the macrocycle encapsulates the fluoroalkane units, leaving a more polarophilic surface.

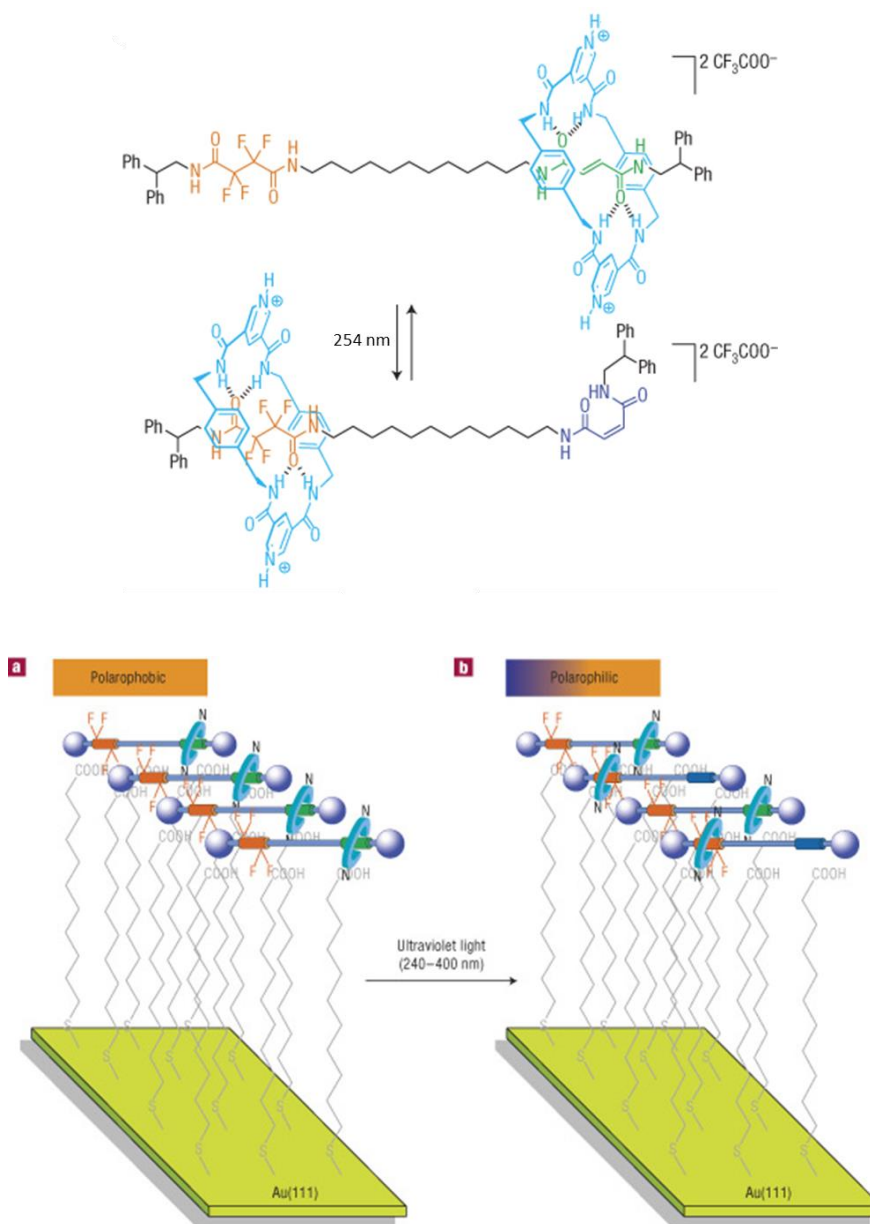


Fig 1.1.3 – positional change of the macrocycle in rotaxane (top), photo-responsive surface based on switchable fluorinated molecular shuttles (bottom). Reprinted with permission from ref^[6].

A 1.25 μL drop of diiodomethane was placed on the prepared surface, and the right-hand side of the drop was irradiated with a perpendicular beam of 240–400 nm light. Therefore, the concentration of fluoroalkane groups is decreased and that part of the surface becomes more polarophilic. The contact angle between the drop and the surface is decreased and the Laplace pressure inside the droplet causes elongation followed by transport forward (Fig 1.1.4). This millimetre-scale directional transport of a liquid on a surface shows macroscopic work against gravity by a MIM based molecular machine.

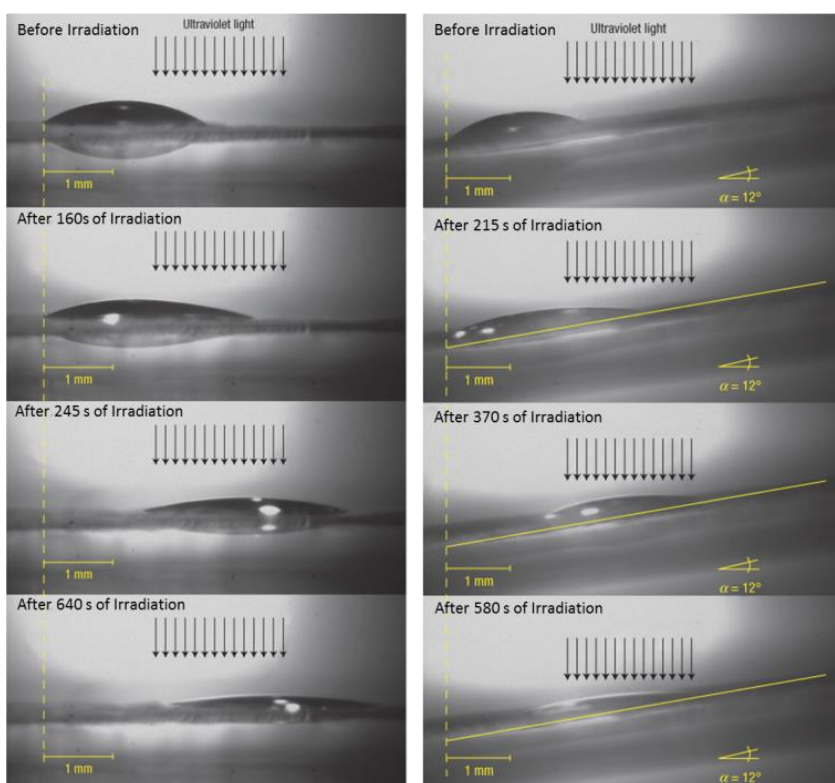


Fig 1.1.4 – light-driven, directional transport of a diiodomethane drop on mica (left), light-driven, directional transport of a diiodomethane drop on mica up a 12° incline against gravity (right). Reprinted with permission from ref^[6].

The application of porphyrin-containing MIMs in energy-transfer devices and processive synthesis machines makes them of interest among chemists. In 2014, Stoddart

and co-workers reported a donor–acceptor [2]catenane, in which the [2]catenane can act as a pushbutton molecular switch where the co-conformations of the [2]catenane can be controlled by addition of acid. Acid protonates the porphyrin ring and the position of the macrocycle changes. The rotation can be reversed by addition of base (Fig 1.1.5).^[7]

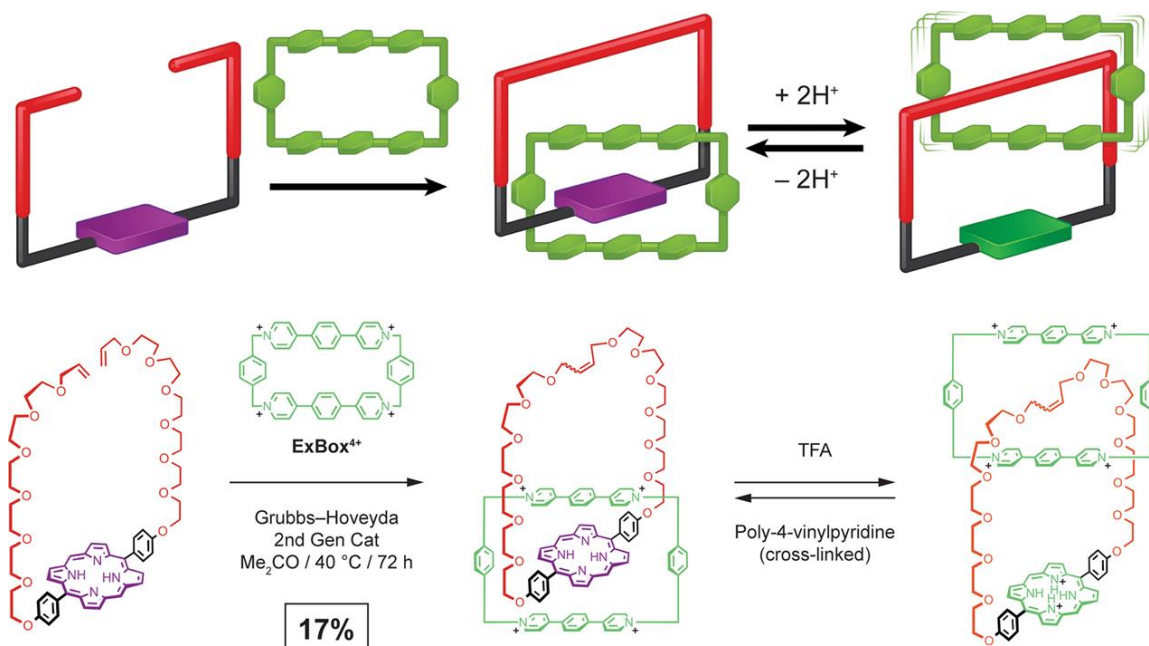


Fig 1.1.5 – synthesis of the [2]catenane from the cyclophane ExBox⁴⁺ and the porphyrin followed by addition of acid (TFA) to protonate the porphyrin ring and the subsequent relative circumrotation of the catenated components positions the porphyrin ring outside the cavity of the cyclophane. Reprinted with permission from ref^[7].

1.1.3 Molecular shuttles

In [2]rotaxanes with two recognition sites, the competitive affinity of ring for the two sites causes the ring to translate between them, so, nanoscale mechanical motions happen in these types of systems.^[8] For most [2]rotaxane molecular shuttles, the macrocyclic ring moves rapidly between the two recognition sites at room temperature. The energy barrier to overcome to interconvert the co-conformational isomers is different depending on the

intramolecular interactions between the axle and wheel components. The first [2]rotaxane temperature-dependent shuttling was reported by Stoddart and co-workers.^[9] The shuttling back and forth of the tetracationic macrocycle between the two hydroquinol stations on the polyether thread with a ΔG_c^\ddagger value of ca. 13 kcal mol⁻¹ was observed by monitoring ¹H NMR spectra at varying temperatures. Fig 1.1.6 shows that the barrier height is dependent on the energy required to break the non-covalent interactions between the macrocycle and recognition station. There are many factors such as solvent and temperature that influence the rate of the shuttling. The effect of water as a solvent on the shuttling rate of [2]rotaxanes bearing hydrogen bonds between macrocycle and stations has been explored. In this system by adding small amounts of water, the translation of a macrocycle along an axle was accelerated significantly.^[11] This effect was attributed to the ability of water to form three-dimensional hydrogen-bonding networks.

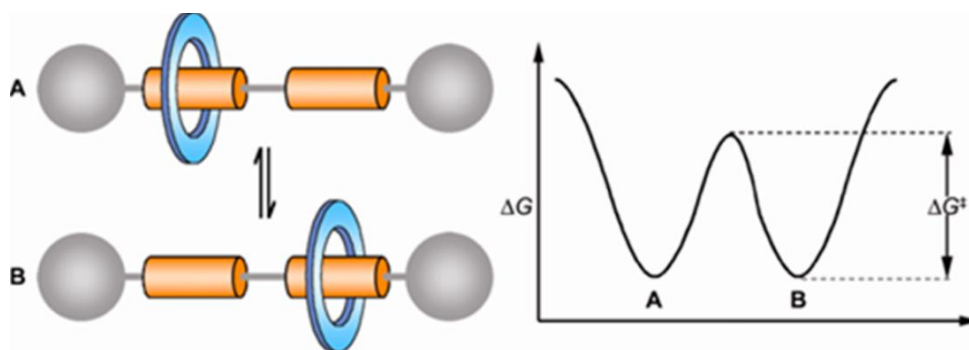


Fig 1.1.6 – energy diagram in degenerate molecular shuttles. Reprinted with permission from ref³¹.

Correlating the rate of shuttling to the length of the axle or track between two stations has been a somewhat controversial issue among chemists. For example, by lengthening the alkyl chain between stations a decrease in the rate of shuttling and an increasing in the activation barrier of ca. 5 kJ mol⁻¹ was reported in 1997. In this report, it was concluded that the increased distance that the macrocycle must travel between peptide sites affects the rate of

translation.^[12] Another study by Brouwer looked at a benzylic amide macrocycle which moves back and forth between two naphthalimide-glycine units along a diphenylethyne spacer or an aliphatic spacer.^[13] The kinetic data obtained from dynamic ¹H NMR spectroscopy demonstrated that rotaxanes with shorter spacers or a rigid diphenylethyne have higher shuttling rates. ¹H NMR spectra at lower temperature for rotaxane **1.1**, **1.2** (Fig 1.1.7) did not show any significant changes, but in the case of **1.3** splitting of signals into pairs was observed. This observation is because of the stronger noncovalent hydrogen-bonding interactions at the lower temperature.

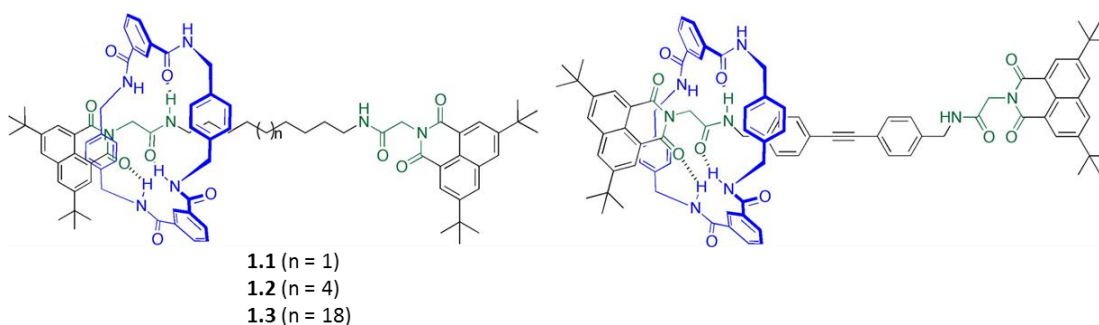


Fig 1.1.7 – structures of degenerate [2]rotaxanes containing flexible (left) and rigid spacers (right). Reprinted with permission from ref^[13].

Recently, Hirose and co-workers also studied the effect of axle length on the activation barrier to ring shuttling.^[14] They chose rigid rod-like structures by incorporating an increasing number of phenylene spacers between the two ammonium stations in order to prevent effects arising from conformational isomerism of the axle. The ¹H NMR spectra of rotaxanes in different solvents such as DMSO and CDCl₃ showed slow ring shuttling on the NMR time scale. The existence of separate sets of signals in all spectra for the complexed and uncomplexed parts of the axle revealed the non-symmetrical nature of the system. They also observed lower barriers for shuttling in DMSO-d₆ than DMF-d₇ due to better solvation

of the positively charged ammonium centers. Interestingly, variable-temperature ^1H NMR spectral data indicated that the activation barriers for ring shuttling are similar at each temperature for each rotaxane irrespective of the length of the axle (Fig 1.1.8). The ΔG^\ddagger value for the rotaxane that contains one phenylene group between the ammonium stations is the same as for the one that contains four phenylenes and is about $16.0 \text{ kcal mol}^{-1}$.

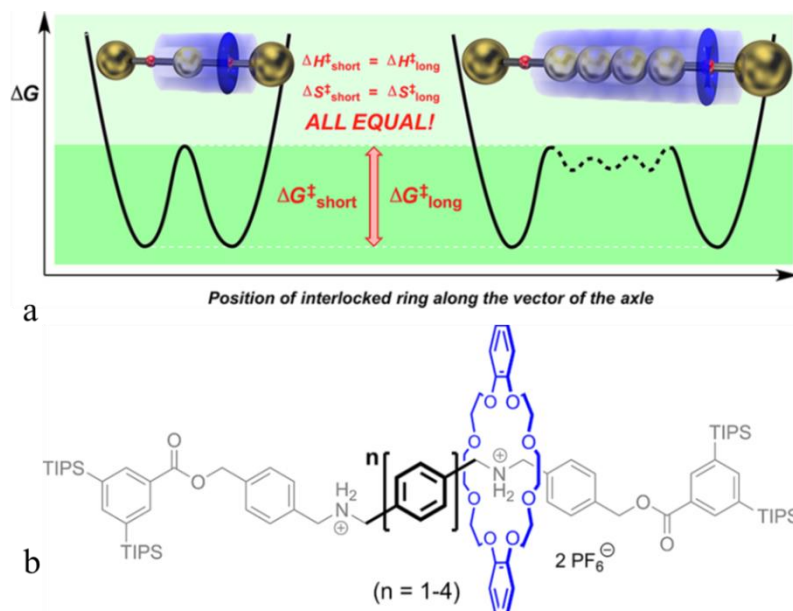


Fig 1.1.8 – representation of axle length and energy barrier (a), The structure of degenerate [2]rotaxane (b). Reprinted with permission from ref¹⁴.

Studies on molecular motions in rotaxanes are prerequisites for their future application in molecular devices. Controlling the shuttling in rotaxanes can be achieved by applying stimuli such as light, pH and temperature differences. In 1994, Stoddart and co-workers reported controlling switching of the ring position in a molecular shuttle by proton concentration changes.^[15] In their rotaxane at neutral pH, the electron poor, positively charged cyclophane macrocycle stayed more on the benzidine station. By adding acid, the benzidine station becomes protonated and the macrocycle relocates to the biphenol station as a result of electrostatic repulsion (Fig 1.1.9).

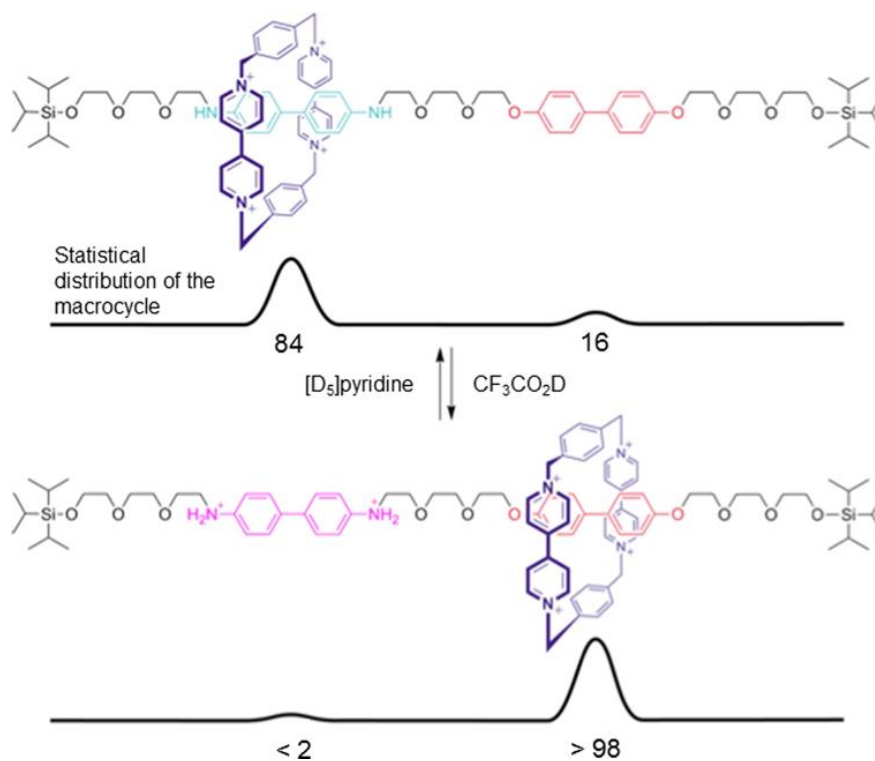


Fig 1.1.9 – pH driven molecular shuttle and equilibrium distribution in [2]rotaxane. Reprinted with permission from ref³.

The effect of additional ions on co-conformation stability has been studied. It was reported that addition of Li^+ ions to a [2]rotaxane containing pyromellitic diimide and naphtho-diimide as two competing π -electron deficient stations lead to formation of strong interactions with the crown ether wheel. Due to stronger ion-dipole interactions with pyromellitic diimide, the crown ether stays more at this station. By addition of [12]crown-4 and removal of the Li^+ ions, the macrocycle returns to its original equilibrium position.^[16] An example of an anion-switchable molecular shuttle was reported by Leigh and co-workers. In their system, a $PdCl$ -coordinated macrocycle drives shuttling from a triazole station to a pyridinium station. By addition of $AgPF_6$, the chloride the ligand is replaced by the non-coordinating PF_6^- counterion and the motion is reversed (Fig 1.1.10).^[17]

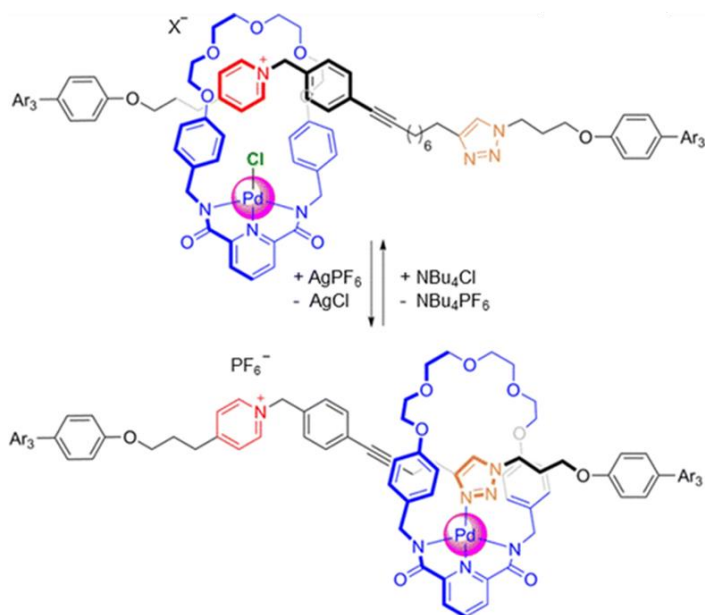


Fig 1.1.10 – chloride-switchable molecular shuttle in [2]rotaxane. Reprinted with permission from ref^[3].

1.2 H-Shaped [2]Rotaxanes

1.2.1 T-shaped [2]pseudorotaxane template based on benzimidazolium axles

The development of new templating motifs for the formation of [2]rotaxanes is highly important for the generation of new types of mechanically interlocked molecules. To this aim, Loeb and co-workers studied the efficiency of imidazolium and benzimidazolium axles to act as recognition sites by determining association constants with 24-membered crown ethers (Fig 1.2.1).^[18] Their studies showed that formation of [2]pseudorotaxanes with T-shaped axles is more favorable due to the rigid shape of the axle and limited degrees of motion. ¹H NMR spectra of equimolar mixtures of axle and wheel demonstrated variations in chemical shifts as a result of NH...O hydrogen bonding, CH...O and π -stacking interactions between the electron poor phenyl rings of the axles and the electron rich catechol rings of DB24C8.

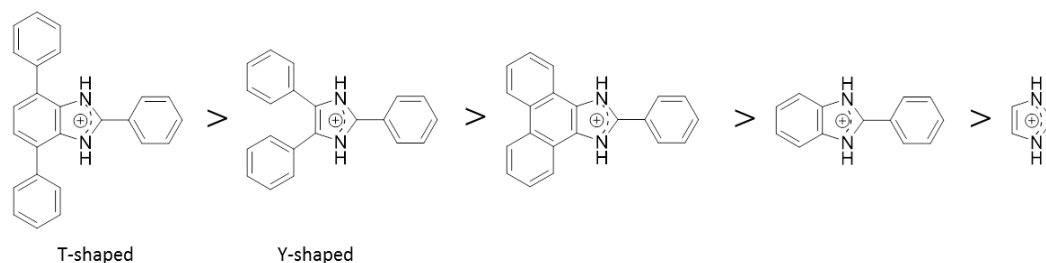


Fig 1.2.1 – variation in templating for a range of imidazolium and benzimidazolium axes in the formation of [2]pseudorotaxanes with the 24-membered crown ether **DB24C8**.

The association constants for the formation of [2]pseudorotaxane with **DB24C8** and the T-shaped 2,4,7- triphenylbenzimidazolium cation were larger than those found for simple imidazolium or benzimidazolium derivatives.^[19]

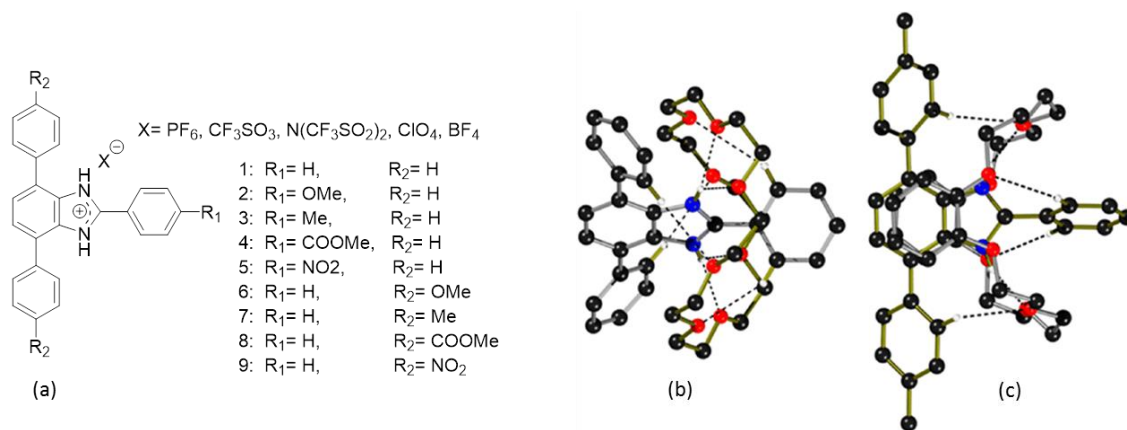


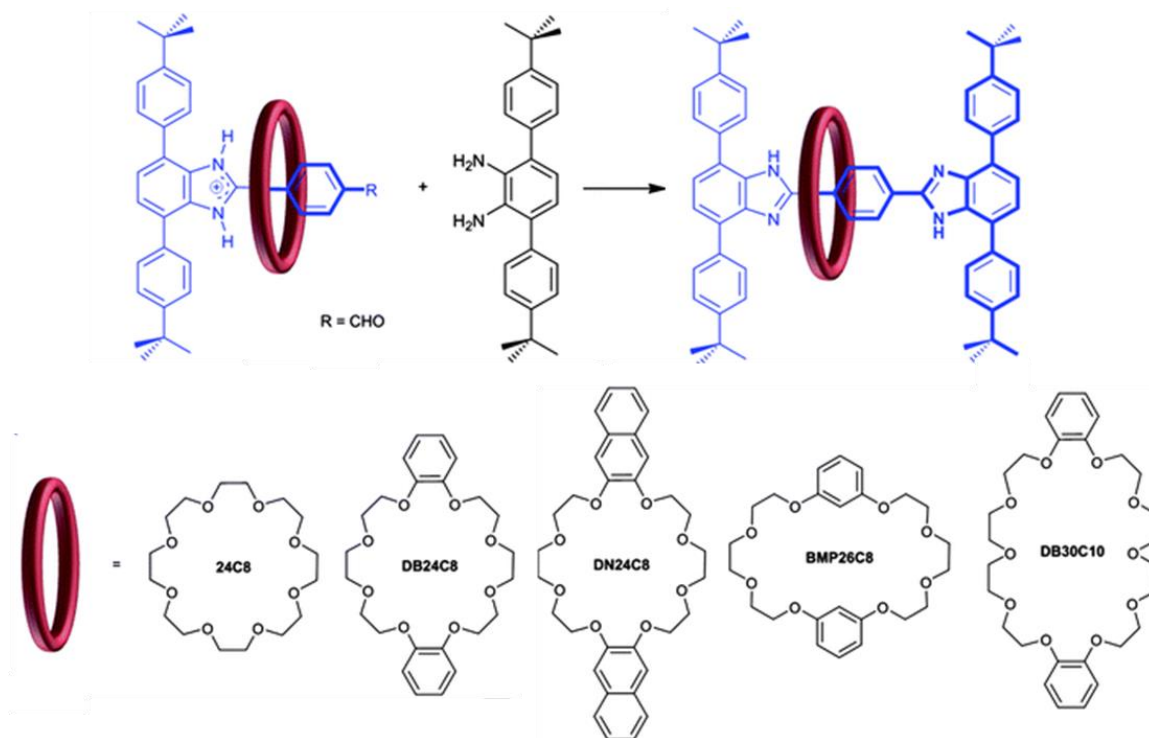
Fig 1.2.2 – a) T-shaped templating motif with various substitutions and salts, b) single-crystal X-ray structure of T-shaped axle with **24C8**, c) single-crystal X-ray structure of T-shaped axle with **DB24C8**. Reprinted with permission from ref^[19].

Studies on the axle substitutions demonstrated electron withdrawing groups increased the acidity of the hydrogen bond donors and the charge on the benzimidazolium rings leading to stronger interactions and higher association constants. X-ray structures of [2]pseudorotaxanes showed hydrogen bonding interactions between axle and wheel

(NH \cdots O and CH \cdots O) and the C-shaped conformation adopted by the **DB24C8** macrocycle is indicative of π -stacking by clamping around the electron poor benzimidazolium ring as shown in Fig 1.2.2 C.

1.2.2 H-shaped [2]rotaxane molecular shuttles based on bis(benzimidazolium) axles

The formation of H-shaped [2]rotaxanes based on bis(benzimidazolium) axles derived from utilizing the 2,4,7-triphenylbenzimidazolium group as a stopper were reported by Loeb and Zhu (Scheme 1.2.1).^[20] They studied the molecular shuttling for H-shaped [2]rotaxanes with a variety of sizes and shapes of crown ether (**24C8**, **DB24C8**, **DN24C8**, **BMP26C8** and **DB30C10**). Their studies showed that [2]pseudorotaxanes containing a 24-membered crown ether have higher association constants while larger crown ethers such as **BMP26C8** and **DB30C10**, have weaker interactions and give the lowest yields for [2]rotaxane preparation. ¹H NMR studies of the neutral H-shaped [2]rotaxanes bearing two recognition sites revealed the macrocyclic rings undergo rapid translation (shuttling) along the axle faster than the NMR timescale. The observation of a single NH signal in the ¹H NMR spectrum represents the average of hydrogen-bonded (NH \cdots O) and free benzimidazole sites. Variable temperature ¹H NMR spectroscopy estimated the average rate of shuttling to be about 10⁷ s⁻¹ in CD₂Cl₂ for these [2]rotaxanes. Protonation of this series of [2]rotaxanes dramatically reduced the rate of shuttling and two separate NH peaks for both complexed and uncomplexed axle appeared in the relevant ¹H NMR spectra.



Scheme 1.2.1 – synthesis of H-shaped [2]rotaxane with a variety of macrocyclic crown ether. Reprinted with permission from ref^[20].

The rate of shuttling was determined by 2D EXSY experiments. The reported rates of shuttling for **24C8** and **DB24C8** were 8.03 and 1.69 s⁻¹ respectively. Thus, the rate of shuttling could be acid-base controlled. Interestingly larger crown ethers in dicationic systems shuttle fast on the NMR time scale. This was rationalized as being due to weaker interactions with the larger crown ethers and the X-ray structure of the dicationic [2]rotaxanes with **BMP26C8** demonstrated the crown ether adopts an S-shaped conformation, and actually interacts simultaneously with the both recognition sites.

Loeb and Zhu also studied controlling the rate of molecular shuttling through external stimulus on these rigid H-shaped [2]rotaxanes (Fig 1.2.3).^[21] Their studies showed by acid-base chemistry, three states of the [2]rotaxane are formed: neutral, monocation and dication. Examples of ¹H NMR spectra for these three forms are shown in Fig 1.2.3. In the ¹H

NMR spectrum of the neutral rotaxane, the singlet NH group arises from fast exchange shuttling between complexed and uncomplexed species but, in the dicationic rotaxane, two sets of peaks are observed as a result of slow exchange between two recognition sites. The monocationic rotaxane contains both neutral and protonated sites but there is no exchange; due to the very large difference in binding strengths the ring resides only at the cationic benzimidazolium site. Since, the [2]rotaxane contains donor nitrogen atoms on benzimidazolium rings, a series of metals (Li^+ , Na^+ and Zn^{2+}) were examined to observe the metal ion binding to the nitrogen of the axle and oxygen of crown ether. Among the mentioned metal ions, Li^+ ion coordinated to nitrogen atom and crown ether oxygen atoms and further studies using 2D EXSY showed addition of one equivalent of Li^+ to the neutral [2]rotaxane caused slow molecular shuttling.

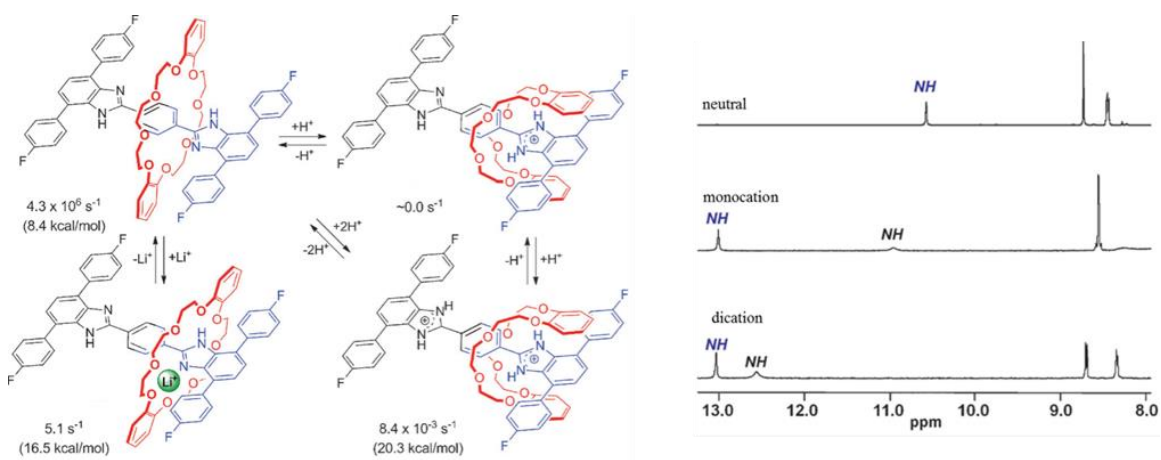


Fig 1.2.3 – four states of H-shaped [2]rotaxane by addition and removal of protons and lithium ions (left), ^1H NMR spectra of neutral, monocation and dication (right). Reprinted with permission from ref^[21].

The rate of shuttling after adding Li^+ ion to the [2]rotaxane was estimated to be somewhere between the rate of shuttling in the neutral and protonated species. By addition of [12]crown-4 ether (**12C4**) the Li^+ could be removed and the neutral rotaxane regenerated.

Recently, Farahani and Loeb have reported molecular shuttles with **24C8** and **DB24C8** wheels and a linear axle with two non-equivalent recognition sites.^[22] The axle combines T-shaped benzimidazolium and Y-shaped imidazolium recognition sites. Their NMR studies of the neutral species showed that the macrocyclic rings undergo fast shuttling on the NMR time scale. This is because the interaction of the crown ether with a neutral recognition site is quite weak. Further ¹H NMR studies on these neutral rotaxanes demonstrated that the interactions between the Y-shaped imidazole unit and the macrocycle is more favorable due to less steric hindrance. In contrast to the neutral [2]rotaxanes, the diprotonated [2]rotaxanes undergo slow exchange on the NMR timescale because of much stronger ion–dipole interactions between the wheel and axle. Since the recognition sites are different in these rotaxanes, there is a competition between the two sites for the binding of the single macrocyclic wheel. In the diprotonated rotaxane, the macrocycles interact with T-shaped site more than the Y-shaped site (Fig 1.2.4).

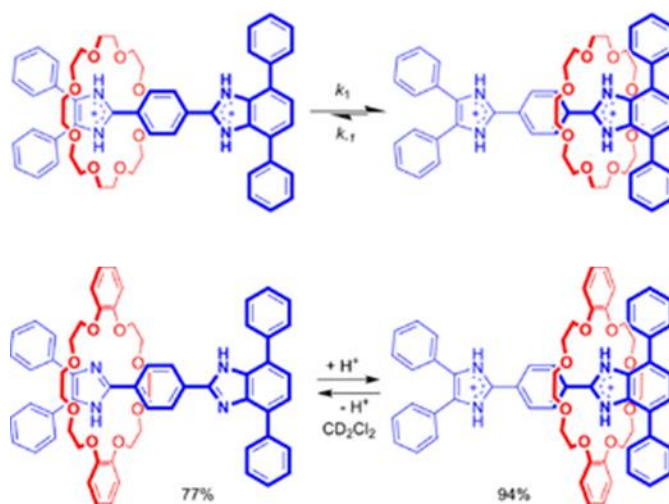


Fig 1.2.4 – interconversion of the co-conformations of the di-protonated [2]rotaxane molecular shuttle (top), acid–base switching of a bistable [2]rotaxane molecular shuttle between the neutral and dicationic versions (bottom). Reprinted with permission from ref^[22].

This leads to an increase in the barrier to motion of the wheels toward the Y-shaped site. This study proved that by protonation/deprotonation of the axle, a pH sensitive, bistable molecular shuttle could be designed. In their very recent publication, Zhu and Loeb investigated new [2] and [3]rotaxanes which combined 1,2-bis(pyridinium)ethane and benzimidazolium recognition sites.^[23] Since the two sites have different binding strengths with a crown ether macrocycle, the translational of the macrocycle could be controlled. ¹H NMR and single crystal X-ray diffraction experiments of the [2]rotaxane showed the **DB24C8** macrocycle adopts an S-shaped co-conformation and is seated in the middle of the 1,2-bis(pyridinium)ethane axle. There are π -stacking interactions between the aromatic rings of the crown ether and the aromatic groups of the pyridinium axle and the four ethylene protons of the -NCH₂CH₂N- linkage form H-bonds with O-atoms of the crown ether. There was no evidence of shuttling in this low energy co-conformation. Treating the [2]rotaxane with two equivalents of acid, converts the neutral benzimidazole sites to protonated ones and the ring moves from the central 1,2-bis(pyridinium)ethane site to the now more favourable benzimidazolium site (Fig 1.2.5).

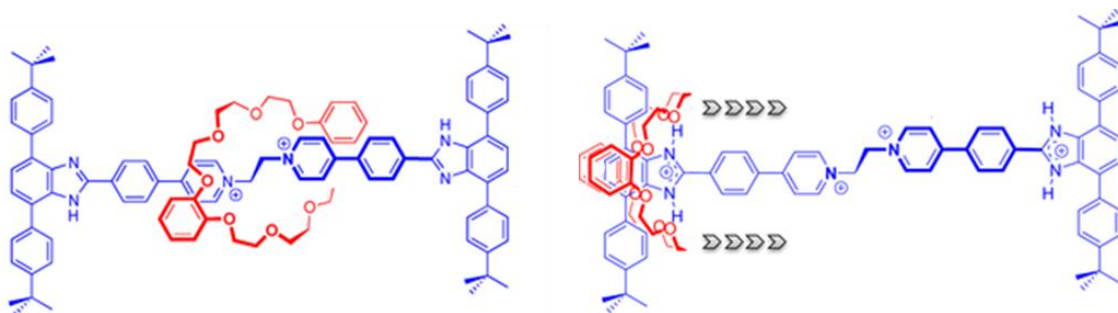


Fig 1.2.5 – no shuttling of the ring (left), the shuttling of the **DB24C8** in protonated [2]rotaxane (right). Reprinted with permission from ref^[23].

Loeb and co-workers also synthesized the [3]rotaxane shown in Fig 1.2.6. The ¹H NMR spectrum of the dicationic [3]rotaxane indicated the two macrocycles shuttle faster than

NMR time scale between the degenerate benzimidazole recognition sites. A variable temperature NMR study of the [3]rotaxane estimated the energy barrier for the simultaneous shuttling of both the wheels to be $9.9 \text{ kcal}\cdot\text{mol}^{-1}$ with a rate of $3.4 \times 10^5 \text{ s}^{-1}$ at 298 K. Protonating the [3]rotaxane to give the tetracationic species caused the crown ethers stay on the two benzimidazolium sites and no shuttling occurred.

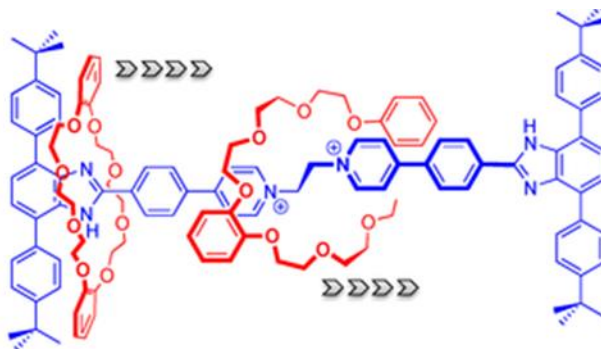


Fig 1.2.6 – shuttling of the **DB24C8** in [3]rotaxane. Reprinted with permission from ref^[23].

1.3 Mechanically interlocked molecules as ligands

1.3.1 Introduction

Studies on the dynamic nature and fundamental switching properties of MIMs in solution give us valuable information for construction of molecular machines. For imposing higher order on these molecules such as rotaxanes and catenanes, they should be fabricated at the nanoscale in the solid state.^[24] Methodologies known to achieve this aim are: attachment to a surface,^[25] incorporation into organic polymers,^[26] tethering between two electrodes^[27] and assembling into the repeating framework of a crystalline lattice.^[28]

1.3.2 Metal-Organic Rotaxane Frameworks (MORFs)

Rotaxanes can be incorporated into metal-organic frameworks to produce one-, two- and three dimensional-periodic coordination polymers. These materials are known as rotaxane coordination polymers (RCPs) or Metal-Organic Rotaxane Frameworks (MORFs) as introduced by Loeb and co-workers.^[29] Kim and co-workers reported the first example of coordination polymers that used [2]pseudorotaxanes as ligands consisting of the protonated diaminoalkane axles and cucurbituril wheels (Fig 1.3.1).^[30,31]

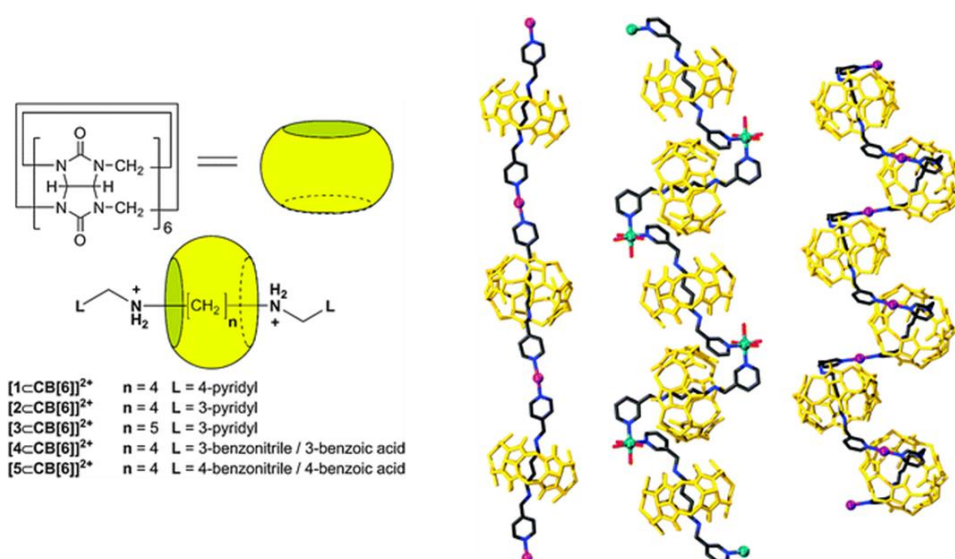


Fig 1.3.1 – the protonated diaminoalkane axles and cucurbituril wheel (left), linear one-periodic coordination polymers (right). Reprinted with permission from ref^[29].

This was followed by Loeb and coworkers who reported their first family of MORFs containing 24-membered crown ether wheels and 1,2-bis(pyridinium)ethane axles. The reaction of a [2]pseudorotaxane linker and $[\text{Co}(\text{H}_2\text{O})_6][\text{BF}_4]_2$ produces yellow/orange crystals that comprise a one-periodic coordination polymer. Each Co(II) centre has an octahedral geometry with two pyridyl groups from the rotaxane, two MeCN molecules and two water molecules. To induce higher orders of dimensionality, non-coordinating solvents were used with two equivalents of linker and one equivalent of $[\text{Cd}(\text{H}_2\text{O})_6][\text{BF}_4]_2$, resulting

in a 2D MORF with square nets. Using larger lanthanide metal ions like Sm(III) ion and an N-oxide pseudorotaxane linker produced 3D MORFs (Fig 1.3.2).^[32]

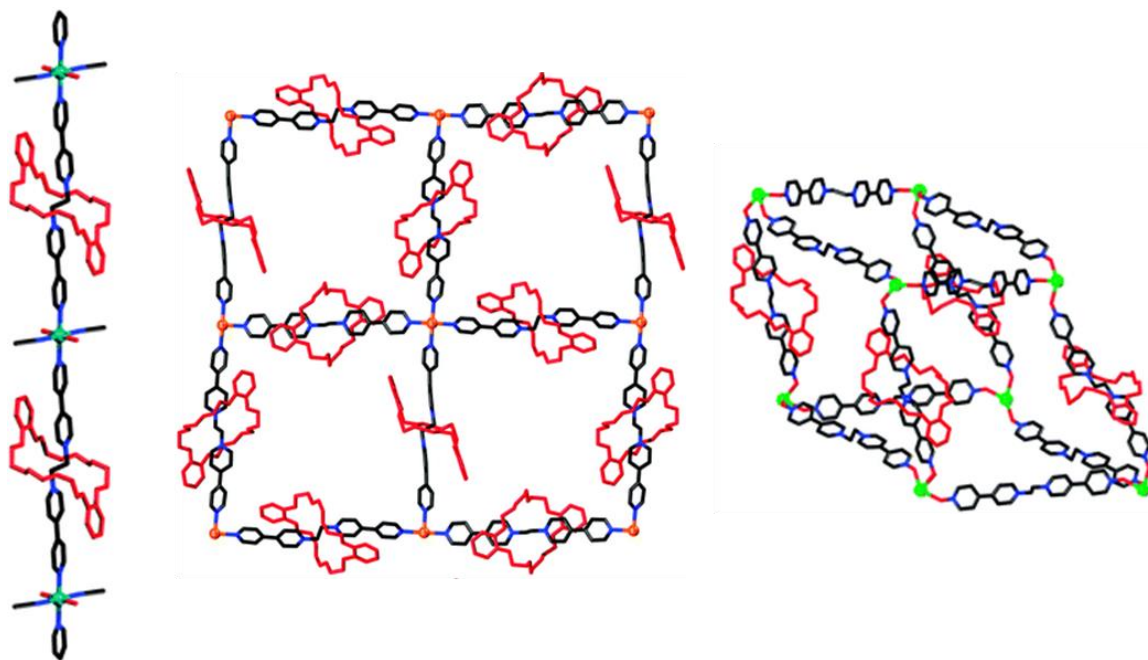


Fig 1.3.2 – the X-ray crystal structure of a 1D MORF with Co(II) ion (left), the X-ray crystal structure of a 2D MORF with Cd(II) ion (middle), and the X-ray crystal structure of a 3D MORF with Sm(III) ion (right). Reprinted with permission from ref^[29].

In 2010, Mercer and Loeb reported the use of [2]rotaxane wheels to create a new type of metal organic rotaxane framework.^[33] In this study, the **DB24C8** wheel was appended with four pyridine donor groups. This crown ether was combined with a 1,2-bis(pyridinium)ethane axle to produce [2]rotaxane ligand **1.4** (Fig 1.3.3). The X-ray crystal structure showed the crown ether adopts S-shaped conformation around the axle, and CH \cdots O, N \cdots O ion dipole and π -stacking interactions between electron-poor pyridinium rings and electron-rich catechol rings.



Fig 1.3.3 – the [2]rotaxane ligands used as the linker (**1.4**). Reprinted with permission from ref^[29].

The synthesized rotaxane reacted with $[\text{Cd}(\text{H}_2\text{O})_6]\text{BF}_4)_2$ and produced X-ray quality crystals of $[\text{Cd}_2\text{Cl}_4(\text{H}_2\text{O})_4(\mathbf{1.4})][\text{BF}_4]_2 \cdot 8(\text{MeNO}_2)$ suitable for X-ray diffraction analysis. Fig 1.3.4 depicts the coordination of ligand **1.4** to Cd(II) ions resulting in a 2D-periodic metal organic rotaxane framework in which the wheels act as the linking units.

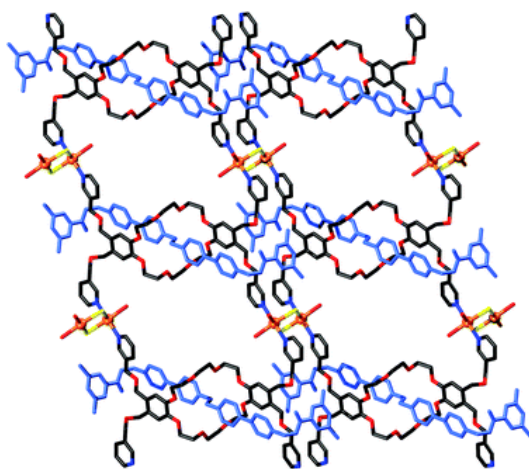


Fig 1.3.4 – representation of The two-periodic coordination polymer consisting of $[\text{Cd}_2\text{Cl}_4(\text{H}_2\text{O})_4]$ nodes and **1.4** rotaxane linkers. Reprinted with permission from ref^[29].

Incorporation of a multidentate [2]rotaxane ligand containing six thioether donor atoms, four attached to **DB24C8** crown ether and two at the termini of a linear axle, into MOF materials was reported by Frank and Loeb.^[34] The new type of morphology was created by reacting this hexa-thioether ligand and AgOTf in which all six thioether S-atoms are bonded to at least one Ag center. The X-ray diffraction study of the crystal showed interpenetrated frameworks in which a void in the lattice is filled with another framework. This interwoven MOF consists of four interlocked nodes, two metal centered through Ag-S bonding and two ligand centered. The 3D metal-organic framework with interweaving axles and wheels is shown in Fig 1.3.5.

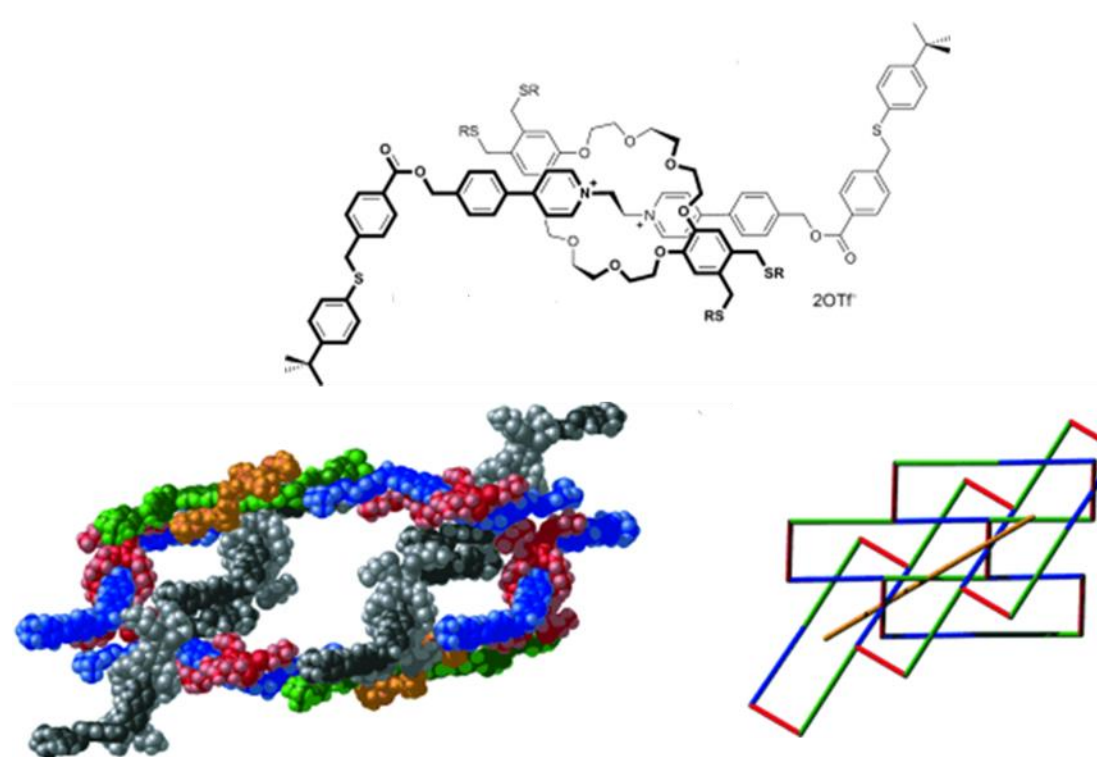


Fig 1.3.5 – multidentate [2]rotaxane ligands with six S-donor atoms (top), space-filling representations of the X-ray structure of MORF (bottom-left), schematic of the full X-ray structure network (bottom-right). Reprinted with permission from ref^[34].

1.4 Dynamic and controlled motion in the solid state

1.4.1 Introduction

Studies on dynamic motions of MIMs in solution are prerequisites for the future application of smart molecules based on MIMs; however arranging these molecules in patterns or condensed phases is quite challenging. Incorporating nanoscale MIMs into metal-organic frameworks is one of the ways to induce higher order on these molecules. In this way dynamic molecular components can undergo rotational or translational motion about the hard structural skeleton of the MOF.

1.4.2 Rotational motion in the solid state

Vukotic, Schurko and Loeb reported, in *Nature Chemistry* the first example of dynamic motion of a MIM inside a MOF material by using a [2]rotaxane as a linker.^[35] The tetracarboxylate [2]rotaxane (**1.5**) was produced through a ring-closing metathesis (RCM) reaction around a charged benzyl-anilinium axle followed by hydrogenation of the double bond and hydrolysis of the four ester groups. The single-crystal X-ray structure of the precursor tetraethyl ester [2]rotaxane showed only a single hydrogen bond between the aniline N-H group on the axle and an oxygen atom of the crown ether wheel. The green crystalline Cu(II)-based MOF with the formula of $[\text{Cu}_2(\mathbf{1.5})(\text{H}_2\text{O})_2] \cdot 3\text{H}_2\text{O}$ and named **UWDM-1** (University of Windsor Dynamic Material) was prepared by combining $\text{Cu}(\text{NO}_3)_2 \cdot 3\text{H}_2\text{O}$ and the tetracarboxylate MIM linker under solvothermal conditions in DMF (Fig 1.4.1). The porous MOF had small void spaces (11%) in the lattice which were occupied with water molecules. By heating the as-synthesized MOF to 150 °C under vacuum (activation method) the water molecules from both the channel and copper centres were removed and the MIM was freed to undergo motion. Powder X-ray diffraction (PXRD) data showed the structure of the MOF was unaffected after activation. To investigate the

dynamic motion of the macrocyclic inside the MOF, ^{13}C and ^2H solid-state NMR (SSNMR) were recorded on activated **UWDM-1**. As the temperature was increased from 292 K to 477 K on activated **UWDM-1**, the ^1H - ^{13}C cross-polarization/magic-angle spinning (CP/MAS) spectra of the crown ether carbons displayed a dramatic increase in resolution.

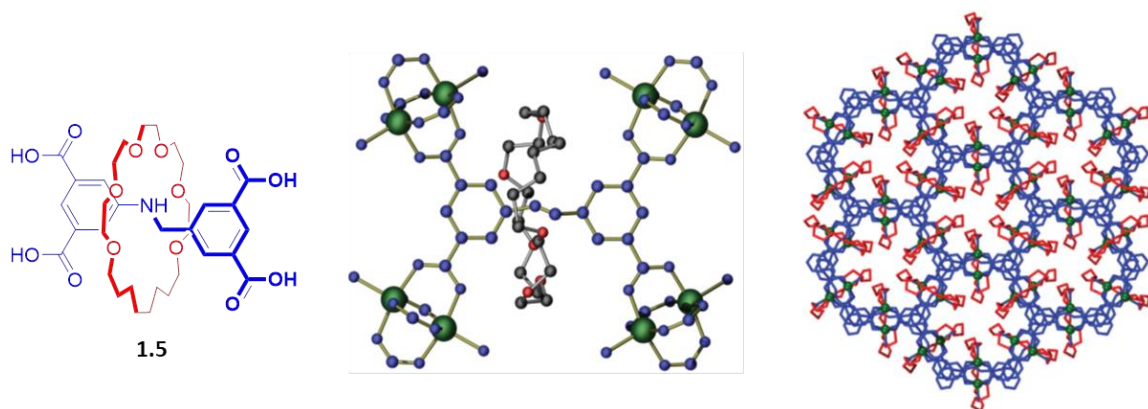


*Fig 1.4.1 – neutral [2]rotaxane **1.5** (left), Ball-and-stick representation of a single unit of the **UWDM-1** (middle), linking polyhedra creating narrow channels along the c-axis (right). Reprinted with permission from ref^[35].*

Similarities between these spectra and the ^{13}C NMR spectrum of the tetraethyl ester rotaxane in solution indicated the crown ether undergoes rapid motion at high temperature (Fig 1.4.2 a). To clarify the nature of the motion, variable-temperature ^2H SSNMR was recorded on **UWDM-1** labelled with deuterium (the double bond of the crown ether was hydrogenated with deuterium gas). Comparing VT ^2H SSNMR spectra of activated **d₂-UWDM-1** (Fig 1.4.2 b) and spectral simulations (Fig 1.4.2 c) with reported ^2H NMR line shapes of simpler molecular systems identified^[36] four kinds of motional regimes: 1) from 160 K to 203 K no motion is observed, 2) from 251 K to 276 K conformational changes of the CH_2 groups occurs (interconverting of the pseudo-axial and pseudo-equatorial C–D positions), 3) at 324 K the CD_2 reorientation is accompanied by rocking, or partial rotation of the ring and 4) above 373 K the ring undergoes full rotation (Fig 1.4.2 d).

Also, the effect of size and shape of the crown ether macrocycles (**22C6**, **24C6**, **B24C6**) on motion in the solid state was studied.^[37] Under the same synthetic conditions, three more MOFs varying different macrocycles were obtained with the same structure as **UWDM-1**. VT ^2H SSNMR spectra, simulations, showed **UWDM-1** with **24C6** macrocycle is the most mobile of the series.

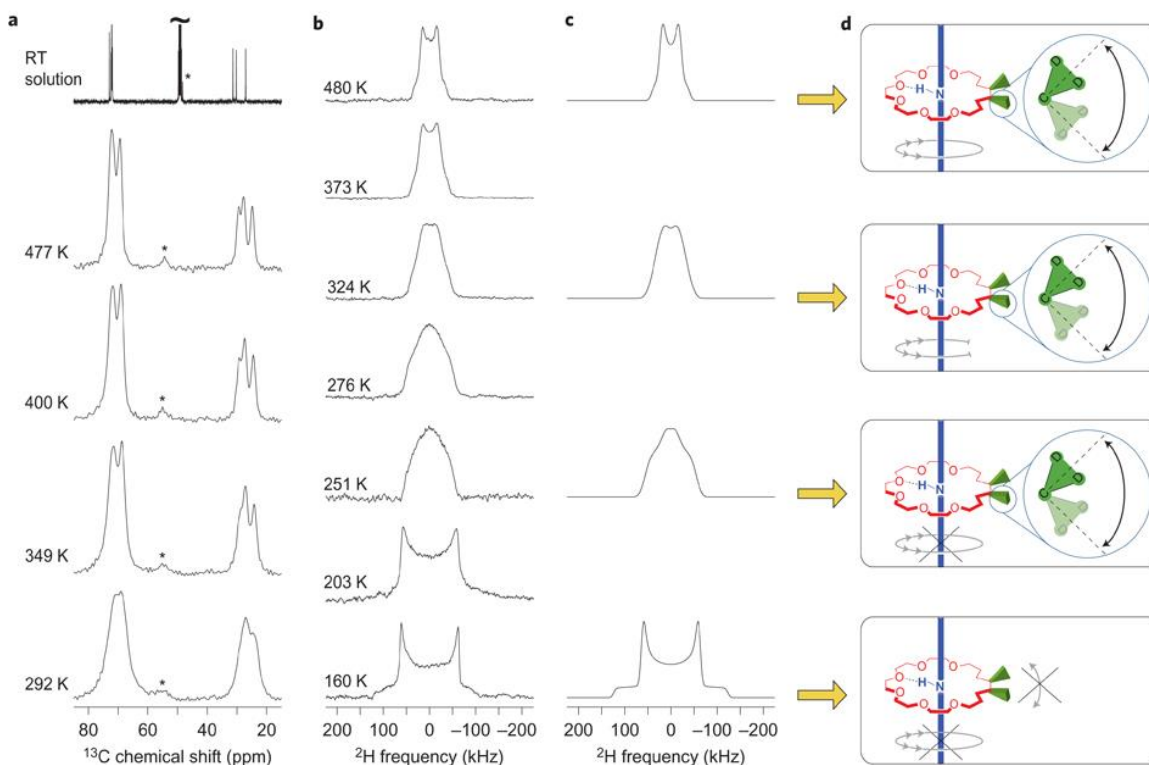
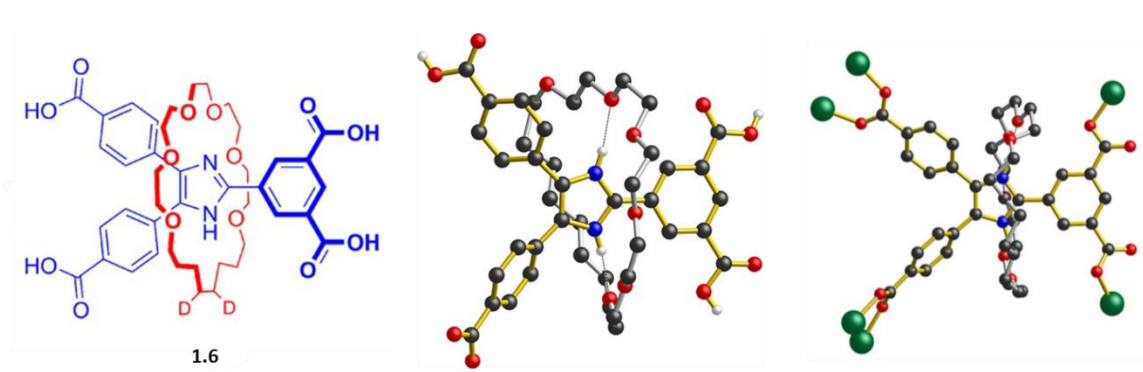


Fig 1.4.2 – a) ^{13}C SSNMR spectra of **UWDM-1**, b) experimental variable temperature ^2H SSNMR spectra of activated d_2 -**UWDM-1**, c) simulated ^2H SSNMR spectra of activated d_2 -**UWDM-1**, d) schematic representations of the dynamic motion. Reprinted with permission from ref^[35].

For **UWDM-1** with **22C6**, no full rotation was observed and partial rotation occurred at temperatures 67 and 100 K higher than the 24-membered ring as a result of stronger hydrogen-bonding interactions between the 22-membered macrocyclic ring and the axle. **UWDM-1** with **B24C6** showed no full or partial rotation. The bulky benzo group of the macrocycle prevented rotation of the macrocycle inside the MOF.

Recently, thermally driven dynamics of a related Y-shaped rotaxane was reported by Farahani, Schurko and Loeb.^[38] In this report, the unsymmetrical rotaxane linker (**1.6**) was incorporated into a Zn(II) based MOF. The formula of the MOF (**UWDM-5**) $\{[\text{Zn}_2(\mathbf{1.6})(\text{NO}_3)(\text{DEF})](\text{DEF})(\text{H}_2\text{O})\}$ was determined by single-crystal X-ray diffraction. The rotaxane imidazole core is protonated (imidazolium) and the crown ether around the recognition site stabilizes the charge and increases the pKa of the imidazolium ion. The charge on the resulting cationic linker is neutralized by a coordinated nitrate ion which is part of the metal node. The imidazolium core remains protonated even during the basic and solvothermal conditions required to make the MOF. The X-ray structure of the rotaxane ligand showed there are two hydrogen bonds between the imidazolium N-atoms and crown ether O-atoms which also occurs in the MOF structure (Fig 1.4.3). To characterize the dynamic motion inside the MOF the double bond of the wheel was again reduced using $\text{D}_2(\text{g})$ and Pd/C. VT ^2H SSNMR of **UWDM-5** displayed similar motion to **UWDM-1**.



*Fig 1.4.3 – rotaxane linker **1.6** with deuterium ($D = ^2\text{H}$) labels (left), X-ray structure of the rotaxane (middle), X-ray structure of MOF **UWDM-5** showing the basic repeating unit (right). Reprinted with permission from ref^[38].*

1.4.3 Translational motion in the solid state

In 2015, Zhu, Schurko and Loeb published a *Nature Chemistry* article titled “A molecular shuttle that operates inside a metal–organic framework”.^[39] For this work, they designed a [2]rotaxane ligand with two benzimidazole recognition sites on the axle and a single [24]crown-8 ether (**24C8**) macrocycle. To identify the shuttling motion inside the MOF by ¹³C SSNMR, the carbon atoms at the 2-positions of the benzimidazole rings of linker (**1.7**) were enriched to 50% ¹³C (Fig 1.4.4). The VT ¹³C NMR spectrum of the precursor ester [2]rotaxane exhibited only a single resonance for ¹³C labelled site in in toluene-d₈ solution indicating that rapid molecular shuttling between the two sites must be occurring. By lowering the temperature, two separate resonances for the occupied and empty recognition sites appeared which allowed determination of an energy barrier to molecular shuttling about $\Delta G^\ddagger = 7.7 \text{ kcal mol}^{-1}$ and a shuttling rate = $1.4 \times 10^7 \text{ s}^{-1}$ at 298 K in toluene-d₈.

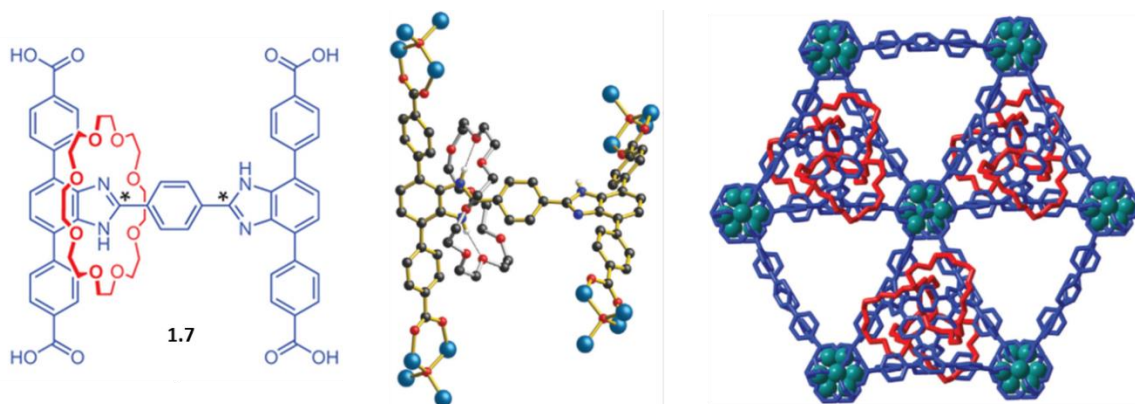


Fig 1.4.4 – neutral [2]rotaxane linker **1.7** enriched with ¹³C shown with asterisks (left), single unit of the linker **1.7** coordinated to four Zn₄O clusters (middle), view of the open channels in the lattice down the c axis with macrocycles (right). Reprinted with permission from ref^[39].

To probe the possibility of translational motion in the solid state, a yellow crystalline Zn(II) based MOF was produced (**UWDM-4**) using zinc(II) tetrafluoroborate hydrate and ligand **1.7** (Fig 1.4.4). The as-synthesized MOF suspected to be in the mono-protonated state (**UWDM-4·HBF₄**) and the macrocycle would occupy only the charged site and no molecular shuttling would be expected. To solve this problem, the as-synthesized MOF (**UWDM-4·HBF₄**) was treated with the strong base N,N,N',N'-tetramethylnaphthalene-1,8-diamine (proton-sponge) in ethanol and removal of HBF₄ was monitored by ¹⁹F NMR spectroscopy. To calculate the rate of shuttling inside the solid-state lattice of the MOF, VT ¹³C SSNMR experiments in a 21.1 T field were performed. At high temperatures (334 K), a single peak was observed and as the temperature is decreased the peak broadens and at 298 K splits into two distinct peaks (Fig 1.4.5 a). It was concluded that rapid molecular shuttling of the macrocyclic ring between the two recognition sites occurs inside the MOF and by simulation of the experimental spectra, the rates of shuttling at various temperatures were determined and the rate of shuttling inside the MOF lattice estimated to be 283 s⁻¹ at 298 K.

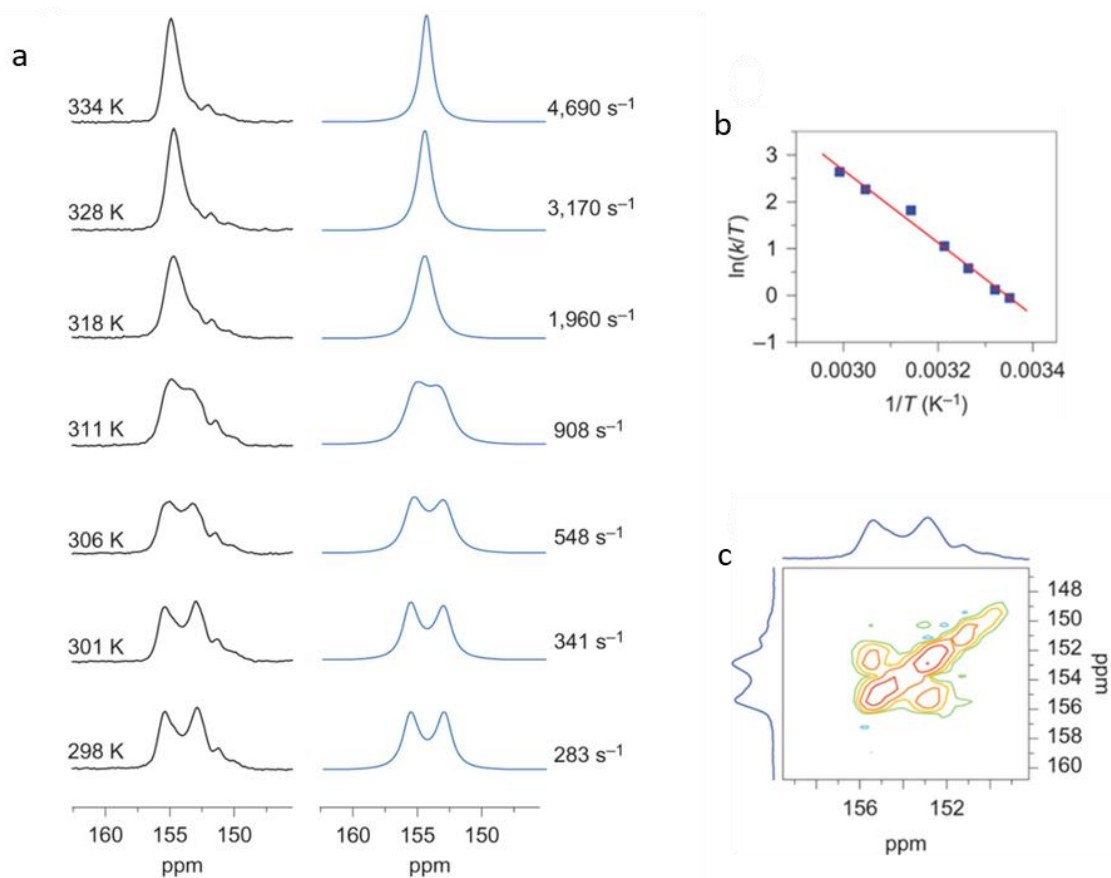


Fig 1.4.5 – ^1H - ^{13}C CP/MAS NMR spectra (experimental, simulation) of a ^{13}C enriched sample of **UWDM-4** (a), Eyring plot created from the VT NMR data (b), ^{13}C 2D EXSY SSNMR spectrum of **UWDM-4** (c). Reprinted with permission from ref^[39].

An Eyring plot of $\ln(k/T)$ versus $1/T$ (Fig 1.4.5 b) allowed the calculation of an activation barrier (ΔG^\ddagger) to this translational motion of 14.1 kcal mol $^{-1}$. As corroborating evidence, 2D SSNMR EXSY experiments also proved molecular shuttling was occurring inside the MOF (Fig 1.4.5 c). This study revealed that molecular shuttling in the solid state is slower than the solution because of a higher energy barrier.

More recently, Stoddart and coworkers described an artificial molecular switch within a robust and porous crystalline material.^[40] They displaced Zr-bound aqua and hydroxyl ligands of a Zr_6 -based metal-organic framework (**NU-1000**) with a trisradical

semirotaxane using the Solvent-Assisted Ligand Incorporation (**SALI**) method. The ^1H NMR spectrum of a digested MOF sample in a D_2SO_4 - $(\text{CD}_3)_2\text{SO}$ mixture showed that approximately, each hexagonal channel was filled by three dumbbells and that half of these dumbbells were encircled by a macrocyclic ring. UV-Vis-NIR reflectance spectroscopy revealed further evidence for the presence of rotaxanes within the MOF (**NU-1000**) (Fig 1.4.6). The ability of these redox-active rotaxane switches to operate within the robust porous framework was confirmed. Ultimately, a thin film of the **NU-1000** MOF crystals incorporated with trisradical rotaxane (**SALI-R^{3(••)}**) on fluorine-doped tin oxide electrode was prepared. Cyclic voltammetry acquired at a scan rate of 50 mV/s revealed a semi-reversible redox wave centered around -250 mV, corresponding to the one-electron reduction of (**SALI-R^{3(••)}**), demonstrating the application of electrochemical molecular switches inside a porous solid state material.

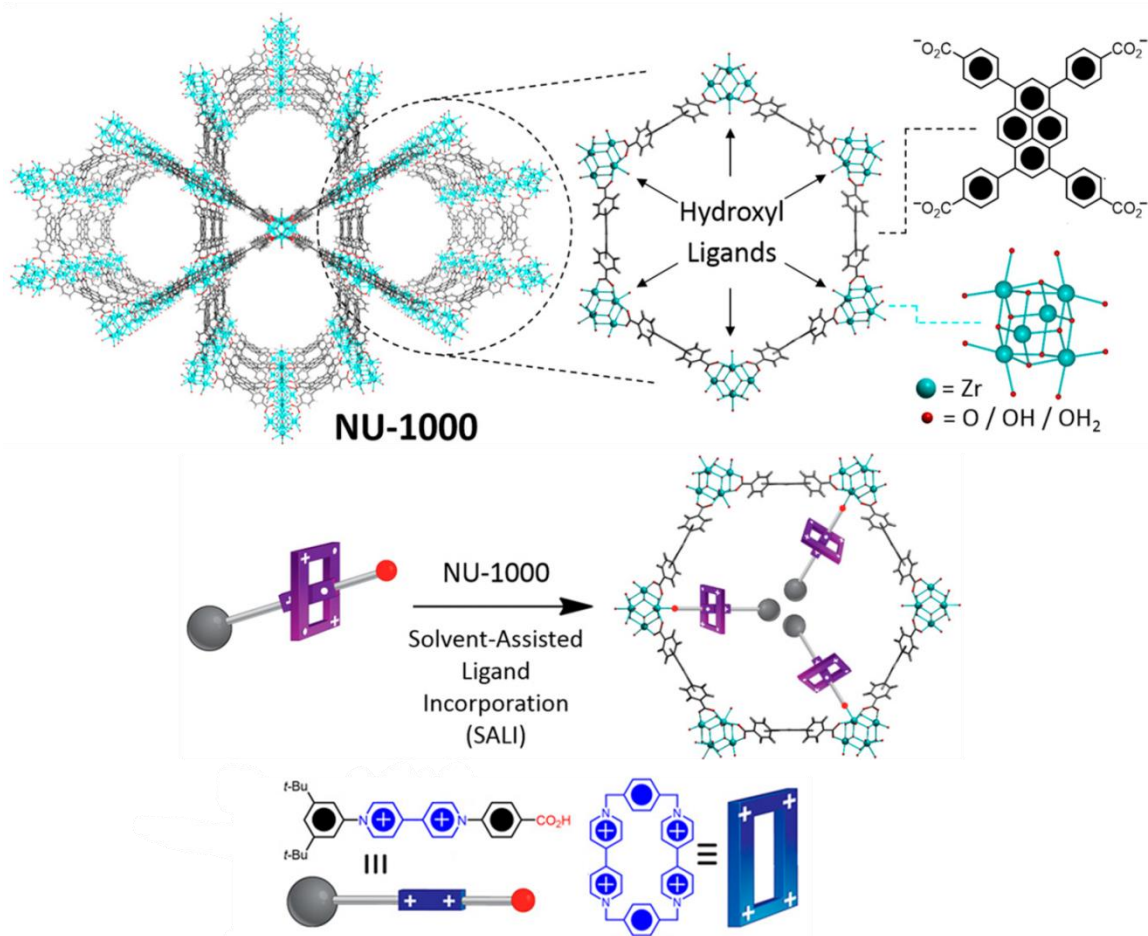


Fig 1.4.6 – top: Zr-based MOF with trihexagonal channels based on tetratopic 4,4',4'',4'''-(pyrene 1,3,6,8-tetrayl)tetrabenzoate linker (**PyTBA**) with a molecular formula of $Zr_6(\mu_3-O)_4(\mu_3-OH)_4(-OH)_4(-OH_2)_4(PyTBA)_2$ (**NU-1000**), bottom: Incorporating the rotaxanes inside the channels of **NU-1000** MOF. Reprinted with permission from ref^[40].

1.5 Scope of Dissertation

Although, [2]rotaxanes like **1.7** through axle and **1.4** through the wheel were successfully incorporated into MOFs, it could be possible to create a MOF using a [2]rotaxane linker with donor atoms attached to *both* the axle and the wheel. In this way, both the axle and wheel could be involved in the propagation of completely independent frameworks. In chapters 2 and 3, the solid-state structures of MOFs derived from interlocked hexadentate linkers with donor atoms on both the axle and wheel will be described (Fig 1.5.1).

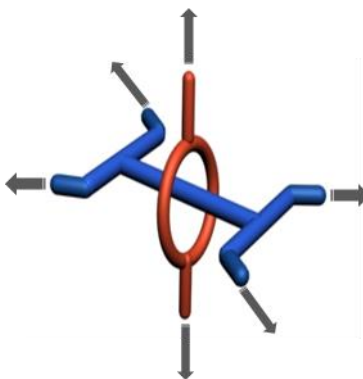


Fig 1.5.1 – cartoon representation of [2]rotaxane linker with donor atoms attached to both the axle and the wheel.

Correlating the rate of shuttling to the length of the axle in rotaxanes is crucial to the development of molecular switches inside the solid state materials. Hence, in chapter 4, the correlation between rigid spacer length and shuttling rate in H-shaped [2]rotaxanes in solution will be considered (Fig 1.5.2).

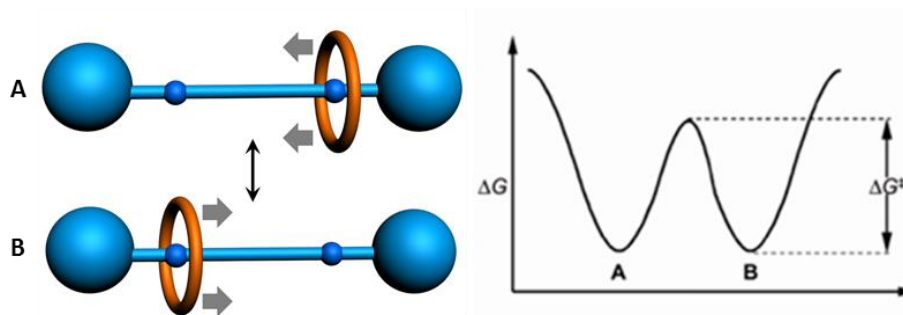


Fig 1.5.2 – cartoon representation of [2]rotaxane and energy diagram in degenerate molecular shuttles. Reprinted with permission from ref^[3].

The shuttling motion inside the Zn-based MOF (**UWDM-4**) was studied previously however, the material was relatively fragile and sensitive to changes in pH and solvent. In chapter 5, pH-control of molecular shuttling rates inside Zr-based MOFs, which is famous for high stability, will be introduced.

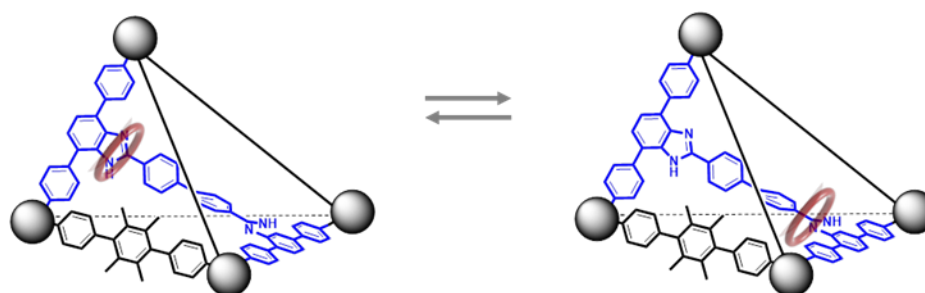


Fig 1.5.3 – representation of shuttling motion inside Zr-based MOF.

In chapter 6, for the first time, a bistable solid-state molecular shuttle will be demonstrated.

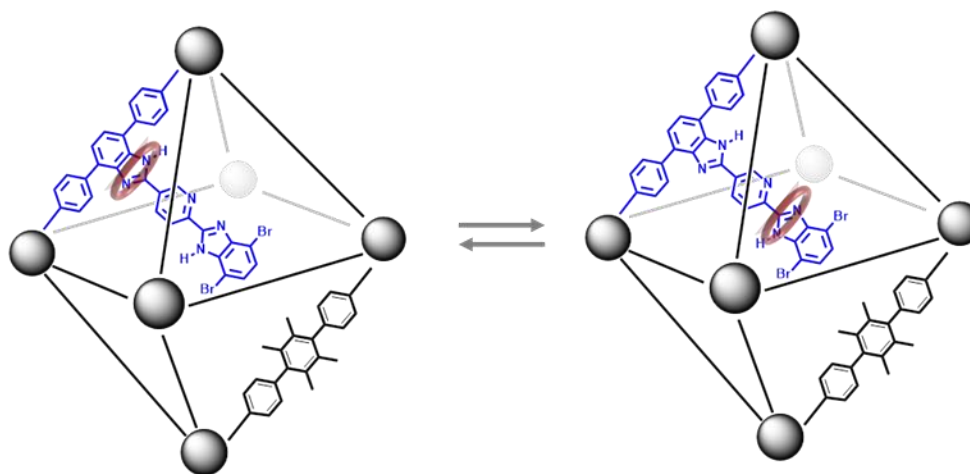


Fig 1.5.4 – representation of bistable shuttling motion inside Zr-based MOF.

1.6 References

1. J. P. Sauvage and D. B. Amabilino, in *Topics in Current Chemistry*, **2012**, vol. 323, pp. 107–126.
2. J. W. Steed and J. L. Atwood, *Nano Today*, **2007**, 2, 707–775.
3. S. Erbas-Cakmak, D. A. Leigh, C. T. McTernan and A. L. Nussbaumer, *Chem. Rev.*, **2015**, 115, 10081–10206.
4. C. Cheng and J. F. Stoddart, *ChemPhysChem*, **2016**, 17, 1780–1793.
5. S. Shinkai, T. Ogawa, T. Nakaji, Y. Kusano, O. Nanabe, *Tetrahedron Lett.*, **1979**, 20, 4569–4572.
6. J. Berná, D. A. Leigh, M. Lubomska, S. M. Mendoza, E. M. Pérez, P. Rudolf, G. Teobaldi and F. Zerbetto, *Nat. Mater.*, **2005**, 4, 704–710.
7. M. Juríček, J. C. Barnes, N. L. Strutt, N. A. Vermeulen, K. C. Ghooray, E. J. Dale, P. R. McGonigal, A. K. Blackburn, A.-J. Avestro and J. F. Stoddart, *Chem. Sci.*, **2014**, 5, 2724–2371.
8. S. Saha, A. H. Flood, J. F. Stoddart, S. Impellizzeri, S. Silvi, M. Venturi and A. Credi, *J. Am. Chem. Soc.*, **2007**, 129, 12159–12171.
9. P. L. Anelli, N. Spencer, and J. F. Stoddart, *J. Am. Chem. Soc.*, **1991**, 113, 5131–5133.
10. E. R. Kay, D. A. Leigh, F. Zerbetto, *Angew. Chem. Int. Ed.*, **2007**, 46, 72–191.
11. M. R. Panman, B. H. Bakker, D. den Uyl, E. R. Kay, D. A. Leigh, W. J. Buma, Brouwer, J. a J. Geenevasen and S. Woutersen, *Nat. Chem.*, **2013**, 5, 929–934.

12. A. S. Lane, D. A. Leigh and A. Murphy, *J. Am. Chem. Soc.*, **1997**, 119, 11092–11093.
13. D. D. Günbaş and A. M. Brouwer, *J. Org. Chem.*, **2012**, 77, 5724–5735.
14. P. G. Young, K. Hirose and Y. Tobe, *J. Am. Chem. Soc.*, **2014**, 136, 7899–7906.
15. F. S. Richard A. Bissell, E. Cordova, A. E. Kaifer, *Nature*, **1994**, 369, 133–137.
16. S. A. Vignon, T. Jarrosson, T. Iijima, H. R. Tseng, J. K. M. Sanders and J. F. Stoddart, *J. Am. Chem. Soc.*, **2004**, 126, 9884–9885.
17. M. J. Barrell, D. A. Leigh, P. J. Lusby and A. M. Z. Slawin, *Angew. Chem. Int. Ed.*, **2008**, 47, 8036–8039.
18. N. Farahani, K. Zhu, N. Noujeim and S. J. Loeb, *Org. Biomol. Chem.*, **2014**, 12, 4824–4827.
19. N. Noujeim, K. Zhu, V. N. Vukotic and S. J. Loeb, *Org. Lett.*, **2012**, 14, 2484–2487.
20. K. Zhu, V. N. Vukotic, N. Noujeim and S. J. Loeb, *Chem. Soc. Rev.*, **2012**, 3, 3265–3271.
21. K. Zhu, V. N. Vukotic and S. J. Loeb, *Angew. Chemie*, **2012**, 124, 2210–2214.
22. N. Farahani, K. Zhu and S. J. Loeb, *ChemPhysChem*, **2016**, 17, 1875–1880.
23. K. Zhu, V. N. Vukotic and S. J. Loeb, *Chem. Asian J.*, **2016**, 11, 3258–3266.
24. S. J. Loeb, *Chem. Commun.*, **2005**, 1511–1518.
25. T. J. Huang, H. R. Tseng, L. Sha, W. Lu, B. Brough, A. H. Flood, B. D. Yu, P. C. Celestre, J. P. Chang, J. F. Stoddart and C. M. Ho, *Nano Lett.*, **2004**, 4, 2065–2071.
26. H. W. Gibson, D. S. Nagvekar, N. Yamaguchi, S. Bhattacharjee, H. Wang, M. J. Vergue and D. M. Hercules, *Macromolecules*, **2004**, 37, 7514–7529.

27. H. Yu, Y. Luo, K. Beverly, J. F. Stoddart, H. R. Tseng and J. R. Heath, *Angew. Chem. Int. Ed.*, **2003**, 42, 5706–5711.
28. (a) M. Albrecht, M. Lutz, A. L. Spek and G. van Koten, *Nature*, **2000**, 406, 970-974; (b) O. M. Yaghi, M. O’Keefe, N. W. Ockwing, H. K. Chae, M. Eddaoudi and J. Kim, *Nature*, **2003**, 423, 705-714.
29. V. N. Vukotic and S. J. Loeb, *Chem. Soc. Rev.*, **2012**, 41, 5896–5906.
30. D. Whang and K. Kim, *J. Am. Chem. Soc.*, **1997**, 119, 451-452.
31. J. E. M. Lewis, S. M. Goldup, P. D. Beer and S. J. Loeb, *Chem. Soc. Rev.*, **2017**, 46, 2577-2591.
32. G. J. E. Davidson and S. J. Loeb, *Angew. Chem. Int. Ed.*, **2003**, 42, 74–77.
33. D. J. Mercer, V. N. Vukotic and S. J. Loeb, *Chem. Commun.*, **2011**, 47, 896–898.
34. N. C. Frank, D. J. Mercer and S. J. Loeb, *Chem. Eur. J.*, **2013**, 19, 14076–14080.
35. V. N. Vukotic, K. J. Harris, K. Zhu, R. W. Schurko and S. J. Loeb, *Nat. Chem.*, **2012**, 4, 456–460.
36. C. I. Ratcliffe, G. W. Buchanan and J. K. Denike, *J. Am. Chem. Soc.*, **1995**, 117, 2900–2906.
37. V. N. Vukotic, C. A. O’Keefe, K. Zhu, K. J. Harris, C. To, R. W. Schurko and S. J. Loeb, *J. Am. Chem. Soc.*, **2015**, 137, 9643–9651.
38. N. Farahani, K. Zhu, C. A. O. Keefe, R. W. Schurko and S. J. Loeb, *ChemPlusChem*, **2016**, 81, 836–841.

39. K. Zhu, C. A. O'Keefe, V. N. Vukotic, R. W. Schurko and S. J. Loeb, *Nat. Chem.*, **2015**, *7*, 514–519.
40. P. R. McGonigal, P. Deria, I. Hod, P. Z. Moghadam, A.-J. Avestro, N. E. Horwitz, I. C. Gibbs-Hall, A. K. Blackburn, D. Chen, Y. Y. Botros, M. R. Wasielewski, R. Q. Snurr, J. T. Hupp, O. K. Farha and J. F. Stoddart, *PNAS*, **2015**, *112*, 11161–11168.

CHAPTER 2

2.1 Formation of a Polythreaded, Metal–Organic Framework

Utilizing an Interlocked Hexadentate, Carboxylate Linker

2.1.1 Introduction

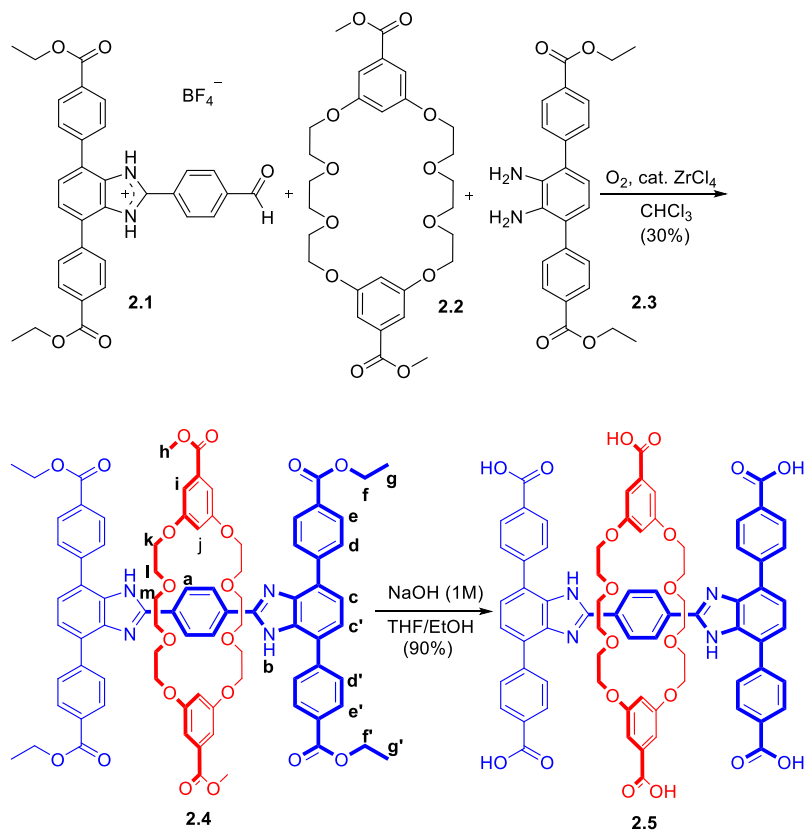
The incorporation of mechanically interlocked molecules (MIMs)^[1] such as rotaxanes, catenanes, and knots into polymeric materials^[2] has become an important area of study to determine the effect that these unique molecular connections might have on the mechanical^[3] (rheology, elasticity), electronic^[4] (ferroelectric, piezoelectric), optical^[5] (nonlinear optics), or host–guest^[6] (absorption, storage) properties of the resulting materials. Most recently, there has been interest in the incorporation of MIMs into metal–organic framework (MOF) materials as a method to organize molecular switches and potentially molecular machines in the solid state.^[7] In particular, novel MOFs have been prepared with rotaxanes as linkers and large amplitude rotational and translational motion (shuttling) characterized by solid-state NMR spectroscopy.^[8] These types of materials, often called metal–organic rotaxane frameworks (MORFs),^[9] were first prepared by simply adding donor atoms to the ends of a linear axle that could thread through a macrocyclic wheel such as a crown ether or a cucurbituril.^[10] This methodology led to examples of 1-, 2- and 3-periodic structures containing [2]rotaxane axles as linkers between metal nodes with macrocyclic wheels threaded onto the framework skeleton.^[11] This was followed by a few examples in which the framework was constructed by utilizing donors attached to the wheels.^[12] We reasoned that it should also be possible to create a [2]rotaxane linker with donor atoms attached to both the axle and the wheel.^[13] This is a particularly attractive idea, because it might be possible for the axle and wheel to be involved in the propagation of

completely independent frameworks that would be interpenetrated only by virtue of the mechanically interlocked nature of the ligand core—a MIM node. Herein, we describe the first example of a metal–carboxylate-derived MOF that combines the interpenetration of frameworks owing to an interlocked ligand node with the classical interpenetration of frameworks that result from the filling of a void in a lattice.^[14] The MOF structure is thus best described as being polythreaded by virtue of this unique combination of two types of interpenetration, that is, through linker (mechanically interlocked) and lattice (*n*-fold interpenetration).^[15]

2.1.2 Results and Discussion

A hexadentate carboxylic acid ligand was constructed by using a previously successful molecular design for a [2]rotaxane that combines a rigid H-shaped axle containing two benzimidazole recognition sites and a single macrocyclic wheel in the form of a crown ether.^[16] Four of the carboxylic acid groups are attached to the ends of the H-shaped axle and the other two are appended to the crown ether wheel. Scheme 2.1 describes the preparation of the [2]rotaxane linker in two steps from known precursors by capping a preformed [2]pseudorotaxane [2.1⊂2.2]⁺ with 2.3 followed by hydrolysis of resulting hexaester 2.4 to yield hexaacid 2.5. The ¹H NMR spectrum of hexaester, [2]rotaxane 2.4 is shown in Fig 2.1; although similar data was obtained for hexaacid, 2.5, the low solubility of this compound limited the utility of these spectra for full characterization and signal assignment (see Experimental 2.2.3). In the neutral forms of these [2]rotaxanes, there is very little interaction between the axle and wheel components. Only two weak NH⋯O interactions between the benzimidazole NH groups and the crown ether O atoms remain from the charge-assisted, noncovalent interaction used to template the formation of this species. Therefore, although the axle is quite rigid and the macrocycle is permanently

locked to the axle, there are a wide variety of possible orientations for the carboxylate groups of the two interlocked components owing to the large amplitude and rotational and translational degrees of freedom available for this molecule.



Scheme 2.1 – synthesis of interlocked, hexadentate carboxylic acid ligand 2.5. Labels are assignments for the resonances observed in the ^1H NMR spectrum shown in Fig 2.1.

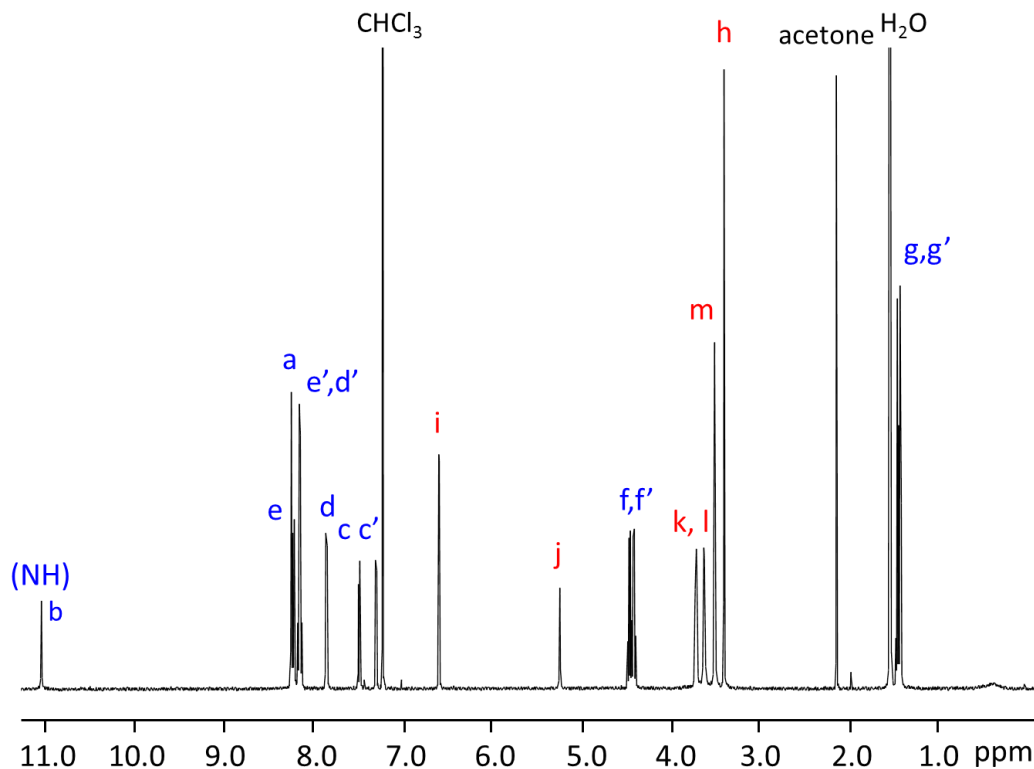


Fig 2.1 – ^1H NMR spectrum of hexaester **2.4** with resonance assignments corresponding to the labeling shown in Scheme 2.1.

The single-crystal X-ray structure of linker **2.5** was determined from crystals with formula $\mathbf{2.5}\cdot(\text{DMSO})_7$ (see Fig 2.2). The two molecules of **2.5** in the asymmetric unit both have a crystallographically imposed center of symmetry and differ only in how they interact with the DMSO solvent molecules. The central phenyl ring and the two benzimidazole groups of the H-shaped axle lie in approximately the same plane, whereas the macrocycle is positioned over the central phenyl ring and bridges the two benzimidazole groups to form two $\text{NH}\cdots\text{O}$ hydrogen bonds ($\text{N}\cdots\text{O}$, 2.90 Å; $\text{N}-\text{H}\cdots\text{O}$ 155° and $\text{N}\cdots\text{O}$, 2.92 Å; $\text{N}-\text{H}\cdots\text{O}$ 167° for two independent centrosymmetric molecules). This is consistent with the chemical shift data observed in solution by ^1H NMR spectroscopy. Although X-ray structures previously determined for similar H-shaped rotaxanes most often reveal that a single macrocyclic

wheel such as dibenzo[24]crown-8 ether prefers to occupy one end of the axle, interacting with only a single benzimidazole recognition site,^[16,8c] there is precedent for larger macrocycles such as dibenzo[30]crown-10 (**DB30C10**) or bis-*meta*-phenylene[26]crown-8 (**BMP26C8**) to interact simultaneously with both NH groups in this fashion.^[17] Most importantly, it is clear from the solid-state structure that the six carboxylic acid groups are well separated and each could potentially act as an independent donor group to a metal centered secondary building unit (SBU) upon deprotonation, that is, result in the formation of a MOF.

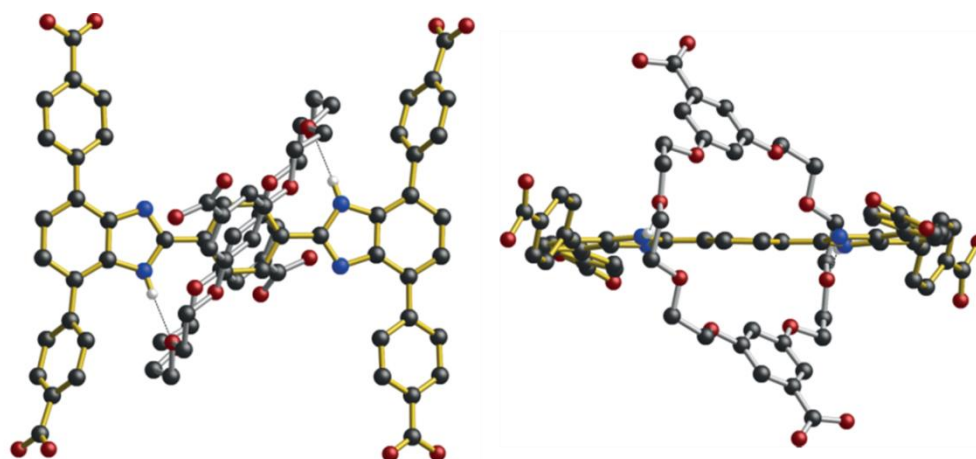


Fig 2.2 – crystal structure of 2.5.(DMSO)₇. view of the H-shaped axle and orientation of the four COOH groups (left), view emphasizing the crown ether wheel and positions of two other COOH groups (right), color key: C black, N blue, O red, H white, axle gold, wheel silver, H-bonds dashed lines, DMSO and H atoms not involved in H-bonding are omitted for clarity, only one of the molecules in the asymmetric unit is shown.

The reaction of **2.5** with zinc nitrate in a solvent mixture of DMF/1,4-dioxane/H₂O (1:1:1) at 90 °C for 48 h produced a solid material in the form of yellow crystals (58 % yield). The material was subsequently analyzed by single-crystal X-ray diffraction and was found to have the formula {[NH₂Me₂]₂[Zn₂(H₂O)₂(**2.5**)](H₂O)_{1.25}}. Fig 2.3 (a) shows the repeating unit

of the material, in which all of the carboxylate ligands of **2.5** are coordinated to a SBU consisting of a single Zn^{II} ion. The combination of two independent Zn^{II} ions and a linker with six negative charges results in a formally anionic framework. This negative charge is balanced by the presence of two cations in the form of dimethylammonium ions, $[NH_2Me_2]^+$, produced during the solvothermal synthesis from the decomposition of DMF^[18]. Fig 2.3 (c) shows the detailed coordination spheres of the two independent Zn^{II} centers. Each Zn^{II} ion has approximately tetrahedral geometry and coordinates to three different carboxylate groups: two from the axle (A), opposite ends of a single triphenylene strut, and one from the macrocyclic wheel (W), as well as a single water molecule. The coordination vectors of the four axle carboxylate groups are essentially coplanar (Fig 2.3, a) with those of the macrocycle, which are oriented in opposite directions ($\approx 180^\circ$ apart), offset by ca. 25° owing to rotation of the ring relative to the H-axle plane (Fig 2.3, b). There are no significant bonding interactions between the axle and wheel; the closest $NH\cdots O$ interaction that could be construed as hydrogen bonding shows a $N\cdots O$ distance of 4.04 Å with a $N-H\cdots O$ angle of 159° . Thus, the positioning of the macrocycle with respect to the wheel is almost certainly dictated by optimizing coordination to the Zn^{II} ions and packing the molecular components rather than the noncovalent interactions between axle and wheel observed for the structure of the free ligand. The overall framework is best described as arising from the threefold interpenetration of individual lattices constructed from alternating axles and wheels, as shown in part (a) of Fig 2.4 (red). However, unlike classical interpenetration for MOFs, in which the interpenetrating lattices simply fill void spaces within the structure, each one of these three lattices must pass through the other two by virtue of the interlocked nature of the linker axle and wheel.

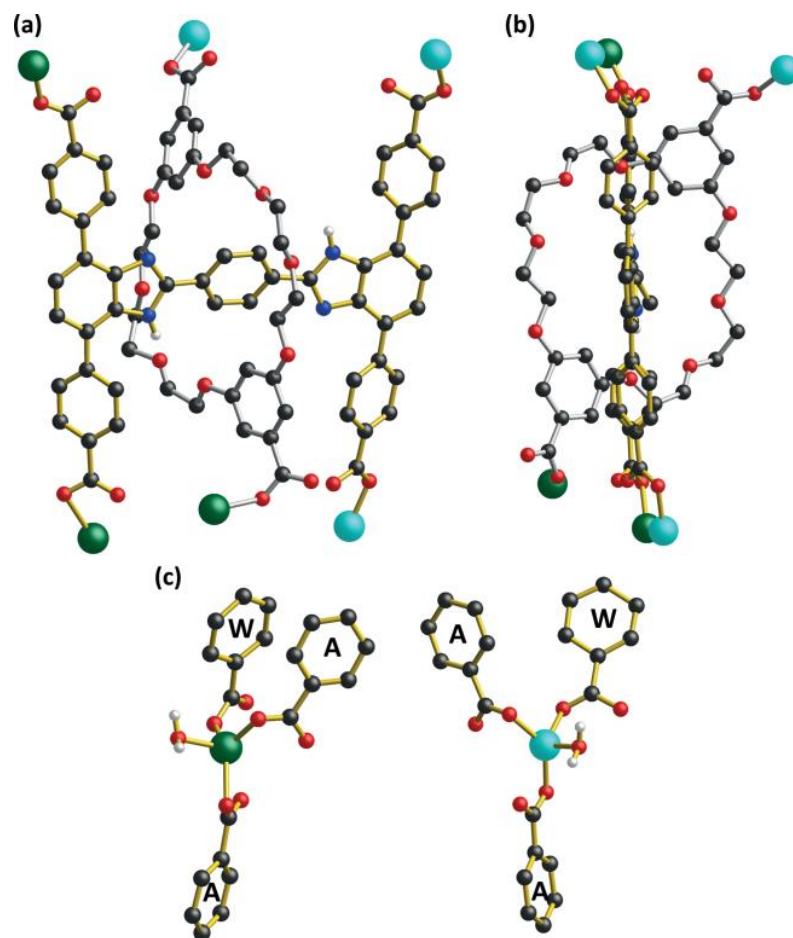


Fig 2.3 – crystal structure of MOF $\{[NH_2Me_2]_2[Zn_2(H_2O)_2(2.5)]\}$, (a) the interlocked core of the MOF showing all bonds to Zn^{II}; coordinated H₂O not shown, (b) the core unit emphasizing the rotation of the wheel relative to the axle, (c) the coordination spheres of the two unique Zn^{II} ions. A = axle, W = wheel, color key: C black, N blue, O red, Zn1 teal, Zn2 cyan, axle gold, wheel silver, cations, solvent, and hydrogen atoms are omitted for clarity.

Fig 2.4 (b, c) shows how a second and then a third lattice interpenetrates through this linker based, mechanical bonding motif. The result is a tightly packed material with an anionic framework, in which the only sizeable voids are filled with the charge-balancing [NH₂Me₂]⁺ cations and a small pocket close to one of the benzimidazole NH groups is occupied by hydrogen-bonded water molecules. Calculations (PLATON) show a total void space of <2

%.^[19] Within one of these single lattices (see Fig 2.4, a, red) the various Zn...Zn distances are, for the H-shaped axle: (1) on the same triphenylene strut, 19.2 and 19.3 Å; (2) between different struts, 10.4 and 15.8 Å; (3) diagonally, 22.8 and 23.5 Å; (4) between two ends of a single macrocycle, 19.0 Å; and (5) between an axle and a wheel, 5.6 and 8.2 Å. The thermal stability of the MOF material was evaluated by variable-temperature powder X-ray diffraction (VT-PXRD), which showed that over the temperature range of 25 to 200 °C there was essentially no loss of crystallinity (see Fig 2.5). These observations are consistent with the nonporous nature of the material. Notably, many materials that contain interpenetrated lattices undergo phase changes or rapid loss of crystallinity owing to the relative motion of one lattice with respect to the others. Given that this material is threaded by interpenetrating one coordinating component through another by formation of a mechanically interlocked linker, this type of lattice motion is much more restricted, and this presumably results in a more robust material. All figures were generated by using the Crystal Maker software.^[21]

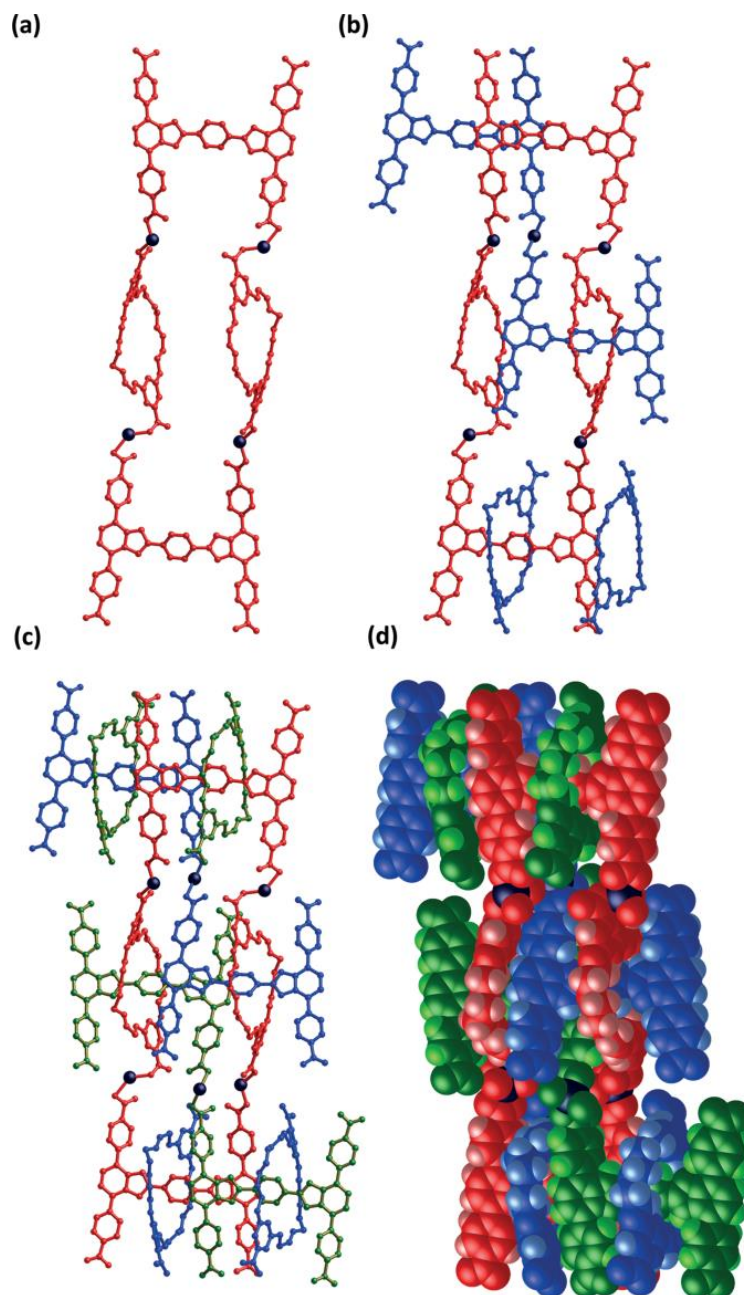


Fig 2.4 – crystal structure of the MOF $\{[NH_2Me_2]_2[Zn_2(H_2O)_2(2.5)]\}$, a) a single 2-periodic, framework (red) with alternating axles and wheels, b) two of the frameworks (red and blue) interpenetrated through the linker, c) three of the frameworks (red, blue and green) interpenetrated through the linker, d) a space-filling model of the three interpenetrated frameworks, color key: frameworks red, blue, green, Zn dark blue, for a), b), and c) hydrogen atoms have been omitted for clarity.

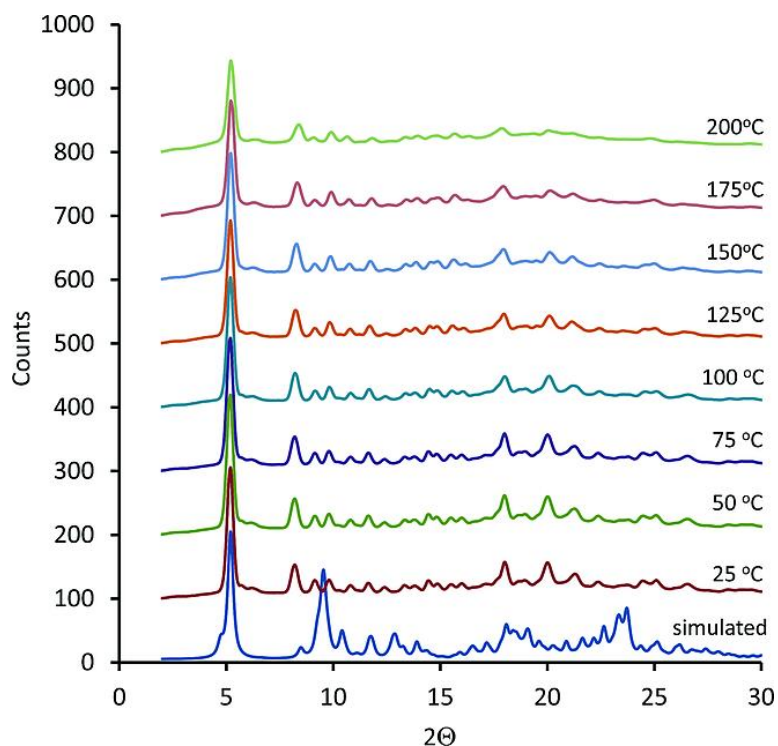


Fig 2.5 – VT-PXRD data for the MOF $\{[NH_2Me_2]_2[Zn_2(H_2O)_2(2.5)]\}$ (simulated pattern created using Diamond 4.0 software)^[20].

2.1.3 Conclusion

The hexadentate carboxylate linker **2.5** provides a truly unique coordination environment for constructing a MOF lattice. In particular, the interlocking of the two components (axle and wheel) provides a highly dynamic scaffold and guarantees that any lattices formed will be threaded. The MOF described herein is a simple example in which only single Zn^{II} ion SBUs are used. The threefold interpenetration of the lattices is a direct result of the interlocked nature of the rotaxane ligand design. This concept adds another level of complexity to the design of interpenetrated and polythreaded lattices and may find applications in the future design of MOF materials with dynamic and mechanical components and the control of bulk materials properties at the molecular level.

2.2. Experimental

2.2.1 General comments

2,1,3-Benzothiadiazole was purchased from TCI Chemicals, Co. 4-Ethoxycarbonylphenylboronic acid, triethylene glycol di(p-toluenesulfonate), and 3,5-dihydroxybenzoic acid were purchased from Sigma–Aldrich, Co., and were used as received. Compounds **2.1**,^[8c] **2.2**^[22] and **2.3**^[8c] (see Scheme 2.1) were prepared according to literature methods. Deuterated solvents were obtained from Cambridge Isotope Laboratories and were used as received. Solvents were dried by using an Innovative Technologies Solvent Purification System. ¹H NMR and ¹³C NMR solution experiments were performed with either a Bruker Avance 300 or 500 instrument at 298 K unless otherwise indicated. Chemical shifts are quoted in ppm relative to tetramethylsilane by using the residual solvent signal as a reference standard. PXRD were recorded with a Bruker D8 Discover diffractometer equipped with a GADDS 2D-detector and operated at 40 kV and 40 mA. Cu-K_α radiation ($\lambda = 1.54187 \text{ \AA}$) was used. Elemental compositions were determined with a Perkin–Elmer 2400 Series II Elemental Analyzer. Thermal gravimetric analyses were conducted with a Mettler Toledo TGA SDTA 851e instrument. Helium (99.99 %) was used to purge the system with a flow rate of 30 mL min⁻¹.

2.2.2 Synthesis of **2.4**

A mixture of **2.1** (100 mg, 0.184 mmol) and **2.2** (300 mg, 0.552 mmol) was stirred in CHCl₃ (30 mL) until a clear solution was obtained. Then, **2.3** (74.4 mg, 0.184 mmol) was added, which was followed by the addition of a small amount of ZrCl₄ (4.28 mg, 0.0184 mmol); this reaction needed to be conducted under an atmosphere of air to effect oxidation. After stirring at room temperature for 2 d, the catalyst was filtered off and the filtrate was concentrated under vacuum. The residue was dissolved in acetonitrile (15 mL) and filtered.

Et₃N (0.5 mL) was added, and after 5 min, a precipitate appeared, which was filtered, yield 82 mg, 30 %, m.p. >250 °C (dec.). ¹H NMR (500 MHz, CDCl₃): δ = 11.07 (s, 2 H), 8.27 (s, 4 H), 8.25 (d, *J* = 8.24 Hz, 4 H), 8.18 (m, 8 H), 7.87 (m, 4 H), 7.52 (d, *J* = 7.50 Hz, 2 H), 7.31 (d, *J* = 7.31 Hz, 2 H), 6.61 (d, *J* = 6.61 Hz, 4 H), 5.26 (t, *J* = 5.26 Hz, 2 H), 4.42 (m, 8 H), 3.74 (m, 8 H), 3.65 (m, 8 H), 3.52 (s, 8 H), 3.42 (s, 6 H), 1.46 (q, *J* = 1.46 Hz, 12 H) ppm. ¹³C NMR (125 MHz, CDCl₃): δ = 166.56, 166.03, 165.74, 158.08, 152.27, 143.19, 142.65, 142.08, 132.99, 130.49, 129.91, 129.52, 129.15, 129.04, 128.82, 128.72, 128.50, 128.01, 124.48, 123.12, 121.42, 106.38, 106.02, 70.10, 66.57, 66.17, 60.92, 60.51, 51.35, 14.08 ppm. C₈₄H₈₂N₄O₂₀ (1467.59): calcd. C 68.75, H 5.63, N 3.82; found C 68.04, H 4.49, N 3.63.

2.2.3 Synthesis of 2.5

1 M NaOH (10 mL) was added to a mixture of **2.4** (80 mg, 0.054 mmol) in THF (6 mL) and EtOH (10 mL). After the mixture was stirred at 80 °C for 20 h, the solvent was removed under reduced pressure. Deionized water (20 mL) was added to dissolve the residue. Then, HBF₄ (48 wt.-% in water) was added to give a pH value of about 6.5. The precipitate that was formed was collected by vacuum filtration and was air dried, yield 65 mg, 90 %, m.p. >250 °C (dec.). ¹H NMR (500 MHz, DMSO-d₆, HBF₄ was added to obtain well-resolved signals): δ = 13.51 (br., 6 H, NH, OH, HBF₄), 8.42 (s, 4 H), 8.20 (d, *J* = 8.20 Hz, 8 H), 8.02 (d, *J* = 8.02 Hz, 8 H), 7.54 (s, 4 H), 6.55 (s, 4 H), 5.60 (s, 2 H), 3.75 (s, 8 H), 3.60 (s, 16 H) ppm. ¹³C NMR (125 MHz, DMSO-d₆): δ = 167.72, 166.96, 158.77, 151.46, 141.78, 140.50, 132.10, 131.44, 130.59, 130.26, 129.78, 129.14, 108.39, 106.84, 105.62, 70.14, 69.48, 66.86 ppm. C₇₄H₆₂N₄O₂₀ (1327.30): calcd. C 66.96, H 4.71, N 4.22. Satisfactory elemental analysis could not be obtained owing to the limited solubility and hygroscopic nature of the compound. ¹H NMR spectroscopy and single-crystal X-ray diffraction studies are consistent with the

proposed formula and structure. Suitable single crystals were obtained by slow diffusion of methanol into a DMSO solution of **2.5** at room temperature.

2.2.4 Synthesis of MOF $[\text{NH}_2\text{Me}_2]_2[\text{Zn}_2(\text{H}_2\text{O})_2(\mathbf{2.5})]$

$\text{Zn}(\text{NO}_3)_2 \cdot 6\text{H}_2\text{O}$ (8.92 mg, 0.03 mmol) and ligand **2.5** (10 mg, 0.0075 mmol) were added to a solution of DMF/1,4-dioxane/ H_2O (1:1:1; 3 mL), to which HBF_4 diethyl ether complex (3 drops) was added. Upon sonication and heating, a clear solution was obtained, and the sample was placed in a programmable oven and heated at a constant rate of $1\text{ }^\circ\text{Cmin}^{-1}$ to $90\text{ }^\circ\text{C}$, kept at that temperature for 48 h, then placed under vacuum in an oven heated to $100\text{ }^\circ\text{C}$ for another 5 h. The pale yellow crystals were collected and washed with DMF, yield 7 mg, 58 % based on MIM ligand **2.5**. The bulk material was determined to be homogeneous by optical microscopy (see Fig 2.6). All attempts to obtain a satisfactory elemental analysis resulted in low C%. X-ray diffraction data collection, solution, and refinement details are given in Table 2.1.

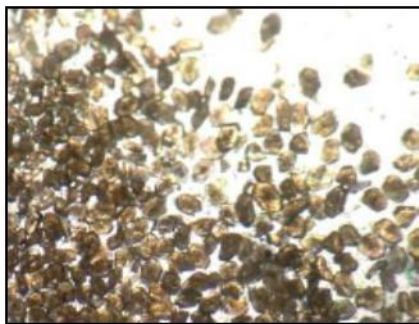


Fig 2.6 – image of crystals of MOF $\{[\text{NH}_2\text{Me}_2]_2[\text{Zn}_2(\text{H}_2\text{O})_2(\mathbf{2.5})](\text{H}_2\text{O})_{1.25}\}$.

2.2.5 Single-Crystal X-ray Diffraction Experiments

Crystals were frozen in paratone oil inside a cryoloop under a cold stream of N₂. Reflection data were collected on a Bruker APEX-II diffractometer using CuK_α radiation and a charge-coupled device (CCD) detector. For both data sets, decay was monitored using 50 standard data frames measured at the beginning and end of data collection. Diffraction data and unit-cell parameters were consistent with the assigned space groups. Lorentzian polarization corrections and empirical absorption corrections, based on redundant data at varying effective azimuthal angles, were applied to the data sets. The structures were solved by direct methods, completed by subsequent Fourier syntheses and refined using full-matrix least-squares methods against |F²| data. All non-hydrogen atoms were refined anisotropically and hydrogen atoms placed in idealized positions and refined using a riding model. Scattering factors and anomalous dispersion coefficients are contained in the SHELXTL program library.^[23] See Table 2.1 (full text) for a summary of the basic experimental details.

2.2.6 Single-crystal X-ray structure of Ligand, 2.5

Crystals of formula 2.5.(DMSO)₇ were of good quality. The asymmetric unit contained two half molecules of the hexa-acid ligand (C₇₄H₆₂N₄O₂₀) and seven molecules of DMSO. The structure was solved in the monoclinic space group *P*2₁/*c*. One of the DMSO molecules was modelled for disorder. Complete details of the structure model and refinement can be obtained from the Cambridge Crystallographic Data Centre at www.ccdc.cam.ac.uk for CCDC accession number 1458990. (CCDC) crystallographic information files for the full details.

2.2.7 Single-crystal X-ray structure of MOF, [NH₂Me₂]₂[Zn₂(H₂O)₂(2.5)]

Crystals of formula [NH₂Me₂]₂[Zn₂(H₂O)(2.5)].(H₂O)_{1.25} were of moderate quality. The asymmetric unit contained one hexa-carboxylate linker (C₇₄H₅₆N₄O₂₀), two zinc ions each with a coordinated water molecule, two [NH₂Me₂]⁺ cations and one and a quarter molecules of water. The structure was solved in the orthorhombic space group *Pbca*. A number of restraints were used to model significant disorder, including one of the Zn(II) ions and attached carboxylate groups. Complete details of the structure model and refinement can be obtained from the Cambridge Crystallographic Data Centre at www.ccdc.cam.ac.uk for CCDC accession number 1458989.

Table 2.1 – X-ray diffraction data collection, solution, and refinement details.

	2.5·(DMSO) ₇	{[NH ₂ Me ₂] ₂ [Zn ₂ (H ₂ O) ₂ (2.5)](H ₂ O) _{1.25} }
Chemical formula	C ₈₈ H ₁₀₄ N ₄ O ₂₇ S ₇	C ₇₈ H _{78.5} N ₆ O _{23.25} Zn ₂
<i>M</i> [g mol ⁻¹]	1874.17	1602.70
Crystal system	monoclinic	orthorhombic
Space group	<i>P2</i> ₁ / <i>c</i>	<i>Pbca</i>
<i>a</i> [Å]	15.1666(9)	37.270(8)
<i>b</i> [Å]	17.9508(11)	10.733(3)
<i>c</i> [Å]	33.565(2)	38.171(9)
<i>α</i> [°]	90	90
<i>β</i> [°]	91.437(2)	90
<i>γ</i> [°]	90	90
<i>V</i> [Å ³]	9135.3(10)	15269(6)
<i>Z</i>	4	8
<i>D</i> _{calcd.} [g cm ⁻³]	1.363	1.394
<i>μ</i> (Cu-K _α) [mm ⁻¹]	2.262	1.454

F(000)	3952	6676
Reflns. collected	121616	39314
Reflns. Independent	16050	8305
Reflns. [$I > 2\sigma(I)$]	14423	5208
R _{int}	0.042	0.066
Parameters refined	1153	1037
Restraints	21	1177
R1	0.0635	0.1515
wR2	0.2011	0.4206
Goodness-of-fit	1.035	1.512
$\Delta\rho$ [$e \text{ \AA}^{-3}$]	1.31	2.50

2.2.8 Decomposition and Analysis of MOF $\{[\text{NH}_2\text{Me}_2]_2[\text{Zn}_2(\text{H}_2\text{O})_2(\mathbf{2.5})]\}$ by ^1H NMR Spectroscopy

A small sample of the MOF (2 mg) was dispersed into 400 μL of DMF and 30 μL of D_2SO_4 (20% in D_2O), and sonicated for 5 min. Although the solution was dilute, there was clear evidence of resonances for both the rotaxane ligand **2.5** and NH_2Me_2 cations; see insert. This provides direct evidence for the presence for NH_2Me_2 cations in the material and justifies their inclusion in the single crystal X-ray structure solution and formulation.

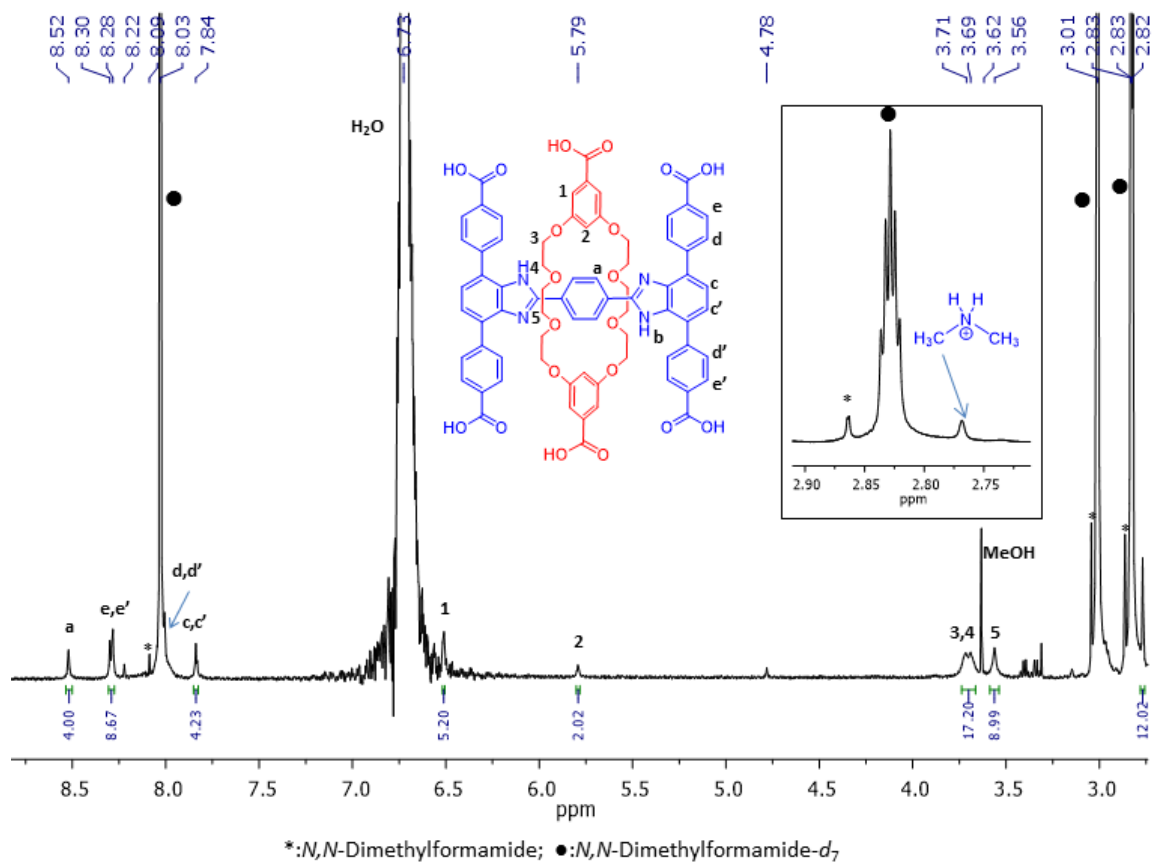


Fig 2.7 – ¹H NMR Spectrum of MOF {[NH₂Me₂]₂[Zn₂(H₂O)₂(**2.5**)](H₂O)₃} after dissolution.

2.3 References

1. a) J. F. Stoddart, *Chem. Soc. Rev.*, **2009**, *38*, 1802–1820; b) J. E. Beves, B. A. Blight, C. J. Campbell, D. A. Leigh, R. T. McBurney, *Angew. Chem. Int. Ed.*, **2011**, *50*, 9260–9327; *Angew. Chem.*, **2011**, *123*, 9428–9499; c) J. F. Stoddart, *Angew. Chem. Int. Ed.*, **2014**, *53*, 11102–11104; *Angew. Chem.*, **2014**, *126*, 11282–11284.
2. a) V. N. Vukotic, S. J. Loeb, *Chem. Soc. Rev.*, **2012**, *41*, 5896–5906; b) B. Zheng, F. Wang, S. Dong, F. Huang, *Chem. Soc. Rev.*, **2012**, *41*, 1621–1636; c) V. Fasano, M. Baroncini, M. Moffa, D. Iandolo, A. Camposeo, A. Credi, D. Pisignano, *J. Am. Chem. Soc.*, **2014**, *136*, 14245–14254; d) S. Erbas-Cakmak, D. A. Leigh, C. T. McTernan and A. L. Nussbaumer, *Chem. Rev.*, **2015**, *115*, 10081–10206.
3. a) A. Harada, R. Kobayashi, Y. Takashima, A. Hashidzume, H. Yamaguchi, *Nat. Chem.*, **2011**, *3*, 34–37; b) O. Lukin, F. Vogtle, *Angew. Chem. Int. Ed.*, **2005**, *44*, 1456–1477; *Angew. Chem.*, **2005**, *117*, 1480–1501; c) S. Li, B. Zheng, J. Chen, S. Dong, Z. Ma, F. Huang, H. W. Gibson, *J. Polym. Sci., Part A* **2010**, *48*, 4067–4073; d) S. Dong, Y. Luo, X. Yan, B. Zheng, X. Ding, Y. Yu, Z. Ma, Q. Zhao, F. Huang, *Angew. Chem. Int. Ed.*, **2011**, *50*, 1905–1909; *Angew. Chem.*, **2011**, *123*, 1945–1949; e) Y. Kohsaka, K. Nakazono, Y. Koyama, S. Asai, T. Takata, *Angew. Chem. Int. Ed.*, **2011**, *50*, 4872–4875; *Angew. Chem.*, **2011**, *123*, 4974–4977.
4. a) M. J. Frampton, H. L. Anderson, *Angew. Chem. Int. Ed.*, **2007**, *46*, 1028–1064; *Angew. Chem.*, **2007**, *119*, 1046–1083; b) J. Buey, T. M. Swager, *Angew. Chem. Int. Ed.*, **2000**, *39*, 608–612; *Angew. Chem.*, **2000**, *112*, 622–626; c) T. Akutagawa, H. Koshinaka, D. Sato, S. Takeda, S.-I. Noro, H. Takahashi, R. Kumai, Y. Tokura, T. Nakamura, *Nature Mater.*, **2009**, *8*, 342–347; d) M. Feng, L. Gao, Z. Deng, W. Ji, X. Guo, S. Du, D. Shi, D. Zhang, D. Zhu, H. Gao, *J. Am. Chem. Soc.*, **2007**, *129*, 2204–2205.

5. a) V. Bermudez, T. Gase, F. Kajzar, N. Capron, F. Zerbetto, F. G. Gatt, D. A. Leigh, S. Zhang, *Electro-Optics*, **2002**, *21*, 39–44; b) M. Horie, T. Sassa, D. Hashizume, Y. Suzuki, K. Osakada, T. Wada, *Angew. Chem. Int. Ed.*, **2007**, *46*, 4983–4986; *Angew. Chem.*, **2007**, *119*, 5071–5074; c) M. Horie, Y. Suzuki, D. Hashizume, T. Abe, T. Wu, T. Sassa, T. Hosokai, K. Osakada, *J. Am. Chem. Soc.*, **2012**, *134*, 17932–17944.
6. Q. Li, W. Zhang, O. S. Miljanic, C.-H. Sue, Y.-L. Zhao, L. Liu, C. B. Knobler, J. F. Stoddart, O. M. Yaghi, *Science*, **2009**, *325*, 855–859.
7. a) H. X. Deng, M. A. Olson, J. F. Stoddart, O. M. Yaghi, *Nat. Chem.*, **2010**, *2*, 439–447; b) A. Coskun, M. Banaszak, R. D. Astumian, J. F. Stoddart, B. A. Grzybowski, *Chem. Soc. Rev.*, **2012**, *41*, 19–35; c) B. M. Rambo, H. Gong, M. O'H, J. L. Sessler, *Acc. Chem. Res.*, **2012**, *45*, 1390–1401; d) P. R. McGonigal, P. Deria, I. Hod, P. Z. Moghadam, A.-J. Avestro, N. E. Horwitz, I. C. Gibbs-Hall, A. K. Blackburn, D. Chen, Y. Y. Botros, W. R. Wasielewski, R. Q. Snurr, J. T. Hupp, O. K. Farha, J. F. Stoddart, *Proc. Natl. Acad. Sci. USA*, **2015**, *112*, 11161–11168.
8. a) V. N. Vukotic, K. J. Harris, K. Zhu, R. W. Schurko, S. J. Loeb, *Nat. Chem.*, **2012**, *4*, 456–460; b) V. N. Vukotic, C. A. O'Keefe, K. Zhu, K. J. Harris, C. To, R. W. Schurko, S. J. Loeb, *J. Am. Chem. Soc.*, **2015**, *137*, 9643–9651; c) K. Zhu, V. N. Vukotic, C. A. O'Keefe, R. W. Schurko, S. J. Loeb, *Nat. Chem.*, **2015**, *7*, 514–519; d) K. Zhu, V. N. Vukotic, C. A. O'Keefe, R. W. Schurko, S. J. Loeb, *J. Am. Chem. Soc.*, **2014**, *136*, 7403–7409.
9. S. J. Loeb, *Chem. Commun.*, **2005**, 1511–1518.
10. a) K. Kim, *Chem. Soc. Rev.* **2002**, *31*, 96–107; b) G. J. E. Davidson, S. J. Loeb, *Angew. Chem. Int. Ed.*, **2003**, *42*, 74–77; *Angew. Chem.*, **2003**, *115*, 78–81; c) D. J. Hoffart, S. J.

- Loeb, *Angew. Chem. Int. Ed.*, **2005**, *44*, 901–904; *Angew. Chem.*, **2005**, *117*, 923–926;
- d) S. J. Loeb, *Chem. Soc. Rev.*, **2007**, *36*, 226–235.
11. a) L. K. Knight, V. N. Vukotic, E. Viljoen, C. B. Caputo, S. J. Loeb, *Chem. Commun.*, **2009**, 5585–5587; b) V. N. Vukotic, S. J. Loeb, *Chem. Eur. J.*, **2010**, *16*, 13630–13637; c) H.-Y. Gong, B. M. Rambo, W. Cho, V. M. Lynch, J. L. Sessler, *Chem. Commun.*, **2011**, *47*, 5973–5975; d) H. Gong, B. M. Rambo, E. Karnas, V. M. Lynch, J. L. Sessler, *Nat. Chem.*, **2010**, *2*, 406–409; e) K. Zhu, S. J. Loeb, *Top. Curr. Chem.*, **2014**, *354*, 213–251; f) H. Gong, B. M. Rambo, C. A. Nelson, V. M. Lynch, X. Zhu, J. L. Sessler, *Chem. Commun.*, **2012**, *48*, 10186–10188.
12. D. J. Mercer, V. N. Vukotic, S. J. Loeb, *Chem. Commun.*, **2011**, *47*, 896–898.
13. N. C. Frank, D. J. Mercer, S. J. Loeb, *Chem. Eur. J.*, **2013**, *19*, 14076–14080.
14. For a review on interpenetration including the interpretation of lattices referred to as catenation, in which two frameworks weave through each other in a mechanical fashion (but does not occur in this structure), see: S. R. Batten, R. Robson, *Angew. Chem. Int. Ed.*, **1998**, *37*, 1460–1494; *Angew. Chem.*, **1998**, *110*, 1558–1595.
15. For a review on the concept of polythreading, see: L. Carlucci, G. Ciani, D. M. Proserpio, *Coord. Chem. Rev.*, **2003**, *246*, 247–289.
16. K. Zhu, V. N. Vukotic, S. J. Loeb, *Angew. Chem. Int. Ed.*, **2012**, *51*, 2168–2172; *Angew. Chem.*, **2012**, *124*, 2210–2214.
17. K. Zhu, V. N. Vukotic, N. Noujeim, S. J. Loeb, *Chem. Sci.*, **2012**, *3*, 3265–3271.
18. For examples of the decomposition of DMF to produce Me_2NH_2^+ , see: a) S. Yang, G. S. B. Martin, J. J. Titman, A. J. Blake, D. R. Allan, N. R. Champness, M. Schroder, *Inorg. Chem.*,

- 2011**, *50*, 9374–9384; b) Z. Lin, Y. Huang, T. Liu, X. Li, R. Cao, *Inorg. Chem.*, **2013**, *52*, 3127–3132.
19. A. L. Spek, *Acta Crystallogr., Sect. D*, **2009**, *65*, 148.
 20. *Diamond*, v. 4.0, Crystal Impact, Bonn, Germany, **2015**.
 21. *Images generated by using CrystalMaker, CrystalMaker Software, Ltd., Oxford, UK, England, UK (www.crystallmaker.com)*.
 22. Z. Xu, X. Huang, J. Liang, S. Zhang, S. Zhou, M. Chen, M. Tang, L. Jiang, *Eur. J. Org. Chem.*, **2010**, 1904–1911.
 23. G. M. Sheldrick, *Acta Cryst.* **2008**, *A64*, 112-115.

CHAPTER 3

3.1 Metal–Organic Frameworks Utilising an Interlocked, Hexadentate Linker Containing a Tetra-carboxylate Axle and a Bis(pyridine) Wheel

3.1.1 Introduction

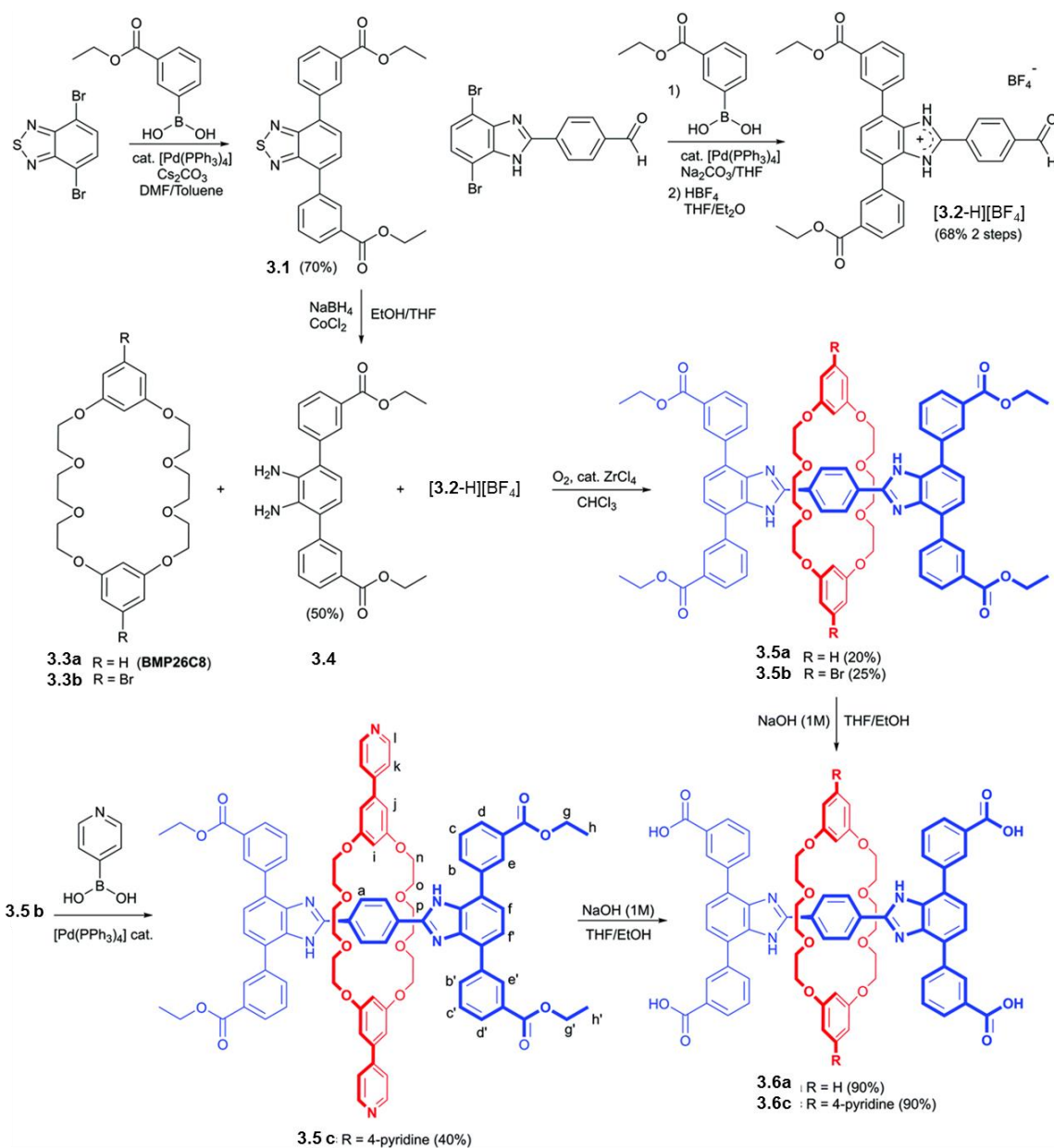
The incorporation of mechanically interlocked molecules^[1-3] (rotaxanes, catenanes, and knots) into polymeric materials^[4-6] is of interest since these unique molecular connections might have interesting structural effects on the mechanical^[7-11] (rheology, elasticity), electronic^[12-15] (ferroelectric, piezoelectric), optical^[16-18] (nonlinear optics), or host–guest^[19] (absorption, storage) properties of the resulting materials. Recently, mechanically interlocked molecules (MIMs) have been incorporated into crystalline metal organic framework (MOF) materials. This provides a way to precisely organize MIM-based molecular switches and potentially molecular machines in the solid state.^[20-23] To this end, MOFs have been prepared with rotaxane linkers that show large amplitude rotational and translational motion (shuttling).^[24-27] These so-called metal organic rotaxane frameworks (MORFs),^[28] were first prepared utilising simple linkers with donor atoms on the ends of a linear axle that was threaded through a macrocyclic wheel such as a crown ether or a cucurbituril.^[29-32] This led to elegant 1-, 2- and 3-dimensional periodic structures containing [2]rotaxane axles as linkers between metal nodes with macrocyclic wheels threaded onto the rigid skeletal backbone of the coordination polymer.^[33-38] We were subsequently interested in the possibility of creating [2]rotaxane linkers with donor atoms on both the axle and the wheel.^[39,40] This is an interesting concept, since it might be possible for the axle and wheel to form independent polymeric networks that would be interpenetrated only

because the ligand core was mechanically interlocked – i.e. a MIM node. Herein, we describe the solid-state structures of MOFs derived from a rotaxane linker that contains four carboxylic acid donors on the axle and two pyridine donors on the wheel. This design was inspired by the well-known Zn(II) and Cu(II) MOFs which have 2D layers supported by carboxylate ligands pillared in the 3rd dimension by a bipyridine ligand.^[41-51] In our case, the two types of ligands (layering and pillaring) are now interlocked and therefore part of the same linker.

3.1.2 Results and Discussion

Two mechanically interlocked (MIM) linkers were constructed using the same H-shaped tetracarboxylic acid axle. One of the linkers contains a bis(meta-phenylene)[24]crown-8 (**BMP26C8**) wheel (**3.6a** R = H) with no donors, while the other contains the same macrocycle substituted with 4-pyridyl donors on the meta-phenylene rings (**3.6c** R = 4-pyridine). The preparations were based on a previously successful molecular design for [2] rotaxanes that combines rigid triphenylene struts, benzimidazolium recognition sites and a single macrocyclic wheel in the form of a crown ether.^[52,53] Scheme 3.1 describes the preparation of tetra ester [2]rotaxanes **3.5a** (R = H) and **3.5b** (R = Br) by condensing preformed [2]pseudorotaxanes [**3.2-H**⊂**3.3a**]⁺ and [**3.2-H**⊂**3.3b**]⁺, which contain a terminal aldehyde group, with diamine **3.4**. **3.5b** can then be converted to **3.5c** (R = 4-pyridine) by Suzuki coupling with 4-pyridyl boronic acid and the resulting ester groups hydrolysed to yield the tetra acid linkers **3.6a** and **3.6c**. The ¹H NMR spectra of tetra ester [2]rotaxanes **3.5a** and **3.5c** are shown in Fig 3.1 a and 3.1 b respectively. Although similar data were obtained for the tetra acids, **3.6a** and **3.6c**, the much lower solubility of these compounds limits the utility of their ¹H and ¹³C NMR spectra for full ¹H peak assignments (see the experimental 3.2.8 and 3.2.11). The ¹H NMR spectra of

3.5a and **3.5c** clearly exhibit separate sets of signals for the axle and wheel components; assignments were made with the aid of 2D NOESY and HMBC experiments.



*Scheme 3.1 – synthesis of mechanically interlocked [2]rotaxane linkers **3.6a** (R = H) and **3.6c** (R = 4 pyridine) from [2]pseudorotaxane precursors using a threading followed by a stoppering methodology, ¹H NMR resonances are labelled according to the numbering shown for **3.5c**.*

In the neutral forms of these [2]rotaxanes, there is very little interaction between the axle and wheel and only weak NH...O interactions between crown ether oxygen atoms and benzimidazole NH groups were detected. This means the macrocycle is free to move rapidly (relative to the NMR timescale) between the two recognition sites which results in simplified, symmetrical spectra. Therefore, although the axle is fairly rigid and the macrocycle permanently interlocked on to the axle, there are a wide variety of possible orientations for the donor groups (four carboxylates for **3.6a**, four carboxylates and two pyridines for **3.6c**) due to the large amplitude, rotational and translation degrees of freedom available to the two interlocked components. Single crystals of **3.6a** (DMF)₂ were grown from a DMF/1,4-dioxane/H₂O (1 : 1 : 1) solution. Fig 3.2a shows the X-ray structure which has a crystallographically imposed center of symmetry. The central phenyl ring and the two benzimidazole groups of the axle are in approximately the same plane while the macrocycle is positioned over the central phenyl and bridges the benzimidazole groups forming two NH...O hydrogen bonds (N...O, 2.99 Å; N-H...O 172°). Although structures for similar H-shaped rotaxanes reveal that a macrocyclic wheel such as dibenzo[24]crown-8 (**DB24C8**) prefers to occupy one end of the axle and interact with only a single benzimidazole recognition site,^[52,53] there is precedence for larger macrocycles such as **BMP26C8** or dibenzo[30]crown-10 (**DB30C10**) to interact simultaneously with both NH groups in this fashion.^[54] Interestingly, the internal H-atoms of the meta-substituted rings of **BMP26C8** are oriented towards the centre of the central phenyl ring of the axle to generate T-shaped CH-π interactions (C...centroid, 3.69 Å, C-H...centroid 169°) which may also contribute to the relative orientation of the macrocycle with respect to the axle.

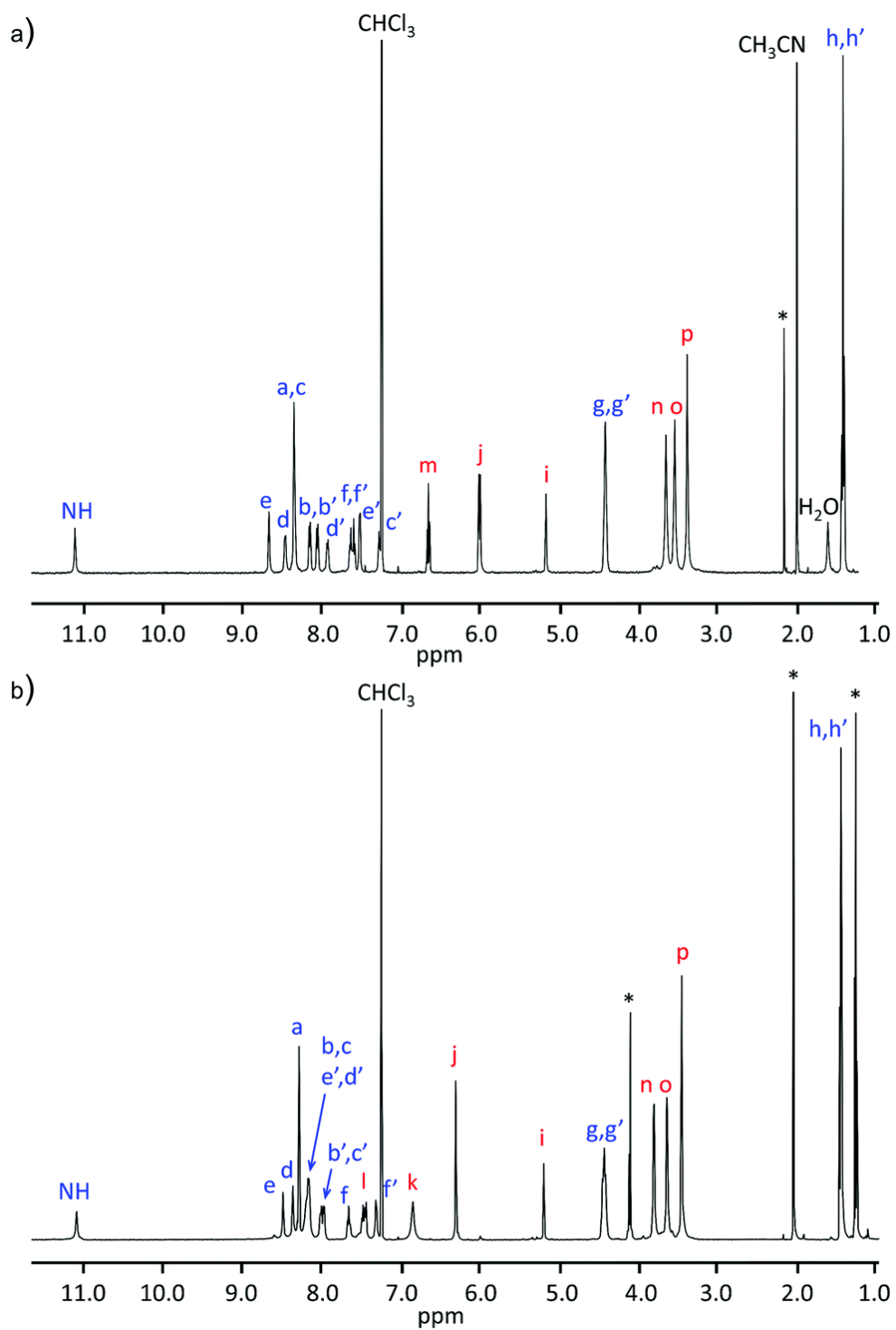


Fig 3.1 – ^1H NMR spectra, (a) tetra ester **3.5a** ($R = \text{H}$), * = acetone and (b) tetra ester **3.5c** ($R = 4\text{-pyridine}$), * = EtOAc. Resonance assignments correspond to the labelling shown in Scheme 3.1 (note: $m = \text{para-H}$ for **3.5a**).

Importantly, the formation of a 1D ribbon via hydrogen-bonding of the four carboxylic acid groups (Fig 3.2b) shows that these acid groups are well separated and could therefore potentially act as independent donors to a metal centred SBU upon deprotonation – i.e. result in the formation of a MOF.

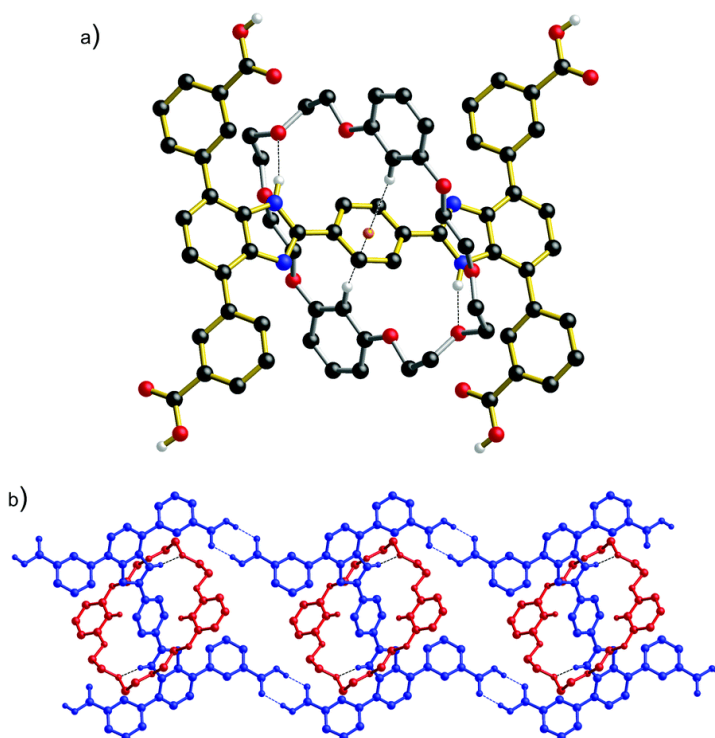


Fig 3.2 – ball-and-stick representations of 3.6a (DMF)₂, (a) the [2]rotaxane linker depicting the relative orientation and intramolecular interactions between the axle and the wheel, colour key: C = black, N = blue, O = red; H = white; centroid = orange; axle = gold bonds, wheel = silver bonds; H-bonds = dotted lines, (b) three molecules making up a portion of a 1D ribbon formed by hydrogen-bonding of the four axle COOH groups, colour key: axles = blue, wheels = red, DMF molecules and H-atoms not involved in H-bonding have been omitted for clarity.

Initially, MOF formation was attempted with **3.6a**. Since this linker contains only four terminal carboxylate groups on the axle, it could be used to determine what type of

framework might be generated when there were no donors on the macrocycle. The reaction of **3.6a** with zinc(II) nitrate in a mixture of DEF/EtOH/H₂O (4 : 2 : 1) at 85 °C for 48 h produced a solid material in the form of yellow crystals; yield 78%. The material (MOF Zn-**3.6a**) was analyzed by single-crystal X-ray diffraction and found to have the formula $\{[\text{Zn}_2(\text{H}_2\text{O})_2(\mathbf{3.6a})](\text{DEF})_2(\text{H}_2\text{O})_2\}$. Fig 3.3a shows the repeating unit of the material in which all of the carboxylate ligands of **3.6a** are coordinated to independent SBUs consisting of pairs of Zn(II) ions. Fig 3.3b shows the details of a single SBU coordination environment. Each of the crystallographically related Zn(II) ions adopts a tetrahedral geometry coordinating to three carboxylate O-atoms (two charged, one neutral) and one water O-atom. Fig 3.3c shows how the coordination of **3.6a** to this SBU propagates into a 2D sheet (blue) that is decorated with **BMP26C8** macrocycles (red). The orientation of the macrocycle with respect to the axle is essentially the same as that found in the structure of the ligand (N...O, 3.17 Å; N-H...O 171°, C...centroid, 3.69 Å, C-H...centroid 164°). This is presumably because the interactions remain unperturbed by coordination of the axle carboxylate groups to Zn(II) ions and the formation of MOF Zn-**3.6a**. Unfortunately, no crystalline material could be isolated from similar reactions involving Cu(II) ions. A mixture of the hexadentate linker **3.6c** and zinc(II) nitrate in DEF/EtOH/H₂O (4 : 2 : 1) was maintained at 85 °C for 48 h. The resulting yellow crystalline solid (yield 77%) was analyzed by single-crystal X-ray diffraction and found to have the formula $\{[\text{Zn}_2(\mathbf{3.6c})](\text{DEF})_2\}$ (MOF Zn-**3.6c**). Fig 3.4a shows the repeating unit in which all of the carboxylate ligands of **3.6c** are coordinated to an SBU consisting of a pair of Zn(II) ions similar to that observed for MOF Zn-**3.6a**. Fig 3.4b shows the details of the coordination environment about the Zn(II) ions.

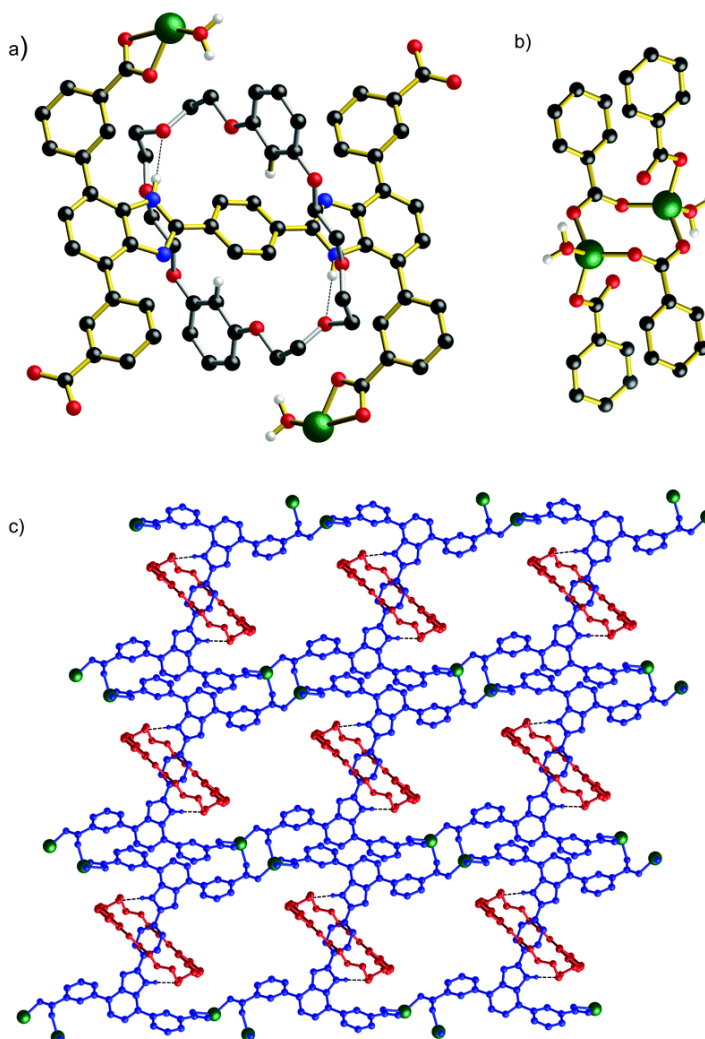


Fig 3.3 – ball-and-stick representations of MOF Zn-3.6a, (a) the interlocked core of the MOF showing bonds to Zn(II), (b) the SBU coordination sphere, colour key: C = black, N = blue, O = red, Zn = teal; axle = gold bonds, wheel = silver bonds, (c) a 2D sheet of interlocked ligands linked by Zn(II) ions, colour key: axles = blue, wheels = red; Zn = teal, solvent and hydrogen atoms not involved in H-bonds have been omitted for clarity.

Each metal ion adopts a tetrahedral geometry coordinating to three carboxylate O-atoms (two charged, one neutral) and one pyridine N-atom. Thus, the major difference between the SBU coordination environment for MOFs Zn-3.6a and Zn-3.6c is that the pyridine groups of linker 3.6c replace the coordinated water molecules found in Zn-3.6a. However,

unlike the monodentate water molecules in MOFs Zn-**3.6a**, the pyridine donors in MOF Zn-**3.6c** are part of the macrocyclic wheel, which is mechanically linked to the tetra carboxylate axle. This results in a polythreaded, 2D network due to the interlocked nature of the linker. This is illustrated in Fig 3.4c which shows a single 2D sheet constructed with interlocked axles (blue) and macrocyclic wheels (red), both of which contribute to the propagation. A mixture of **3.6c** and copper(II) nitrate in DEF/EtOH/H₂O (2: 1: 1) plus 3 drops of 5% HNO₃(aq) was maintained at 85 °C for 48 h. The isolated blue crystalline solid (yield 35%) was analyzed by single-crystal X-ray diffraction and found to have the formula {[Cu(**3.6c**)](H₂O)₂(DEF)_{1.5}}. Fig 3.5a shows the repeating unit of the material designated MOF Cu-**3.6c**. The major difference between this Cu(II) MOF and the previously described Zn(II) MOFs is that the metal : linker ratio is only 1 : 1 for Cu-**3.6c** whereas it is 2 : 1 for Zn-**3.6a** and Zn-**3.6c**. As a result, only two of the carboxylate groups of linker **3.6c** are deprotonated and the single Cu(II) ions adopt a square planar geometry bonding to two carboxylate O-atoms (both charged) and the two pyridine N-atoms, each pair having a trans disposition; see Fig 3.5b. As shown in Fig 3.5c, this result in the propagation of two independent lattices—orange axles linked to red wheels and blue axles linked to green wheels—which are then threaded, blue⊂red and orange⊂green. This unique topology is only possible because linker **3.6c** contains both pairs of donors (carboxylates and pyridines) on different components of an interlocked [2]rotaxane linker and clearly demonstrates the novelty of utilising mechanically bonded systems in coordination polymers.

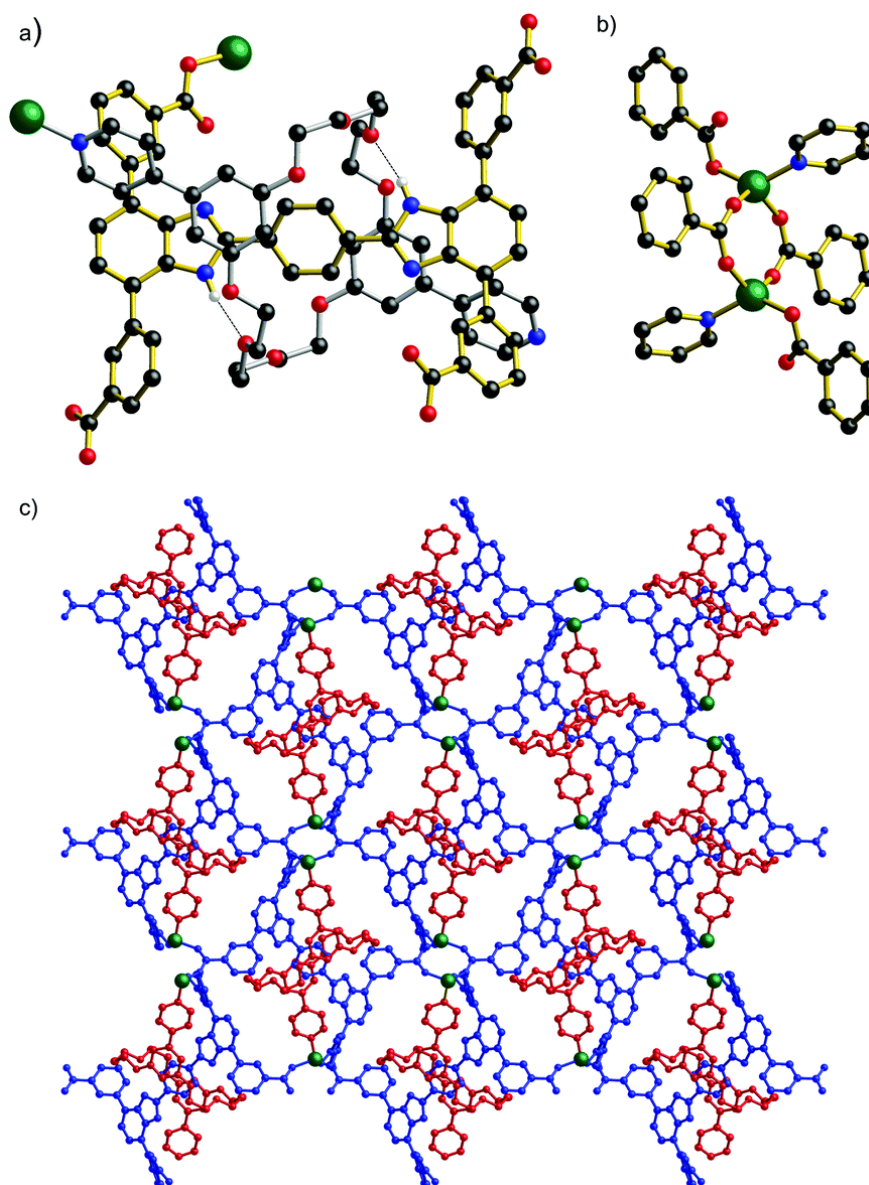


Fig 3.4 – ball-and-stick representations of MOF Zn-3.6c, (a) the interlocked core of the MOF showing bonds to Zn(II), (b) the SBU coordination sphere, colour key: C = black, N = blue, O = red, Zn = teal; axle = gold bonds, wheel = silver bonds, (c) the 2D sheet of interlocked ligands linked by Zn(II) ions, colour key: axles = blue, wheels = red; Zn = teal, solvent and hydrogen atoms not involved in H-bonds have been omitted for clarity.

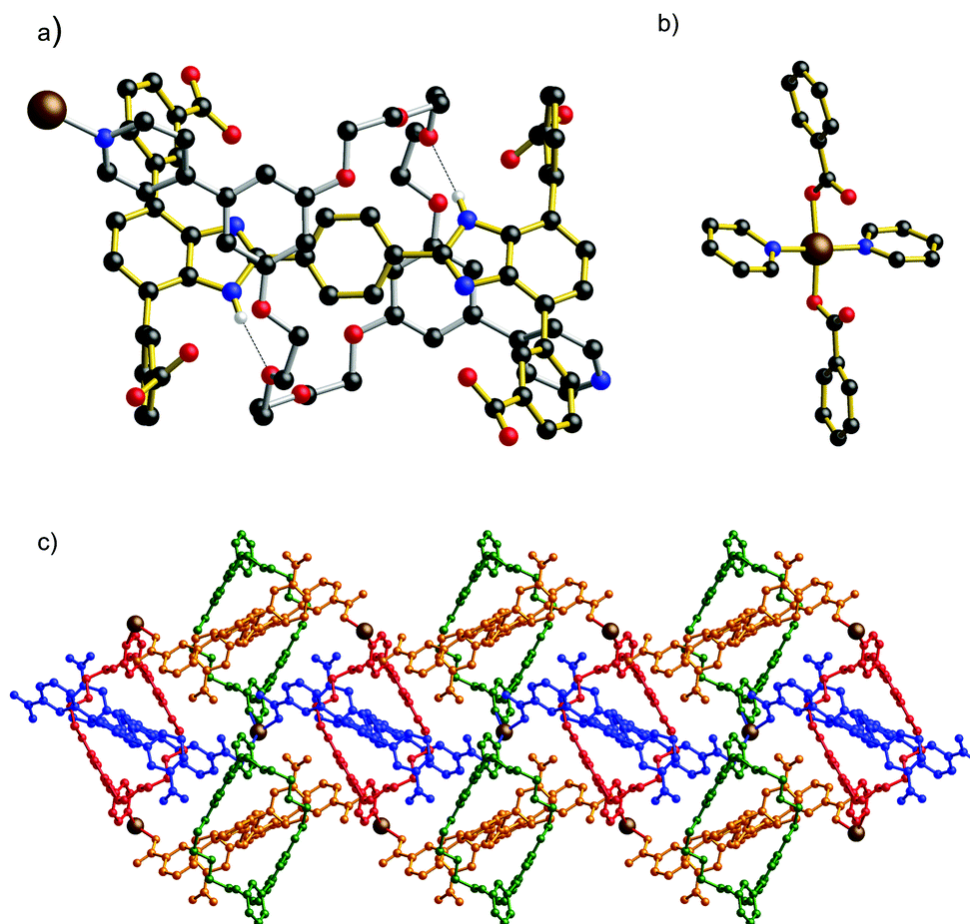


Fig 3.5 – ball-and-stick representations of MOF Cu-3.6c, (a) the interlocked core of the MOF showing bonds to Cu(II), (b) the coordination sphere of the Cu(II) ions, colour key: C = black, N = blue, O = red, Cu = brown; axle = gold bonds, wheel = silver bonds, (c) two sets of independent 3D lattices (orange axles linked to red wheels and blue axles linked to green wheels) that are interpenetrated (blue \subset red and orange \subset green) solely by virtue of the interlocked nature of the linker, Solvent and hydrogen atoms not involved in H-bonds have been omitted for clarity.

3.1.3 Conclusion

The design of linker **3.6c** was inspired by the structures of Cu(II) and Zn(II) MOFs that contain 2D layers of carboxylate linkers pillared by bipyridine ligands.^[41-51] By incorporating these two types of donors (carboxylates and pyridines) into separate but

interlocked components of a rotaxane, it has been demonstrated herein that two normally independent lattices can be threaded together by interlocking of the linker components. This is a significant step towards our ultimate goal of creating a material with a network of independent lattices controlled by the switching of an interlocked linker.

3.2. Experimental

3.2.1 General comments

Precursors 1-bromo-3,5-dihydroxybenzene,^[55] 3,6-di-bromobenzene-1,2-diamine,^[56] 4-(4,7-dibromo-1H-benzo[d]imidazol-2-yl)benzaldehyde^[57] and **BMP26C8** (ref. 54) were synthesized according to published literature procedures. Triethyleneglycoldi(p-tosylate) was purchased from Sigma-Aldrich Chemicals and used as received. Deuterated solvents were obtained from Cambridge Isotope Laboratories and used as received. ¹H and ¹³C spectra were recorded on Bruker Avance 300 or 500 instruments. All peak positions are listed in ppm relative to TMS. Melting point measurements were performed on MPA100 melting point apparatus. Column chromatography was performed using Silicycle Ultra-Pure silica gel (230–400 mesh).

3.2.2 Synthesis of 3.1

4,7-Dibromo-2,3-benzothiadiazole (2.26 g, 7.7 mmol), 3-ethoxycarbonylphenyl boronic acid (3 g, 15.4 mmol), Pd(PPh₃)₄ (800 mg, 0.69 mmol), and Cs₂CO₃ (7.52 g, 23.1 mmol) were added to a 100 mL Schlenk flask, degassed and backfilled with N₂. DMF (25 mL) and toluene (25 mL) were added and the solution was refluxed (110 °C) for 24 h. The solution was cooled to room temperature, CHCl₃ was added and filtered. Solvents were evaporated, and the residue was extracted with DCM/1 M HCl (3×) followed by DCM/brine.

The organic solution was dried over anhydrous MgSO_4 and evaporated. The resulting solids were filtered, air dried and recrystallized from ethanol producing a yellow solid; yield 2.3 g (70%). Mp: 120–122 °C. ^1H NMR (500 MHz, CDCl_3 , 298 K): δ = 1.40 (t, 6H, J = 7.1 Hz), 4.40 (q, 4H, J = 7.1 Hz), 7.61 (t, 2H, J = 7.7 Hz), 7.82 (s, 1H), 8.13 (d, 2H, J = 7.8), 8.19 (d, 2H, J = 7.7 Hz), 8.60 (s, 2H). ^{13}C NMR (126 MHz, CDCl_3): δ = 166.71, 154.16, 137.77, 133.92, 133.04, 131.28, 130.49, 129.73, 128.96, 128.58, 61.46, 14.64. HR-MS (ESI): calc'd for $[\text{M} + \text{H}]^+$, $[\text{C}_{24}\text{H}_{21}\text{O}_4\text{S}]^+$, m/z = 433.1217, found m/z = 433.1222.

3.2.3 Synthesis of 3.2

4-(4,7-dibromo-1H-benzo[d]imidazol-2-yl)- benzaldehyde (1.5 g, 3.94 mmol), 3-ethoxycarbonylphenyl boronic acid (1.51 g, 7.78 mmol) and $\text{Pd}(\text{PPh}_3)_4$ (350 mg, 0.3 mmol) were added to a 500 mL Schlenk flask which was degassed and backfilled with N_2 . 2 M Na_2CO_3 (200 mL) and THF (160 mL) were added, and the mixture was refluxed (80 °C) for 24 h. The solution was cooled to room temperature and the organic phase was separated and extracted with EtOAc/brine. The organic phase was dried over anhydrous MgSO_4 and evaporated. The resulting solids were filtered, air dried and recrystallized from CH_3CN producing a pale-yellow solid; yield 1.65 g (80%). Mp: 104–108 °C. ^1H NMR (500 MHz, CD_2Cl_2 , 298 K): δ = 1.44 (m, 6H), 4.41 (m, 4H), 7.48 (d, 1H, J = 7.6 Hz), 7.64 (m, 3H), 7.92 (d, 1H, J = 7.5 Hz), 8.01 (d, 2H, J = 8.2 Hz), 8.09 (d, 1H, J = 7.7 Hz), 8.15 (d, 1H, J = 7.8 Hz), 8.31 (d, 2H, J = 8.1 Hz), 8.38 (s, 1H), 8.43 (d, 1H, J = 7.8 Hz), 8.88 (s, 21H), 10.09 (s, 1H), 10.14 (br s, 1H). ^{13}C NMR (126 MHz, CD_2Cl_2): δ = 191.78, 167.02, 166.57, 142.73, 138.82, 138.63, 137.64, 135.31, 133.91, 133.76, 132.64, 132.14, 131.19, 131.17, 130.67, 130.45, 129.90, 129.29, 129.24, 128.81, 128.79, 127.54, 125.01, 124.43, 122.81, 61.72, 61.44, 14.50. HR-MS (ESI): calc'd for $[\text{M} + \text{H}]^+$, $[\text{C}_{32}\text{H}_{27}\text{N}_2\text{O}_5]^+$, m/z = 519.1914, found m/z = 519.1920.

3.2.4 Synthesis of [3.2-H][BF₄]

3.2 (1.38 g, 2.6 mmol) was dissolved in THF (40 mL). The tetrafluoroboric acid diethyl ether complex (750 μ L, 5.51 mmol) was added dropwise. After 30 min, the resulting white solid was filtered, washed with ether and air dried; yield 1.2 g, (85%). Mp: 260–265 °C. ¹H NMR (500 MHz, CD₃CN, 298 K): δ = 1.38 (t, 6H, *J* = 7.1 Hz), 4.38 (q, 4H, *J* = 7.1 Hz), 7.76 (m, 4H), 7.95 (d, 2H, *J* = 7.6 Hz), 8.17 (s, 4H), 8.19 (d, 2H, *J* = 7.1 Hz), 8.32 (s, 2H), 10.13 (s, 1H), 12.50 (br s, 2H). ¹³C NMR (126 MHz, CD₃CN): δ = 193.06, 167.03, 151.64, 140.81, 136.84, 134.54, 132.89, 131.46, 131.12, 131.01, 130.88, 130.80, 128.75, 128.66, 127.78, 62.35, 14.73. HR-MS (ESI): calc'd for [M - BF₄]⁺, [C₃₂H₂₇N₂O₅]⁺, *m/z* = 519.1914; found *m/z* = 519.1926.

3.2.5 Synthesis of 3.3b

A 2 L Schlenk flask was filled with CH₃CN (1000 mL) and K₂CO₃ (21.6 g, 156.65 mmol), degassed and backfilled with N₂. 1-Bromo-3,5-dihydroxybenzene (7.85 g, 31.33 mmol) and triethyleneglycol-di(*p*-tosylate) (14.36 g, 31.33 mmol) were added in portions over 4 days under reflux. The solution was cooled to room temperature, filtered and washed with CHCl₃. The organic solvents were evaporated and the solids were extracted with brine and CHCl₃. After removing the organic solvent, the solids were recrystallized from CH₃CN producing a white solid; yield 2.1 g (11%). Mp: 124–127 °C. ¹H NMR (500 MHz, CDCl₃): δ = 3.70 (s, 8H) 3.70, 3.80 (m, 8H), 4.02 (m, 8H), 6.39 (t, 2H, *J* = 2.2), 6.64 (d, 4H, *J* = 2.2). ¹³C NMR (126 MHz, CDCl₃): δ = 98.10, 88.64, 85.59, 83.19, 75.62, 75.26, 74.79. Elemental analysis (%): calc'd for C₂₄H₃₀Br₂O₈: C, 47.54; H, 4.99. found: C, 47.20; H, 4.58.

3.2.6 Synthesis of 3.4

(2 g, 4.6 mmol) was dissolved in THF/EtOH (1 : 3) (160 mL). NaBH₄ (690 mg, 18.4 mmol) was added in portions. After addition, CoCl₂·6H₂O (50 mg, 0.21 mmol) was added. The resulting black mixture was refluxed for 4 h, cooled to room temperature and then filtered. The filtrate was concentrated and extracted with brine and DCM. The combined organic phase was dried over anhydrous Na₂SO₄. The solvents were evaporated and the solids were recrystallized from methanol. Yield: 940 mg (50%). Mp: 135–140 °C. ¹H NMR (500 MHz, CDCl₃, 298 K): δ = 1.38 (t, 6H, *J* = 7.1 Hz), 3.58 (br, s, 4H), 4.37 (q, 4H, *J* = 7.1 Hz), 6.79 (s, 2H), 7.53 (t, 2H, *J* = 7.7 Hz), 7.66 (m, 2H), 8.05 (m, 2H), 8.17 (s, 2H). ¹³C NMR (126 MHz, CDCl₃): δ = 166.76, 140.10, 133.87, 132.60, 131.50, 130.56, 129.27, 128.79, 128.05, 121.27, 61.43, 14.65. HR-MS (ESI): calc'd for [M + H]⁺, [C₂₄H₂₅N₂O₄]⁺, *m/z* = 405.1809; found *m/z* = 405.1814.

3.2.7 Synthesis of 3.5a

[3.2-H][BF₄] (300 mg, 0.55 mmol) and BMP26C8 (970 mg or 2.21 mmol) were stirred in CHCl₃ (30 mL) until a clear solution was obtained. 3.4 (223 mg, 0.55 mmol) was then added, followed by ZrCl₄ (1.28 mg, 0.005 mmol). The mixture was stirred at room temperature for 12 h, filtered and the filtrate was concentrated under vacuum. The solid was dissolved in CH₃CN (20 mL) and filtered. Et₃N (0.15 mL) was added to the filtrate. The resulting pale-yellow solid was filtered, recrystallized from CH₃CN, and air dried. Yield 148 mg (20%). Mp: 165–170 °C. ¹H NMR (500 MHz, CDCl₃, 298 K): δ = 1.41 (t, 12H, *J* = 7.1 Hz), 3.39 (s, 8H), 3.55 (s, 8H), 3.66 (s, 8H), 4.42 (m, 8H), 5.17 (s, 2H), 6.00 (d, 4H, *J* = 8.2 Hz), 6.65 (d, 2H, *J* = 8.2 Hz), 7.27 (d, 2H, *J* = 7.2 Hz), 7.52 (d, 2H, *J* = 7.5 Hz), 7.61 (m, 4H), 7.93 (d, 2H, *J* = 6.9 Hz), 8.06 (d, 2H, *J* = 7.7 Hz), 8.15 (d, 2H, *J* = 7.5 Hz), 8.35 (s, 6H), 8.46 (d, 2H, *J* = 7.1 Hz), 8.68 (s, 2H), 11.13 (s, 2H). ¹³C NMR (126 MHz, CDCl₃): δ = 167.08, 166.64, 158.96, 152.99,

142.52, 139.63, 139.06, 134.61, 133.85, 131.19, 130.77, 130.34, 130.06, 129.04, 128.73, 128.48, 123.67, 121.66, 116.44, 106.00, 101.66, 70.46, 70.07, 66.19, 61.43, 60.97, 14.49. HR-MS (ESI): calc'd for $[M + H]^+$, $[C_{80}H_{79}N_4O_{16}]^+$, $m/z = 1351.5486$, found $m/z = 1351.5491$.

3.2.8 Synthesis of 3.6a

To **3.5a** (120 mg, 0.088 mmol) in THF (15 mL) and ethanol (25 mL) was added 1 M NaOH (15 mL). After the reaction mixture was stirred at 80 °C for 24 h, the solvent was removed on a rotary evaporator. Deionized water (15 mL) was added to dissolve the residue. The solution was acidified with 2 M HCl to give a pH value of approx. 5. The resulting precipitate was collected by vacuum filtration and air dried; yield 98 mg (90%). $M_p > 300$ °C. 1H NMR (500 MHz, DMSO- d_6 , 298 K): $\delta = 3.52$ (s, 8H), 3.57 (s, 8H), 3.73 (s, 8H), 5.51 (s, 8H), 6.06 (d, 4H, $J = 6.2$ Hz), 6.66 (t, 2H, $J = 8.05$ Hz), 7.30 (d, 2H, $J = 7.7$ Hz), 7.51 (d, 2H, $J = 7.65$ Hz), 7.67 (t, 2H, $J = 7.7$ Hz), 7.74 (t, 2H, $J = 7.7$ Hz), 7.99 (d, 3H, $J = 8.1$ Hz), 8.07 (d, 2H, $J = 7.5$ Hz), 8.24 (s, 2H), 8.39 (s, 3H), 8.52 (d, 2H, $J = 7.7$ Hz), 8.56 (s, 2H), 12.02 (s, 2H), 13.12 (br s, 4H). ^{13}C NMR (126 MHz, DMSO- d_6): $\delta = 167.45$, 167.26, 158.63, 152.34, 141.79, 138.36, 138.20, 133.83, 133.24, 133.13, 130.93, 130.58, 129.34, 129.01, 128.73, 128.43, 128.31, 127.81, 124.61, 123.34, 121.07, 105.64, 100.61, 69.70, 68.81, 65.85, 39.97, 39.88, 39.81, 39.72, 39.64, 39.55, 39.38, 39.21, 39.05, 38.88. HR-MS (ESI): calc'd for $[M + H]^+$, $[C_{72}H_{63}N_4O_{16}]^+$, $m/z = 1239.4239$, found $m/z = 1239.4226$.

3.2.9 Synthesis of 3.5b

[3.2-H][BF₄] (700 mg, 1.29 mmol) and crown ether **3.3b** (1.56 g or 2.58 mmol) were stirred in CHCl₃ (40 mL) until a clear solution was obtained. **3.4** (520 mg, 1.29 mmol) was added followed by ZrCl₄ (4 mg, 0.017 mmol). The mixture was stirred at room temperature for 12 h, filtered and the filtrate was concentrated under vacuum. The solid was dissolved in CH₃CN (30 mL) and filtered. Et₃N (0.2 mL) was added to the filtrate. The white solid was

filtered, washed with hot CH₃CN, and air dried. Yield 460 mg (25%). Mp: 117–121 °C. ¹H NMR (500 MHz, DMSO-d₆, 298 K): δ = 1.38 (m, 12H), 3.52 (s, 8H), 3.56 (s, 8H), 3.73 (s, 8H), 4.40 (m, 8H), 5.44 (s, 2H), 6.19 (s, 4H), 7.33 (d, 2H, *J* = 7.6 Hz), 7.53 (d, 2H, *J* = 7.6 Hz), 7.7 (t, 2H, *J* = 7.7 Hz), 7.80 (t, 2H, *J* = 7.7 Hz), 8.04 (t, 4H, *J* = 9.2 Hz), 8.11 (d, 2H, *J* = 7.8 Hz), 8.32 (s, 6H), 8.53 (d, 2H, *J* = 8 Hz), 8.71 (s, 2H), 11.96 (s, 2H). ¹³C NMR (126 MHz, DMSO-d₆): δ = 166.01, 165.89, 159.13, 152.28, 141.92, 138.80, 138.62, 134.17, 133.68, 133.29, 130.74, 130.60, 130.07, 129.43, 129.40, 129.34, 129.09, 128.76, 128.27, 127.78, 127.69, 124.46, 123.53, 121.41, 121.29, 108.93, 100.08, 69.71, 68.82, 66.46, 60.97, 60.80, 14.26. HR-MS (ESI): calc'd for [M + H]⁺, [C₈₀H₇₇Br₂N₄O₁₆]⁺, *m/z* = 1507.3696, found *m/z* = 1507.3701.

3.2.10 Synthesis of 3.5c

3.5b (400 mg, 0.280 mmol), 4-pyridyl boronic acid (75.8 mg, 0.616 mmol) and Pd(PPh₃)₄ (98 mg, 0.084 mmol) were added to a 100 mL Schlenk flask, degassed and backfilled with N₂. 2 M Na₂CO₃ (30 mL) and THF (30 mL) were added and the mixture was refluxed (80 °C) for 24 h. The solution was cooled to room temperature and the organic phase was separated and extracted with DCM/brine. The organic solvent was dried over Na₂SO₄ and evaporated. The solids were filtered, air dried and recrystallized from CH₃CN producing a white solid; yield 168 mg (40%). Mp: 130–135 °C. ¹H NMR (500 MHz, CDCl₃, 298 K): δ = 1.42 (t, 12H, *J* = 7.1 Hz), 3.45 (s, 8H), 3.64 (s, 8H), 3.80 (s, 8H), 4.46 (m, 8H), 5.20 (s, 2H), 6.31 (s, 4H), 8.86 (br s, 4H), 7.31 (d, 2H, *J* = 7.5 Hz), 7.45 (m, 4H), 7.65 (m, 2H), 7.98 (m, 4H), 8.17 (m, 8H), 8.30 (s, 4H), 8.38 (s, 2H), 8.50 (s, 2H), 11.11 (s, 2H). ¹³C NMR (126 MHz, CDCl₃): δ = 166.98, 166.80, 159.32, 152.81, 149.34, 147.85, 142.45, 139.46, 139.15, 138.72, 134.15, 133.77, 133.56, 131.22, 130.72, 130.58, 130.47, 130.14, 128.79, 128.55, 128.35, 124.59, 123.78, 121.87, 121.28, 116.46, 104.94, 101.29, 70.56, 70.05, 66.54, 61.52,

60.97, 14.52. HR-MS (ESI): calc'd for $[M + H]^+$, $[C_{90}H_{85}N_6O_{16}]^+$, $m/z = 1505.6017$, found $m/z = 1505.6022$.

3.2.11 Synthesis of 3.6c

To **3.5c** (150 mg, 0.099 mmol) in tetrahydrofuran (15 mL) and ethanol (25 mL) was added 1 M NaOH (15 mL). After the reaction mixture was stirred at 80 °C for 24 h, the solvent was removed on a rotary evaporator. Deionized water (15 mL) was added to dissolve the residue. The solution was acidified with 2 M HCl to give a pH value of approx. 5. The precipitate was collected by vacuum filtration and air dried. Yield 124 mg (90%). Mp: 260–265 °C. 1H NMR (500 MHz, DMSO- d_6): $\delta = 3.54$ (s, 8H), 3.56 (s, 8H), 3.89 (s, 8H), 5.52 (s, 2H), 6.38 (s, 4H), 7.06 (s, 4H), 7.26 (s, 4H), 7.47 (m, 4H), 7.64 (m, 2H), 7.71 (m, 3H), 7.77 (m, 4H), 7.92 (m, 2H), 8.02 (s, 4H), 8.07 (s, 3H), 8.15 (m, 6H), 8.28 (s, 6H), 8.49 (m, 8H), 8.87 (s, 2H), 11.85 (s, 2H, NH), 12.95 (s, 2H, protonated pyridine), 13.07 (br s, 4H, acid). ^{13}C NMR (126 MHz, DMSO- d_6): $\delta = 167.65, 167.45, 160.22, 159.18, 152.50, 150.12, 149.36, 142.02, 138.62, 138.48, 133.90, 133.31, 131.58, 131.28, 131.20, 129.56, 129.18, 128.48, 127.98, 127.65, 124.67, 121.34, 120.94, 105.21, 104.30, 102.47, 101.55, 70.10, 69.91, 69.04, 68.88, 67.45, 66.40$. HR-MS (ESI): calc'd for $[M + H]^+$, $[C_{82}H_{69}N_6O_{16}]^+$, $m/z = 1393.4765$, found $m/z = 1393.4771$.

3.2.12 Synthesis of MOF Zn-3.6a

3.6a (10 mg, 0.007 mmol) and $Zn(NO_3)_2 \cdot 6H_2O$ (4.5 mg, 0.015 mmol) were added to a solution of DEF/EtOH/ H_2O (2 : 1 : 0.5 mL). Upon sonication and heating, a clear solution was obtained. The sample was then placed in a programmable oven and heated at a constant rate of 1 °C min^{-1} to 85 °C and kept at that temperature for 24 h. The resulting pale yellow crystals were collected and washed with DEF followed by EtOH, yield 9 mg (78%). $C_{82}H_{92}N_6O_{22}Zn_2$ (1644.48): calcd C: 59.89, H: 5.64, N: 5.11; found C: 60.06, H: 5.36, N: 5.11.

3.2.13 Synthesis of MOF Zn-3.6c

3.6c (4.56 mg, 0.003 mmol) and $\text{Zn}(\text{NO}_3)_2 \cdot 6\text{H}_2\text{O}$ (4.86 mg, 0.016 mmol) were added to a solution of DEF/EtOH/ H_2O (2 : 1 : 0.5 mL). Upon sonication and heating, a clear solution was obtained. The sample was then placed in a programmable oven and heated at a constant rate of $1\text{ }^\circ\text{C min}^{-1}$ to $85\text{ }^\circ\text{C}$ and kept at that temperature for 24 h. The resulting pale yellow crystals were collected and washed with DEF followed by EtOH, yield 4 mg (77%). $\text{C}_{92}\text{H}_{90}\text{N}_8\text{O}_{18}\text{Zn}_2$ (1726.53): calcd C: 64, H: 5.25, N: 6.49; found C: 54.81, H: 4.43, N: 6.17.

3.2.14 Synthesis of MOF Cu-3.6c

3.6c (10 mg, 0.007 mmol) and $\text{Cu}(\text{NO}_3)_2 \cdot 2.5\text{ H}_2\text{O}$ (6.66 mg, 0.028 mmol) were added to a solution of DEF/EtOH/ H_2O (2 : 1 : 1 mL) followed by 5% HNO_3 (3 drops). Upon sonication and heating, a clear solution was obtained. The sample was then placed in a programmable oven and heated at a constant rate of $1\text{ }^\circ\text{C min}^{-1}$ to $85\text{ }^\circ\text{C}$ and kept at that temperature for 48 h. The resulting blue crystals were collected and washed with DEF followed by EtOH, yield 4 mg (35%). All attempts to obtain a satisfactory elemental analysis resulted in low C%.

3.2.15 Single-Crystal X-ray Diffraction Experiments

Crystals were frozen in paratone oil inside a cryoloop under a cold stream of N_2 . X ray intensity data were collected at 173(2) K using a Bruker D8 Venture diffractometer equipped with a PHOTON 100 CMOS area detector. The raw area detector data frames were reduced and corrected for absorption effects using the SAINT+ and SADABS programs.^[58] Final unit cell parameters were determined by least squares refinement taken from the data set. Diffraction data and unit-cell parameters were consistent with the assigned space groups. The structures were solved by direct methods with SHELXT.^[59] Subsequent

difference Fourier calculations and full-matrix least-squares refinement against $|F^2|$ were performed with SHELXL-2014^[59] using OLEX2.^[60] All non-hydrogen atoms were refined anisotropically and hydrogen atoms placed in idealized positions and refined using a riding model. See Table 3.1 and 3.2 for a summary of data collection, solution and refinement details. Complete details of the structures can be obtained from the Cambridge Crystallographic Data Centre at www.ccdc.cam.ac.uk for CCDC accession numbers 1519348-1519352.

3.2.16 X-ray structure of Linker 3.6a

Crystals of formula **3.6a**(DMF)₂ were of good quality. Data were collected using MoK α radiation ($\lambda = 0.71073 \text{ \AA}$). The asymmetric unit contained half a molecule of the tetra-acid ligand (C₇₄H₆₂N₄O₂₀) and one molecule of DMF. The structure was solved in the triclinic space group P-1. No restraints were required. See Table 3.1 for details.

3.2.17 X-ray structure of MOF Zn-3.6a

Crystals of formula {[Zn₂(H₂O)₂(**3.6a**)](DEF)₂(H₂O)₂} were of good quality. Data were collected using MoK α radiation ($\lambda = 0.71073 \text{ \AA}$). The asymmetric unit contained half a tetra-carboxylate linker, one zinc(II) ion with a coordinated water molecule, two molecules of DEF and two molecules of water. The structure was solved in the triclinic space group P-1. No restraints were required. See Table 3.1 for details.

Table 3.1 – single-crystal X-ray data collection, solution and refinement details for **3.6a** and MOFs Zn-**3.6a**.

CCDC No.	1519348	1519349
Compound	3.6a (DMF) ₂	{[Zn ₂ (H ₂ O) ₂ (3.6a)](DEF) ₂ (H ₂ O)}
Formula	C _{76.8} H _{73.2} N _{5.6} O _{17.6}	C ₈₂ H ₈₈ N ₆ O ₂₂ Zn ₂
<i>M</i> [g mol ⁻¹]	1356.21	1640.32
Crystal system	triclinic	triclinic
Space group	P-1 (No. 2)	P-1 (No. 2)
<i>a</i> [Å]	8.0014(3)	8.2465(4)
<i>b</i> [Å]	14.3032(6)	14.4619(6)
<i>c</i> [Å]	15.5636(8)	15.5490(8)
α [°]	76.9517(16)	97.0926(17)
β [°]	79.6241(15)	94.778(2)
γ [°]	81.520(2)	102.6227(18)
<i>V</i> [Å ³]	1696.19(13)	1898.76(15)
<i>Z</i>	1	1
<i>D</i> _{calcd.} [g cm ⁻³]	1.328	1.435
μ [mm ⁻¹]	0.095	0.714
Reflections	6336	7692
<i>R</i> _{int}	0.0222	0.0407
Parameters	474	568
Restraints	0	156
<i>R</i> 1 [I > 2σ(I)] ^a	0.0449	0.0403
<i>R</i> 1 (all data)	0.0665	0.0541
<i>wR</i> 2 [I > 2σ(I)] ^b	0.1059	0.0954
<i>wR</i> 2 (all data)	0.1179	0.1027
GoF (<i>F</i> ²)	1.019	1.026
$\Delta\rho$ [e Å ⁻³]	+0.48 (-0.24)	+0.62 (-0.60)

^a $R1 = \sum ||F_o| - |F_c|| / \sum |F_o|$; $R2w = [\sum [w(F_o^2 - F_c^2)^2] / \sum [w(F_o^2)^2]]^{1/2}$, ^b $w = q[\sigma^2(F_o^2) + (aP)^2 + bP]$.

3.2.18 X-ray structure of MOF Zn-3.6c

Crystals of formula {[Zn₂(**3.6c**)](DEF)₂} were of good quality. Data was collected using Cu_{Kα} radiation ($\lambda = 1.54178$ Å). The asymmetric unit contained half a molecule of the linker

3.6c coordinated to one zinc(II) ion and one molecule of DEF in the lattice. The structure was solved in the monoclinic space group $P2_1/c$. One of the ethyl groups of the DEF molecule was disordered with approximately 50:50 site occupancy; the C-C bonds were restrained to 1.40 Å and SIMU used to even out the electron density on these atoms. See Table 3.2 for details.

3.2.19 X-ray structure of MOF Cu-3.6c

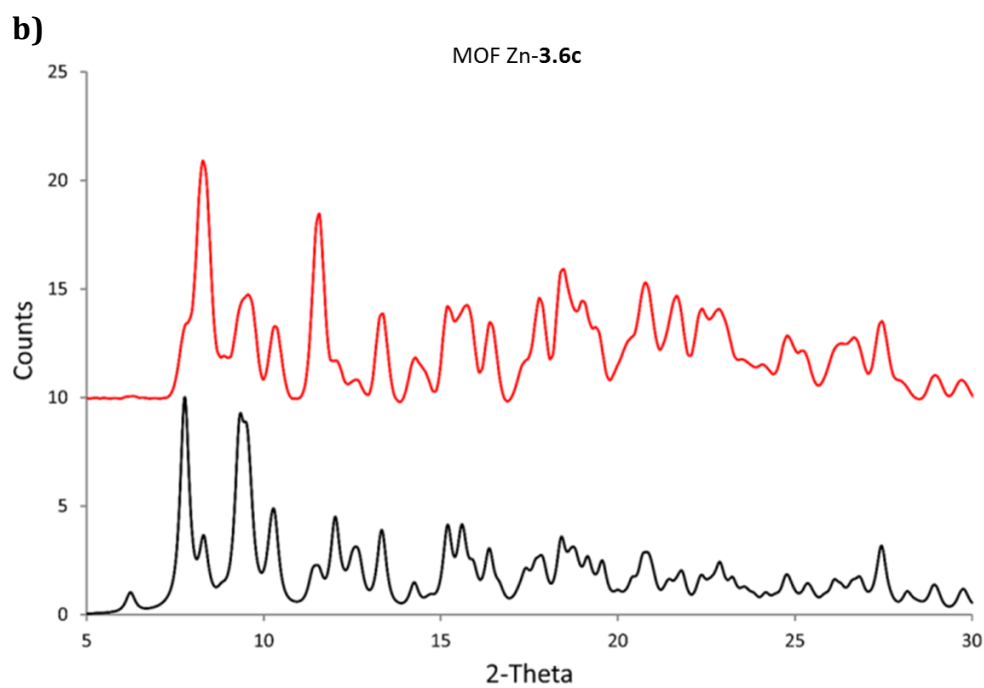
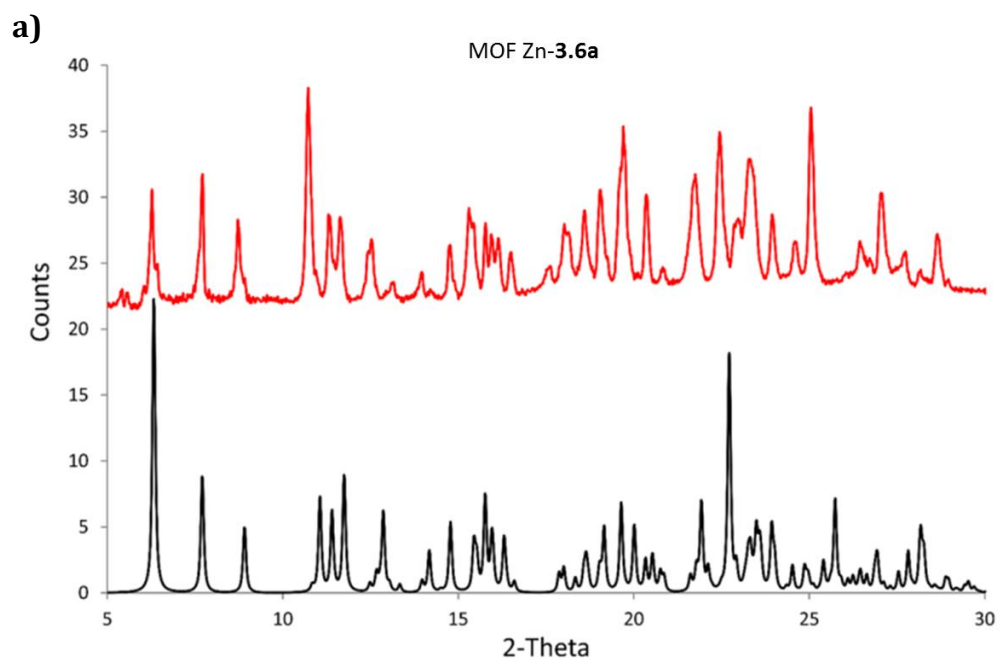
Crystals of formula $\{[\text{Cu}(\mathbf{3.6c})](\text{DEF})_x(\text{H}_2\text{O})_x\}$ were of moderate quality. Data were collected using $\text{Cu}_{K\alpha}$ radiation ($\lambda = 1.54178$ Å). The asymmetric unit contained half a molecule of linker **3.6c** coordinated to one copper(II) ion with one partially occupied molecule of DEF and one fully occupied molecule of water in the lattice. The structure was solved in the monoclinic space group $P2_1/n$. The full extent of the disorder was discovered and modelled with the necessary restraints (numerous AFIX, SAME, FLAT commands were required); three PARTS for the axle component and disordered DEF and water molecules. Although this provided a chemically sensible result and reasonable final residuals, the data to parameters/restraints ratio was clearly unacceptable. The solid-state structure and atom connectivity is sensible. See Table 3.2 and archived CIF files for more details.

Table 3.2 – single-crystal X-ray data collection, solution and refinement details for Zn-3.6c and Cu-3.6c.

CCDC No.	1519350	1519351
Compound	{[Zn ₂ (3.6c)](DEF) ₄ }	{[Cu(3.6c)](DEF) _{1.5} (H ₂ O) ₂ }
Formula	C ₁₀₂ H ₁₀₈ N ₁₀ O ₂₀ Zn ₂	C _{89.5} H _{86.5} CuN _{7.5} O _{19.5}
<i>M</i> [g mol ⁻¹]	1924.72	1641.03
Crystal system	monoclinic	monoclinic
Space group	P2 ₁ /c (No. 14)	P2 ₁ /n (No. 14)
<i>a</i> [Å]	11.4221(4)	17.2427(6)
<i>b</i> [Å]	21.2742(8)	14.0544(5)
<i>c</i> [Å]	19.0647(7)	17.5540(8)
α [°]	90	90
β [°]	95.4192(19)	103.263(2)
γ [°]	90	90
<i>V</i> [Å ³]	4611.9(3)	4140.5(3)
<i>Z</i>	2	2
<i>D</i> _{calcd.} [g cm ⁻³]	1.386	1.006
μ [mm ⁻¹]	1.285	1.320
Reflections	6673	6343
<i>R</i> _{int}	0.0558	0.0495
Parameters	562	1066
Restraints	74	2324
<i>R</i> 1 [<i>I</i> > 2σ(<i>I</i>)] ^a	0.0683	0.1241
<i>R</i> 1 (all data)	0.0889	0.1674
<i>wR</i> 2 [<i>I</i> > 2σ(<i>I</i>)] ^b	0.1795	0.3419
<i>wR</i> 2 (all data)	0.1957	0.3843
GoF (<i>F</i> ²)	1.074	1.488
$\Delta\rho$ [e Å ⁻³]	+1.06 (-0.37)	+0.55 (-0.41)

^a $R1 = \sum ||F_o| - |F_c|| / \sum |F_o|$; $R2w = [\sum [w(F_o^2 - F_c^2)^2] / \sum [w(F_o^2)^2]]^{1/2}$, ^b $w = q[\sigma^2(F_o^2) + (aP)^2 + bP]$.

3.2.20 Powder X-ray Diffraction Experiments



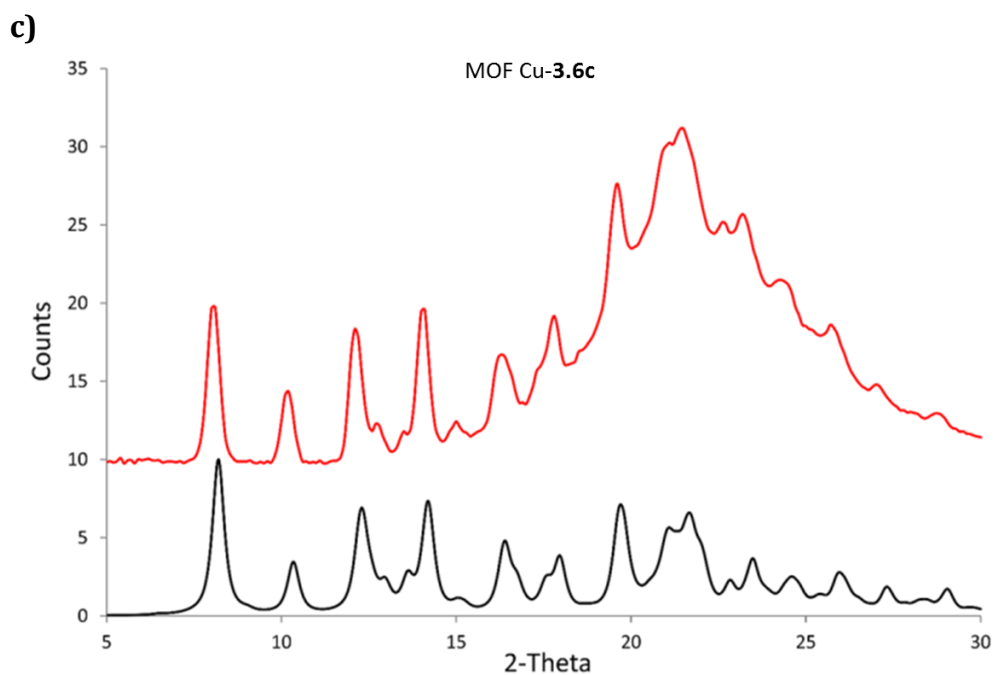


Fig 3.6 – a) comparison of PXRD of MOF Zn-3.6a (in red) and simulated from the single crystal X-ray structures (in black); b) comparison of PXRD of MOF Zn-3.6c (in red) and simulated from the single crystal X-ray structures (in black); c) comparison of PXRD of MOF Cu-3.6c (in red) and simulated from the single crystal X-ray structures (in black).

3.3 References

1. J. F. Stoddart, *Chem. Soc. Rev.*, **2009**, *38*, 1802–1820.
2. J. E. Beves, B. A. Blight, C. J. Campbell, D. A. Leigh, R. T. McBurney, *Angew. Chem. Int. Ed.*, **2011**, *50*, 9260–9327.
3. J. F. Stoddart, *Angew. Chem. Int. Ed.*, **2014**, *53*, 11102–11104.
4. V. N. Vukotic, S. J. Loeb, *Chem. Soc. Rev.*, **2012**, *41*, 5896–5906.
5. B. Zheng, F. Wang, S. Dong, F. Huang, *Chem. Soc. Rev.*, **2012**, *41*, 1621–1636.
6. V. Fasano, M. Baroncini, M. Moffa, D. Iandolo, A. Camposeo, A. Credi, D. Pisignano, *J. Am. Chem. Soc.*, **2014**, *136*, 14245–14254.
7. A. Harada, R. Kobayashi, Y. Takashima, A. Hashidzume, H. Yamaguchi, *Nat. Chem.*, **2011**, *3*, 34–37.
8. O. Lukin, F. Vogtle, *Angew. Chem. Int. Ed.*, **2005**, *44*, 1456–1477.
9. S. Li, B. Zheng, J. Chen, S. Dong, Z. Ma, F. Huang, H. W. Gibson, *J. Polym. Sci., Part A* **2010**, *48*, 4067–4073.
10. S. Dong, Y. Luo, X. Yan, B. Zheng, X. Ding, Y. Yu, Z. Ma, Q. Zhao, F. Huang, *Angew. Chem. Int. Ed.*, **2011**, *50*, 1905–1909.
11. Y. Kohsaka, K. Nakazono, Y. Koyama, S. Asai, T. Takata, *Angew. Chem. Int. Ed.*, **2011**, *50*, 4872–4875.
12. M. J. Frampton, H. L. Anderson, *Angew. Chem. Int. Ed.*, **2007**, *46*, 1028–1064.
13. J. Buey, T. M. Swager, *Angew. Chem. Int. Ed.*, **2000**, *39*, 608–612.

14. T. Akutagawa, H. Koshinaka, D. Sato, S. Takeda, S.-I. Noro, H. Takahashi, R. Kumai, Y. Tokura, T. Nakamura, *Nature Mater.*, **2009**, *8*, 342–347.
15. M. Feng, L. Gao, Z. Deng, W. Ji, X. Guo, S. Du, D. Shi, D. Zhang, D. Zhu, H. Gao, *J. Am. Chem. Soc.*, **2007**, *129*, 2204–2205.
16. V. Bermudez, T. Gase, F. Kajzar, N. Capron, F. Zerbetto, F. G. Gatt, D. A., Leigh, S., Zhang, *Electro-Optics*, **2002**, *21*, 39–44.
17. M. Horie, T. Sassa, D. Hashizume, Y. Suzuki, K. Osakada, T. Wada, *Angew. Chem. Int. Ed.*, **2007**, *46*, 4983–4986.
18. M. Horie, Y. Suzuki, D. Hashizume, T. Abe, T. Wu, T. Sassa, T. Hosokai, K. Osakada, *J. Am. Chem. Soc.*, **2012**, *134*, 17932–17944.
19. Q. Li, W. Zhang, O. S. Miljanic, C.-H. Sue, Y.-L. Zhao, L. Liu, C. B. Knobler, J. F. Stoddart, O. M. Yaghi, *Science*, **2009**, *325*, 855–859.
20. H. X. Deng, M. A. Olson, J. F. Stoddart, O. M. Yaghi, *Nat. Chem.*, **2010**, *2*, 439–447.
21. A. Coskun, M. Banaszak, R. D. Astumian, J. F. Stoddart, B. A. Grzybowski, *Chem. Soc. Rev.*, **2012**, *41*, 19–35
22. B. M. Rambo, H. Gong, M. O'H, J. L. Sessler, *Acc. Chem. Res.*, **2012**, *45*, 1390–1401.
23. P. R. McGonigal, P. Deria, I. Hod, P. Z. Moghadam, A.-J. Avestro, N. E. Horwitz, I. C. Gibbs-Hall, A. K. Blackburn, D. Chen, Y. Y. Botros, W. R. Wasielewski, R. Q. Snurr, J. T. Hupp, O. K. Farha, J. F. Stoddart, *Proc. Natl. Acad. Sci. USA*, **2015**, *112*, 11161–11168.
24. V. N. Vukotic, K. J. Harris, K. Zhu, R. W. Schurko, S. J. Loeb, *Nat. Chem.*, **2012**, *4*, 456–460.

25. V. N. Vukotic, C. A. O'Keefe, K. Zhu, K. J. Harris, C. To, R. W. Schurko, S. J. Loeb, *J. Am. Chem. Soc.*, **2015**, *137*, 9643–965120.
26. K. Zhu, V. N. Vukotic, C. A. O'Keefe, R. W. Schurko, S. J. Loeb, *Nat. Chem.*, **2015**, *7*, 514–519.
27. K. Zhu, V. N. Vukotic, C. A. O'Keefe, R. W. Schurko, S. J. Loeb, *J. Am. Chem. Soc.*, **2014**, *136*, 7403–7409.
28. S. J. Loeb, *Chem. Commun.*, **2005**, 1511–1518.
29. K. Kim, *Chem. Soc. Rev.* **2002**, *31*, 96–107.
30. G. J. E. Davidson, S. J. Loeb, *Angew. Chem. Int. Ed.*, **2003**, *42*, 74–77.
31. D. J. Hoffart, S. J. Loeb, *Angew. Chem. Int. Ed.*, **2005**, *44*, 901–90420. H. X. Deng, M. A. Olson, J. F. Stoddart, O. M. Yaghi, *Nat. Chem.*, **2010**, *2*, 439–447.
32. S. J. Loeb, *Chem. Soc. Rev.*, **2007**, *36*, 226–235.
33. L. K. Knight, V. N. Vukotic, E. Viljoen, C. B. Caputo, S. J. Loeb, *Chem. Commun.*, **2009**, 5585–5587.
34. V. N. Vukotic, S. J. Loeb, *Chem. Eur. J.*, **2010**, *16*, 13630–13637.
35. H. Gong, B. M. Rambo, C. A. Nelson, V. M. Lynch, X. Zhu, J. L. Sessler, *Chem. Commun.*, **2012**, *48*, 10186–10188.
36. K. Zhu, S. J. Loeb, *Top. Curr. Chem.*, **2014**, *354*, 213–251.
37. H. Gong, B. M. Rambo, C. A. Nelson, V. M. Lynch, X. Zhu and J. L. Sessler, *Chem. Commun.*, **2012**, 10186–10188.

38. D. J. Mercer, V. N. Vukotic, S. J. Loeb, *Chem. Commun.*, **2011**, 47, 896–898.
39. N. C. Frank, D. J. Mercer, S. J. Loeb, *Chem. Eur. J.*, **2013**, 19, 14076–14080.
40. G. Gholami, K. Zhu and S. J. Loeb, *Eur. J. Inorg. Chem.*, **2016**, 27, 4524-4529.
41. D. N. Dybtsev, H. Chun and K. Kim, *Angew. Chem., Int. Ed.*, **2004**, 43, 5033-5036.
42. H. Chun, D. N. Dybtsev, H. Kim and K. Kim, *Chem. – Eur. J.*, **2005**, 11, 3521-3529.
43. B. Q. Ma, K. L. Mulfort and J. T. Hupp, *Inorg. Chem.*, **2005**, 44, 4912-4914.
44. T. Gadzikwa, B. S. Zeng, J. T. Hupp and S. T. Nguyen, *Chem. Commun.*, **2008**, 3672-3674.
45. T. Gadzikwa, O. K. Farha, C. D. Malliakas, M. G. Kanatzidis, J. T. Hupp and S. T. Nguyen, *J. Am. Chem. Soc.*, **2009**, 131, 13613-13615.
46. O. K. Farha and J. T. Hupp, *Acc. Chem. Res.*, **2010**, 43, 1166-1175.
47. O. K. Farha, C. D. Malliakas, M. G. Kanatzidis and J. T. Hupp, *J. Am. Chem. Soc.*, **2010**, 132, 950-952.
48. W. Bury, D. Fairen-Jimenez, M. B. Lalonde, R. Q. Snurr, O. K. Farha and J. T. Hupp, *Chem. Mater.*, **2013**, 25, 739-744.
49. B. L. Chen, C. D. Liang, J. Yang, D. S. Contreras, Y. L. Clancy, E. B. Lobkovsky, O. M. Yaghi and S. Dai, *Angew. Chem., Int. Ed.*, **2006**, 45, 1390-1393.
50. B. L. Chen, S. Q. Ma, F. Zapata, F. R. Fronczek, E. B. Lobkovsky and H. C. Zhou, *Inorg. Chem.*, **2007**, 46, 1233-1236.
51. I. H. Park, K. Kim, S. S. Lee and J. J. Vittal, *Cryst. Growth Des.*, **2012**, 12, 3397-3401.

52. K. Zhu, V. N. Vukotic and S. J. Loeb, *Angew. Chem., Int. Ed.*, **2012**, 51, 2168-2172.
53. N. Farahani, K. Zhu and S. J. Loeb, *ChemPhysChem*, **2016**, 17, 1875-1880.
54. K. Zhu, V. N. Vukotic, N. Noujeim and S. J. Loeb, *Chem. Sci.*, **2012**, 3, 3265-3271.
55. C. Simocko, T. C. Young and K. B. Wagener, *Macromolecules*, **2015**, 48, 5470-5473.
56. J. P. Anzenbacher, K. Jursikova, D. Aldakov, M. Marquez and R. Pohl, *Tetrahedron*, **2004**, 60, 11163-11168.
57. S. D. Uzun, N. A. Unlu, M. Sendur and F. E. Kanik, *Colloids Surf., B*, **2013**, 112, 74-80.
58. Bruker, *SAINT+ and SADABS*, Bruker AXS Inc., Madison, Wisconsin, USA, 2012.
59. G. M. Sheldrick, *Acta Crystallogr., Sect. C: Cryst. Struct. Commun.*, **2015**, 71, 3-8.
60. O. V. Dolomanov, L. J. Bourhis, R. J. Gildea, J. A. K. Howard, H. Puschmann, *J. Appl. Cryst.*, **2009**, 42, 339-341.
61. D. C. Palmer, *CrystalMaker*, CrystalMaker Software Ltd, Begbroke, Oxfordshire, England, 2014.

CHAPTER 4

4.1 Influence of Axle Length on the Rate and Mechanism of Shuttling in Rigid H-shaped [2]Rotaxanes

4.1.1 Introduction

One of the earliest classes of mechanically interlocked molecules (MIMs) to be investigated for dynamic motion was the molecular shuttle.^[1] The first such system reported by Stoddart in 1991, consisted of a tetracationic macrocycle that translocated between two identical electron-rich aromatic groups attached to a flexible polyether chain.^[2] The energy barrier for this to and fro motion was determined to be 13 kcal mol⁻¹ in acetone solution. Since that pioneering work, many different structural versions of the molecular shuttle have been prepared and the corresponding energy barriers to translational motion measured.^[3]

A number of studies have attempted to correlate the rate of shuttling to the structure of the molecular path along which the ring must travel.^[4] In particular, the conformational freedom of the track along which the ring shuttles, can have a significant effect on the barrier. For example, when the track is a flexible polyether or hydrocarbon chain folding can cause a significant increase to the shuttling barrier and clearly a very long track would require a non-linear trajectory with several different sized energy barriers.^[5] Studies have shown that folded conformations can impede shuttling by presenting steric barriers^[6] and flexibility can even change the mechanism by allowing the wheel to simultaneously interact with both initial and final recognition sites.^[7] Even answering a seemingly simple question such as—*is there a relationship between the shuttling rate and the distance between the recognition sites?*—can be difficult.

In an elegant study in 2014, Hirose and co-workers prepared a series of degenerate molecular shuttles with alkyl ammonium recognition sites and a rigid track comprised of phenyl rings; Fig 4.1.^[8] By incorporating an increasing number of phenylene spacers in the axle ($n = 1-4$), they were able to extend the distance between the two ammonium N-atoms from 6.9 ($n = 1$) to 19.6 Å ($n = 4$). This eliminated the effects of conformational isomerism and it was concluded that “axle length does not affect switching dynamics in degenerate molecular shuttles with rigid spacers”.

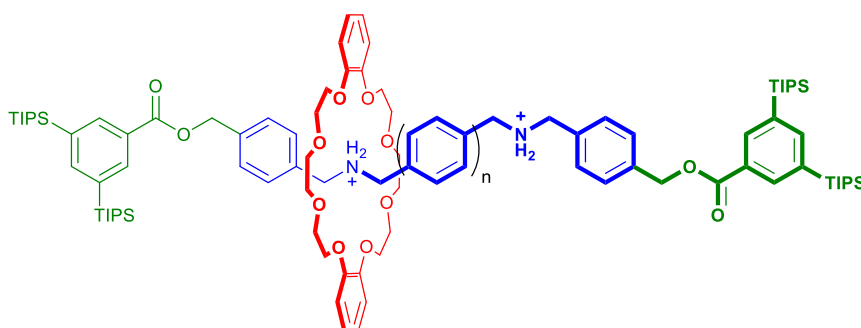


Fig 4.1 – Hirose and co-worker's degenerate molecular shuttle with alkyl ammonium recognition sites and phenylene spacers ($n = 1-4$).^[8]

During our investigations to incorporate molecular shuttles into solid-state materials by using rotaxanes as linkers for metal-organic frameworks (MOFs),^[9] we prepared a series of [2]rotaxane molecular shuttles with a rigid H-shaped axle.^[10] We rationalised that it should also be possible to extend this motif by adding an increasing number of phenyl rings, or equally rigid groups, to prepare a series of molecular shuttles with a fairly wide variation in shuttling track length. As in Hirose's work, these could then be used to more accurately probe the effect of track length—the distance between recognition sites—on the rate of shuttling without the previously encountered flexibility of the axle being an issue. These

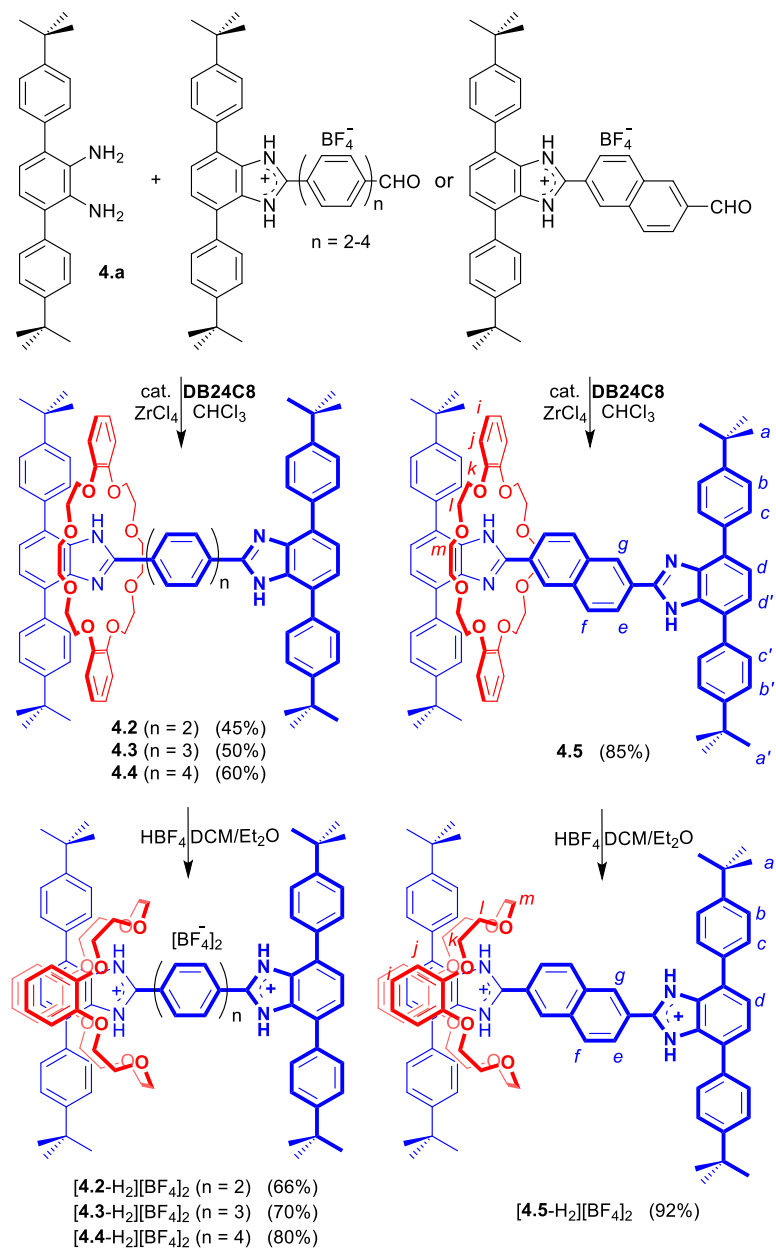
new elongated [2]rotaxanes would also be amenable to incorporation into solid-state materials.

Although our study herein corroborates Hirose's major tenant that axle length does not appreciably affect shuttling rate, it expands significantly upon their work as our system can be studied in both neutral and dicationic forms. We also add a cautionary tale about oversimplifying the mechanism of shuttling as we show it can be easily short circuited, even in a rigid molecular design. We report herein, the preparation of a series of five rigid, H-shaped [2]rotaxane molecular shuttles comprised of two equivalent benzimidazolium recognition sites, a track containing $n = 1-4$ phenyl rings or a naphthyl ring and a single dibenzo[24]crown-8 ether, **DB24C8** macrocycle. The distance between the N-atoms of the two recognition sites varies between 7.4 and 20.3 Å and the rate of shuttling can be measured for both neutral benzimidazole and dicationic benzimidazolium species.

4.1.2 Results and Discussion

4.1.2.1 Preparation and characterisation of molecular shuttles

Preparation of the required aldehyde precursors with $n = 2-4$ and N_p spacers are described in the experimental section 4.2. Formation of the [2]rotaxanes was accomplished by condensation between the appropriate aldehyde with $n = 2-4$ or N_p and diamine **4.a** in the presence of **DB24C8** utilising $ZrCl_4$ as catalyst as outlined in Scheme 4.1. The neutral species **4.2-4.5** were isolated initially and then converted to the dicationic versions [**4.2-H₂**]²⁺-[**4.5-H₂**]²⁺ by protonation with HBF_4 .



Scheme 4.1 – preparation of rigid, H-shaped [2]rotaxane molecular shuttles containing 2, 3 and 4 phenyl rings or a naphthyl group along the track. Preparation of various aldehyde precursors (n = 2–4, Np) are described in the experimental 4.2.2. The n = 1 analogue was previously prepared as described in ref.^[11] H-atom labels are for NMR spectral assignments shown in Fig. 4.2.

The ^1H NMR spectra of the neutral [2]rotaxanes display resonances for both axle and wheel protons that are indicative of molecular shuttling at a rate that is fast compared to the NMR timescale. As an example, Fig 4.2a shows that for **4.5** there are significant interactions resulting from hydrogen bonding between the axle and wheel—for example a down field shift of the NH peak from 9.77 to 10.69 ppm—but only averaged signals are observed.

For the dicationic version $[\mathbf{4.5-H_2}]^{2+}$, the non-covalent interactions between axle and wheel are much stronger due to additional ion-dipole and π -stacking interactions and the ^1H NMR spectra show individual resonances for all axle protons as the rate of shuttling is now slow on the NMR timescale; see Fig 4.2b.

An analysis of the non-covalent interactions between axle and wheel can be obtained from the solid-state structure. Fig 4.3 shows the results of X-ray diffraction experiments for both the neutral and dicationic pair **4.5** and $[\mathbf{4.5-H_2}][\text{BF}_4]_2$. Most importantly, the structures verify the array of non-covalent interactions observed from the solution NMR studies. In the neutral species **4.5**, the only significant interaction is a bifurcated hydrogen bond between the benzimidazole NH and crown ether O-atoms, while for the dication, $[\mathbf{4.5-H_2}]^{2+}$, the **DB24C8** wheel is clamped around the benzimidazolium core and involved in extensive charge-assisted hydrogen bonding accompanied by π -stacking interactions.^[12]

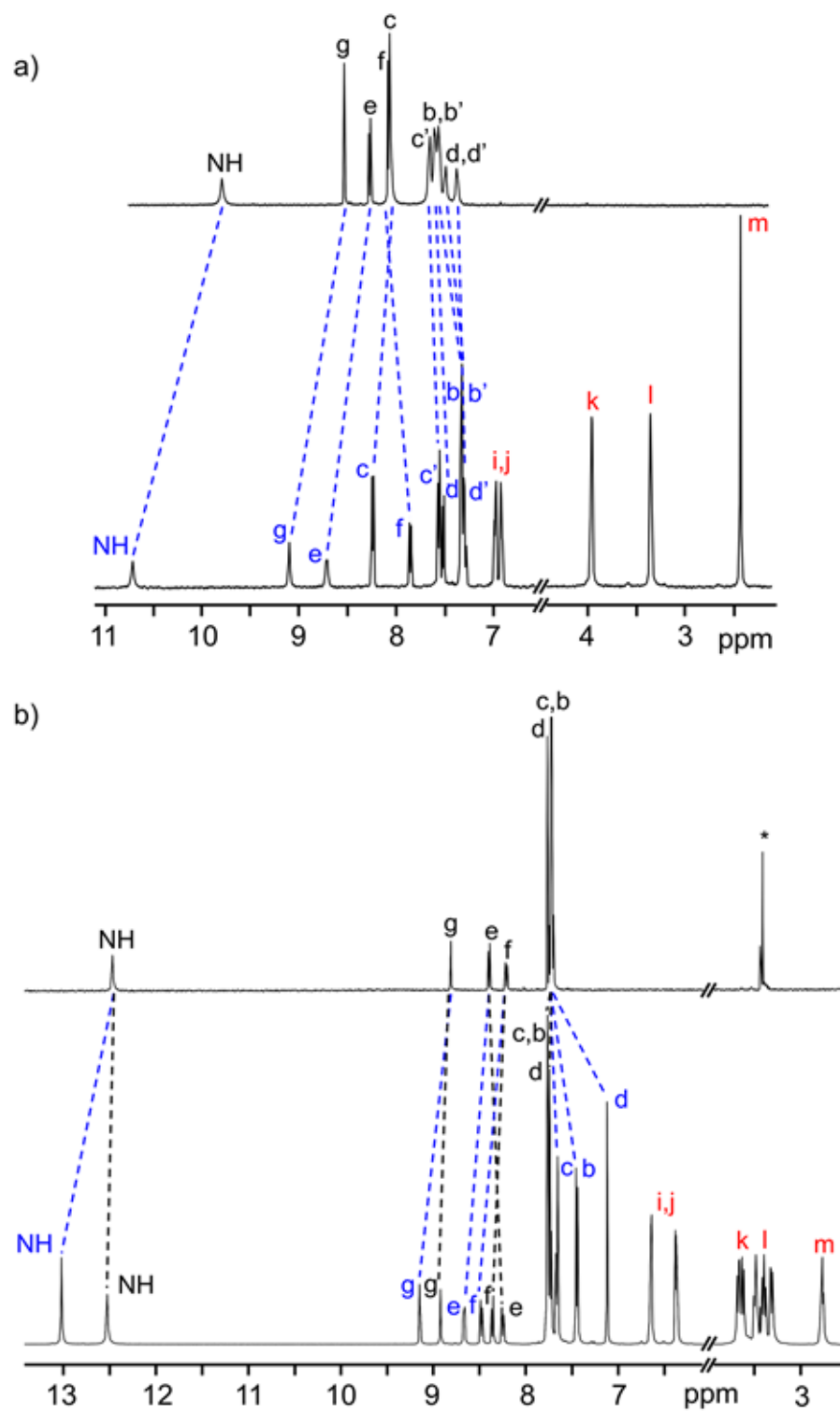
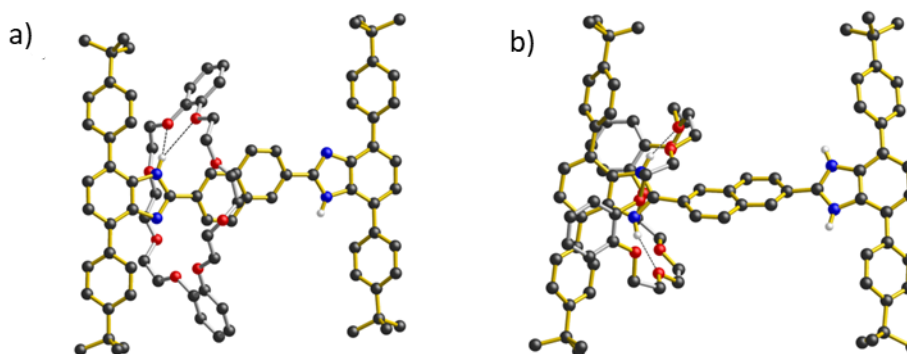


Fig 4.2 – a) ^1H NMR spectra (500 MHz, CD_2Cl_2 , 298 K) of naked axle of **4.5** (top) and neutral [2]rotaxane **4.5** (bottom), b) ^1H NMR spectra (500 MHz, CD_3CN , 298 K) of naked axle of

*[4.5-H₂]²⁺ (top) and dicationic [2]rotaxane [4.5-H₂]²⁺ (bottom). The change in chemical shifts due to threading of the **DB24C8** wheel on the axle are highlighted. Colour key: blue = [2]rotaxane axle, red = crown ether wheel, black = naked axle. H-atom labels are as shown in Scheme 4.1.*



*Fig 4.3 – ball-and-stick representations of the X-ray structures of [2]rotaxanes: a) **4.5** ($n = Np$) and b) **[4.5-H₂][BF₄]₂** ($n = Np$). Only H-atoms involved in hydrogen bonds are shown for clarity. Color key: red = O; blue = N, black = C; white = H; gold bonds = axle; silver bonds = wheel.*

4.1.2.2 Measurement of shuttling rates

Shuttling rates for both the neutral and dicationic [2]rotaxanes were measured using ¹H NMR spectroscopy. Since for the neutral series, **4.1-4.5**, the rate of shuttling was fast on the NMR timescale at room temperature, variable temperature studies were used to obtain rates at different temperatures and these fit to the Eyring equation (see experimental section 4.2.20). Since both signals from complexed and uncomplexed axle recognition site protons were observed in the ¹H NMR spectra for the dicationic species **[4.2-H₂]²⁺-[4.5-H₂]²⁺**, EXSY experiments were used to determine the rates of shuttling at room temperature. Table 4.1 summarizes the shuttling rates and energy barriers for both the neutral and dicationic series.

[2]rotaxane	k (s ⁻¹)	ΔG^\ddagger (kcal mol ⁻¹)
4.1	1.0 x 10 ⁷	7.7 ^c
4.2	6.2 x 10 ³	9.0
4.3	3.3 x 10 ³	9.6
4.4	4.7 x 10 ³	9.2
4.5	3.1 x 10 ³	9.8
[4.1 -H ₂] ²⁺	17.0 x 10 ⁻¹	17.3 ^d
[4.2 -H ₂] ²⁺	6.1 x 10 ⁻³	20.2 ^e
[4.3 -H ₂] ²⁺	7.8 x 10 ⁻³	20.1 ^e
[4.4 -H ₂] ²⁺	9.0 x 10 ⁻³	19.8 ^f
[4.5 -H ₂] ²⁺	12.4 x 10 ⁻³	20.0 ^d

^a Obtained from fit to VT data; reported at coalescence temperature, see Experimental section 4.2.20.

^b Obtained from 2D EXSY data; reported at RT. ^c Estimated from coalescence temperature see Experimental section 4.2.22. ^d 298 K. ^e 295 K. ^f 293 K.

Table 4.1 – shuttling data from ¹H NMR experiments for (**4.1–4.5**)^a in CD₂Cl₂ and ([**4.1**-H₂]²⁺-[**4.5**-H₂]²⁺)^b in CD₃CN.

Fig 4.4 shows a plot of the energy barriers to shuttling, for all the [2]rotaxane molecular shuttles (neutral and charged) as a function of the distance between the benzimidazole N-atoms on the axle. For the most part, the data corroborates Hirose and co-workers' conclusion that axle length does not affect the shuttling rate. The neutral species **4.2–4.5** have a fairly low barrier to shuttling of approximately 9.7 kcal/mol (blue horizontal line), while the dicationic compounds [**4.1**-H₂]²⁺-[**4.5**-H₂]²⁺ have a substantially larger energy barrier of approximately 20.1 kcal/mol (red horizontal line). Surprisingly however, for both the neutral and dicationic species, it appears that the energy barriers for the shortest (n = 1) compounds are outliers. They appear to have significantly lower energy barriers. In order to try and understand these observations, we turned to DFT calculations.

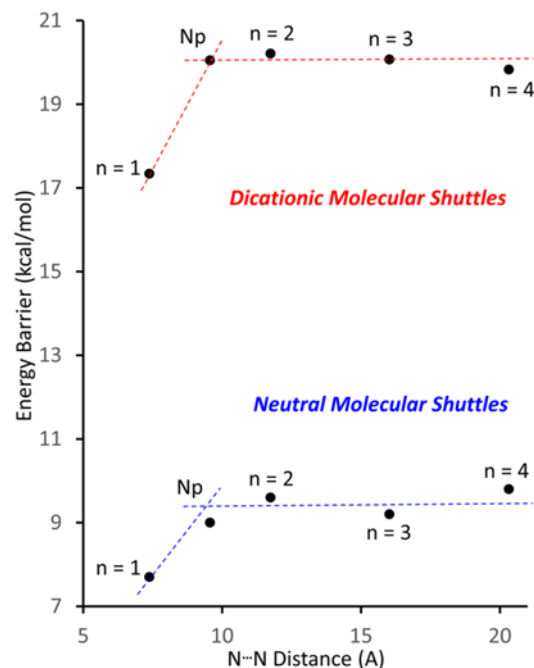
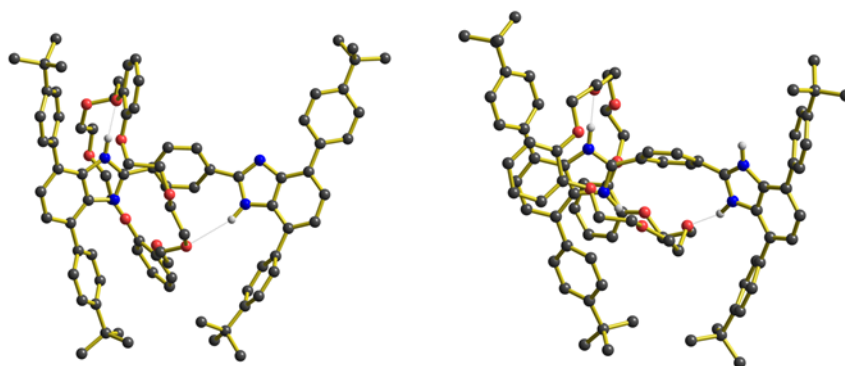


Fig 4.4 – plots of the energy barrier to translational motion in the molecular shuttles versus the distance between N-atoms on opposite ends of the track. Dotted lines are for visualisation purposes only. (n = number of phenyl rings, Np = naphthyl).

4.1.2.3 DFT calculations

Energy barriers to molecular shuttling and transition state structures were determined for two sets of molecular shuttles, **4.1–4.4** and $[\mathbf{4.1-H_2}]^{2+}-[\mathbf{4.4-H_2}]^{2+}$, with varying track lengths defined by $n = 1-4$ phenyl rings using DFT calculations (B3LYP/6-31G**, PCM $\epsilon = 8.93$). The calculated energy barrier for both (neutral and charged) series showed the same trends as the experimentally obtained data, where for $n = 2-4$ the shuttling energies are similar and fairly insensitive to the distance between the recognition sites (see experimental 4.2.29). However, as was observed for the experimental measurements, the calculated energy barriers for the molecular shuttling were significantly lower for the shortest $n = 1$ systems (neutral and charged). Moreover, DFT geometry optimizations of the transition states (TS) for these molecules provided a rational

explanation for the observed differences between the energy barriers. For both the **4.1** and $[\mathbf{4.1-H}_2]^{2+}$, the TS structures showed that the short length of the axles allows interaction of the crown ether wheel with *both* recognition sites at the same time. These interactions are stabilized by hydrogen bonds between the H-shaped axle and the **DB24C8** macrocycle with $\text{NH}\cdots\text{O}$ values between 1.9 and 2.7 Å. The predicted TS structures for **4.1** and $[\mathbf{4.1-H}_2]^{2+}$ are shown in Fig 4.5. These TS structures provide a shortcut in terms of the energy barrier to shuttling as interactions holding the wheel unit in place are never completely severed. On the other hand, for $n = 2-4$ this type of geometrical structure for the TS is not possible, see experimental 4.2.29. Furthermore, it is interesting that the structures at the TS position show that for $n=1$ (neutral and charged) the H-shaped axle bends, which allows both recognitions sites to be closer to the **DB24C8** macrocycle (see Fig 4.5), but for $n = 2-4$ (neutral and charged) the H-shaped axle remains straight, the recognition sites are further apart and the wheel interacts only with the central aromatic rings in the TS geometry (see experimental 4.2.29).



*Fig 4.5 – structural representations of the transition states for molecular shuttling as determined by DFT calculations. left, **4.1** and right, $[\mathbf{4.1-H}_2]^{2+}$. $\text{NH}\cdots\text{O}$ interactions are shown as dotted lines.*

4.1.2.4 Further experimental evidence: a transition state “snap-shot”

For all of the neutral molecular shuttles, the energy barriers to translational motion (measured in CD_2Cl_2) are quite low and this is undoubtedly due to the minimal interactions that bind the wheel to the recognition site—primarily a single $\text{NH}\cdots\text{O}$ hydrogen bond and some weak $\text{CH}\cdots\text{O}$ interactions. In this respect it should be noted that previous attempts to measure association constants for [2]pseudorotaxanes formation between neutral T-shaped benzimidazole axles and 24-membered crown ether wheels were unsuccessful, even in completely non-competitive solvents such as toluene^[13]. Only charged benzimidazolium axles have been successfully used for the template preparation of H-shaped MIMs.

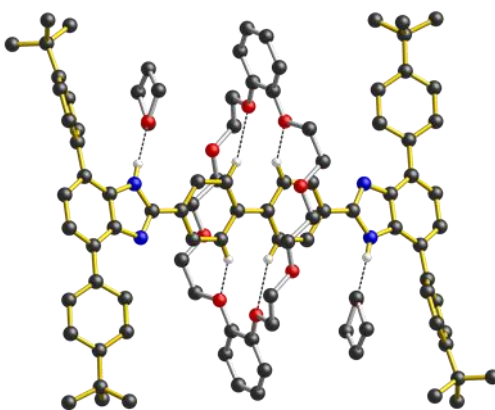


*Fig 4.6 – ball-and-stick representation of the single-crystal X-ray structure of the [2]rotaxane molecular shuttle **4.2** ($n = 2$) crystallized from THF (crystal formula **4.2**. $(\text{THF})_4$). Only H-atoms involved in hydrogen bonds are shown for clarity. Color key: red = O; blue = N; black = C; white = H; gold bonds = axle; silver bonds = wheel.*

It was therefore interesting to note that when the neutral molecular shuttle **4.2** was crystallized from the hydrogen-bond accepting solvent THF, the solvent interacts with the benzimidazole NH groups rather than the **DB24C8** macrocycle. (Only a single set of peaks was observed in the ^1H NMR spectrum of **4.2** (THF-d_3) and **4.1-Br** (CD_2Cl_2) even at the

lowest accessible temperature). Fig 4.6 shows the X-ray crystal structure of **4.2**·(THF)₄ in which a molecule of THF hydrogen bonds to each of the benzimidazole NH groups and the **DB24C8** macrocycle is displaced to a position between the two axle phenyl groups.

This is presumably a position where there are only very weak interactions are possible between phenyl H-atoms and crown ether O-atoms and can be thought of as “snapshot” of the crown ether position during a cycle of molecular shuttling between the two recognition sites along a rigid biphenyl axle. Indeed, this positioning of the crown ether on the axle is very similar to that calculated for the transition state structure of this shuttling process using DFT.

The identification by DFT and inference from experiment that for the shorter ($n = 1$) molecular shuttles the macrocyclic ring can adopt a conformation that allows interaction with *both* recognition states simultaneously is an important aspect of the shuttling mechanism for these rigid molecular systems. In an effort to induce this type of ambivalent structural conformation between axle and wheel, a model [2]rotaxane **R₁-Br** with one phenyl ring as the spacer was prepared. This compound lacks: 1) the aromatic groups at the 4- and 7-positions of the benzimidazole units of the axle as they are replaced by Br-atoms and 2) the aromatic groups of the crown ether since the wheel is simply **24C8**.^[13]

As shown for the X-ray structure of **4.1-Br** in Fig 4.7, the absence of secondary CH···O stabilizing interactions between axle and wheel—only the primary NH···O hydrogen bonds remain—the flexible **24C8** macrocyclic can indeed span the two recognition sites and is involved in a centrosymmetric conformation utilizing two NH···O hydrogen bonds to simultaneously interact with both benzimidazole sites; conceptually mimicking the transition state calculated for **4.1** using DFT. (Only a single set of peaks was observed in the

^1H NMR spectrum of **4.2** (THF- d_8) and **4.1-Br** (CD_2Cl_2) even at the lowest accessible temperature).

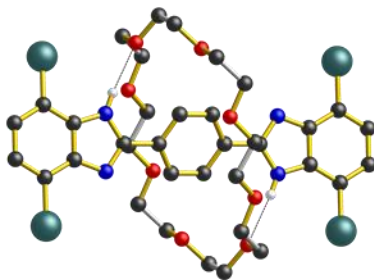


*Fig 4.7 – ball-and-stick representation of the single-crystal X-ray structure of the [2]rotaxane molecular shuttle **4.1-Br** ($n = 1$). Only H-atoms involved in hydrogen bonds are shown for clarity. Color key: teal = bromine, red = O; blue = N, black = C; white = H; gold bonds = axle; silver bonds = wheel.*

4.1.3 Conclusion

This study not only corroborates Hirose and co-workers' conclusions about the translational motion in molecular shuttles with a rigid axle – that the length of the axle does not affect the shuttling rate⁸ –it expands upon that single system demonstrating that, with one significant exception, both the neutral and dicationic forms of a class of rigid H-shaped [2]rotaxanes also show length-independent shuttling rates. Most importantly, we were able to identify a mechanism for shuttling that can act to lower the usual energy barrier if the axle length is short enough, even in a very rigid system. Finally, a pair of single-crystal X-ray structures provide interesting mechanistic insight into: 1) what the transition state structure for the passage of a **DB24C8** macrocycle between two well separated neutral recognition sites (two phenyl rings) during a shuttling event might look like and 2) what the structure of a “short-cut” transition state for a neutral shuttle with a short and rigid axle (one phenyl ring) could resemble.

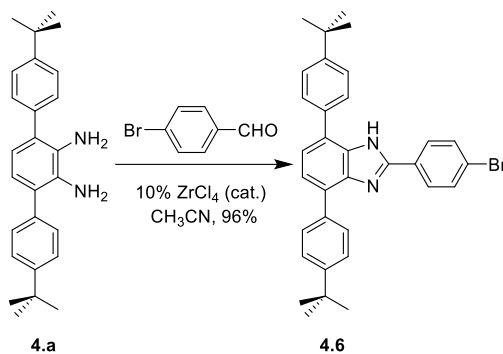
4.2. Experimental

4.2.1 General comments

4,7-Di(4'-t-butylphenyl)-benzothiodiazole,^[14]1,2-diamino-3,6-di(4'-t-butylphenyl)benzene (**4.a**),^[11] terphenyl-4,4'-dicarbaldehyde,^[15] 4'-bromo-4-triphenylbenzaldehyde^[16] and naphthalene-2,6-dicarbaldehyde^[17] were synthesized according to literature methods. Dibenzo[24]crown-8 ether **DB24C8** was purchased from TCI Chemical. 4,4'-dibromobiphenyl, 1,4-dibromobenzene and 4-t-butylphenylboronic acid were purchased from Sigma-Aldrich. The solvents were dried and distilled prior to use. Deuterated solvents were obtained from Cambridge Isotope Laboratories and used as received. ¹H, ¹³C, and 2D NMR spectra were recorded on Brüker Avance 500 or 300 instruments. All peak positions are listed in ppm relative to TMS. Melting point measurements were performed on MPA100 melting point apparatus. Column chromatography was performed using Silicycle Ultra-Pure Silica Gel (230–400 mesh).

4.2.2 Synthesis of 4.6

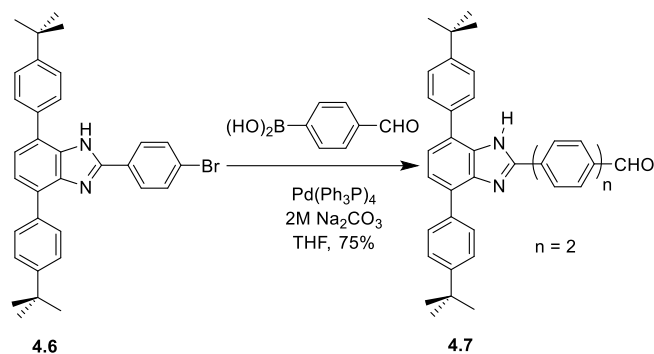
ZrCl₄ (3.20 mg, 0.0136 mmol) was added to a round bottom flask containing **4.a** (505 mg, 0.136 mmol). Bromobenzaldehyde (25.3 mg, 0.136 mmol) was diluted with CHCl₃ in a small vial and then transferred to the round bottom flask containing **4.a** and ZrCl₄. The orange solution was stirred for 24 h at RT. Then solvents were removed and a white solid residue was obtained. Yield 96% (70 mg). Mp: 257-259 °C. ¹H NMR (300 MHz, CDCl₃, 298 K) δ = 1.45 (s, 18H), 7.50 (s, 2H), 7.63, (m, 8H, J = 7.6 Hz), 7.97 (d, 4H, J = 7.9 Hz), 9.52 (br s, 1H). ¹³CNMR (300 MHz, CDCl₃, 298K) δ = 31.51, 34.79, 123.01, 124.57, 128.29, 128.52, 128.72, 132.23, 135.52, 150.37, 150.74. IR (neat): 3358, 3031, 2691, 2902, 2866, 1602, 1493, 1474, 1461, 1425, 1260 cm⁻¹. HR-MS (ESI): calcd for [M+H]⁺, [C₃₃H₃₃BrN₂]⁺, m/z = 537.1906, found m/z = 537.1905.



Scheme 4.2 – synthesis of 4.6.

4.2.3 Synthesis of 4.7

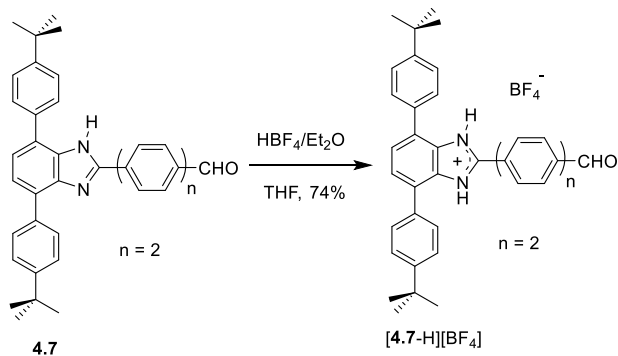
4.6 (100 mg, 0.178 mmol), 4-formylphenylboronic acid (69.46 mg, 0.391 mmol) and Pd(PPh₃)₄ (20.5 mg, 0.018 mmol) were added to a 100 mL Schlenk flask, degassed and backfilled with N₂. A solution of 2M Na₂CO₃ (11 mL, 120 eq.) and THF (11 mL, 120 eq.) were added and the yellow solution was refluxed (80 °C) for 24 h. The solution was cooled to room temperature; the organic layer was extracted with ethyl acetate (2 x 50 mL) and then dried over anhydrous MgSO₄. CH₃CN (20 mL) was added, the solution heated to reflux and then cooled to room temperature. The resulting solids were filtered and air dried producing a yellow solid. Yield 75% (91 mg). Mp: 191-194 °C. ¹H NMR (500 MHz, CDCl₃, 298 K) δ = 1.41 (s, 18H), 7.38 (d, 1H, *J* = 7.7 Hz), 7.55 (d, 1H, *J* = 7.7 Hz), 7.58 (d, 1H, *J* = 7.5 Hz), 7.56 (d, 2H, *J* = 7.5 Hz), 7.60 (d, 2H, *J* = 8.5 Hz), 7.64 (d, 2H, *J* = 8.5 Hz), 7.75 (d, 2H, *J* = 8.6) 7.80(d, 2H, *J* = 8.2 Hz), 7.97 (d, 2H, *J* = 8.45 Hz), 7.12 (d, 2H, *J* = 8.5 Hz), 8.18 (d, 2H, *J* = 8.5 Hz), 9.63 (s, 1H), 10.08 (s, 1H). ¹³C NMR (126 MHz, CDCl₃, 298 K) δ = 191.94, 150.91, 150.29, 146.10, 142.30, 140.96, 135.67, 135.46, 133.26, 131.43, 130.37, 129.97, 128.98, 127.72, 127.63, 127.41, 126.32, 125.47, 124.44, 123.39, 122.28, 34.64, 31.41. HR-MS (ESI): calcd for [M+H]⁺, [C₄₀H₃₈N₂O]⁺, *m/z* = 563.3018, found *m/z* = 563.3032.



Scheme 4.3 – synthesis of **4.7**.

4.2.4 Synthesis of **[4.7-H][BF₄]**

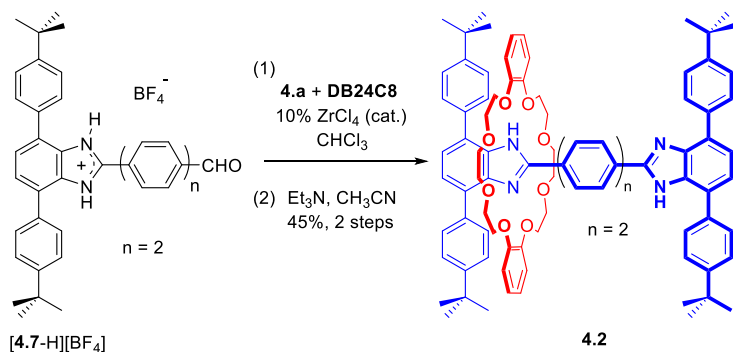
4.7 (118 mg, 0.220 mmol) was dissolved in diethyl ether (100 mL). Tetrafluoroboric acid diethyl ether complex (22 μL , 0.24 mmol) was added in a dropwise fashion. The resulting yellow solid was vacuum filtered and washed with ether. Yield 74% (87 mg). Mp: 214-217 °C. ¹H NMR (500 MHz, CD₃CN, 298 K) δ = 1.42 (s, 18H), 7.69 (s, 10H), 7.95 (d, 2H, J = 8.3 Hz), 8.01 (dd, 4H, J = 8.03 Hz), 8.15 (d, 2H, J = 8.6 Hz), 10.10 (s, 1H), 12.60 (br s, 2H). ¹³C NMR (125 MHz, CD₃CN, 298 K) δ = 192.32, 152.26, 151.06, 144.45, 132.50, 132.50, 130.41, 130.20, 129.94, 128.53, 128.21, 128.06, 127.59, 127.14, 126.43, 121.66, 121.66, 34.48, 30.60. HR-MS (ESI): calculated for $[\text{M}+\text{H}]^+$, $[\text{C}_{40}\text{H}_{38}\text{N}_2\text{O}]^+$, m/z = 563.3062, found m/z = 563.3063.



Scheme 4.4 – synthesis of **[4.7-H][BF₄]**.

4.2.5 Synthesis of 4.2

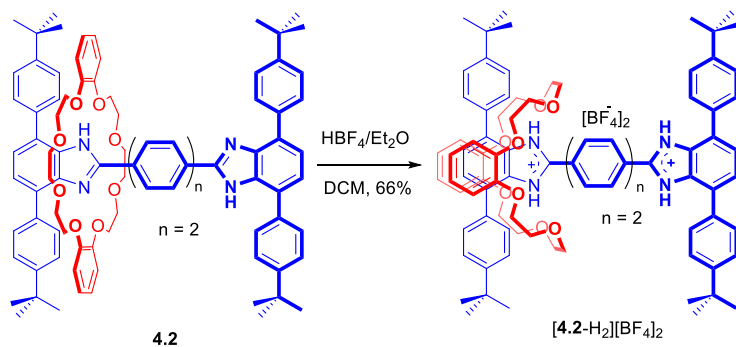
DB24C8 (179 mg, 0.399 mmol) was added to [**4.7-H**][BF₄] (65 mg, 0.109 mmol) in a round bottom flask. CHCl₃ (30 mL) was added and stirred at RT until a clear solution gained. 1,2-Diamino-3,6-di(4-*t*-butylphenyl)benzene **4.a** (41 mg, 0.109 mmol) was added, followed by ZrCl₄ (26 mg, 0.01 mmol) and the yellow solution was stirred at room temperature for 24 h. Then the mixture was filtered, solvents were evaporated and CH₃CN (30 mL) was added to dissolve the solids. After filtration the mixture, Et₃N (0.2 mL) was added to the filtrate and the formation of crystals was observed. The solids were filtered and air dried. Yield 45% (65 mg). Mp: >300 °C. ¹H NMR (500 MHz, CD₂Cl₂, 298 K) δ = 1.29 (d, 36H), 2.62 (s, 8H), 3.45 (s, 8H), 4.01 (s, 8H), 6.91 (m, 4H), 6.98 (m, 4H), 7.30 (d, 2H, *J* = 5.7 Hz), 7.32 (d, 4H, *J* = 8.4 Hz), 7.37 (d, 4H, *J* = 8.4 Hz), 7.55 (d, 2H, *J* = 7.3 Hz), 7.57 (d, 4H, *J* = 8.6 Hz), 7.80 (d, 4H, *J* = 8.4 Hz), 8.23 (d, 4H, *J* = 8.2 Hz), 8.66 (d, 4H, *J* = 8.5 Hz), 10.7 (s, 2H). ¹³C NMR (300 MHz, CDCl₃, 298K) δ = 152.46, 150.51, 148.86, 142.83, 135.93, 130.89, 129.66, 129.34, 128.18, 126.81, 126.23, 125.54, 123.43, 121.55, 121.26, 112.12, 69.38, 68.91, 68.60, 34.81, 31.53, 31.43. HR-MS (ESI): calcd for [M+H]⁺, [C₉₀H₉₈N₄O₈]⁺, *m/z* = 1363.7463, found *m/z* = 1363.7483.



Scheme 4.5 – synthesis of **4.2**.

4.2.6 Synthesis of [4.2-H₂][BF₄]₂

Tetrafluoroboric acid (2.8 μ L, 0.032 mmol) was added to **4.2** in CH₂Cl₂ (1 mL). After 30 min, the CH₂Cl₂ was removed and diethyl ether (20 mL) was added. The solution was sonicated and vacuum filtered. Yield 66% (13.7 mg). Mp: 217-220 °C. ¹H NMR (500 MHz, CD₃CN, 298 K) δ = 1.44 (s, 36H), 2.95 (m, 4H), 3.36 (m, 8H), 3.52 (m, 4H), 3.65 (m, 8H), 6.63 (m, 4H), 6.62 (m, 4H), 7.10 (s, 1H), 7.43 (d, 4H, J = 7.3 Hz), 7.62 (d, 4H, J = 7.3 Hz), 7.72 (d, 10H, J = 7.6 Hz), 8.12 (m, 4H, J = 8.1 Hz), 8.23 (d, 2H, J = 8.2 Hz), 8.54 (d, 2H, J = 8.5 Hz), 12.32 (s, 2H), 12.89 (s, 2H). ¹³C NMR (75 MHz, CD₃CN, 298 K) δ = 152.36, 152.11, 151.13, 150.95, 147.34, 142.23, 132.61, 132.33, 130.60, 129.96, 129.28, 128.75, 128.64, 128.10, 127.31, 126.72, 126.54, 126.34, 125.90, 124.91, 120.84, 112.49, 69.98, 69.74, 67.86, 34.55, 30.68. HR-MS (ESI): calculated for [M-(BF₄)₂]²⁺, [C₉₀H₁₀₀N₄O₈]²⁺, m/z = 682.3765, found m/z = 682.3756.

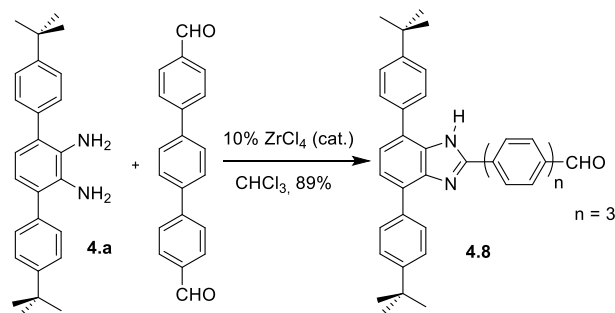


Scheme 4.6 – synthesis of [4.2-H₂][BF₄]₂.

4.2.7 Synthesis of 4.8

4.a (65 mg, 0.174 mmol) and terphenyl-4,4'-dicarbaldehyde (0.25 g, 0.873 mmol) were dissolved in CHCl₃. ZrCl₄ (4 mg, 0.017 mmol) was added. After 24 h stirring, the solution was filtered and solvent removed. The crude product was purified by column chromatography (SiO₂, dichloromethane). Yield: 100 mg, 89%. Mp: 185-190 °C. ¹H NMR

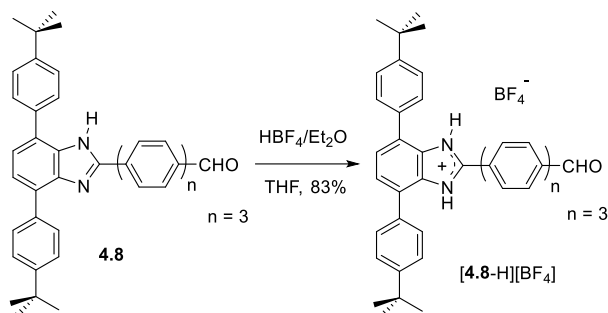
(300 MHz, CDCl₃, 298 K) δ = 1.42 (s, 18H), 7.47 (s, 2H), 7.58 (d, 4H, J = 7.5 Hz), 7.76 (m, 8H), 7.97 (d, 2H, J = 7.9 Hz), 8.1 (d, 2H, J = 8 Hz), 10.07 (s, 1H). ¹³C NMR (126 MHz, CDCl₃, 298 K) δ = 192.00, 151.12, 151.05, 146.58, 142.12, 141.89, 140.37, 139.69, 139.16, 135.63, 135.40, 130.46, 129.20, 127.98, 127.77, 127.66, 127.54, 127.33, 34.77, 31.50. H-MS (ESI): calcd for [M+H]⁺, [C₄₆H₄₃N₂O]⁺, m/z = 639.3370, found m/z = 639.3375.



Scheme 4.7 – synthesis of **4.8**.

4.2.8 Synthesis of [4.8-H][BF₄]

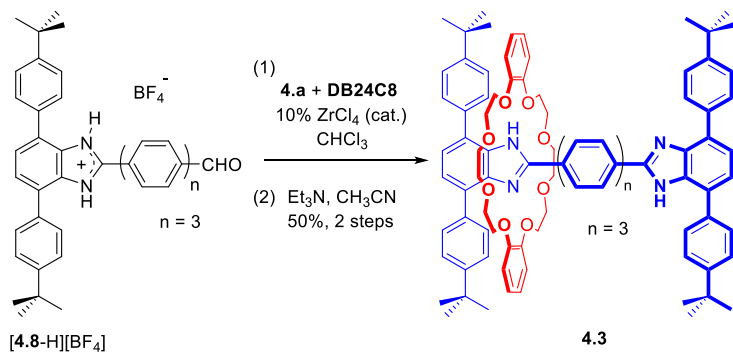
4.8 (100 mg, 0.16 mmol) was dissolved in THF (15 mL) and tetrafluoroboric acid diethyl ether complex (24 μ L, 0.176 mmol) was added. The resulting yellow solid was vacuum filtered and washed with diethyl ether. Yield 83% (93 mg). Mp: >300 °C. ¹H NMR (500 MHz, CD₃CN, 298 K) δ = 1.44 (s, 18H), 7.72 (m, 10H), 7.93 (m, 2H), 7.98 (s, 2H), 8.03 (d, 1H, J = 6.5 Hz), 8.07 (m, 2H), 8.17 (m, 2H), 10.08 (s, 1H), 12.45 (s, 2H). ¹³C NMR (125 MHz, CD₃CN, 298 K) δ = 153.12, 133.39, 131.25, 130.99, 130.76, 129.40, 128.94, 128.82, 128.64, 128.41, 128.01, 127.30, 71.00, 35.35, 31.45, 27.22. H-MS (ESI): calcd for [M-BF₄]⁺, [C₄₆H₄₃N₂O]⁺, m/z = 639.3370, found m/z = 639.3375.



Scheme 4.8 – synthesis of [4.8-H][BF₄].

4.2.9 Synthesis of 4.3

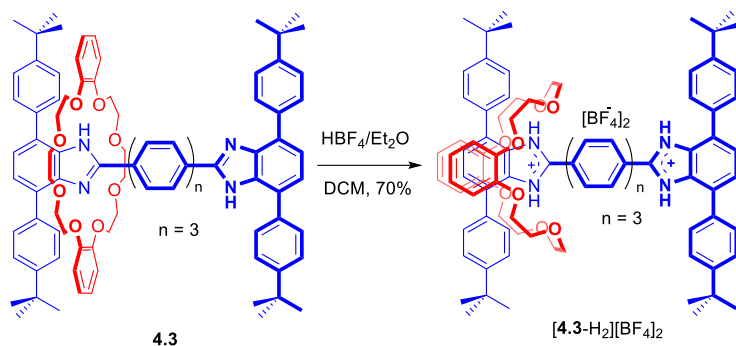
DB24C8 (0.25 g, 0.56 mmol) was added to [4.8-H][BF₄] (90 mg, 0.14 mmol) in a round bottom flask. CHCl₃ (20 mL) was added and the mixture stirred at RT until a clear solution formed. **4.a** (52.4 mg, 0.14 mmol) was added, followed by ZrCl₄ (32.6 mg, 0.014 mmol) and the yellow solution was stirred at RT for 24 h. The solution was filtered, solvents were evaporated and CH₃CN (20 mL) was added to dissolve the solids. After filtration the mixture, Et₃N (0.2 mL) was added to filtrate and solids were formed. The solution was filtered and air dried producing a white solid. Yield 50% (110 mg). Mp: 230-235 °C. ¹H NMR (500 MHz, CD₂Cl₂, 298 K) δ = 1.31 (s, 36H), 2.64 (s, 8H), 3.48 (s, 8H), 4.03 (s, 8H), 6.93 (m, 4H), 7.01 (m, 4H), 7.32 (m, 10H), 7.55 (d, 2H, *J* = 7.7 Hz), 7.59 (d, 4H, *J* = 8.2 Hz), 7.79 (d, 8H, *J* = 7.8 Hz), 8.26 (d, 4H, *J* = 8.2 Hz), 8.7 (d, 4H, *J* = 8.1 Hz), 10.77 (s, 2H). ¹³C NMR (125 MHz, CD₂Cl₂, 298 K) δ = 30.82, 30.92, 34.19, 68.00, 68.27, 68.74, 111.48, 120.63, 120.92, 122.79, 124.92, 125.61, 126.16, 127.00, 127.56, 128.72, 128.97, 129.14, 130.24, 135.31, 135.54, 139.27, 140.22, 148.25, 149.85, 150.12, 151.86. HR-MS (ESI): calcd for [M+H]⁺, [C₉₆H₁₀₃N₄O₈]⁺, *m/z* = 1439.7770, found *m/z* = 1439.7786.



Scheme 4.9 – synthesis of **4.3**.

4.2.10 Synthesis of **[4.3-H₂][BF₄]₂**

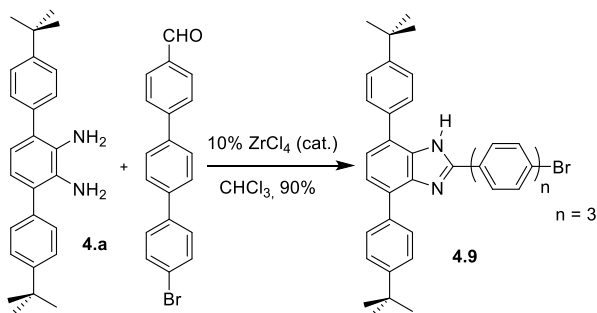
Tetrafluoroboric acid was added dropwise to **4.3** in CH₂Cl₂. After 30 min, CH₂Cl₂ was removed and diethyl ether was added. The solid was filtered and recrystallized from CH₃CN. Yield 70% (12 mg). Mp: >300°C. ¹H NMR (500 MHz, CD₃CN, 298 K) δ = 1.44 (d, 36H), 2.96 (dd, 4H), 3.15 (m, 4H), 3.34 (m, 8H), 3.55 (m, 8H), 6.34 (m, 4H), 6.63 (m, 4H), 7.08 (s, 2H), 7.44 (d, 4H, *J* = 8.35 Hz), 7.64 (d, 4H, *J* = 8.35 Hz), 7.72 (m, 12H), 8.01 (m, 4H), 8.11 (m, 4H), 8.18 (d, 2H, *J* = 8.5 Hz), 8.53 (d, 2H, *J* = 8.4 Hz), 12.33 (s, 2H), 12.91 (s, 2H). ¹³C NMR (125 MHz, CD₃CN, 298 K) δ = 31.41, 35.26, 68.56, 70.44, 70.65, 113.19, 121.50, 121.76, 125.30, 125.49, 126.57, 126.95, 127.20, 127.87, 128.33, 128.50, 128.68, 128.81, 129.32, 129.45, 130.00, 130.73, 131.16, 132.93, 133.37, 139.57, 144.11, 148.05, 151.93, 152.05, 152.77, 153.01. HR-MS (ESI): calcd for [M-(BF₄)₂]²⁺, [C₉₆H₁₀₄N₄O₈]²⁺, *m/z* = 1440.7843, found *m/z* = 1440.7831.



Scheme 4.10 – synthesis of $[4.3-H_2][BF_4]_2$.

4.2.11 Synthesis of 4.9

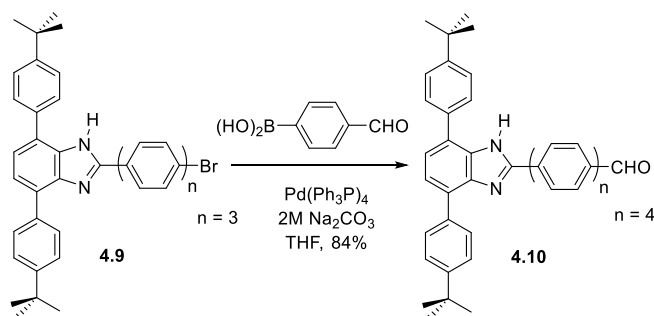
4.a (300 mg, 0.805 mmol) and 4'-bromo-4-triphenylbenzaldehyde (271 mg, 0.805 mmol) were dissolved in $CHCl_3$. $ZrCl_4$ (18.7 mg, 0.08 mmol) was added. After 24 h stirring, the solution was filtered and solvent removed. The crude product was purified by recrystallization with ethyl acetate. Yield 90% (500 mg). Mp: 238-240°C. 1H NMR (500 MHz, $CDCl_3$, 298 K) δ = 1.42 (s, 18H), 7.45 (s, 2H), 7.52 (d, 2H, J = 7.5 Hz), 7.58 (d, 2H, J = 7.5 Hz), 7.65 (d, 3H, J = 7.6 Hz), 7.72 (dd, 4H, J = 7.7 Hz), 7.8 (s, 3H), 8.19 (d, 2H, J = 8.1 Hz), 10.01 (s, 1H). ^{13}C NMR (125 MHz, $CDCl_3$, 298 K) δ = 31.50, 34.81, 121.91, 123.29, 126.09, 127.35, 127.47, 127.65, 128.40, 128.71, 132.09, 135.16, 139.47, 139.61, 142.37, 150.85, 150.99. H-MS (ESI): calcd for $[M+H]^+$, $[C_{45}H_{42}BrN_2]^+$, m/z = 689.2526, found m/z = 689.2531.



Scheme 4.11 – synthesis of **4.9**.

4.2.12 Synthesis of 4.10

4.9 (300 mg, 0.43 mmol), 4-formylphenylboronic acid (65.2 mg, 0.43 mmol) and $\text{Pd}(\text{PPh}_3)_4$ (34 mg, 0.029 mmol) were added to a 100 mL Schlenk flask, degassed and backfilled with N_2 . A solution of 2M Na_2CO_3 (100 mL) and THF (100 mL) were added and the yellow solution refluxed (80 °C) for 24 h. The solution was cooled to room temperature, the organic layer was extracted with CH_2Cl_2 (2 x 50 mL) and the solution was dried over anhydrous MgSO_4 . The product was recrystallized from acetonitrile to give a yellow solid, Yield 85% (260 mg). Mp: 185-190 °C, ^1H NMR (500 MHz, CD_2Cl_2 , 298 K) δ = 1.42 (s, 18H), 7.39 (d, 1H, J = 7.7 Hz), 7.52 (d, 1H, J = 7.7 Hz), 7.58 (d, 2H, J = 8.4 Hz), 7.64 (dd, 4H, J = 8.4 Hz), 7.80 (d, 4H, J = 8.6 Hz), 7.81 (s, 4H), 7.85 (dd, 4H, J = 6.5 Hz), 7.97 (d, 2H, J = 8.3 Hz), 8.08 (d, 2H, J = 8.4 Hz), 8.18 (d, 2H, J = 8.4 Hz), 9.7 (s, 1H), 10.06 (s, 1H). ^{13}C NMR (125 MHz, CD_2Cl_2 298K) δ = 192.04, 150.71, 135.89, 130.50, 129.26, 128.13, 127.82, 127.79, 127.71, 127.39, 126.79, 125.63, 124.80, 123.38, 122.28, 70.78, 34.94, 31.42. HR-MS (ESI): calcd for $[\text{M}+\text{H}]^+$, $[\text{C}_{52}\text{H}_{47}\text{N}_2\text{O}]^+$, m/z = 715.3683, found m/z = 715.3688.

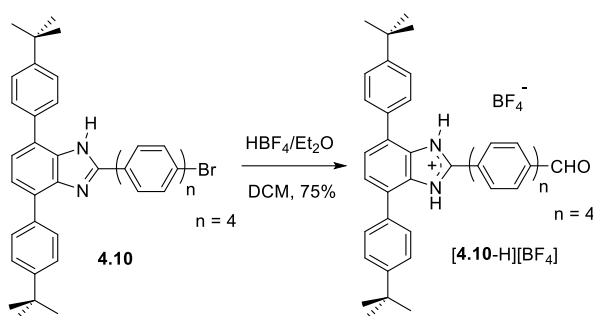


Scheme 4.12 – synthesis of **4.10**.

4.2.13 Synthesis of [4.10-H][BF₄]

Tetrafluoroboric acid was added dropwise to **4.10** in CH_2Cl_2 . After 30 min, CH_2Cl_2 was removed and diethyl ether was added. The solids were filtered and recrystallized from

CH₃CN. Yield 75% (150 mg) Mp: 235-240 °C. ¹H NMR (500 MHz, CD₃CN, 298 K) δ = 1.45 (s, 18H) 7.73 (m, 10H), 7.8 (d, 4H, J = 7.8 Hz), 7.93 (d, 4H, J = 8.4 Hz), 7.96 (d, 2H, J = 8.3 Hz), 8.01 (d, 2H, J = 8.4 Hz), 8.06 (d, 2H, J = 8.6 Hz), 8.1 (d, 2H, J = 8.5 Hz), 10.08 (s, 1H), 12.33 (s, 2H). ¹³C NMR (125 MHz, CD₃CN, 298 K) δ = 193.21, 153.23, 152.19, 146.79, 146.50, 141.38, 140.87, 139.78, 139.00, 136.61, 133.49, 131.30, 131.07, 130.83, 129.53, 128.85, 128.82, 128.60, 128.52, 128.46, 128.10, 127.43, 121.59, 35.47, 31.58. HR-MS (ESI): calcd for [M-BF₄]⁺, [C₅₂H₄₇N₂O]⁺, m/z = 715.3683, found m/z = 715.3688.

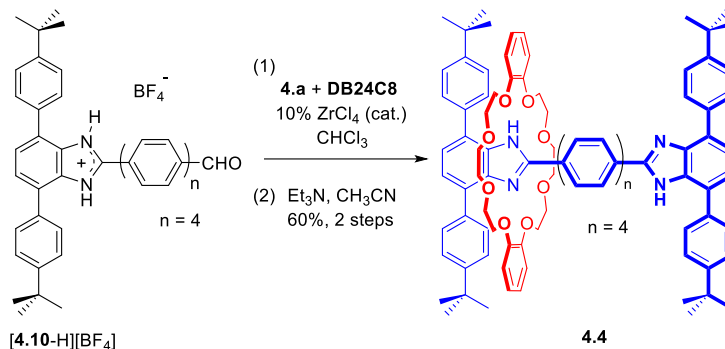


Scheme 4.13 – synthesis of [4.10-H][BF₄].

4.2.14 Synthesis of 4.4

DB24C8 (0.25 g, 0.56 mmol) was added to [4.10-H][BF₄] (90 mg, 0.14 mmol) in a round bottom flask. CHCl₃ (20 mL) was added and the mixture stirred at room temperature until a clear solution formed. **4.a** (52.4 mg, 0.14 mmol) was added, followed by ZrCl₄ (32.6 mg, 0.014 mmol) and the yellow solution was stirred at RT for 24 h. The solution was filtered, solvents were evaporated and CH₃CN (20 mL) was added to dissolve the solids. After filtration the mixture, Et₃N (0.2 mL) was added to the filtrate and formation of a solid was observed. The solution was filtered and air dried producing a white solid. Yield 60% (120 mg). Mp: >300 °C. ¹H NMR (500 MHz, CD₂Cl₂, 298 K) δ = 1.32 (36H), 2.62 (s, 8H), 3.46 (s, 8H), 4.01 (s, 8H), 6.92 (m, 4H), 6.98 (m, 4H), 7.30 (dd, 6H, J = 7.7 Hz), 7.37 (d, 4H, J = 8.4 Hz), 7.53 (d, 2H, J = 7.7 Hz), 7.57 (d, 4H, J = 8.3 Hz), 7.76 (m, 12H), 8.24 (d, 4H, J = 8.4 Hz),

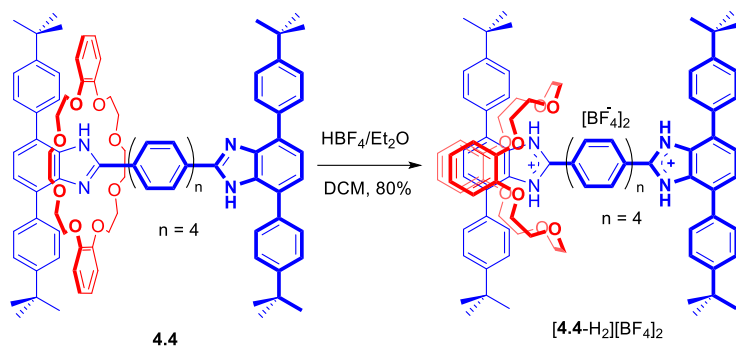
8.69 (d, 4H, $J = 8.1$ Hz), 10.76 (s, 2H). ^{13}C NMR (125 MHz, CD_2Cl_2 , 298 K) $\delta = 30.13, 31.03, 31.47, 31.57, 34.85, 53.43, 53.65, 53.86, 54.08, 54.30, 68.66, 68.94, 69.41, 112.15, 121.29, 121.58, 123.45, 125.17, 125.58, 126.27, 126.84, 127.68, 127.73, 128.22, 129.39, 129.83, 130.93, 135.97, 136.21, 139.87, 140.00, 142.89, 148.92, 150.52, 152.53$. HR-MS (ESI): calcd for $[\text{M}+\text{H}]^+$, $[\text{C}_{102}\text{H}_{107}\text{N}_4\text{O}_8]^+$, $m/z = 1516.8117$, found $m/z = 1516.8123$.



Scheme 4.14 – synthesis of **4.4**.

4.2.15 Synthesis of [4.4-H₂][BF₄]₂

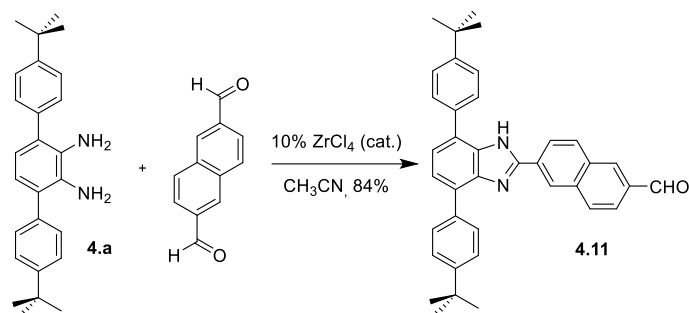
Tetrafluoroboric acid was added dropwise to **4.4** in CH_2Cl_2 . After 30 min, CH_2Cl_2 was removed and diethyl ether was added. The solid was filtered and recrystallized from CH_3CN . Yield 80% (13.5 mg). Mp: > 300 °C. ^1H NMR (500 MHz, CD_3CN , 298 K) $\delta = 1.43$ (s, 36H), 2.95 (m, 4H), 3.33 (m, 8H), 3.55 (m, 4H), 3.65 (m, 8H), 6.32 (m, 4H), 6.61 (m, 4H), 7.07 (s, 2H), 7.43 (d, 4H, $J = 8.3$ Hz), 7.62 (d, 4H, $J = 8.3$ Hz), 7.69 (m, 12H), 7.92 (m, 8H), 8.06 (m, 4H), 8.16 (d, 2H, $J = 8.5$ Hz), 8.51 (d, 2H, $J = 8.3$ Hz), 12.29 (s, 2H), 12.90 (s, 2H). ^{13}C NMR (125 MHz, CD_3CN , 298 K) $\delta = 31.47, 35.34, 68.65, 70.54, 70.75, 113.28, 121.59, 125.55, 126.67, 126.96, 127.07, 127.33, 128.00, 128.40, 128.55, 128.59, 128.78, 129.43, 129.54, 130.11, 130.75, 131.25, 133.01, 133.40, 133.48, 139.03, 140.75, 146.42, 148.14, 152.12, 152.86, 153.12$. HR-MS (ESI): calcd for $[\text{M}-(\text{BF}_4)_2]^{2+}$, $[\text{C}_{102}\text{H}_{108}\text{N}_4\text{O}_8]^{2+}$, $m/z = 1516.8156$, found $m/z = 1516.8153$.



Scheme 4.15 – synthesis of $[4.4-H_2][BF_4]_2$.

4.2.16 Synthesis of 4.11

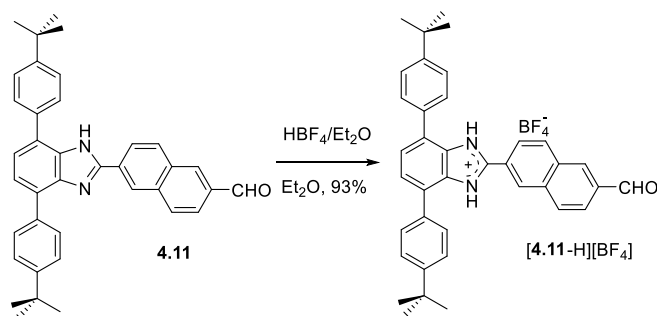
4.a (130 mg, 0.36 mmol), naphthalene-2,6-dicarbaldehyde (330 mg, 1.8 mmol), and $ZrCl_4$ (4.2 mg, 0.18 mmol) were added to 50 mL of CH_3CN . The mixture was stirred in open air at room temperature for 24 h. Et_3N (0.5 mL) and $CHCl_3$ (20 mL) were added and the mixture was filtered. The solvents of the filtrate were removed on a rotary evaporator. The residue was purified by column chromatography using dichloromethane as eluent. Further washing with acetonitrile gave the pure product as a pale yellow solid. Yield: 162 mg, 84%. Mp: 280-283 °C. 1H NMR (300 MHz, $DMSO-d_6$, 298 K) δ = 12.93 (s, 1H), 10.18 (s, 1H), 9.03 (s, 1H), 8.64 (s, 1H), 8.58 (d, 1H, J = 8.7 Hz), 8.30 (d, 1H, J = 8.7 Hz), 8.18 (d, 1H, J = 8.7 Hz), 8.14 (d, 2H, J = 8.4 Hz), 7.96 (d, 1H, J = 8.7 Hz), 7.70 (d, 2H, J = 8.4 Hz), 7.60 (d, 2H, J = 8.4 Hz), 7.57 (d, 2H, J = 8.4 Hz), 7.50 (d, 1H, J = 8.4 Hz), 7.31 (d, 1H, J = 8.4 Hz), 1.39 (s, 9H), 1.37 (s, 9H). ^{13}C NMR (75 MHz, $DMSO-d_6$, 298 K) δ = 193.5, 152.2, 150.5, 150.1, 142.7, 136.3, 135.9, 135.6, 135.0, 134.7, 134.3, 133.3, 131.1, 130.4, 130.1, 129.2, 128.7, 127.2, 126.7, 126.3, 125.7, 125.5, 124.2, 123.7, 121.8, 31.7, 31.7. HR-MS (ESI): calcd for $[M+H]^+$, $[C_{38}H_{37}N_2O]^+$, m/z = 537.2861, found m/z = 537.2907.



Scheme 4.16 – synthesis of **4.11**.

4.2.17 Synthesis of [4.11-H][BF₄]

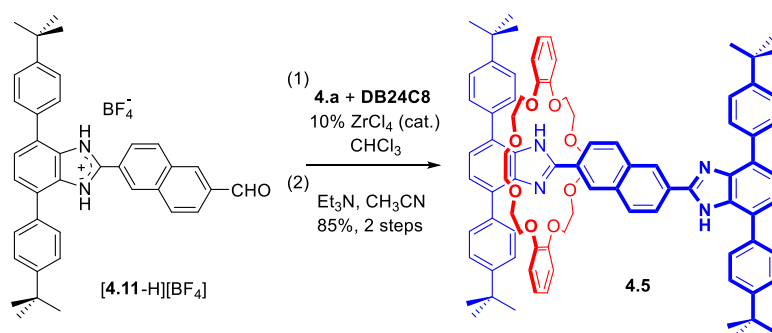
Tetrafluoroboric acid diethyl ether complex (36 μL , 0.26 mmol) was added to a mixture of **4.11** (130 mg, 0.24 mmol) in diethyl ether (100 mL) with stirring. After stirred for 10 min, the resulting white solid was filtered, rinsed with diethyl ether and air dried. Yield: 141 mg, 93%. Mp 240–243 °C. ^1H NMR (500 MHz, CD_3CN , 298 K) δ = 12.45 (br s, 2H), 10.21 (s, 1H), 8.76 (s, 1H), 8.60 (s, 1H), 8.38 (d, 1H, J = 8.5 Hz), 8.23 (d, 1H, J = 8.5 Hz), 8.15 (d, 1H, J = 8.5 Hz), 8.08 (d, 1H, J = 8.5 Hz), 7.72 (s, 2H), 7.70 (m, 8H), 1.42 (s, 18H). ^{13}C NMR (125 MHz, CD_3CN , 298 K) δ = 192.4, 152.3, 150.9, 136.6, 135.1, 134.75, 133.8, 132.4, 131.4, 130.9, 130.2, 130.0, 128.6, 127.6, 127.3, 126.5, 125.9, 124.5, 121.7, 34.5, 30.6. HR-MS (ESI): calcd for $[\text{M-BF}_4]^+$, $[\text{C}_{38}\text{H}_{37}\text{N}_2\text{O}]^+$, m/z = 537.2900, found m/z = 537.2908.



Scheme 4.17 – synthesis of $[\text{4.11-H}][\text{BF}_4]$.

4.2.18 Synthesis of 4.5

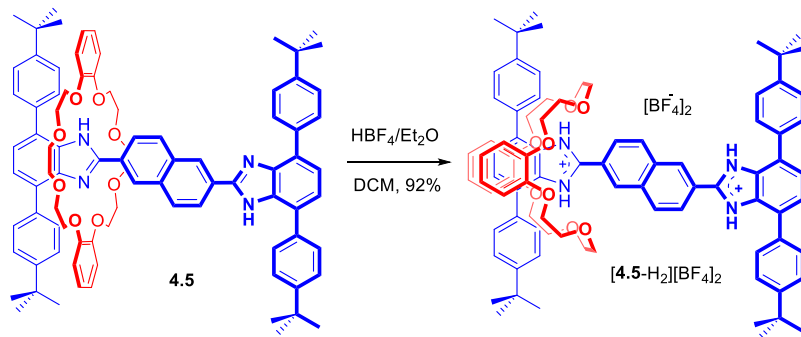
[**4.11-H**][BF₄] (94 mg, 0.15 mmol) and **DB24C8** (135 mg, 0.30 mmol) were stirred in CHCl₃ (20 mL) until a clear solution resulted. **4.a** (57 mg, 0.154 mmol) was added followed by ZrCl₄ (3.6 mg, 0.015 mmol). The mixture was stirred at room temperature overnight, filtered and the filtrate was concentrated under vacuum. The residue was washed with diethyl ether twice and air dried. The dried solid was dissolved in CH₃CN (30 mL) and filtered. Et₃N (0.2 mL) was added to the filtrate. The mixture was heated to reflux and allowed to cool to room temperature. The pale yellow solid was filtered, washed with CH₃CN, and air dried. Yield: 171 mg. 85%. Mp: > 300 °C. ¹H NMR (500 MHz, CD₂Cl₂, 298 K) δ = 10.70 (br s, 1H), 9.08 (s, 2H), 8.70 (d, 2H, *J* = 4.2 Hz), 8.22 (d, 4H, *J* = 8.5 Hz), 7.81 (d, 2H, *J* = 4.2 Hz), 7.54 (d, 4H, *J* = 8.5 Hz), 7.49 (d, 2H, *J* = 8.4 Hz), 7.32 (m, 10H), 6.96 (m, 8H), 3.97 (s, 8H), 3.36 (s, 8H), 2.44 (s, 8H), 1.25 (s, 36H). ¹³C NMR (125 MHz, CD₃CN, 298 K) δ = 192.4, 152.3, 150.9, 136.6, 135.1, 134.75, 133.8, 132.4, 131.4, 130.9, 130.2, 130.0, 128.6, 127.6, 127.3, 126.5, 125.9, 124.5, 121.7, 34.5, 30.6. ¹³C NMR (75 MHz, CD₂Cl₂) δ 152.47, 150.45, 150.13, 148.53, 142.57, 135.77, 135.56, 133.53, 133.42, 130.62, 129.03, 128.64, 128.27, 127.82, 126.99, 125.93, 125.18, 124.77, 123.10, 121.20, 121.03, 111.87, 69.08, 68.55, 68.34, 34.50, 34.45, 31.18, 31.11. HR-MS (ESI): calcd for [M+H]⁺, [C₈₈H₉₇N₄O₈]⁺, *m/z* = 1337.7301, found *m/z* = 1337.7306.



Scheme 4.18 – synthesis of **4.5**.

4.2.19 Synthesis of [4.5-H₂][BF₄]₂

Tetrafluoroboric acid diethyl ether complex (28 μ L, 0.20 mmol) was added to a mixture of **4.5** (67 mg, 0.05 mmol) in dichloromethane (10 mL) with stirring. The solvent of the mixture was removed under vacuum. The residue was washed by diethyl ether and air dried. Yield: (70 mg) 92%. Mp: > 300 $^{\circ}$ C. ¹H NMR (500 MHz, CD₃CN, 298 K) δ = 12.99 (br s, 2H), 12.46 (br s, 2H), 9.13 (s, 1H), 8.87 (s, 1H), 8.65 (d, 1H, J = 4.1 Hz), 8.44 (d, 1H, J = 4.1 Hz), 8.34 (d, 1H, J = 4.1 Hz), 8.21 (d, 1H, J = 4.1 Hz), 7.71-7.77 (m, 6H), 7.65 (d, 4H, J = 8.5 Hz), 7.44 (d, 4H, J = 8.5 Hz), 7.13 (s, 2H), 8.38 (d, 1H, J = 8.5 Hz), 8.23 (d, 1H, J = 8.5 Hz), 8.15 (d, 1H, J = 8.5 Hz), 8.08 (d, 1H, J = 8.5 Hz), 7.13 (s, 2H), 6.64 (m, 4H), 6.37 (m, 4H), 3.66-3.35 (m, 8H), 3.60 (m, 4H), 3.48 (m, 4H), 3.39 (m, 4H), 2.75 (m, 4H), 1.43 (s, 36H). ¹³C NMR (125 MHz, CD₃CN, 298 K) δ = 152.31, 152.15, 150.85, 150.57, 147.34, 133.72, 133.53, 132.51, 132.47, 132.23, 131.64, 130.26, 130.06, 129.30, 129.23, 128.89, 128.83, 128.57, 127.69, 127.37, 126.53, 126.44, 126.13, 126.02, 125.92, 125.13, 121.30, 120.88, 112.55, 69.93, 69.82, 67.83, 34.51, 30.66, 30.64. HR-MS (ESI): calcd for [M-BF₄]⁺, [C₄₄H₅₀N₂O₄]⁺, m/z = 670.3765, found m/z = 670.3732.



Scheme 4.19 – synthesis of [4.5-H₂][BF₄]₂.

4.2.20 Determination of the rate of shuttling for neutral [2]Rotaxanes

The shuttling rates were calculated from a line shape analysis of the NMR spectra using the program DNMR71.EXE.^[18]

$$K_c = \pi\Delta\nu / \sqrt{2}$$

k_c is the rate of shuttling at coalescence temperature. $\Delta\nu$ is the limiting chemical shift (in Hz) between the exchanging proton resonances and can be determined by variable-temperature NMR. The Eyring equation,^[19] $\Delta G_c^\ddagger = -RT_c \ln(k_c h / k_B T_c)$, was used to estimate ΔG_c^\ddagger and extrapolate the rate of shuttling to other temperatures. T_c is the coalescence temperature, R is the gas constant, h is Planck's constant, and k_B is Boltzmann's constant. The neutral species **4.1** could not be cooled down far enough to attain the limiting chemical shifts. We observed the coalescence temperature at 183 K, but nothing further. This data has been published^[11] and the VT spectra are available in the ESI of that article. By assuming the separation of the limiting peaks to be approximately 1000 Hz – this is about the average of the other (n = 2,3,4) samples – we roughly estimated an upper value for ΔG_c^\ddagger to be 7.73 kcal/mol.

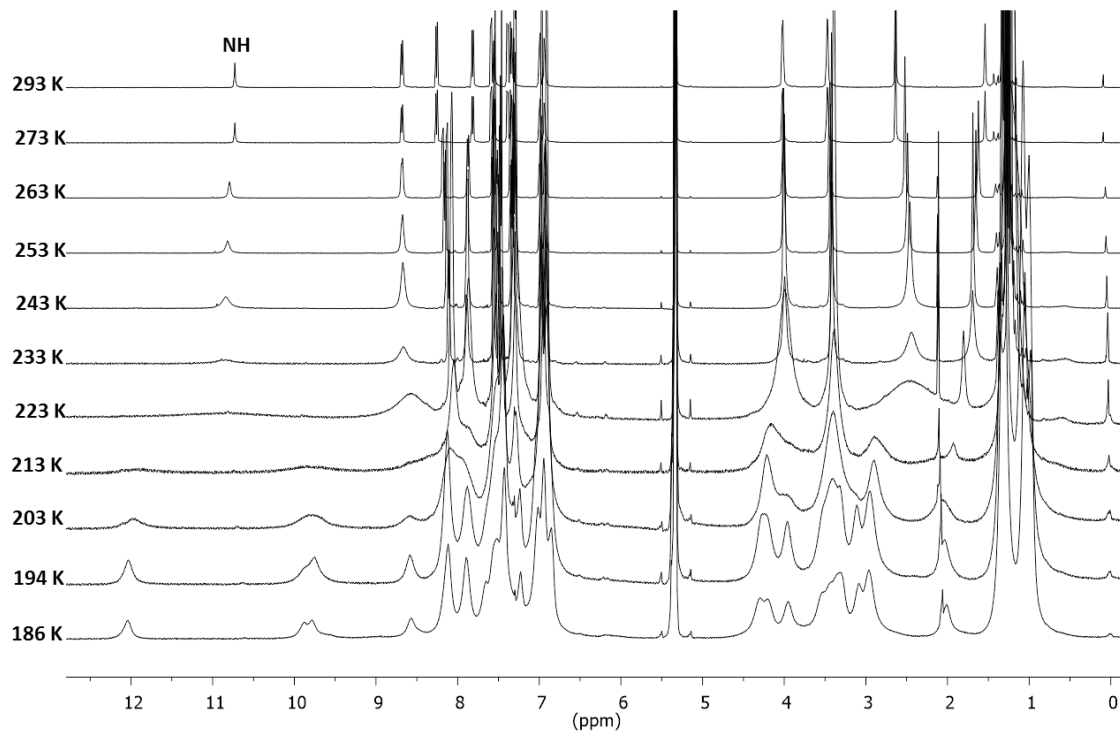


Fig 4.8 – variable temperature ^1H NMR of **4.2** (500 MHz, CD_2Cl_2).

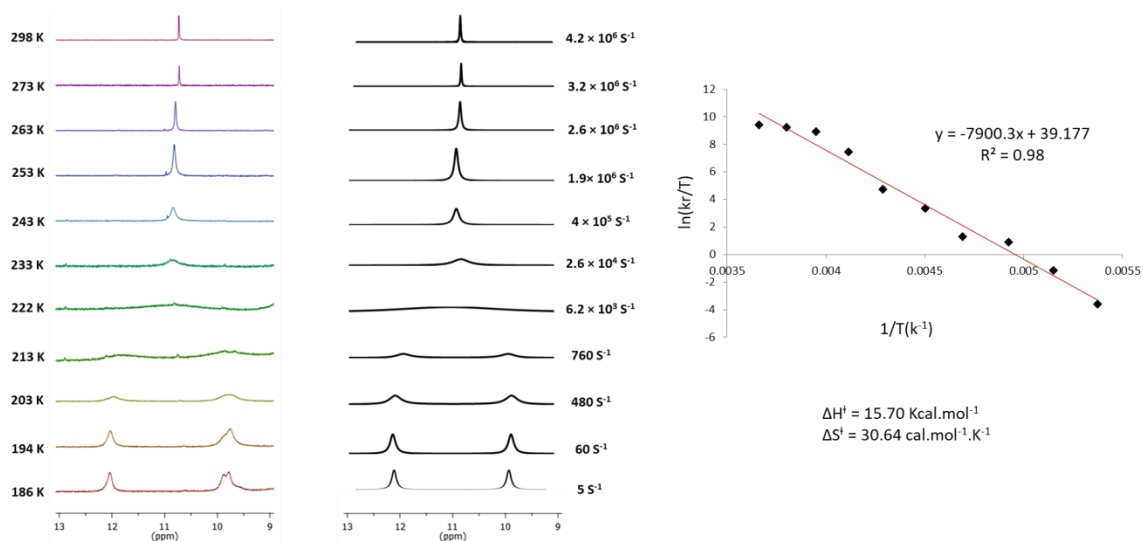


Fig 4.9 – comparison of the experimental and simulation ^1H NMR data (left) and Eyring plot generated from the simulated data (right) for **4.2**.

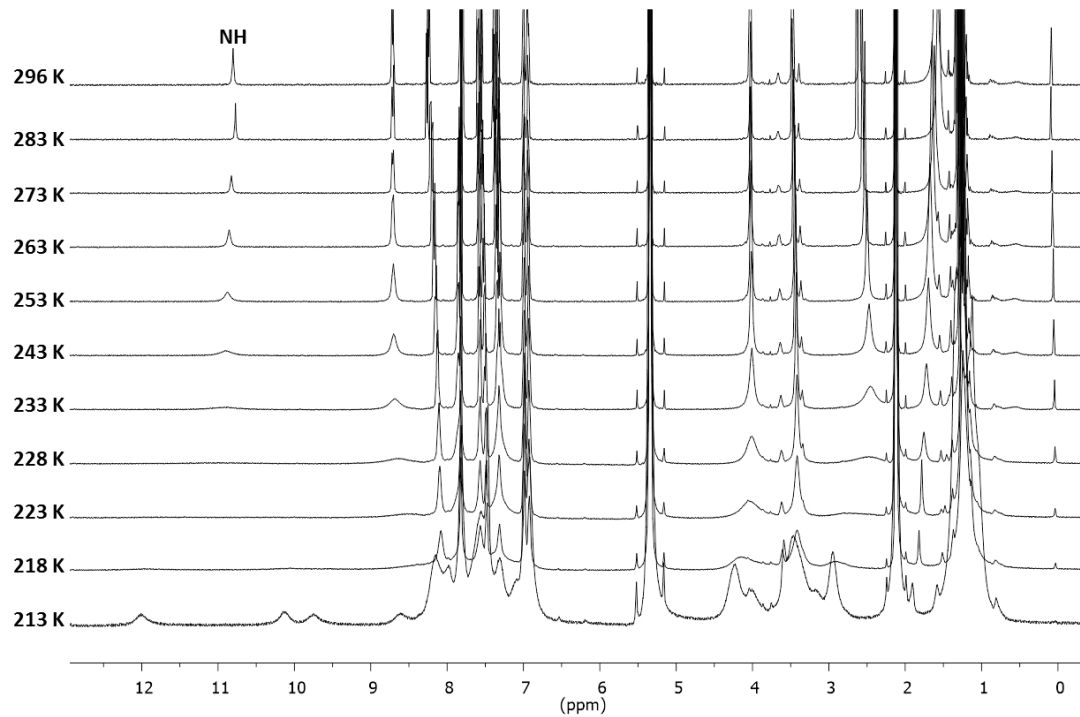


Fig 4.10 – variable temperature ^1H NMR of **4.3** (500 MHz, CD_2Cl_2).

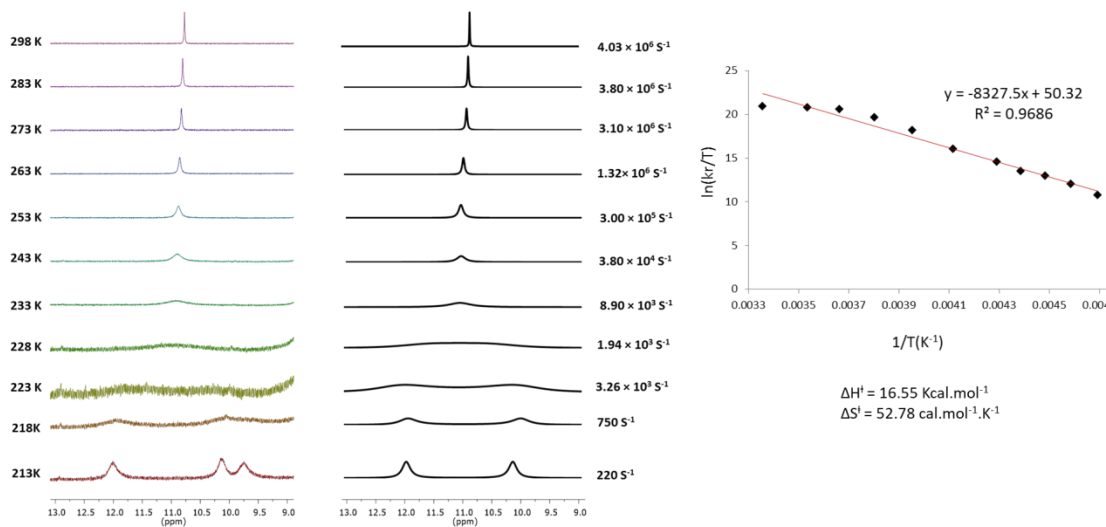


Fig 4.11 – comparison of the experimental and simulation ^1H NMR data (left) and Eyring plot generated from the simulated data (right) for **4.3**.

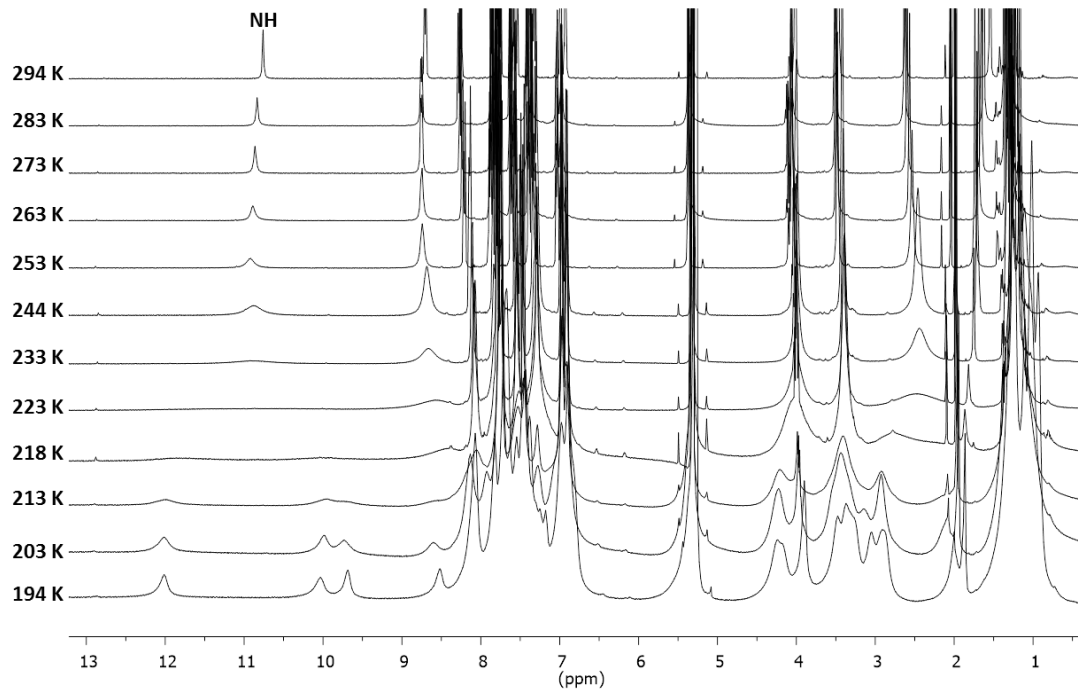


Fig 4.12 – variable temperature ^1H NMR of **4.4** (500 MHz, CD_2Cl_2).

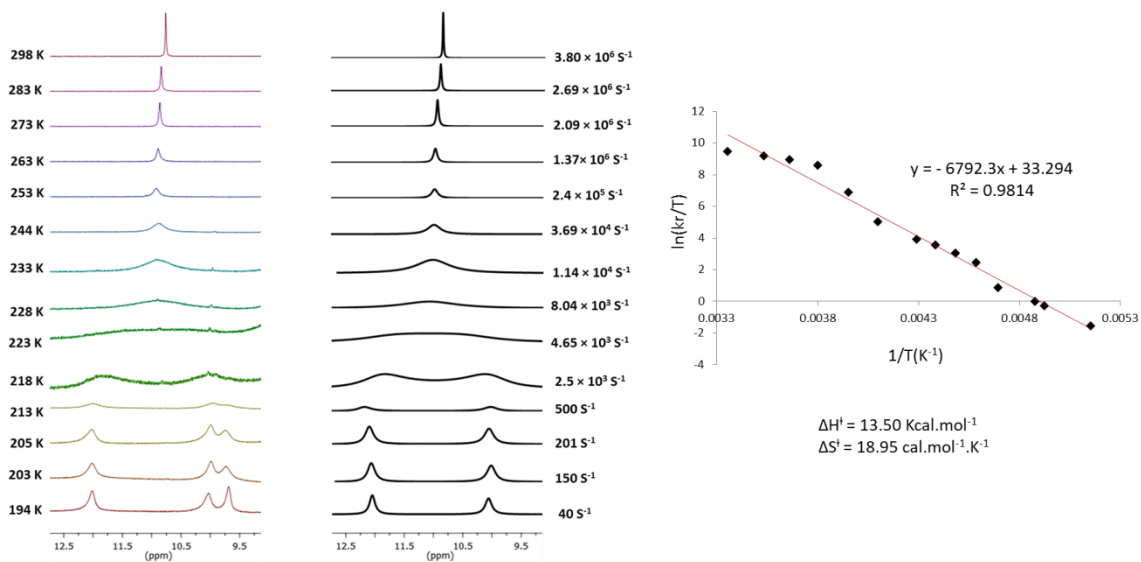


Fig 4.13 – comparison of the experimental and simulation ^1H NMR data (left) and Eyring plot generated from the simulated data (right) for **4.4**.

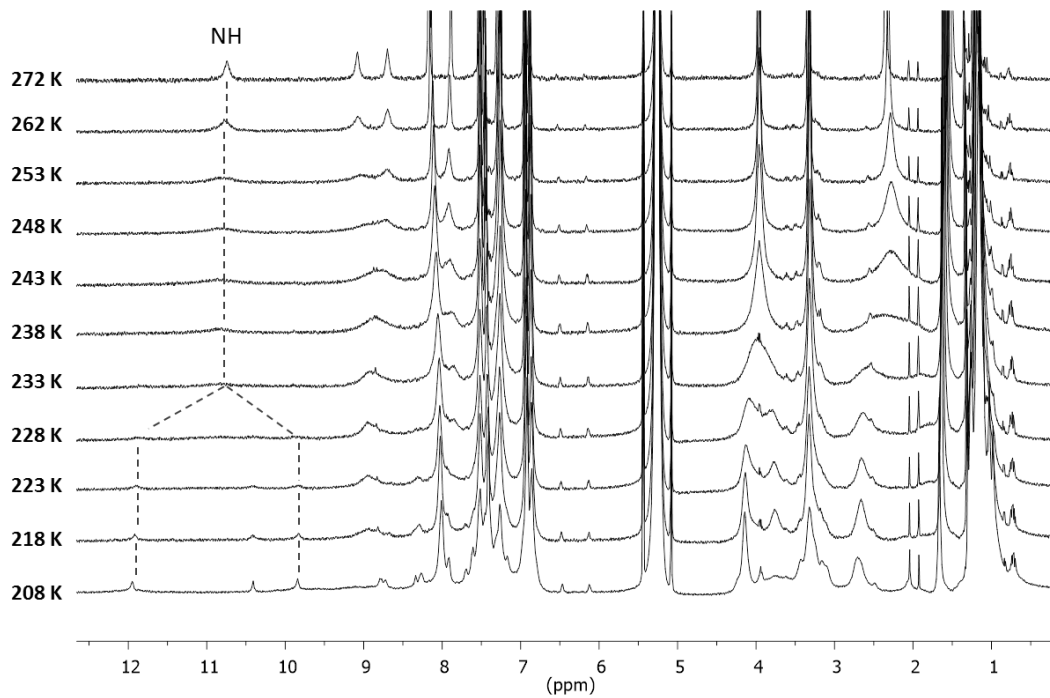


Fig 4.14 – variable temperature ^1H NMR of **4.5** (500 MHz, CD_2Cl_2).

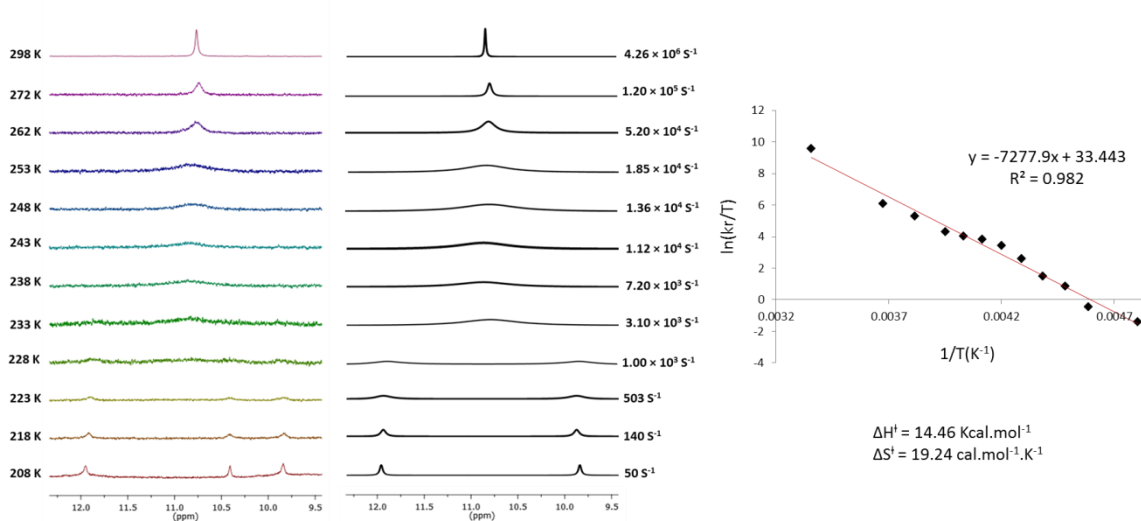


Fig 4.15 – comparison of the experimental and simulation ^1H NMR data (left) and Eyring plot generated from the simulated data (right) for **4.5**.

4.2.21 Shuttling rates for series of neutral [2]rotaxanes

Table 4.2 – summary of shuttling rates for neutral [2]rotaxane molecular shuttles.

shuttle	$\Delta\nu(\text{Hz})$	$T_c(\text{K})$	$k_c(\text{s}^{-1})$	$k_{(298\text{K})}(\text{s}^{-1})$	$\Delta G_c^\ddagger(\text{kcal/mol})$	$\Delta G_{(298)}^\ddagger(\text{kcal/mol})$
4.2	1080	222	6200	4.20×10^6	9.01	8.41
4.3	932	228	3264	4.03×10^6	9.56	8.44
4.4	999	223	4650	3.80×10^6	9.18	8.47
4.5	609	233	3100	4.26×10^6	9.80	8.40

4.2.22 Determination of the rate of shuttling for dicationic [2]Rotaxanes

The shuttling rate for dicationic [2]rotaxanes can be obtained by using the equations shown below, where I_{AA} and I_{BB} are the diagonal peak intensities and I_{AB} and I_{BA} are the cross-peak intensities. k is the sum of the forward, k_1 , and backward, k_{-1} , pseudo-first order rate constants for the shuttling process. k_1 and k_{-1} are equal due to the identical stations and thus the observed pseudo-first order rate constant, k_{obs} can be determined. R is the ideal gas constant, h is Planck's constant and k_B is Boltzmann's constant.

$$r = (I_{AA} + I_{BB}) / (I_{AB} + I_{BA}), \quad k = 1/\tau_m \ln(r + 1/r - 1), \quad k = k_1 + k_{-1}, \quad k_{\text{obs}} = k_1 = k_{-1}$$

$$\Delta G^\ddagger = -RT \ln(k_{\text{obs}} h / k_B T)$$

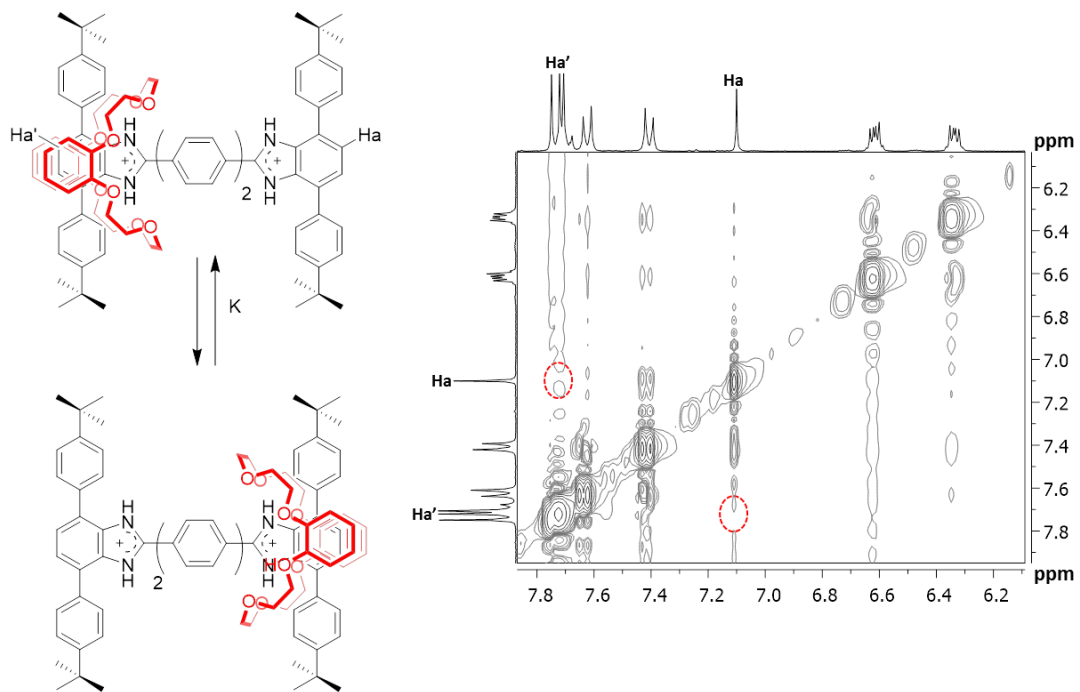


Fig 4.16 – partial 2D ^1H - ^1H EXSY (300 MHz, 295K, CD_3CN) spectrum of $[\mathbf{4.2}\text{-H}_2][\text{BF}_4]_2$.

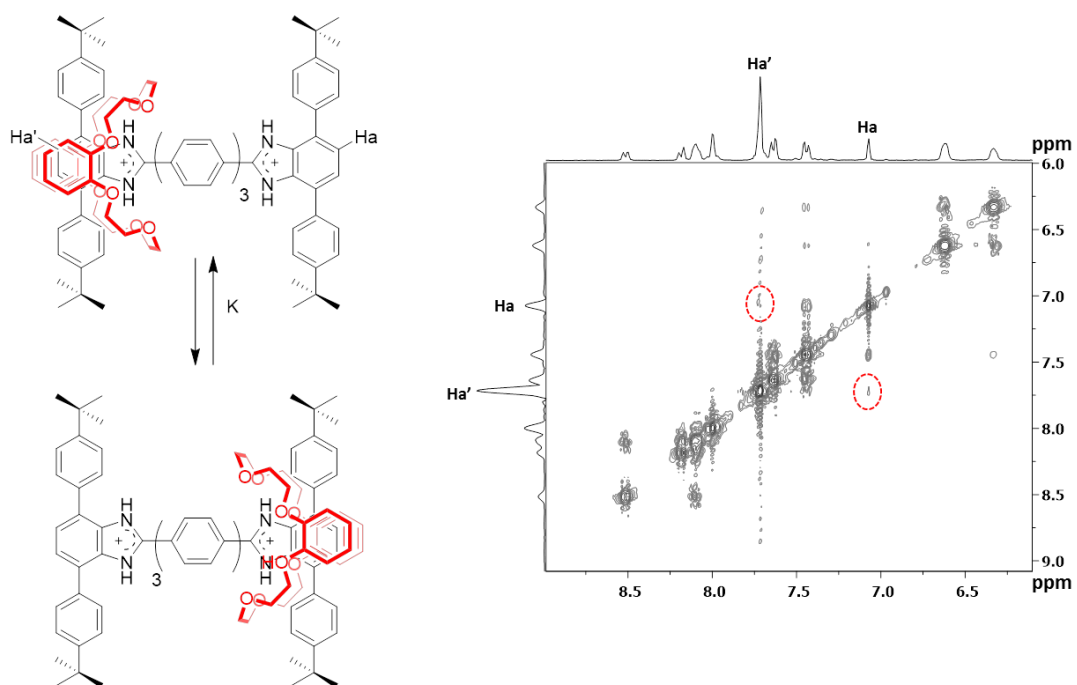


Fig 4.17 – partial 2D ^1H - ^1H EXSY (300 MHz, 295K, CD_3CN) spectrum of $[\mathbf{4.3}\text{-H}_2][\text{BF}_4]_2$.

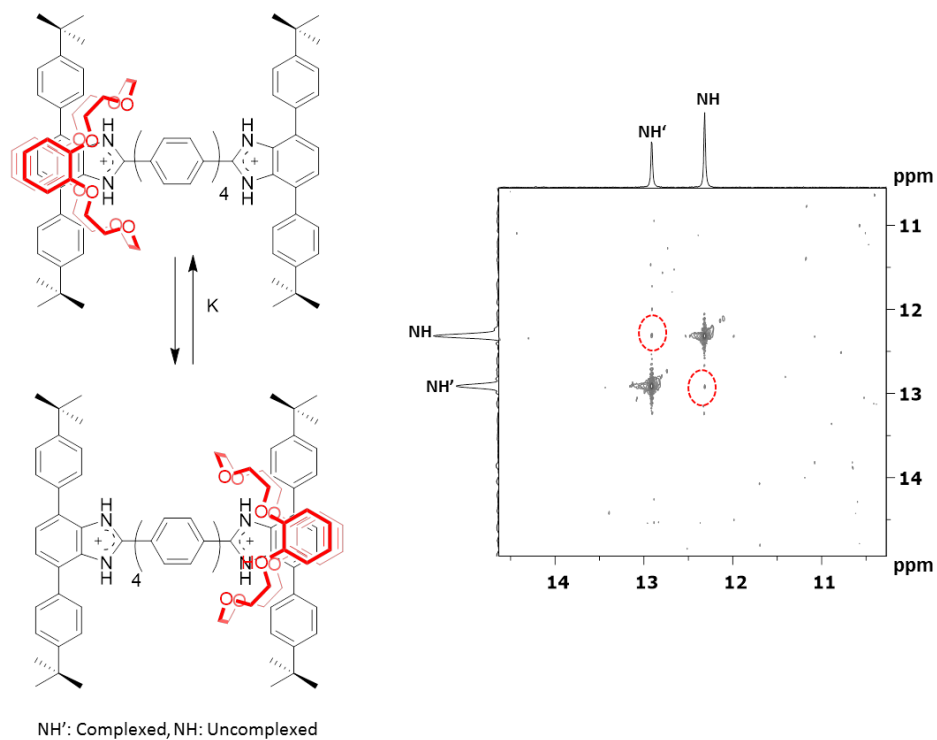


Fig 4.18 – partial 2D ^1H - ^1H EXSY (300 MHz, 293K, CD_3CN) spectrum of $[\mathbf{4.4}\text{-H}_2][\text{BF}_4]_2$.

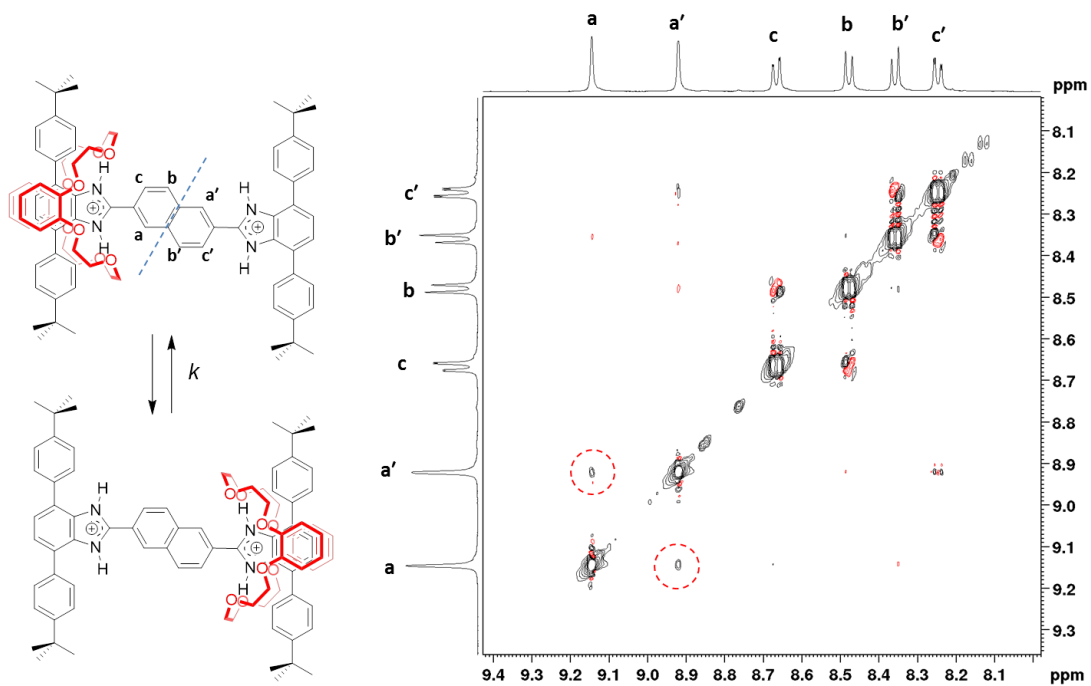


Fig 4.19 – partial 2D ^1H - ^1H EXSY (300 MHz, 298K, CD_3CN) spectrum of $[\mathbf{4.5}\text{-H}_2][\text{BF}_4]_2$.

4.2.23 Shuttling rates for series of dicationic [2]rotaxanes

Table 4.3 – summary of shuttling rates for dicationic [2]rotaxane molecular shuttles.

shuttle	I_{AA}	I_{BB}	I_{AB}	I_{BA}	k_{obs} (s ⁻¹)	ΔG^\ddagger (kcal/mol)	T (K)
[4.2-H ₂][BF ₄] ₂	0.3421	0.0887	0.0013	0.00001	0.0061	20.21	295
[4.3-H ₂][BF ₄] ₂	1.7451	1.3902	0.0094	0.0033	0.0078	20.07	295
[4.4-H ₂][BF ₄] ₂	0.3385	0.3464	0.0016	0.0016	0.0090	19.83	293
[4.5-H ₂][BF ₄] ₂	0.9899	1.0000	0.0060	0.0063	0.0124	20.05	298

4.2.24 Details of single X-ray crystal structure determinations

General: Crystals were frozen in paratone oil inside a cryoloop under a cold stream of N₂. X-ray intensity data were collected at 173(2) K using a Bruker APEX diffractometer equipped with an APEX area detector. The raw area detector data frames were reduced and corrected for absorption effects using the SAINT+ and SADABS programs.^[20] Final unit cell parameters were determined by least-squares refinement taken from the data set. Diffraction data and unit-cell parameters were consistent with the assigned space groups. The structures were solved by direct methods with SHELXT.^[21] Subsequent difference Fourier calculations and full-matrix least-squares refinement against |F²| were performed with SHELXL-2014^[21] using OLEX2.^[22] All non-hydrogen atoms were refined anisotropically and hydrogen atoms placed in idealized positions and refined using a riding model. See Tables 4.4 and 4.5 for a summary of data collection, solution and refinement details. Complete details of the structures can be obtained from the Cambridge Crystallographic

Data Centre at www.ccdc.cam.ac.uk for CCDC accession numbers 1563641, 1563642, 1563643 and 1563644.

4.2.25 X-ray structure of [2]Rotaxane 4.5

Single crystals were obtained from slow evaporation of a DMF solution of **4.5**. Crystals of formula **4.5**(DMF)₂ were of good quality. Data was collected using MoK α radiation ($\lambda = 0.71073 \text{ \AA}$). The asymmetric unit contained one molecule of the [2]rotaxane (C₈₈H₉₆N₄O₈) and two molecules of DMF. The structure was solved in the triclinic space group P-1 (#2). One of the *t*Bu groups was disordered and modelled with occupancies of 81:19 using PART and FVAR. See Table 4.4 for details.

4.2.26 X-ray structure of [2]Rotaxane [4.5-H₂][BF₄]₂

Single crystals were obtained from slow evaporation of a toluene solution of **4.5-H₂**[BF₄]₂. Crystals of formula [**4.5-H₂**][BF₄]₂(toluene)₄ were of good quality. Data was collected using MoK α radiation ($\lambda = 0.71073 \text{ \AA}$). The asymmetric unit contained one molecule of the dicationic [2]rotaxane (C₈₈H₉₈N₄O₈), two BF₄ anions, three molecules of toluene and one water molecule. The structure was solved in the triclinic space group P-1 (#2). Two of the *t*Bu groups were disordered and both modelled with occupancies of 53:47 using PART and FVAR. Both anions were disordered and restrained with SAME & SIMU commands and modelled with occupancies of 84:16 and 79:21 respectively using PART and FVAR. The toluene molecules were included as rigid groups using a combination of SADI restraints. See Table 4.4 for details.

4.2.27 X-ray structure of [2]Rotaxane 4.2 from THF

Single crystals were obtained from slow evaporation of a THF solution of **4.2**. Crystals of formula **4.2**(THF)₄ were of good quality. Data was collected using CuK α radiation ($\lambda = 1.54178 \text{ \AA}$). The asymmetric unit contained half a molecule of the [2]rotaxane (C₉₀H₉₈N₄O₈) and two molecules of THF. The structure was solved in the triclinic space group P-1 (#2). Both *t*Bu groups were disordered and modelled as rigid groups using SADI and SIMU with occupancies of 54:46 and 68:32 respectively using PART and FVAR. One of the THF molecules was disordered modelled with occupancies of 75:25 using PART and FVAR. See Table 4.5 for details.

4.2.28 X-ray structure of [2]Rotaxane 4.1-Br

Single crystals were obtained from slow evaporation of an ethyl acetate solution of **4.1-Br**. Crystals of formula **4.1-Br** were of good quality. Data was collected using MoK α radiation ($\lambda = 0.71073 \text{ \AA}$). The asymmetric unit contained half a molecule of the [2]rotaxane (C₃₆H₄₂Br₄N₄O₈); no anions, no solvent. The structure was solved in the triclinic space group P-1 (#2). No restraints were required. See Table 4.5 for details.

Table 4.4 – Single-crystal X-ray data collection, solution and refinement details for **4.5** and **[4.5-H₂][BF₄]₂**.

CCDC No.	1563641	1563642
Compound	4.5 (DMF) ₂	[4.5- H ₂][BF ₄] ₂ (H ₂ O)(toluene) ₃
Formula	C ₉₄ H ₁₁₀ N ₆ O ₁₀	C ₁₀₉ H ₁₂₄ B ₂ F ₈ N ₄ O ₉
<i>M</i> [g mol ⁻¹]	1483.87	1807.73
Crystal system	Triclinic	Triclinic
Space group	P-1 (No. 2)	P-1 (No. 2)
<i>a</i> [Å]	14.3220(13)	14.2079(9)
<i>b</i> [Å]	15.9818(16)	18.9576(11)
<i>c</i> [Å]	20.0611(16)	20.1063(13)
α [°]	107.703(4)	97.249(3)
β [°]	90.106(4)	100.114(3)
γ [°]	110.238(4)	108.536(3)
<i>V</i> [Å ³]	4074.8(7)	4957.8(5)
<i>Z</i>	2	2
<i>D</i> _{calcd.} [g cm ⁻³]	1.209	1.211
μ [mm ⁻¹]	0.078	0.086
Reflections	8510	20185
<i>R</i> _{int}	0.1148	0.0518
Parameters	1007	1400
Restraints	114	328
<i>R</i> 1 [<i>I</i> > 2σ(<i>I</i>)] ^a	0.1041	0.1057
<i>R</i> 1 (all data)	0.2001	0.1744
<i>wR</i> 2 [<i>I</i> > 2σ(<i>I</i>)] ^b	0.2151	0.2079
<i>wR</i> 2 (all data)	0.2713	0.2555
GoF (<i>F</i> ²)	1.026	1.106
$\Delta\rho$ [e Å ⁻³]	+0.39 (-0.41)	+0.63 (-0.63)

$$^a R1 = \sum ||F_o| - |F_c|| / \sum |F_o|; wR2 = [\sum [w(F_o^2 - F_c^2)^2] / \sum [w(F_o^2)^2]]^{1/2}$$

$$^b w = q[\sigma^2(F_o^2) + (aP)^2 + bP]^{-1}.$$

Table 4.5 – Single-crystal X-ray data collection, solution and refinement details for **4.2** and **4.1-Br**.

CCDC No.	1563643	1563644
Compound	4.2 (THF) ₄	4.1-Br
Formula	C ₁₀₆ H ₁₃₀ N ₄ O ₁₂	C ₃₆ H ₄₂ Br ₄ N ₄ O ₈
<i>M</i> [g mol ⁻¹]	1652.13	978.37
Crystal system	Triclinic	Triclinic
Space group	P-1 (No. 2)	P-1 (No. 2)
<i>a</i> [Å]	12.0595(2)	9.6346(14)
<i>b</i> [Å]	12.5637(3)	10.1658(15)
<i>c</i> [Å]	16.8685(3)	11.2070(17)
α [°]	74.7825(11)	68.379(2)
β [°]	76.6602(12)	82.740(2)
γ [°]	70.7332(11)	68.992(2)
<i>V</i> [Å ³]	2298.72(8)	10682(13)
<i>Z</i>	1	1
<i>D</i> _{calcd.} [g cm ⁻³]	1.193	1.706
μ [mm ⁻¹]	0.607	4.281
Reflections	8028	3839
<i>R</i> _{int}	0.0557	0.0518
Parameters	664	235
Restraints	100	0
<i>R</i> 1 [<i>I</i> > 2σ(<i>I</i>)] ^a	0.0584	0.0374
<i>R</i> 1 (all data)	0.0962	0.0438
<i>wR</i> 2 [<i>I</i> > 2σ(<i>I</i>)] ^b	0.1379	0.0995
<i>wR</i> 2 (all data)	0.1570	0.1042
GoF (<i>F</i> ²)	1.037	1.032
$\Delta\rho$ [e Å ⁻³]	+0.36 (-0.23)	+0.99 (-0.36)

$$^a R1 = \sum ||F_o| - |F_c|| / \sum |F_o|; wR2 = [\sum [w(F_o^2 - F_c^2)^2] / \sum [w(F_o^2)^2]]^{1/2}$$

$$^b w = q[\sigma^2(F_o^2) + (aP)^2 + bP]^{-1}.$$

4.2.29 Methods and Computational Details

Quantum mechanics calculations were carried out in the framework of the Density Functional Theory (DFT) methods incorporated in the GAUSSIAN09 package.^[23] The ground state equilibrium structures and the transition state (TS) structures of the dibenzo[24]crown-8 (**DB24C8**) macrocycle and an H-shaped axle, forming a rotaxane, were

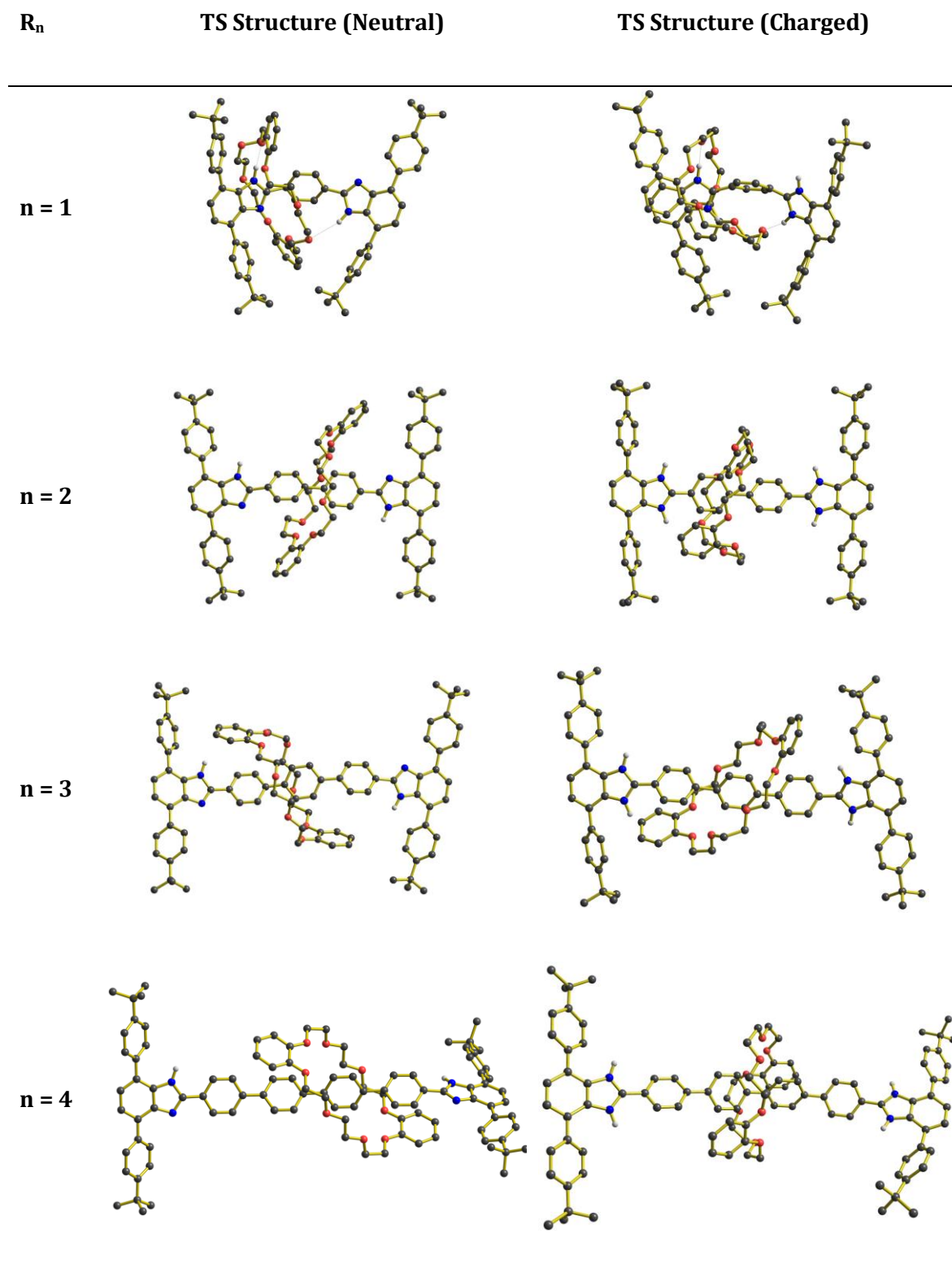
fully optimized without symmetry restraints. The track length of the axle was varied in terms of the amount (n) of phenylene spacers, increasing from n=1 to n=4. The Becke-3-parameter-Lee-Yang-Parr hybrid functional (B3LYP),^[24] which incorporates 20% of Hartree-Fock exact exchange, was employed as it has been reported to achieve good agreement with X-ray geometrical structures of even large molecular systems.^[25] The Gaussian-type basis set 6-31G(d,p)^[26] was employed for all atoms and the dispersion correction (DFT-D3) to the energy was included in all the calculations using the Grimme scheme.^[27]

Molecular structures of the starting and finishing points for the shuttling of the rotaxane, which were constructed with the **DB24C8** macrocycle in each extreme of the axle, were optimized to find stationary point geometries. The structures of the TS between these geometries were optimized by applying Schlegel's synchronous-transit-guided quasi-Newton (QST3) method.^[28] The nature of the found stationary points on the potential energy surface (PES) was characterized by the computation of the harmonic vibrational frequencies obtained by the examination of the Hessian matrix, which is constituted by the second derivative of energy with respect to the spatial coordinates of the systems. The transition states were verified to be first order saddle points with only one negative eigenvalue. Implicit solvation effects were taken into account by means of the Polarized Continuum Model (PCM) using dichloromethane (DCM, $\epsilon = 8.93$).^[29]

Table 4.6 – Calculated thermochemistry values and energy barriers for **4.1** – **4.4** and $[\mathbf{4.1-H_2}]^{2+}$ – $[\mathbf{4.4-H_2}]^{2+}$.

n	Charge	Start	TS	Finish	ΔG^\ddagger (AU) _{Th}	ΔG^\ddagger (kcal mol ⁻¹) _{Th}
1	0	-4077.19	-4077.17	-4077.19	0.018	11.1
2	0	-4308.18	-4308.15	-4308.18	0.027	17.1
3	0	-4539.17	-4539.14	-4539.17	0.033	20.5
4	0	-4770.17	-4770.14	-4770.17	0.033	20.9
1	+2	-4078.08	-4078.05	-4078.07	0.029	18.0
2	+2	-4309.08	-4309.02	-4309.07	0.054	34.1
3	+2	-4540.08	-4540.01	-4540.07	0.068	42.6
4	+2	-4771.07	-4771.00	-4771.06	0.074	46.4

Table 4.7 – Calculated TS structures for 4.1 – 4.4 and [4.1-H₂]²⁺ – [4.4-H₂]²⁺.



4.3 References

1. a) J. O. Jeppesen, S. A. Vignon, J. F. Stoddart, *Chem. Eur. J.*, **2003**, 9, 4611–4625; b) J. D. Crowley, S. M. Goldup, A.-L. Lee, D. A. Leigh, R. T. McBurney, *Chem.Soc.Rev.*, 2009, 38, 1530–1541; c) S. F. M. van Dongen, S. Cantekin, J. A. A. W. Elemans, A. E. Rowan, R. J. M. Nolte, *Chem. Soc. Rev.*, **2014**, 43, 99–122; d) V. Balzani, A. Credi, F. M. Raymo, J. F. Stoddart, *Angew. Chem., Int. Ed.*, **2000**, 39, 3348–3391; e) H. Tian, Q.-C. Wang, *Chem. Soc. Rev.*, **2006**, 35, 361–374.
2. P. L. Anelli, N. Spencer and J. F. Stoddart, *J. Am. Chem. Soc.*, **1991**, 113, 5131–5133.
3. a) L. Charles, P. J. Dwyer, T. J. Dwyer, *Chem. Rev.*, **1990**, 90 (6), 935–967; b) C.-F. Lee, D. A. Leigh, R. G. Pritchard, D. Schultz, S. J. Teat, G. A. Timco, R. E. P. Winpenny, *Nature*, **2009**, 458, 314–318; b) Q. Gan, Y. Ferrand, C. Bao, B. Kauffmann, A. Grélard, H. Jiang, I. Huc, *Science*, **2011**, 331, 1172–1175.
4. a) J. Baggerman, N. Haraszkiewicz, P. G. Wiering, G. Fioravanti, M. Marcaccio, F. Paolucci, E. R. Kay, D. A. Leigh, A. M. Brouwer, *Chem. Eur. J.*, **2013**, 19, 5566–5577; b) D. D. Gunbas, A. M. Brouwer, *J. Org. Chem.*, **2012**, 77, 5724–5735; c) H. Li, Y.-L. Zhao, A. C. Fahrenbach, S.-Y. Kim, W. F. Paxton, J. F. Stoddart, *Org. Biomol. Chem.*, **2011**, 9, 2240–2250.
5. D. D. Günbaş, A. M. Brouwer, *J. Org. Chem.*, **2012**, 77, 5724–5735.
6. M. Hmadeh, A.C. Fahrenbach, S. Basu, A. Trabolsi, D. Benitez, H. Li, A.-M. Albrecht-Gary, M. Elhabiri, J. F. Stoddart, *Chem. Eur. J.*, **2011**, 17, 6076–6087.
7. V. Balzani, A. Credi, M. Venturi, *Chem. Soc.Rev.* **2009**, 38, 1542–1550.
8. P. G. Young, K. Hirose and Y. Tobe, *J. Am. Chem. Soc.*, **2014**, 136, 7899–7906.

9. a) K. Zhu, C. a O'Keefe, V. N. Vukotic, R. W. Schurko and S. J. Loeb, *Nat. Chem.*, **2015**, 7, 514–519; b) G. Gholami, K. Zhu, J.S. Ward, P. E. Kruger, S. J. Loeb, *Eur. J. Inorg. Chem.* **2016**, 4524–4529; c) G. Gholami, G. Baggi, K. Zhu, S. J. Loeb, *Dalton Trans.*, **2017**, 46, 2462–2470.
10. a) K. Zhu, V. N. Vukotic, S. J. Loeb, *Chem. Asian J.*, 11, **2016**, 3258 –3266; b) G. Baggi, S. J. Loeb, *Angew. Chem. Int. Ed.*, **2016**, 55, 12533 –12537; c) K. Zhu, V. N. Vukotic, S. J. Loeb, *Angew. Chem. Int. Ed.*, 124, **2012**, 2210–2214; d) K. Zhu, V. N. Vukotic, N. Noujeim, S. J. Loeb, *Chem. Asian J.*, **2016**, 11, 3258-3266.
11. K. Zhu, V. N. Vukotic, N. Noujeim, S. J. Loeb, *Chem. Sci.*, **2012**, 3, 3265-3271.
12. N. Noujeim, K. Zhu, V. N. Vukotic, S. J. Loeb, *Org. Lett.*, **2012**, 14 (10), 2484-2487.
13. N. Farahani, K. Zhu, S. J. Loeb, *ChemPhysChem*, **2016**, 17, 1875–1880.
14. H. Akpınar, A. Balan, D. Baran, E. Unver, L. Toppare, *Polymer*, **2010**, 51, 6123–6131.
15. M. Kozakova, M. Budesi'nsky, J. Hodacova, *Synthetic Communication*, **2005**, 35, 161-167.
16. H. C.hun Cheng, P. P. Yu Chen, Y. Oliver Su, *Dalton Trans.*, **2014**, 43, 1424-1433.
17. G.-Y. Xie, L. Jiang, T.-B. Lu, *Dalton Trans.*, **2013**, 42, 14092–14099.
18. DNMR71.EXE, Reich, H. J., *J. Chem. Educ. Software*, **1996**.
19. Sutherland, I. O. *Annu. Rep. NMR Spectrosc.* **1971**, 4, 71.
20. Bruker, *SAINT+* and *SADABS*. Bruker AXS Inc., Madison, Wisconsin, USA, **2012**.
21. G. M. Sheldrick, *Acta Cryst.* **2015**, C71, 3-8.

22. O. V. Dolomanov, L. J. Bourhis, R. J. Gildea, J. A. K. Howard, H. Puschmann, *J. Appl. Cryst.*, **2009**, *42*, 339-341.
23. M. J. Frisch, G. W. Trucks, H. B. Schlegel, G. E. Scuseria, M. A. Robb, J. R. Cheeseman, G. Scalmani, V. Barone, B. Mennucci, G. A. Petersson, H. Nakatsuji, M. Caricato, X. Li, H. P. Hratchian, A. F. Izmaylov, J. Bloino, G. Zheng, J. L. Sonnenberg, M. Hada, M. Ehara, K. Toyota, R. Fukuda, J. Hasegawa, M. Ishida, T. Nakajima, Y. Honda, O. Kitao, H. Nakai, T. Vreven, J. A. Montgomery, Jr., J. E. Peralta, F. Ogliaro, M. Bearpark, J. J. Heyd, E. Brothers, K. N. Kudin, V. N. Staroverov, R. Kobayashi, J. Normand, K. Raghavachari, A. Rendell, J. C. Burant, S. S. Iyengar, J. Tomasi, M. Cossi, N. Rega, J. M. Millam, M. Klene, J. E. Knox, J. B. Cross, V. Bakken, C. Adamo, J. Jaramillo, R. Gomperts, R. E. Stratmann, O. Yazyev, A. J. Austin, R. Cammi, C. Pomelli, J. W. Ochterski, R. L. Martin, K. Morokuma, V. G. Zakrzewski, G. A. Voth, P. Salvador, J. J. Dannenberg, S. Dapprich, A. D. Daniels, O. Farkas, J. B. Foresman, J. V. Ortiz and J. Cioslowski and D. J. Fox, Gaussian 09, Revision E.01, Gaussian, Inc., Wallingford CT, **2009**.
24. (a) A. D. Becke, *J. Chem. Phys.* **1993**, *98*, 5648; (b) P. J. Stephens, F. J. Devlin, C. F. Chabalowski, M. J. Frisch, *J. Phys. Chem.* **1994**, *98*, 11623-11627.
25. (a) S. Tortorella, M. M. Talamo, A. Cardone, M. Pastore, F. De Angelis. *J. Phys.: Condens. Matter.* **2016**, *28*, 074005 (11 pp); (b) M Pastore, E Mosconi, F De Angelis, M. Grätzel. *J. Phys. Chem. C.* **2010**, *114*, 7205-7212; (c) M. N. Glukhovtsev, R. D. Bach, C. J. Nagel. *J. Phys. Chem. A.* **1997**, *101*, 316.
26. M. J. Frisch, J. A. Pople, J. S. Binkley. *J. Chem. Phys.* **1984**, *80*, 3265-3269.
27. S. Grimme, J. Antony, S. Ehrlich, H. Krieg, *J. Chem. Phys.* **2010**, *132*, 154104 (19 pp).
28. C. Peng, H. B. Schlegel. *Israel J. Chem.* **1993**, *33*, 449-454.

29. M. Cossi, N. Rega, G. Scalmani and V. Barone, *J. Comput. Chem.*, **2003**, 24, 669-681.

CHAPTER 5

5.1 pH-Control of Molecular Shuttling Inside Zr-based MOFs

5.1.1 Introduction

Molecular shuttles—interlocked molecular assemblies in which a macrocyclic ring is able to move back and forth between two recognition sites—have been studied due to their potential applications in many fields such as drug delivery,^[1] smart polymers,^[2] catalysis,^[3] and sensors.^[4] Almost all studies on molecular shuttles have been in solution where the motion is incoherent and random.^[6,7] To impose higher order on molecular shuttles, they can be incorporated into solid-state materials such as metal–organic frameworks (MOFs). To this aim, Loeb recently reported the translational motion of a molecular shuttle inside a crystalline, solid-state material.^[8] The variable-temperature (VT) ¹³C solid-state NMR (SSNMR) of a specially designed Zn(II) based MOF, **UWDM-4** (University of Windsor Dynamic Material), demonstrated translational motion of a [2]rotaxane—a MIM (mechanically interlocked molecule) linker with one ring and two recognition sites—in the solid state. However, there was no control over the degenerate shuttling of the rotaxane in this MOF. One straightforward method to control shuttling of this rotaxane would be by acid/base chemistry, as the neutral and charged species have very different energy barriers to shuttling. For acid/base control of molecular shuttling of rotaxanes inside MOFs, a highly stable framework is needed and Zn-based MOFs are not suitable. However, Zr-based MOFs are well known for their exceptional thermal, chemical and mechanical stability, and could therefore be used in pH control of molecular shuttles inside MOF materials. Thus a Zr-based material was targeted.

The super stability of Zr-based MOFs arises from strong coordination bonds between Zr(IV) ions and carboxylate ligands. The **UiO** (University of Oslo) series of Zr-based^[9,10]

MOFs such as **UiO-68** with terphenyl dicarboxylates (**TPDC**) as organic linkers were the first examples of this type of unprecedented stable MOFs. To date no single crystal of **UiO-68** has been reported, but the very closely related material **PCN-57**^[11] (Porous Coordination Network) with 2',3',5',6'-tetramethylterphenyl-4,4'' dicarboxylate (**TTTP**) linkers could be crystalized from DMF in a form suitable for single-crystal X-ray diffraction. The crystal structure is made up of polyhedral cages (tetrahedral and octahedral) connected with carboxylate ligands between $Zr_6O_4(OH)_4(CO_2)_{12}$ clusters; see Fig 5.1.

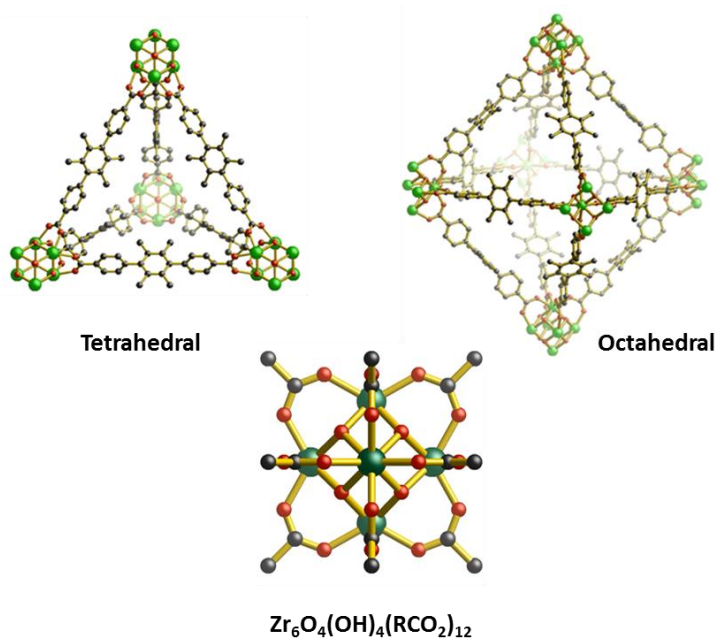


Fig 5.1 – tetrahedral and octahedral cages in the single-crystal X-ray structure of **PCN-57** (top) and a single $Zr_6O_4(OH)_4(CO_2)_{12}$ cluster (bottom).^[11]

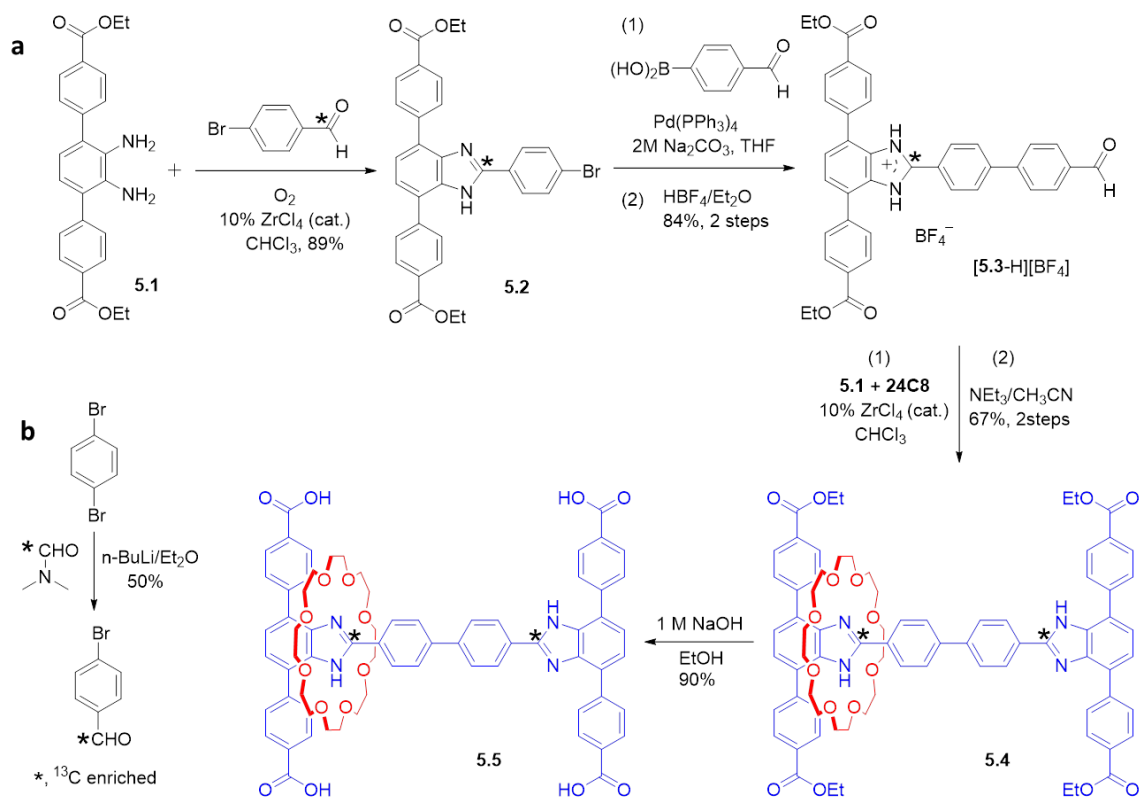
Herein, we describe the robust and dynamic MOFs **UWDM-6** and **UWDM-7** which contain Zr_6 clusters and terphenyl linkers and are based directly on the structures of known materials **PCN-57** and **UiO-68** respectively. To accomplish this, a new [2]rotaxane molecular shuttle linker **5.5** (Scheme 5.1) was synthesized and characterized. Preparation

of MOFs **UWDM-6** and **UWDM-7** was then accomplished by doping—incorporating in a stoichiometric fashion—**5.5** into the known structures of **PCN-57** and **UiO-68**.

5.1.2 Results and discussion

A new molecular shuttle linker, **5.5**, was prepared as outlined in Scheme 5.1a. In a one-pot reaction, the preformed [2]pseudorotaxane [**5.3-H**⊂**24C8**]⁺ (from the reaction of [24]crown-8 ether (**24C8**) and [**5.3-H**][BF₄]) containing a terminal aldehyde function was condensed with an equivalent of diamine **5.1** and then oxidized with a catalytic amount of ZrCl₄ to produce, after treatment with Et₃N, the neutral tetraethyl ester [2]rotaxane, **5.4**^[14,15] (the ¹H NMR spectrum of **5.4** is shown in the experimental section 5.2.7, see Fig 5.7). The tetra ester was then hydrolysed to yield the tetra acid linker **5.5**. For identification of the shuttling motion in the MOF by ¹³C SSNMR, the carbon atoms at the 2-positions of the benzimidazole rings of **5.5** (shown with asterisks in Scheme 5.1a) were enriched to 50% ¹³C by using ¹³C enriched 1-bromo4-benzaldehyde prepared as shown in Scheme 5.1b.

To study the dynamics of the designed MIM linker, first a ¹³C enriched sample of the tetraethyl ester MIM, **5.4**, was subjected to a VT ¹³C NMR study in a toluene-d₈ solution. Monitoring the ¹³C labelled site (asterisk in Scheme 5.1a) as a function of temperature showed that macrocycle undergoes rapid molecular shuttling between the two benzimidazole recognition sites faster than the NMR timescale at room temperature (see experimental 5.2.8). At lower temperatures, two separate resonances for the occupied and empty recognition sites were observed. This study allowed us to estimate the rate and energy barrier of molecular shuttling to be 6.1 × 10⁶ s⁻¹ and 7.9 kcal mol⁻¹ respectively at 298 K in toluene-d₈.



*Scheme 5.1 – a) major steps in the synthesis of a molecular shuttle MOF linker **5.4** (see experimental 5.2.1-5.2.7 for full synthetic details), b) the synthetic route used to enrich the MOF linker with ^{13}C to aid in characterization of the shuttling motion by ^1H - ^{13}C CP/MAS SSNMR.*

As a prelude to controlling the rate of shuttling motion of the [2]rotaxane inside the MOF by acid–base chemistry, shuttling motion of the diprotonated [2]rotaxane [**5.4**-H₂]²⁺ was also studied in solution. The ^{13}C NMR spectrum of [**5.4**-H₂]²⁺ showed two sets of peaks which means the macrocyclic wheel undergoes slow shuttling motion at 298 K, and 2D EXSY ^{13}C NMR experiments demonstrated the rate of shuttling to be about 0.19 s⁻¹ at 320 K with an energy barrier of 19.8 kcal mol⁻¹. Moreover, the NMR studies on the monoprotonated [2]rotaxane [**5.4**-H]⁺ showed the macrocyclic wheel preferred the charged site and does not shuttle toward the neutral site (see experimental 5.2.8).

To understand the translational motion of the macrocyclic ring in a solid-state material, we designed the Zr-based MOF, **UWDM-6**, based on the known MOF **PCN-57**. Fig 5.2 shows the design of **UWDM-6** in which two linking edges of **PCN-57** are replaced with a single [2]rotaxane linker.

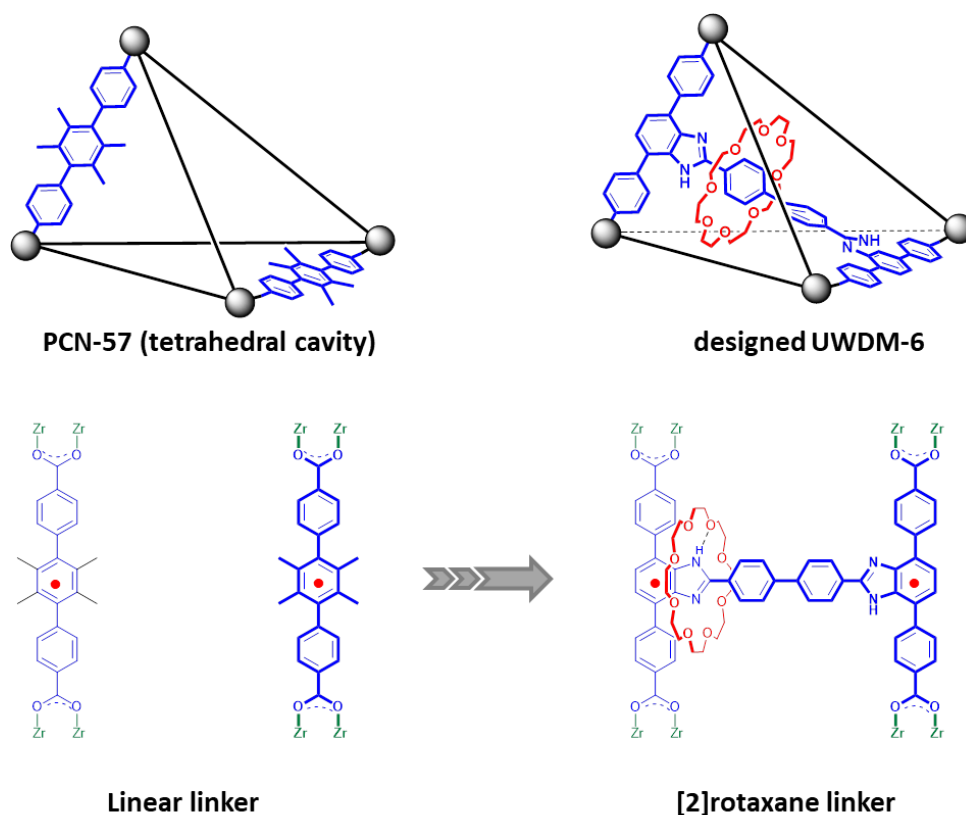


Fig 5.2 – designing **UWDM-6** with the same tetrahedral cavity as **PCN-57**, the [2]rotaxane linker was designed as a linear ligand to span the same distance between the centroids of linking terphenyl groups (shown with •).

UWDM-6 was prepared using *both* linkers **5.5** and 2',3',5',6'-tetramethylterphenyl-4,4'' dicarboxylic acid (**H₄TTTP**). Zirconium (IV) tetrachloride was combined with **5.5** and **H₄TTTP** in a ratio of 6:1:4 in 2 mL of N,N-dimethylformamide along with 5 drops of

trifluoroacetic acid (TFA) and heated to 90 °C for 24 h (Fig 5.3a). This yielded white microcrystals designated **UWDM-6**.

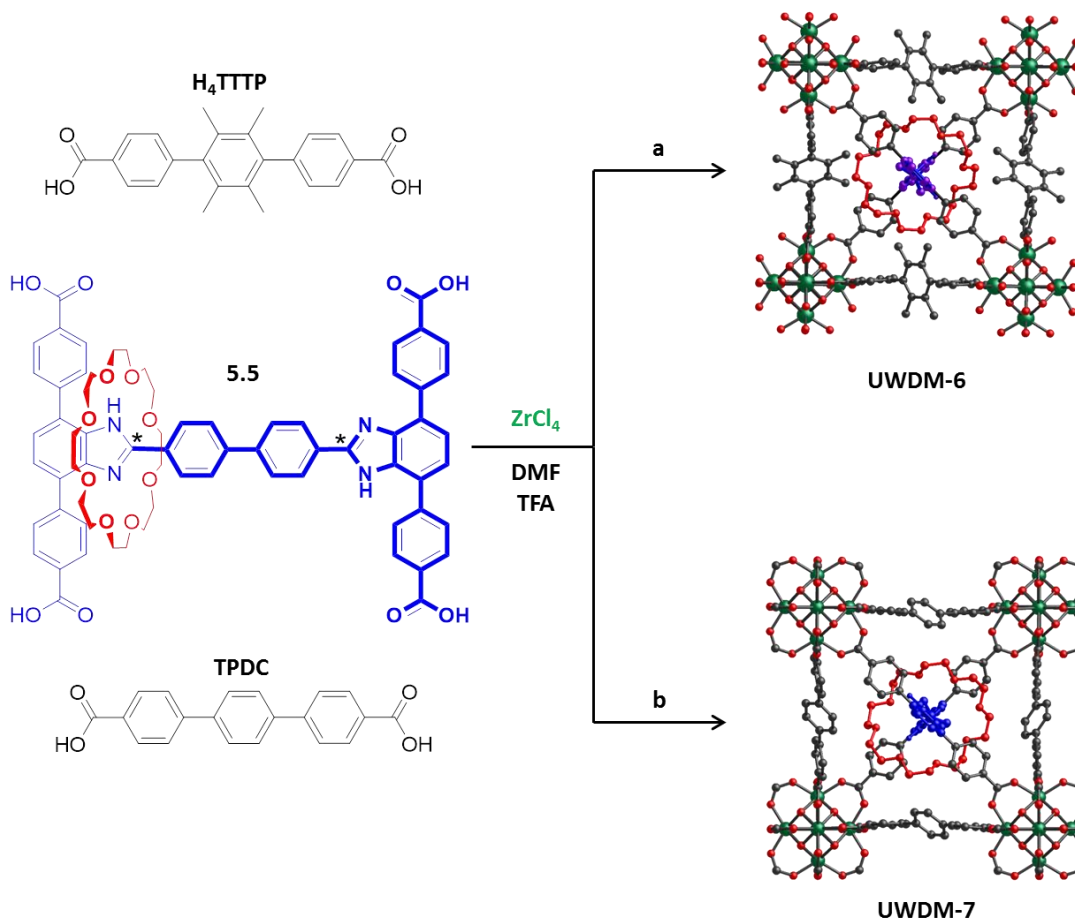
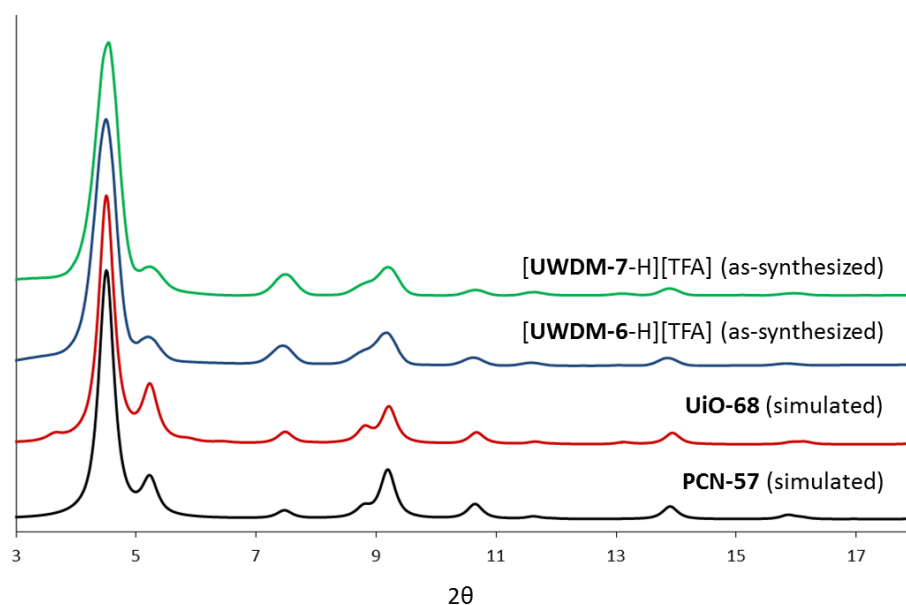


Fig 5.3 – synthetic route for making **UWDM-6** and **UWDM-7** (TFA: trifluoroacetic acid). Structures of **UWDM-6** and **UWDM-7** shown were generated from the X-ray structure of **PCN-57** using Material Studio.

The powder X-ray diffraction (PXRD) pattern for **UWDM-6** was similar to that reported for **PCN-57** (Fig 5.4). A portion of **UWDM-6** was digested in a DMSO/K₃PO₄ (saturated solution in D₂O) and analyzed by ¹H NMR spectroscopy to prove the presence of linker **5.5** within the framework. This experiment showed the ratio of **TTTP** to **5.5** was about 4:1 (see experimental 5.2.9). To determine if all four carboxylate groups of **5.5** are actually

coordinated to zirconium, samples of **UWDM-6** and **PCN-57** were subjected to ^{13}C SSNMR experiments. The spectrum showed only one single peak at about 170 ppm for **UWDM-6** similar to that observed for **PCN-57** indicating that all the carboxylate groups are involved in coordination to the Zr_6 clusters (see experimental 5.2.10). Based on previous MOF syntheses with related benzimidazole linkers, we assumed that the as-synthesized MOF material contained the linker in the mono-protonated state, so we assigned it formula $\text{Zr}_6(\text{TTTP})_4[\text{5.5-H}]^+[\text{CF}_3\text{COO}]^-$ (**[UWDM-6-H][TFA]**). Since, the interaction of the macrocycle with the charged benzimidazolium recognition site is much stronger than the neutral site; no molecular shuttling would be expected to occur in this state. As a result, we treated as-synthesized **[UWDM-6-H][TFA]** with the strong base *N,N,N',N'*-tetramethylnaphthalene-1,8-diamine (proton-sponge) in ethanol to make a neutral MOF.



*Fig 5.4 – PXRD (bottom to top) simulated from the single crystal X-ray structure of **PCN-57**, simulated from Material Studio software of **UiO-68**, as-synthesized **[UWDM-6-H][TFA]** and as-synthesized **[UWDM-7-H][TFA]**.*

Deprotonation of [UWDM-6-H][TFA] to UWDM-6 was inferred by a significant change in the fluorescence colour and intensity of the solid upon UV irradiation at 345 nm (see experimental 5.2.11).

To address whether or not the macrocyclic ring of linker **5.5** could shuttle between the recognition sites inside the MOF material, a ^{13}C -enriched sample of UWDM-6 was subjected to ^{13}C SSNMR experiments. Fig 5.5a shows the solid-state ^{13}C NMR spectrum of UWDM-6 with two single peaks at room temperature. To determine the rate of shuttling, VT ^{13}C SSNMR spectra were recorded on a sample of UWDM-6. However, this experiment showed no variation with temperature indicating that there was no molecular shuttling occurring inside UWDM-6. In order to understand the surprising failure of the shuttle to undergo translation motion, even at increased temperatures, the structure of the material was further investigated using the software package Material Studio.

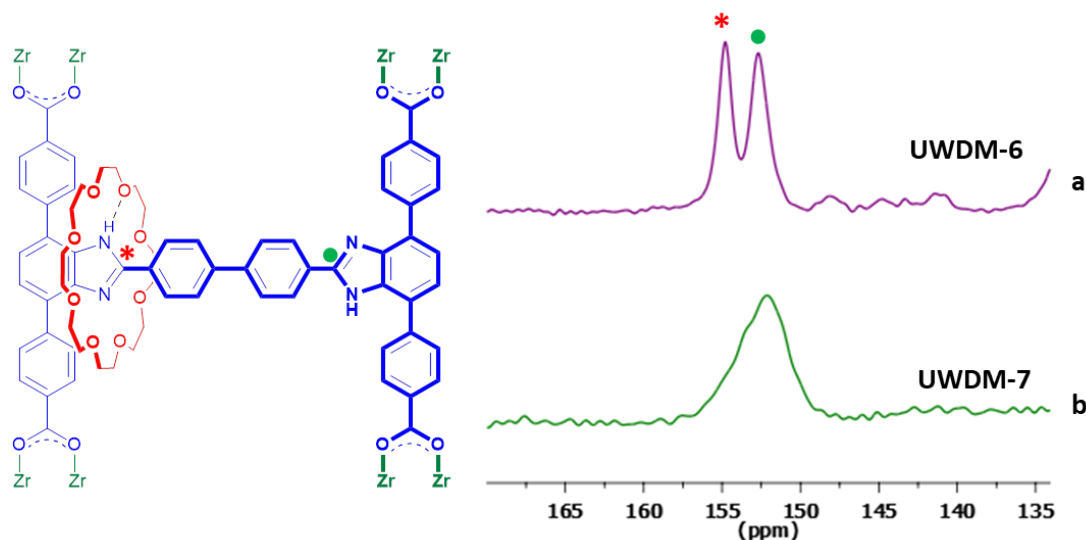


Fig 5.5 – partial ^{13}C SSNMR spectra of neutral UWDM-6 and UWDM-7 (acquired at 9.4 T), (* = occupied site, • = unoccupied site).

This study revealed that there is very likely steric hindrance from the methyl groups of the **TTTP** linker which prevents the macrocycle from shuttling inside the solid state material—the barrier is too high and the ring is essentially locked in position. As a result, the two single peaks in the ^{13}C SSNMR spectra are interpreted as meaning the macrocycle resides at one recognition site and cannot shuttle to the other.

To remove the hindrance presented by the methyl groups, the organic linker **H₄TTTP** was replaced by the analogous linker **H₄TPDC** (this linker does not have any methyl groups) and the MOF, **UWDM-7** (Fig 5.3b) obtained using the same procedure as for **UWDM-6**. The ^{13}C SSNMR spectrum of **UWDM-7** showed one single broad peak at room temperature (Fig 5.5b). This observation infers that the macrocyclic ring undergoes shuttling inside the solid state material. Unfortunately, VT ^{13}C SSNMR experiments on **UWDM-7** did not allow resolution of the two-site exchange, which is presumably fast on the NMR time scale and it was therefore not possible to determine an estimation of the shuttling rate inside the solid state. It is very likely that the poor crystallinity of **UWDM-7** and the fast shuttling of the macrocyclic wheel inside the MOF contribute to this dilemma.

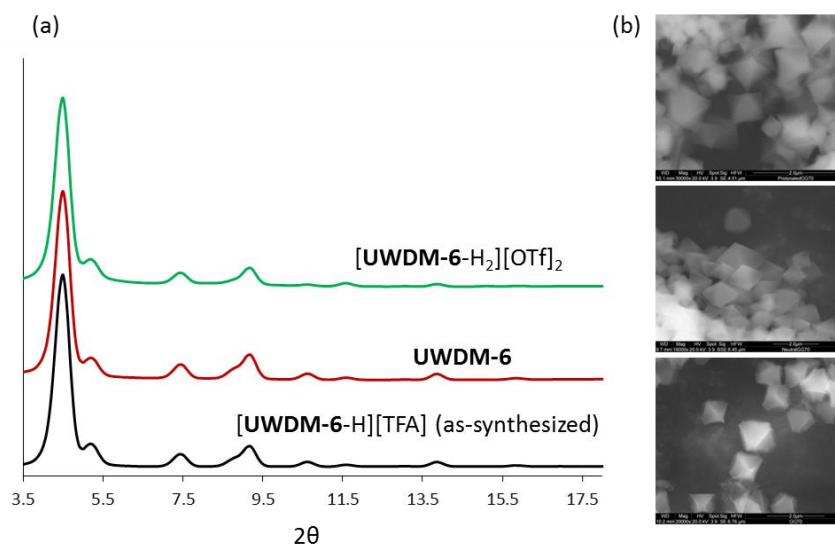


Fig 5.6 – a) PXRD of as-synthesized **[UWDM-6-H][TFA]**, **UWDM-6** and **[UWDM-6-H₂][OTf]₂**, b) SEM of **[UWDM-6-H₂][OTf]₂**, **UWDM-6** and **[UWDM-6-H][TFA]** from top to bottom.

To further assess the stability of the constructed MOFs to acid/base treatments, the as-synthesized **[UWDM-6-H][TFA]** was treated with both the strong base N,N,N',N'-tetramethylnaphthalene-1,8-diamine (proton-sponge) and triflic acid (CF₃SO₃H). Powder X-ray diffraction (PXRD) experiments and scanning electron microscopy/energy-dispersive X-ray spectroscopy (SEM/EDX) measurements were investigated on these acid/base treated samples. Also the thermal stability of the MOFs was evaluated by variable-temperature powder X-ray diffraction (VT-PXRD), over the temperature range of 25 to 175 °C. The result of these different experiments clearly showed there was retention of the framework integrity with essentially no loss of crystallinity of the MOFs (see experimental 5.2.12) (Fig 5.6) even after fairly harsh chemical treatments.

5.1.3 Conclusions

Two Zr-based MOF materials **UWDM-6** and **UWDM-7** using a mixture of linear and [2]rotaxane linkers have been successfully prepared. Both MOFs were stable under

acid/base and high temperature conditions. VT ^{13}C SSNMR experiments of **UWDM-6** demonstrated that the translational motion of the macrocyclic wheel was impeded due to steric hindrance inside the cavity of the MOF. This limitation for shuttling was removed by changing the linear linker in **UWDM-7**; however, the poor crystallinity of this MOF did not allow determination of the exact rate of shuttling inside the Zr-based MOF.

5.2. Experimental

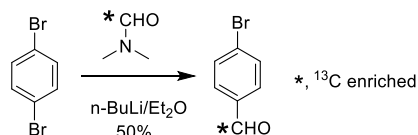
5.2.1 General comments

1,4-Dibromobenzene and 4-formylphenylboronic acid were purchased from Sigma-Aldrich. Compound **5.1** was prepared according to the literature method.^[8] Deuterated solvents were obtained from Cambridge Isotope Laboratories and used as received. Solvents were dried using an Innovative Technologies Solvent Purification System. ¹H and ¹³C NMR solution experiments were performed on a Bruker Avance 500 instrument at 298 K unless otherwise indicated. Chemical shifts are quoted in ppm relative to tetramethylsilane using the residual solvent peak as a reference standard. Powder XRD measurements were recorded on a Bruker D8 Discover diffractometer equipped with a GADDS 2D-detector and operated at 40 kV and 40 mA. CuK_α radiation was used and the initial beam diameter was 0.5 mm. Melting points were recorded on a Stanford Research Systems, Opti Melt MPA100 instrument. SSNMR spectra were acquired using a Varian Infinity Plus console equipped with a 9.4 T Oxford magnet at resonance frequencies of 100.5 MHz for ¹³C. Experiments were conducted using a Chemagnetics 4 mm HX MAS probe. Samples were packed into zirconia rotors and temperatures calibrated using the ²⁰⁷Pb isotropic shift of PbNO₃.

5.2.2 Synthesis of 4-bromobenzaldehyde-¹³C

A solution of 1,4-dibromobenzene (3.22 g, 0.0136 mol) in Et₂O (30 mL) was cooled to -78 °C. 1.6 M n-BuLi in hexane (7.5 mL, 0.0136 mol) was added dropwise over a period of 75 min and stirred for 2 h then ¹³C-DMF (1.0 g, 0.0149 mol) was added over a period of 30 min. The mixture was allowed to warm to RT and stirred for 3 h. The mixture cooled in an ice-bath, diluted with 1 M HCl (150 mL) and extracted with Et₂O. The combined organic layers were dried over anhydrous MgSO₄. Evaporation of the solvent gave crude product

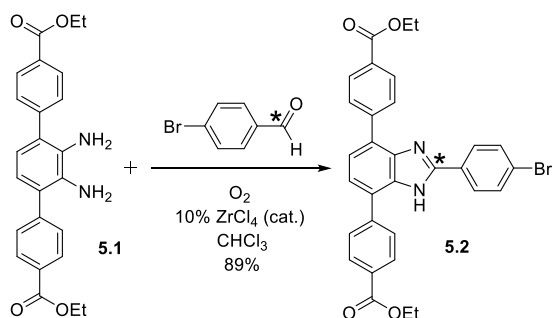
which was purified by column chromatography (SiO_2 , n-hexane/ CHCl_3 (4:1)) R_f : 0.3. Yield: 50% (1.1 g). Mp: 65-70 °C. ^1H NMR (500 MHz, CDCl_3 , 298 K): δ = 7.68 (d, 2H, J = 8.2 Hz), 7.74 (m, 2H), 9.80 (d, 1H, $\text{H-}^{13}\text{C}$ O, J = 175.4 Hz). ^{13}C NMR (126 MHz, CDCl_3): δ = 191.18, 167.57, 132.62, 132.58, 131.13, 131.10, 129.93. HR-MS (ESI): calculated for $[\text{M}+\text{H}]^+$, $[\text{}^{13}\text{C}_1\text{C}_6\text{H}_5\text{BrO}]^+$, m/z = 184.9450, found m/z = 184.9617.



Scheme 5.2 – synthesis of 4-bromobenzaldehyde- ^{13}C .

5.2.3 Synthesis of 5.2

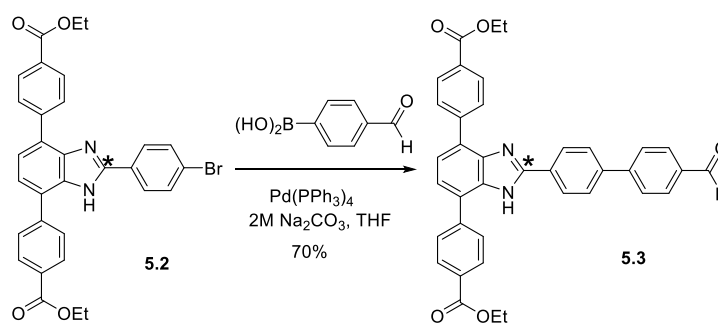
4-Bromobenzaldehyde- ^{13}C (368 mg, 1.97 mmol) and **1** (800 mg, 1.97 mmol) were dissolved in CHCl_3 in a small flask and then ZrCl_4 (45 mg, 0.19 mmol) was added. The solution was stirred for 24 h at room temperature. After filtration, solvent was removed and the resulting yellow solids were washed with CH_3CN . Yield 85% (955 mg). Mp: 165-170 °C. ^1H NMR (500 MHz, CDCl_3 , 298 K): δ = 1.42 (t, 6H, J = 3.6 Hz), 4.40 (q, 4H, J = 3.6 Hz), 7.53 (s, 4H), 7.94 & 8.02 (br, 6H), 8.21 (d, 4H, J = 8 Hz). ^{13}C NMR (125 MHz, DMSO-d_6 , 298 K): δ = 166.57, 151.96, 132.28, 129.41, 128.99, 128.90, 60.60, 14.20. HR-MS (ESI): calc for $[\text{M}+\text{H}]^+$, $[\text{}^{13}\text{C}_1\text{C}_{30}\text{H}_{26}\text{BrN}_2\text{O}_4]^+$, m/z = 570.0996, found m/z = 570.1102.



Scheme 5.3 – synthesis of **5.2**.

5.2.4 Synthesis of 5.3

5.2 (900 mg, 1.57 mmol), 4-formylphenylboronic acid (520 mg, 3.46 mmol) and $\text{Pd}(\text{PPh}_3)_4$ (181 mg, 0.156 mmol) were added to a 250 mL Schlenk flask, degassed and backfilled with N_2 . The following solvents were added, 2 M Na_2CO_3 (80 mL) and THF (80 mL) and the solution was refluxed (80 °C) for 24 h. The solution was cooled to room temperature, the organic layer was extracted with EtOAc (2 x 50 mL) and the solution dried over anhydrous MgSO_4 . Solvents removed and solids recrystallized from Acetonitrile. Yield 70% (650 mg). Mp: 155-160 °C. ^1H NMR (500 MHz, CD_3CN): δ = 1.39 (t, 6H), 4.38 (q, 4H), 7.44 (d, 1H, J = 7.8 Hz), 7.63 (d, 1H, J = 7.9 Hz), 7.87 (d, 4H, J = 8.5 Hz), 7.91 (d, 2H, J = 8.2 Hz), 7.99 (d, 2H, J = 8.3 Hz), 8.15 (m, 4H), 8.28 (m, 2H), 8.36 (d, 2H, J = 7.9 Hz), 10.05 (s, 1H), 10.91 (s br, 1H). ^{13}C NMR (126 MHz, CD_3CN): δ = 193.23, 167.10, 153.41, 146.60, 143.47, 142.02, 136.86, 131.11, 131.03, 130.91, 130.25, 130.23, 129.78, 128.93, 128.71, 128.67, 128.64, 124.51, 123.09, 61.83, 14.63. H-MS (ESI): calcd for $[\text{M}+\text{H}]^+$, $^{13}\text{C}_1\text{C}_{37}\text{H}_{31}\text{N}_2\text{O}_5^+$, m/z = 596.2154, found m/z = 596.2266.

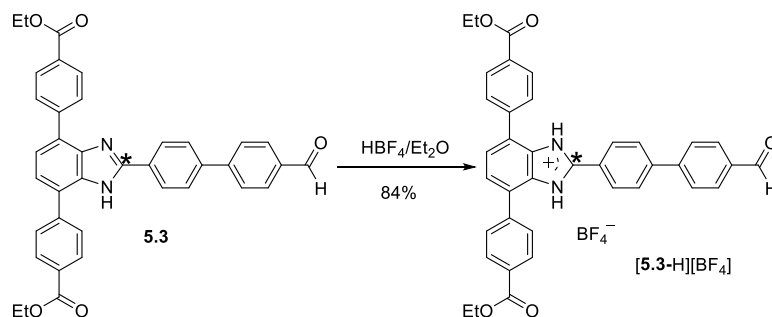


Scheme 5.4 – synthesis of **5.3**.

5.2.5 Synthesis of $[\mathbf{5.3-H}][\text{BF}_4]$

5.3 (500 mg, 0.83 mmol) was dissolved in THF (10 mL). Tetrafluoroboric acid diethyl ether complex (125 μL , 0.924 mmol) was added and stirred for 30 min. The yellow solid was vacuum filtered and washed with ether. Yield 90% (450mg). Mp: 200-205 °C. ^1H NMR

(500 MHz, CD₃CN, 298 K): δ = 1.41 (t, 6H), 4.40 (q, 4H), 7.78 (s, 2H), 7.86 (d, 4H, J = 8.2 Hz), 7.95 (d, 2H, J = 8.2 Hz), 8.04 (t, 4H, J = 8.8 Hz), 8.15 (m, 2H), 8.24 (d, 4H, J = 8.2 Hz), 10.08 (s, 1H). ¹³C NMR (75 MHz, CD₃CN): δ = 193.24, 166.90, 152.45, 145.37, 140.73, 137.50, 132.14, 131.24, 131.19, 130.26, 129.34, 129.30, 129.07, 128.56, 128.54, 128.28, 62.15, 14.36. HR-MS (ESI): Calculated for [M-BF₄]⁺, [¹³C₁C₃₇H₃₁N₂O₅]⁺, m/z = 596.2153; found m/z = 596.2258.

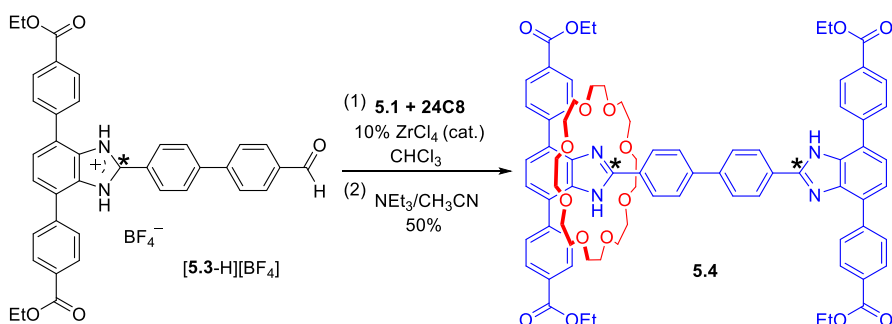


Scheme 5.5 – synthesis of [5.3-H][BF₄].

5.2.6 Synthesis of 5.4

24C8 (300 mg, 0.85 mmol) was added to [5.3-H][BF₄] (341 mg, 0.56 mmol) in a round bottom flask. CHCl₃ (25 mL) was added and stirred at room temperature until a clear solution formed. 1,2-Diamino-3,6-di(4-*t*-butylphenyl)benzene **5.1** (230 mg, 0.56 mmol) was added, followed by ZrCl₄ (13 mg, 0.05 mmol) and the solution was stirred at room temperature for 24 h. The solution was filtered, solvent was evaporated, CH₃CN (25 mL) was added and filtered. Et₃N (0.5 mL) was added to the filtration. The solution was filtered and air dried producing a white solid. Yield 50% (380 mg). Mp: 240-245 °C. ¹H NMR (500 MHz, CD₂Cl₂, 298 K): δ = 1.43 (m, 12H), 3.21 (s, 32H), 4.41 (m, 8H), 7.40 (d, 2H, J = 7.7 Hz), 7.60 (d, 2H, J = 7.8 Hz), 7.82 (d, 4H, J = 8.1 Hz), 7.90 (d, 4H, J = 8.3 Hz), 8.19 (m, 8H), 8.35 (d, 4H, J = 8.2 Hz), 8.55 (d, 4H, J = 8.2 Hz), 10.86 (brs 2H). ¹³C NMR (126 MHz, CD₂Cl₂): δ = 166.83, 166.50, 153.59, 143.52, 143.47, 143.01, 141.75, 133.65, 130.84, 130.42, 130.07, 129.89, 129.77, 129.73, 129.47, 128.93, 126.95, 125.21, 123.53, 122.17, 70.84, 70.02, 61.46,

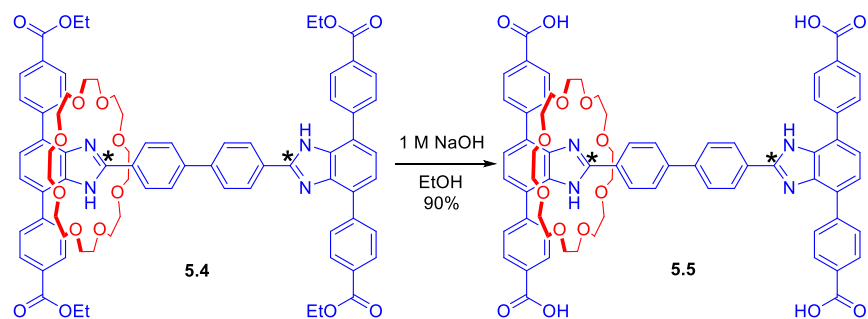
61.09, 26.91, 14.48. HR-MS (ESI): calculated for $[M+H]^+$, $[^{13}\text{C}_1\text{C}_{77}\text{H}_{83}\text{N}_4\text{O}_{16}]^+$, $m/z = 1332.5725$, found $m/z = 1331.5797$.



Scheme 5.6 – synthesis of **5.4**.

5.2.7 Synthesis of **5.5**

To **5.4** (250 mg, 0.187 mmol) in tetrahydrofuran (20 mL) and ethanol (40 mL), 1 M NaOH (40 mL) was added. After the reaction mixture was stirred at 80 °C for 24 h, the solvent was removed on a rotary evaporator. Deionized water (20 mL) was added to dissolve the residue. Then 0.1 N HCl was added to give a pH value of about 5. The precipitate was collected by vacuum filtration and air dried. Yield: 90% (215 mg). Mp: >300 °C. ¹H NMR (500 MHz, DMSO-d₆): δ = 3.19 (s, 32H), 7.41 (d, 2H, *J* = 7.3 Hz), 7.66 (d, 2H, *J* = 7.4 Hz), 7.89 (d, 4H, *J* = 7.5 Hz), 8.15 (m, 4+8H), 8.44 (d, 4H, *J* = 7.7 Hz), 8.59 (d, 4H), 12.56 (s, 2H), 13.03 (s br, 4H). ¹³C NMR (126 MHz, DMSO-d₆): δ = 167.37, 167.22, 153.45, 152.61, 142.54, 142.29, 142.23, 140.43, 133.43, 129.86, 129.76, 129.37, 129.28, 129.24, 129.07, 129.00, 128.90, 128.82, 127.17, 125.02, 123.25, 121.48, 69.16. HR-MS (ESI): $[M+H]^+$, $[^{13}\text{C}_1\text{C}_{69}\text{H}_{67}\text{N}_4\text{O}_{16}]^+$, $m/z = 1220.4470$, found $m/z = 1220.4562$.



Scheme 5.7 – synthesis of 5.5.

5.2.8 ^1H NMR spectrum of 5.4 with resonance assignments labeling

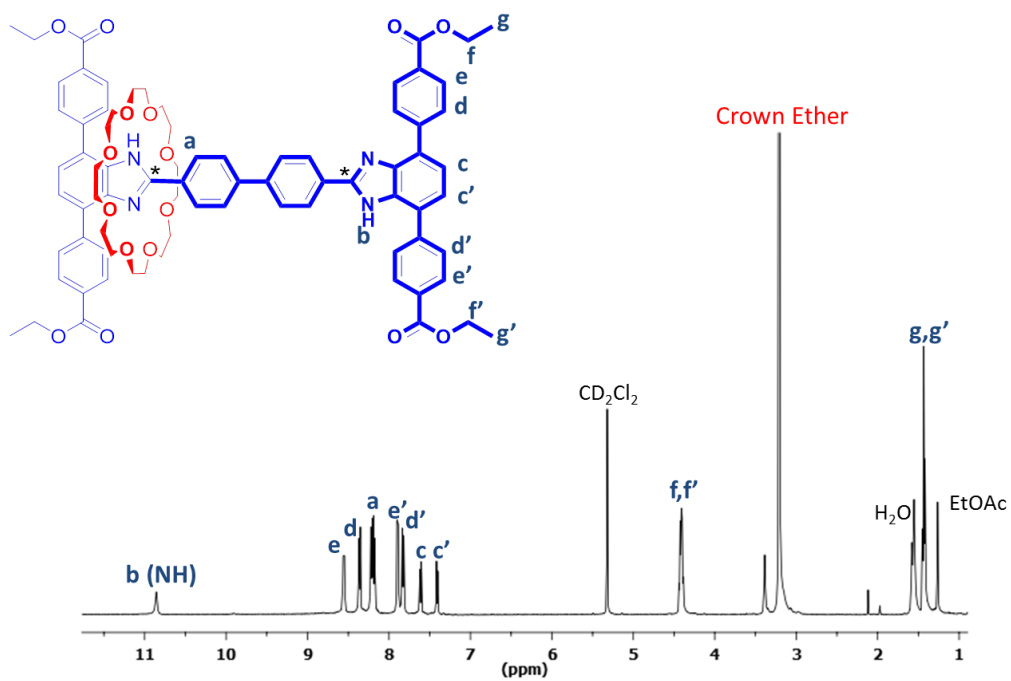


Fig 5.7 – ^1H NMR spectrum of 5.4.

5.2.9 Determination of the rates of shuttling for 5.4, [5.4-H]⁺, [5.4-H₂]²⁺ in solution

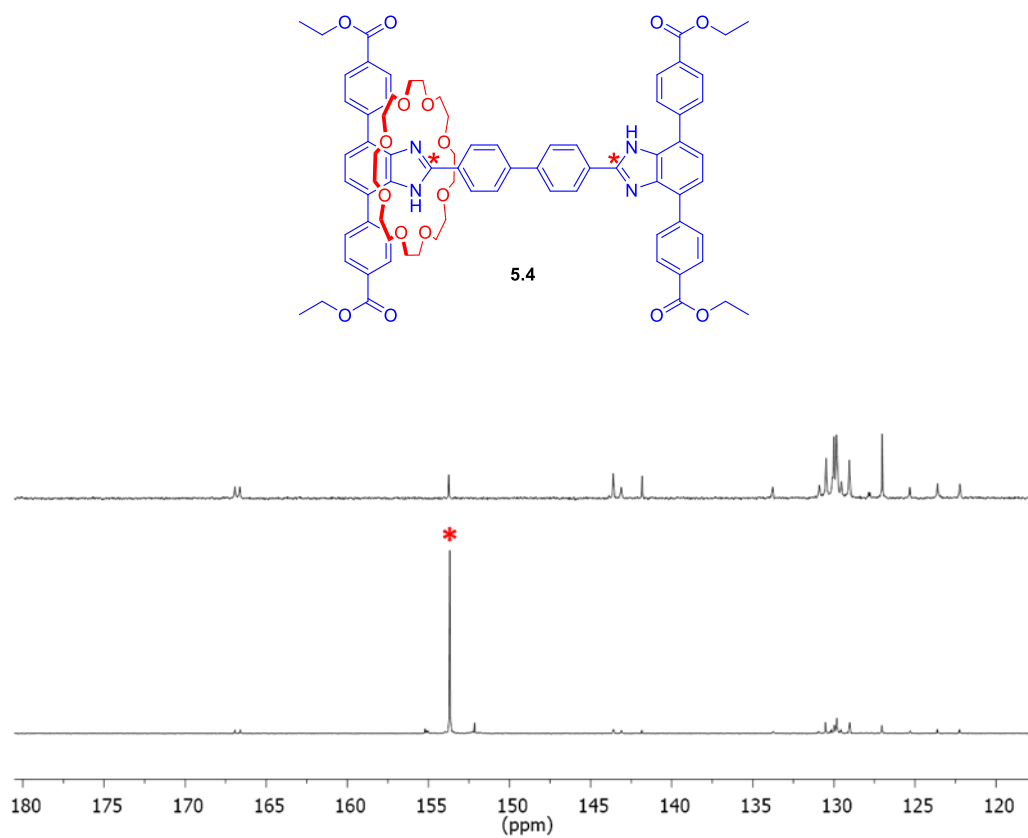


Fig 5.8 – solution ¹³C NMR spectra (125 MHz, CD₂Cl₂, 298 K) of **5.4** non-enriched (top) and a ¹³C-enriched **5.4** (bottom), (* = ¹³C-enriched atoms).

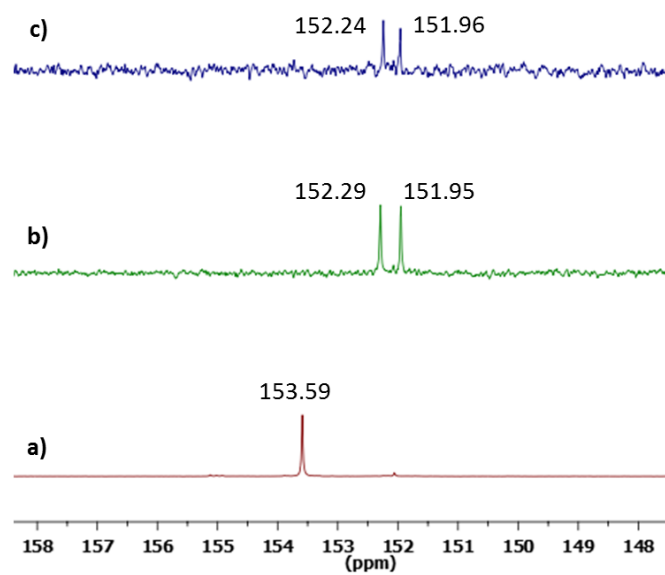


Fig 5.9 – partial ^{13}C NMR solution spectra (125 MHz, CD_2Cl_2 , 298K) of a) **5.4** (neutral rotaxane linker), b) $[\mathbf{5.4-H}]^+$ (+1 charged rotaxane linker) the sites are different and resolved, one is charged and occupied the other is neutral and unoccupied, c) $[\mathbf{5.4-H}_2]^{2+}$ (+2 charged rotaxane linker).

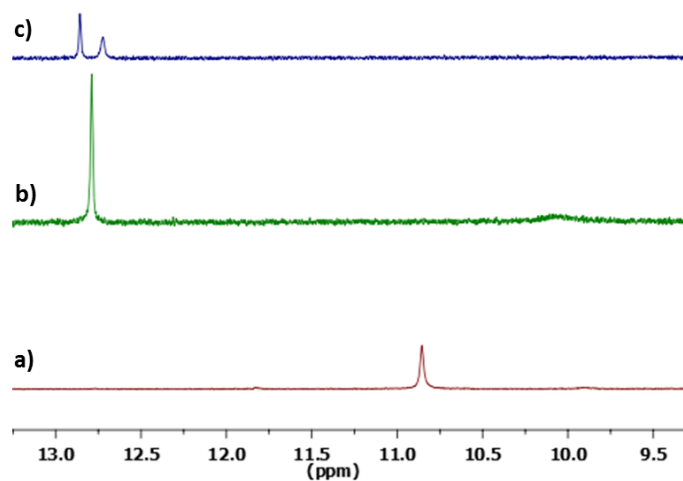


Fig 5.10 – partial ^1H NMR solution spectra (500 MHz, CD_2Cl_2 , 298 K) of a) **5.4** (neutral rotaxane linker), b) $[\mathbf{5.4-H}]^+$ (+1 charged rotaxane linker) the sites are different and resolved

one is charged and occupied the other is neutral and unoccupied, c) [5.4-H₂]²⁺ (+2 charged rotaxane linker).

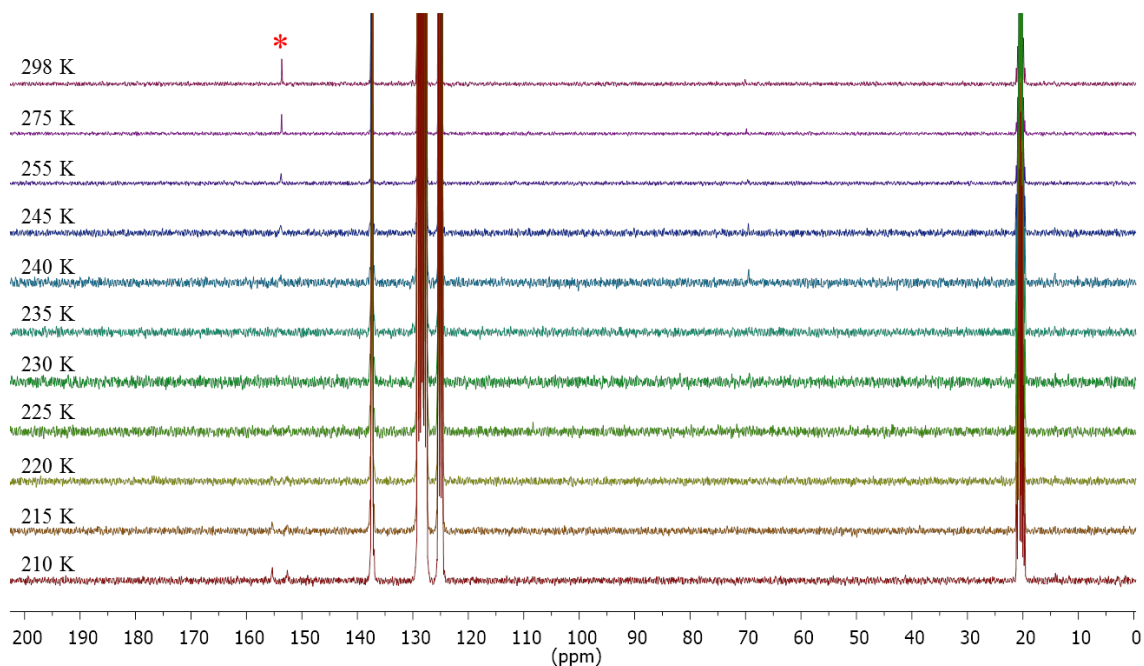


Fig 5.11 – variable temperature ¹³C NMR spectra of neutral 5.4 in toluene-d₈ (* = ¹³C-enriched atoms, (toluene-d₈ was chosen as a solvent since it has very low melting point and polarity).

The shuttling rates were calculated from a line shape analysis of the NMR spectra using the program DNMR71.EXE^[17]. Free energies of activation (ΔG^\ddagger) were estimated using the Eyring equation: $\Delta G^\ddagger = -RT \ln (kh/k_B T)$, where R is the ideal gas constant, h is Planck's constant and k_B is Boltzmann's constant. The enthalpic (ΔH^\ddagger) and entropic (ΔS^\ddagger) contributions to the transition state were calculated from Eyring plots: $\ln (k/T) = - (\Delta H^\ddagger/RT) + (\Delta S^\ddagger/R) + \ln (k_B/h)$.

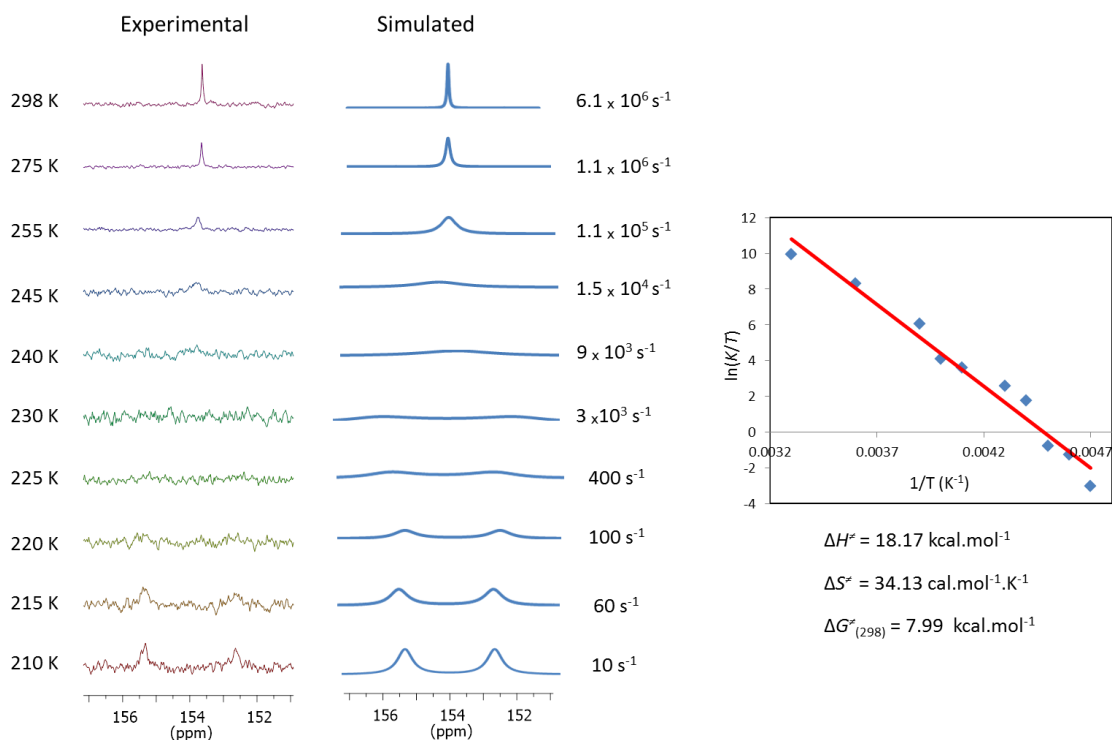


Fig 5.12 – comparison of the experimental and simulation ¹³C NMR data (left) for the ¹³C-enriched carbon of neutral **5.4**, Eyring plot (right) for the shuttling of neutral **5.4** generated from the simulated data.

The shuttling rate for [5.4-H₂]²⁺ can be obtained by using the equations shown below, where I_{AA} and I_{BB} are the diagonal peak intensities and I_{AB} and I_{BA} are the cross-peak intensities. k is the sum of the forward, k_1 , and backward, k_{-1} , pseudo-first order rate constants for the shuttling process. k_1 and k_{-1} are equal due to the identical stations and thus the observed pseudo-first order rate constant, k_{obs} can be determined. R is the ideal gas constant, h is Planck's constant and k_B is Boltzmann's constant.

$$r = (I_{AA} + I_{BB}) / (I_{AB} + I_{BA}), \quad k = 1/\tau_m \ln(r + 1/r - 1), \quad k = k_1 + k_{-1}, \quad k_{obs} = k_1 = k_{-1}$$

$$\Delta G^\ddagger = -RT \ln(k_{obs} h / k_B T)$$

Table 5.1 – kinetic parameters for shuttling process of $[5.4-H_2]^{2+}$ (no shuttling was observed at 268 K).

T (K)	I_{AA}	I_{BB}	I_{AB}	I_{BA}	k_{obs} (S ⁻¹)	ΔG^\ddagger (kcal mol ⁻¹)
320 K	19889000	19369000	2539400	2826600	0.27	19.6
330 K	5104100	5035800	1031000	1375300	0.43	19.9

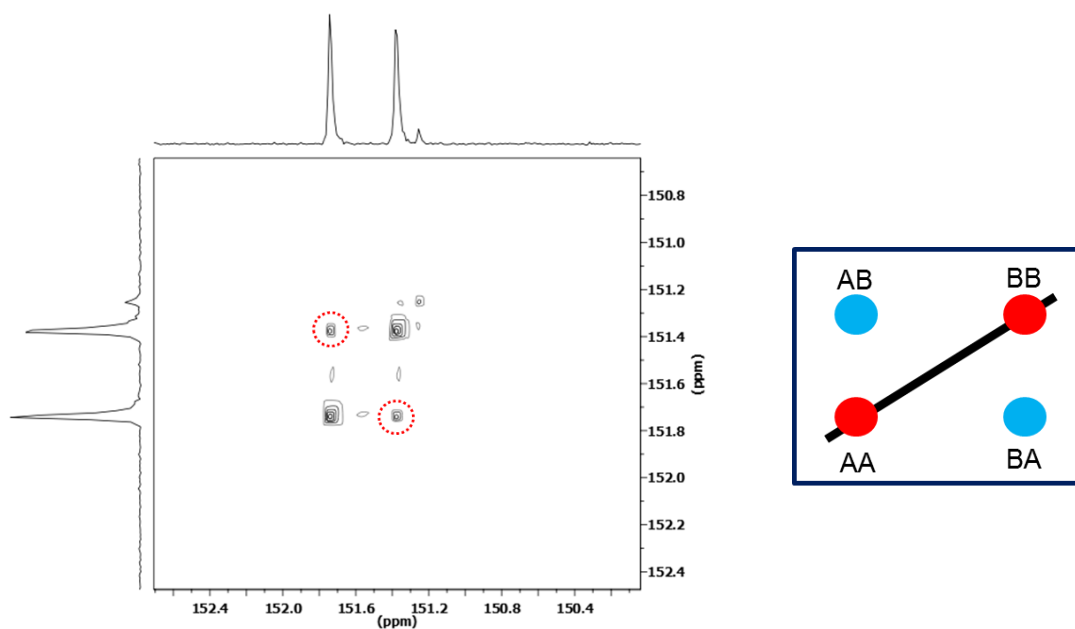


Fig 5.13 – partial 2D EXSY ^{13}C NMR (500 MHz, 320 K, CD_3CN with $\tau_m = 500$ ms) spectrum of $[5.4-H_2]^{2+}$.

5.2.10 Analysis of MOFs: UWDM-6 and UWDM-7 by ^1H NMR Spectroscopy

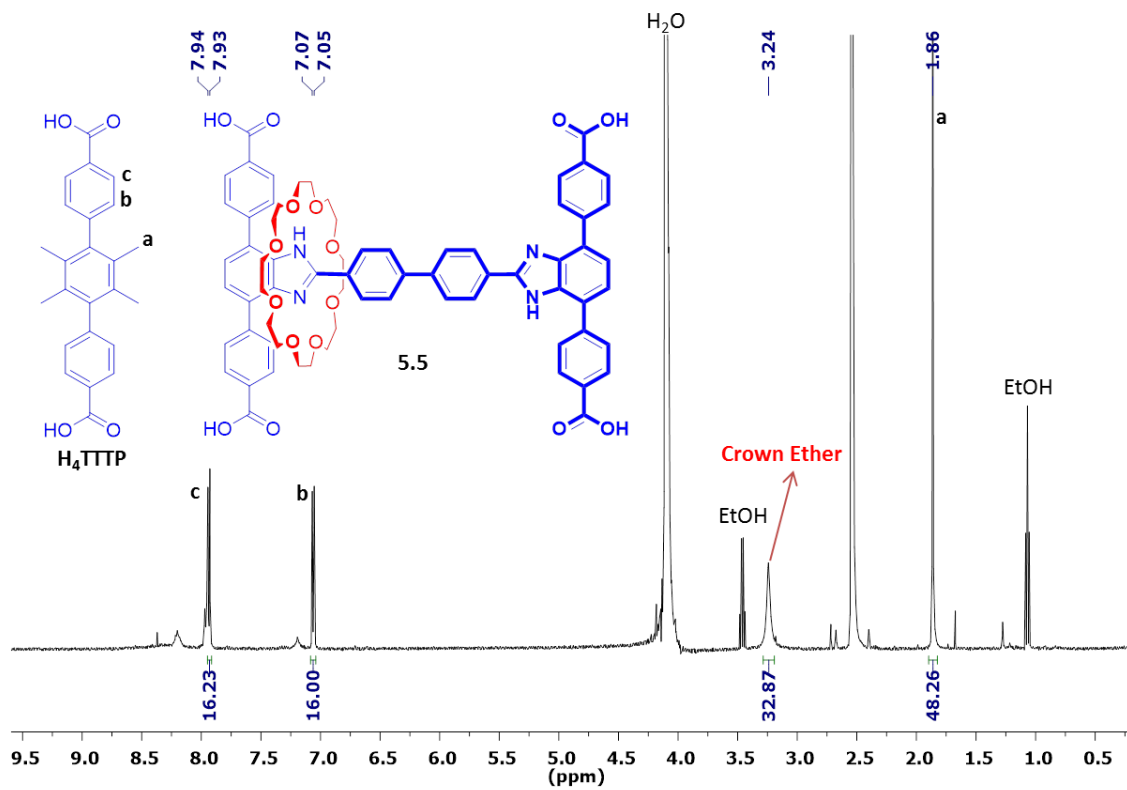


Fig 5.14 – ^1H NMR of **UWDM-6** after digestion (500 MHz, DMSO-d_6), the integration shows the ratio of H_4TTTP to 5.5 is about 4:1.

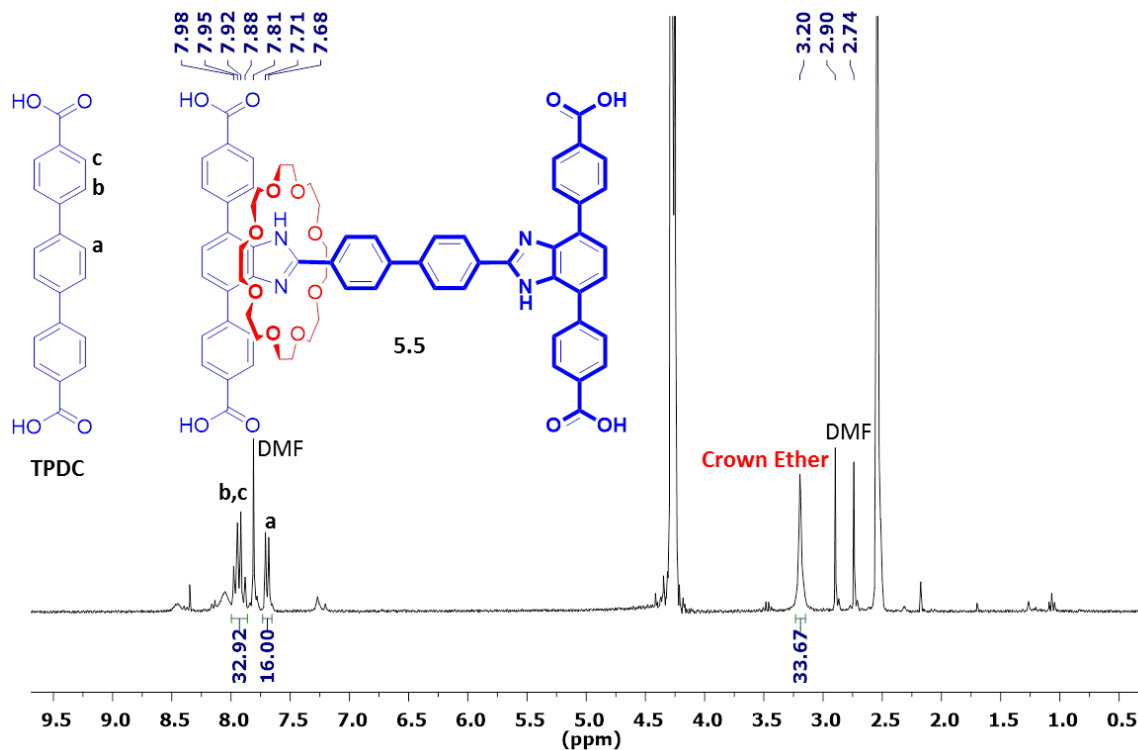


Fig 5.15 – ¹H NMR of **UWDM-7** after digestion (500 MHz, DMSO-d₆), the integration shows the ratio of **TPDC** to **5.5** is about 4:1.

5.2.11 Comparing the ¹³C SSNMR of [UWDM-6-H][TFA] and PCN-57

The presence of only single peak of carboxylic acid group in ¹³C SSNMR of known **PCN-57** and [UWDM-6-H][TFA] showed all carboxylate groups of **5.5** linker are incorporated into Zr-MOFs.

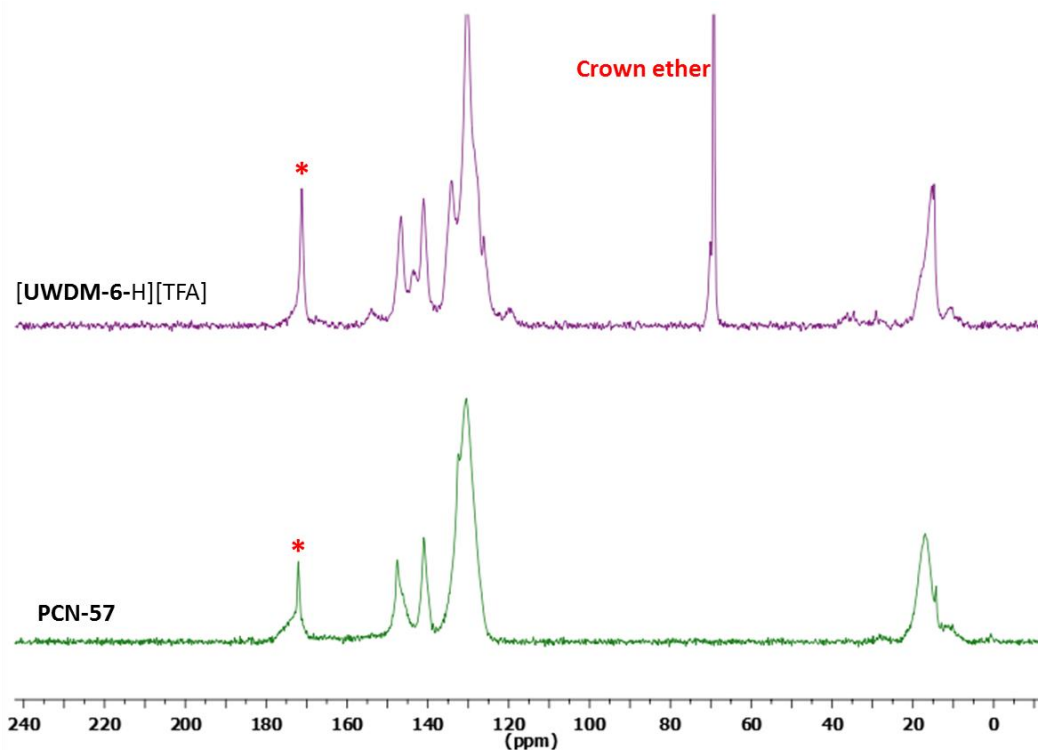


Fig 5.16 – ^{13}C SSNMR of $[\text{UWDM-6-H}][\text{TFA}]$ and PCN-57 (* = carboxylic acid group).

5.2.12 Comparing optical microscope images of microcrystals of UWDM-6 (three states) and 5.5 (three states) in solution under UV irradiation

Tetrafluoroboric acid diethyl ether complex (2 μL , 0.015 mol) was added to a **5.4** (20 mg, 0.015 mmol) solution in CH_2Cl_2 (2 mL). The mixture was stirred for 5 min. Ether was added to precipitate the product. The solids were filtered, washed with some ether and air dried giving to $[\text{5.4-H}_2][\text{BF}_4]_2$.

10 mg of $[\text{5.4-H}_2][\text{BF}_4]_2$ dissolved in mixture of CH_3CN (2 mL) and H_2O (1 mL) and sonicated for 5 min. Then CH_3CN was removed, solids were filtered and air dried to yield $[\text{5.4-H}][\text{BF}_4]$.

The as-synthesized MOF, $[\text{UWDM-6-H}][\text{TFA}]$ (50 mg), was soaked in a 0.07 mol/L solution of proton sponge® (*N,N,N',N'*-tetramethyl-1,8-naphthalenediamine) in ethanol (60

mg in 4 mL EtOH). The mixture was kept in the dark at room temperature for 72 h (solvent replaced every 12 h and the qualitative level of deprotonation was monitored by UV irradiation). The crystals were then washed with fresh ethanol once and re-soaked in fresh ethanol for 2 h. The solids were filtered, air-dried and were activated at 160 °C for 12 h giving to **UWDM-6**.

25 mg of **UWDM-6** was soaked in a 2 M solution of $\text{CF}_3\text{SO}_3\text{H}$ in ethanol at 60 °C for 24 h (solvent replaced every 12 h). Then the microcrystals were filtered, washed with ethanol, air dried and were activated at 160 °C for 12 h giving to $[\text{UWDM-6-H}_2][\text{OTf}]_2$.

The same methods were done on **UWDM-7** for acid/base treatment. And the results of optical microscope images of three states of **UWDM-7** were similar to **UWDM-6**.

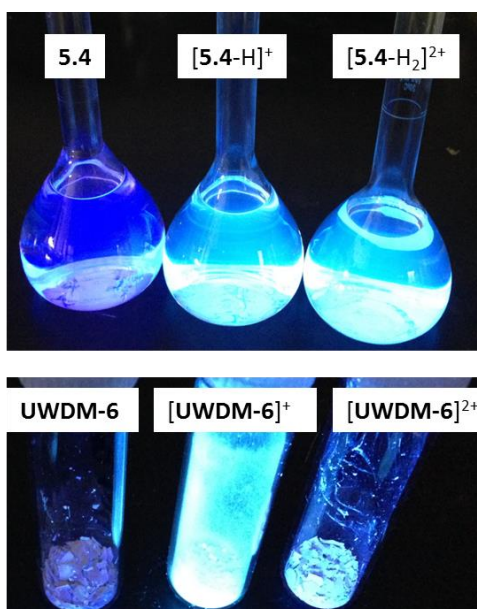


*Fig 5.17 – optical images of three states of 5.4 linkers in CD_2Cl_2 and microcrystals of **UWDM-6** under UV irradiation.*

5.2.13 Variable Temperature PXRD data for UWDM-6

Powder X-ray diffraction (PXRD) measurements were recorded on a Brüker D8 Discover diffractometer equipped with a GADDS 2D-detector and operated at 40 kV and 40 mA. CuK α radiation ($\lambda = 1.54187 \text{ \AA}$) was used and the initial beam diameter was 0.5 mm. Samples were mounted in a 0.5 mm boron-rich capillary tube on a goniometer head. Data was collected as rotation frames at 2θ value of 18° for 15 min.

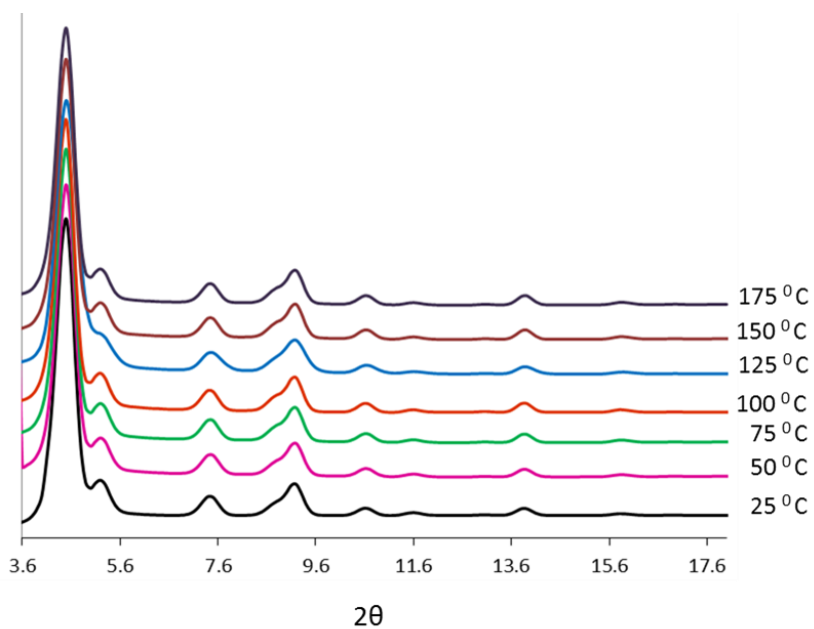


Fig 5.18 – variable temperature PXRD analysis of UWDM-6.

5.2.14 ^{13}C SSNMR of $[\text{UWDM-6-H}][\text{TFA}]$, UWDM-6 and $[\text{UWDM-6-H}_2][\text{OTf}]_2$

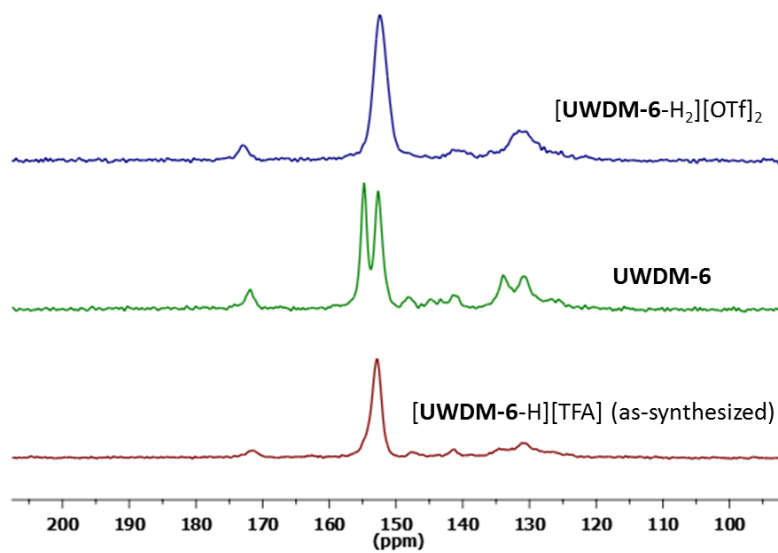


Fig 5.19 – partial ^{13}C SSNMR of the three states of **UWDM-6** (neutral, 1+, 2+).

5.3. References

1. R. Barat, T. Legigan, I. Tranoy-Opalinski, B. Renoux, E. Péraudeau, J. Clarhaut, P. Poinot, A. E. Fernandes, V. Aucagne, D. A. Leigh and S. Papot, *Chem. Sci.*, **2015**, *6*, 2608–2613.
2. F. H. S. Li, J. Chen, B. Zheng, S. Dong, Z. Ma, H. W. Gibson, *J. Polym. Sci. Part A*, **2010**, *48*, 4067–4073.
3. V. Blanco, D. A. Leigh, V. Marcos, J. A. Morales-Serna and A. L. Nussbaumer, *J. Am. Chem. Soc.*, **2014**, *136*, 4905–4908.
4. N. D. Suhan, L. Allen, M. T. Gharib, E. Viljoen, S. J. Vella and S. J. Loeb, *Chem. Commun.*, **2011**, *47*, 5991–5993.
5. S. J. Loeb, *Chem. Soc. Rev.*, **2007**, *36*, 226–235.
6. J. W. Choi, A. H. Flood, D. W. Steurman, S. Nygaard, A. B. Braunschweig, N. N. P. Moonen, B. W. Laursen, Y. Luo, E. Delonno, A. J. Peters, J. O. Jeppesen, K. Xu, J. F. Stoddart and J. R. Heath, *Chem. Eur. J.*, **2006**, *12*, 261–279.
7. E. R. Kay, D. A. Leigh and F. Zerbetto, *Angew. Chem. Int. Ed.*, **2007**, *46*, 72–191.
8. K. Zhu, C. A. O’Keefe, V. N. Vukotic, R. W. Schurko and S. J. Loeb, *Nat. Chem.*, **2015**, *7*, 514–519.
9. J. H. Cavka, S. Jakobsen, U. Olsbye, N. Guillou, C. Lamberti, S. Bordiga and K. P. Lillerud, *J. Am. Chem. Soc.*, **2008**, *130*, 13850–13851.
10. S. Øien, D. Wragg, H. Reinsch, S. Svelle, S. Bordiga, C. Lamberti and K. P. Lillerud, *Cryst. Growth Des.*, **2014**, *14*, 5370–5372.

11. H. L. Jiang, D. Feng, T. F. Liu, J. R. Li and H. C. Zhou, *J. Am. Chem. Soc.*, **2012**, 134, 14690–14693.
12. J.-S. Qin, S. Yuan, Q. Wang, A. Alsalmeh and H.-C. Zhou, *J. Mater. Chem. A*, **2017**, 5, 4280–4291.
13. S. Yuan, J. S. Qin, L. Zou, Y. P. Chen, X. Wang, Q. Zhang and H. C. Zhou, *J. Am. Chem. Soc.*, **2016**, 138, 6636–6642.
14. Y. Bai, Y. Dou, L.-H. Xie, W. Rutledge, J.-R. Li and H.-C. Zhou, *Chem. Soc. Rev.*, **2016**, 45, 2327–2367.
15. K. Zhu, V. N. Vukotic and S. J. Loeb, *Angew. Chemie - Int. Ed.*, **2012**, 51, 2168–2172.
16. K. Zhu, V. N. Vukotic, N. Noujeim and S. J. Loeb, *Chem. Soc. Rev.*, **2012**, 3, 3265–3271.
17. DNMR71.EXE, Reich, H. J., *J. Chem. Educ. Software*, **1996**.

CHAPTER 6

6.1 A Bistable Molecular Shuttle that Switches Inside a Zr-MOF

6.1.1 Introduction

Bistable [2]rotaxane molecular shuttles—mechanically interlocked molecules (MIMs) that can adopt two different translational, co-conformations in response to an external stimulus such as a chemical, electrochemical, or photochemical—are molecular switches and have been studied due to their potential applications from drug delivery to molecular electronic devices.^[1-3] In a degenerate [2]rotaxane molecular shuttle, composed of a linear dumbbell shaped axle with two distinct recognition sites and a single macrocyclic wheel that moves back and forth between sites, there is an equilibrium between two co-conformations. This degenerate [2]rotaxane molecular shuttle can be designed to be a bistable molecular switch^[4-7] by introducing a large difference in the affinity of macrocycle for the two competing recognition sites. The thermodynamic preference for a particular co-conformation in the bistable molecular switch can be reversed by using an external stimulus (Fig 6.1).^[8,9]

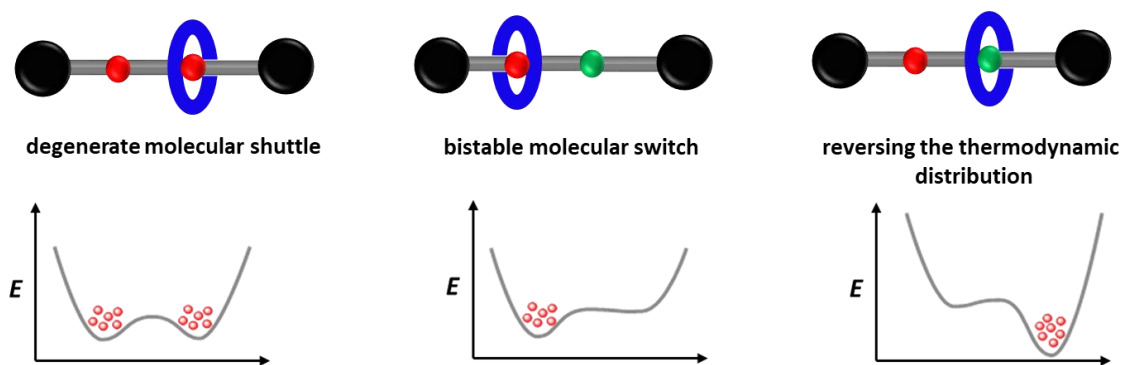


Fig 6.1 – representations of a degenerate molecular shuttle, a bistable molecular switch and reversing the thermodynamic preference by using external perturbation (top), thermodynamic distribution for the presence of macrocycle between the two recognition sites (bottom).

[2]Rotaxane molecular shuttles with two equivalent benzimidazole recognition sites that the macrocycle can shuttle between have been reported by Loeb.^[16] Here we design and synthesize a novel bistable molecular switch with two different recognition sites (see Fig 6.2); the macrocycle prefers to reside on the site for which there is stronger binding affinity. In this [2]rotaxane design, the macrocycle could be translocated to the pyridine unit nearby when metal ion such as Li^+ or an equivalent of acid is added.

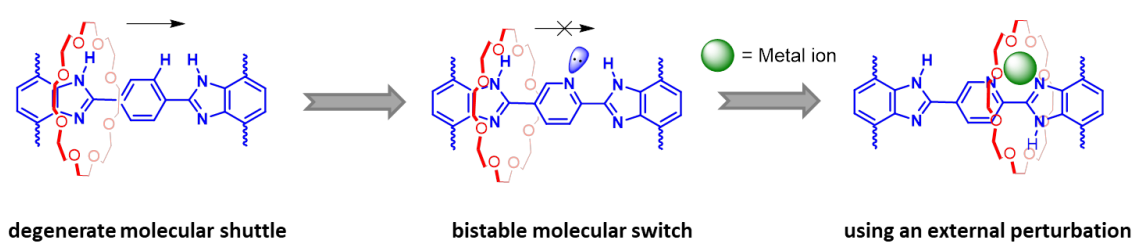


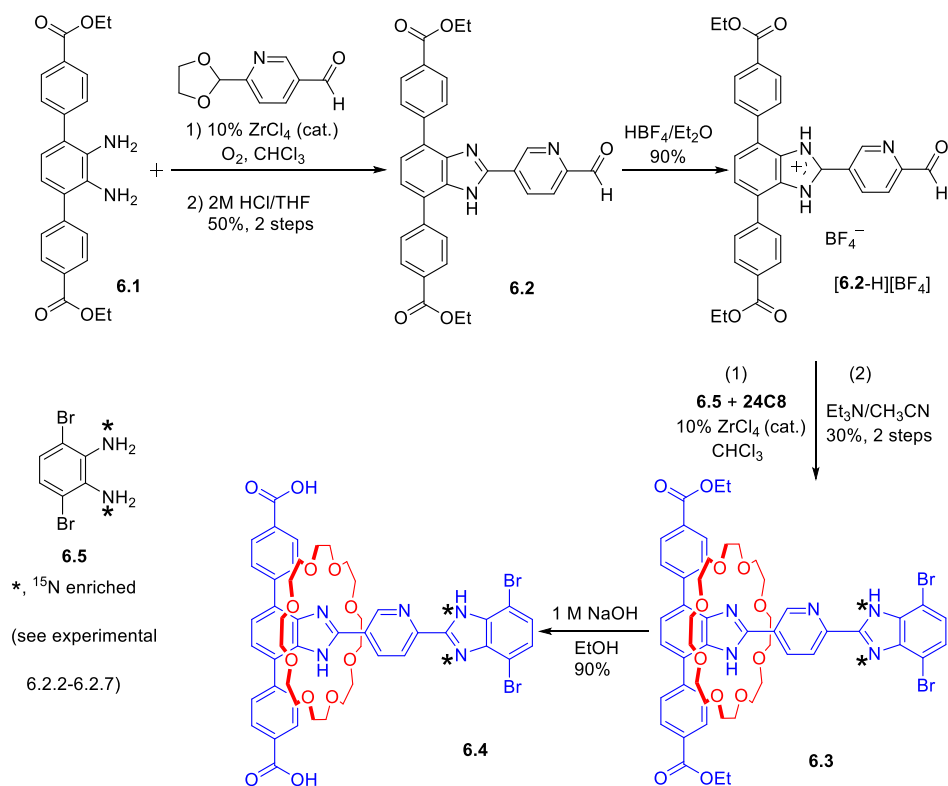
Fig 6.2 – representation of the new design of a bistable molecular switch and the macrocycles translation in response to an external perturbation.

A number of studies on bistable [2]rotaxane molecular switches have been carried in solution where the motion is incoherent and random.^[10,11] It is desirable to impose higher order on these molecules by incorporating them into solid-state materials. Metal-organic frameworks (MOFs)^[12,13] which include interlocked components as linkers is one type of solid state material that can address this aim. Notably, Loeb reported the preparation of Zn-based MOF containing a degenerate [2]rotaxane molecular shuttle as a linker in which the macrocyclic wheel can undergo translational motion inside the solid state materials.^[14] Herein, we have designed and synthesized a new Zr-based MOF, **UWDM-8** (University of Windsor Dynamic Material), containing a non-degenerate [2]rotaxane and terphenyl linkers based on the structure of the known MOF material **PCN-57**^[15] (Porous Coordination Network). In this prepared MOF, reversible translational motion of the macrocycle between the two non-equivalent sites was performed by changing the pH. It was proposed that the

reversible molecular switching inside the MOF could be monitored by a 2D ^{15}N - ^1H SSNMR experiment and triggered by changing the environment of the hydrogen-bonding of the benzimidazole site adjacent to the pyridine unit.

6.1.2 Results and discussion

Scheme 6.1 outlines the major steps in the synthesis of a new bistable molecular shuttle linker, **6.4**. The [2]rotaxane linker, **6.4**, was prepared by capping a preformed [2]pseudorotaxane [**6.2**-H \subset **24C8**]⁺ with **6.5** followed by hydrolysis of the resulting diester [2]rotaxane (**6.3**) to yield **6.4**.^[16] For eventual identification of the translational motion of the macrocycle by ^{15}N SSNMR in the MOF in response of external perturbation, the nitrogen atoms at the benzimidazole rings of **6.4** (shown with asterisks in Scheme 6.1) were enriched to 50% ^{15}N by using **6.5** (see experimental 6.2.2-6.2.11 for full synthetic details). Thus, it was expected that when the macrocycle relocates from its initial position to the desired site by adding an external perturbation, that through-space correlation will be observed between the hydrogen atoms of the macrocycle and the ^{15}N -enriched benzimidazole site by ^{15}N SSNMR spectroscopy.



Scheme 6.1 – major steps in the synthesis of a molecular shuttle linker (see experimental 6.2 for full synthetic details).

It was first necessary to demonstrate that the molecular switch can operate in response to a chemical perturbation in solution. By adding one equivalent of acid to **6.3** to give **[6.3-H]⁺**, ¹H NMR spectra showed significant changes in chemical shifts indicative of relocating the macrocycle due to the change in thermodynamic preference for the protonated recognition site (see Fig 6.3). Furthermore, addition of lithium triflate to the neutral [2]rotaxane solution yields **[6.3.Li]⁺** in which there is stronger binding affinity between Li⁺ ion, nitrogen atoms and crown ether oxygen atoms; and this caused similarly significant chemical shifts in spectrum the ¹H NMR similar to **[6.3-H]⁺** (see Fig 6.3).

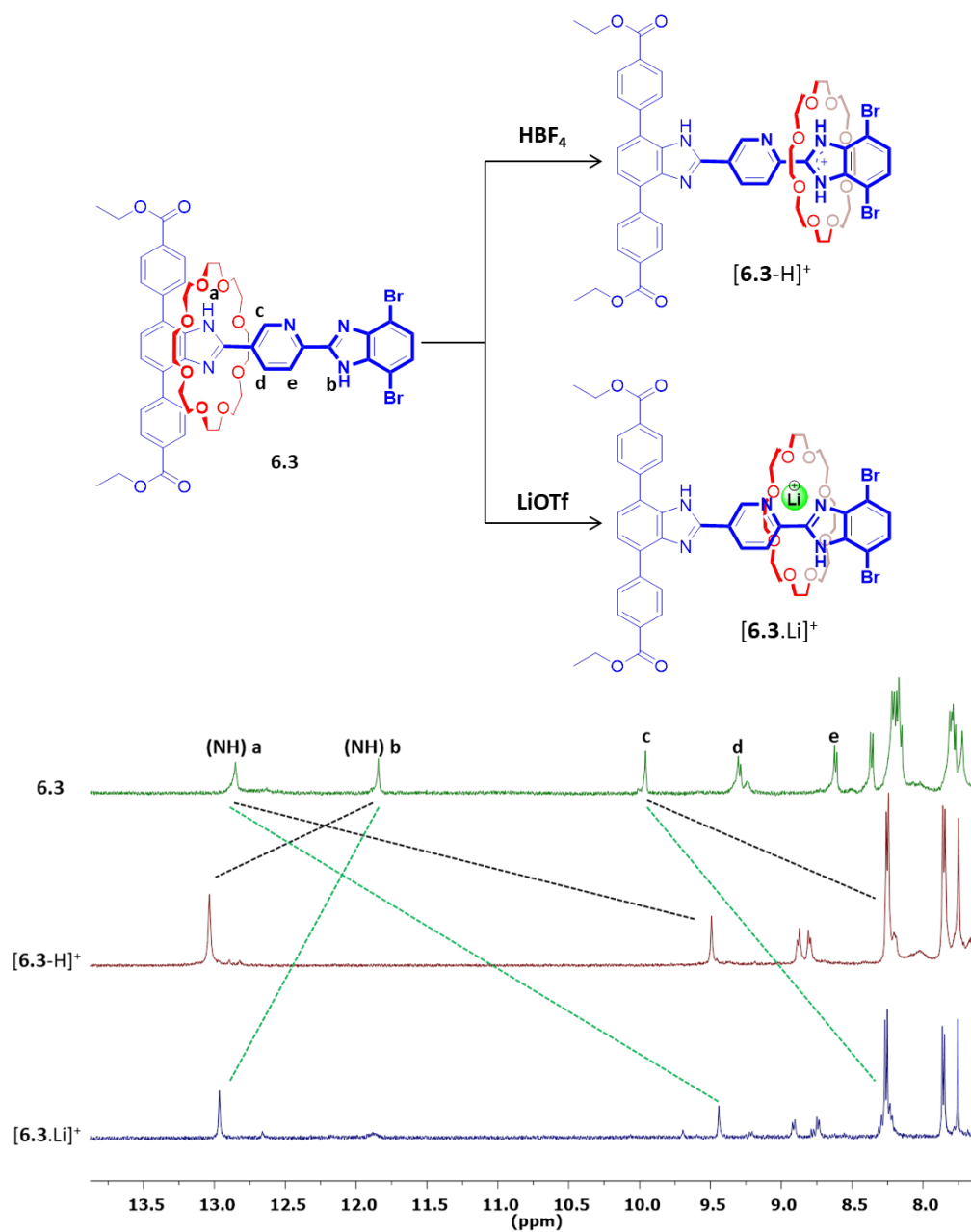


Fig 6.3 – relocating of **24C8** as a result of adding chemical perturbation (top), partial ^1H NMR of **6.3**, $[\mathbf{6.3}\text{-H}]^+$ and $[\mathbf{6.3}\text{.Li}]^+$ in CDCl_3 with resonance assignments (bottom).

To achieve a bistable solid-state molecular switch, **6.4** was incorporated into a Zr-based MOF. To this aim, zirconium (IV) tetrachloride was combined with **6.4** and **H₄TTTP** (2',3',5',6'-tetramethylterphenyl-4,4'' dicarboxylic acid) in a ratio of 6:1:5 in 2 mL

N,N-dimethylformamide with 5 drops of trifluoroacetic acid (TFA) and heated to 100 °C for 24 h (Fig 6.4). This yielded white microcrystals designated **UWDM-8**.

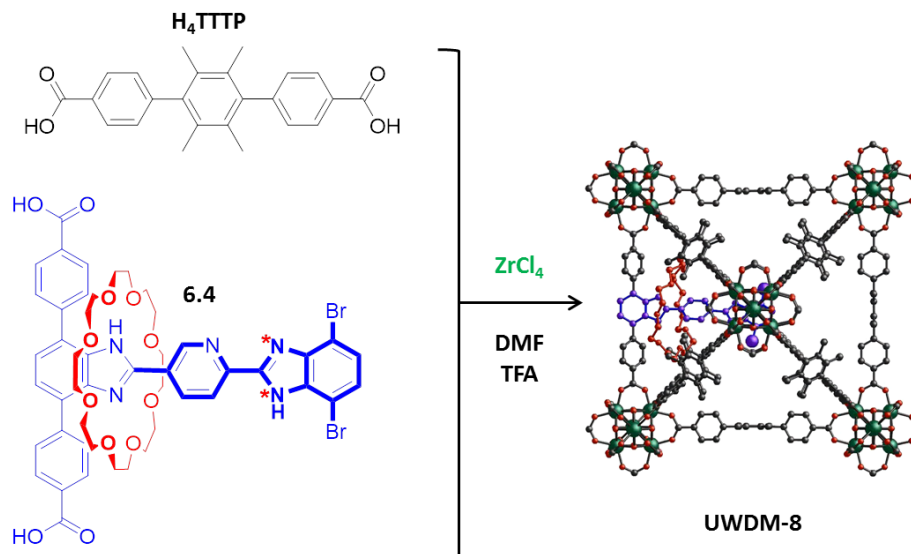


Fig 6.4 – synthetic route for making **UWDM-8** (TFA: trifluoroacetic acid). A structure of **UWDM-8** shown was generated from the X-ray structure of **PCN-57** using Material Studio.

The powder X-ray diffraction (PXRD) pattern of **UWDM-8** was similar to that reported for **PCN-57** (Fig. 6.5). To prove the presence of **6.4** linker within the framework, a portion of **UWDM-8** was digested in a DMSO/ K_3PO_4 (saturated solution in D_2O) and analyzed by 1H NMR spectroscopy. This experiment showed the ratio of **TTTP** to **6.4** was about 5:1 (see experimental 6.2.12). This represents the replacement of a single **TTTP** linker by a [2]rotaxane. Molecular modeling using Materials Studio suggests that this likely means there is one molecular switch is incorporated per octahedral cavity as the [2]rotaxane is probably too large for the smaller tetrahedral cavities.

Based on previous MOF syntheses with related benzimidazole linkers, we assumed that the as-synthesized MOF material contained the linker in the mono-protonated state, so we assigned it formula $Zr_6(TTTP)_5[6.4-H]^+[CF_3COO]^-$ (**[UWDM-8-H][TFA]**). From the

solution studies, it is expected that the macrocycle in [**UWDM-8-H**][TFA] resides on the ^{15}N -enriched benzimidazolium recognition site; thus, the correlation between the ^{15}N -enriched site and the hydrogens of the crown ether should be observed in ^1H - ^{15}N SSNMR. However, when the as-synthesized MOF ([**UWDM-8-H**][TFA]) is treated with the strong base N,N,N',N' -tetramethylnaphthalene-1,8-diamine (proton-sponge) in ethanol to make neutral MOF (**UWDM-8**) this observation should be switched off since the crown ether will no longer be in close proximity to the ^{15}N -enriched benzimidazolium recognition site.

Deprotonation of [**UWDM-8-H**][TFA] to **UWDM-8** was inferred by a significant change in the fluorescence colour and intensity of the solid upon UV irradiation at 345 nm. Powder X-ray diffraction (PXRD) experiments on **UWDM-8** showed retention of the framework integrity and crystallinity of the MOF after treating with base (Fig 6.5).

^1H - ^{15}N 2D SSNMR on [**UWDM-8-H**][TFA] showed no correlation between the ^{15}N -enriched atoms of the site and the hydrogens of the crown ether which indicates that the macrocycle does not reside on the ^{15}N -enriched benzimidazolium recognition site. However, further ^1H - ^{15}N 2D SSNMR studies on **UWDM-8** did reveal a correlation between the ^{15}N enriched site and linker methyl groups. It is therefore likely that steric hindrance from the methyl groups of the **TTTP** linker prevents the macrocycle from translocating to the ^{15}N -enriched benzimidazolium recognition site (see experimental 6.2.13) similar to what was observed for **UWDM-6**.

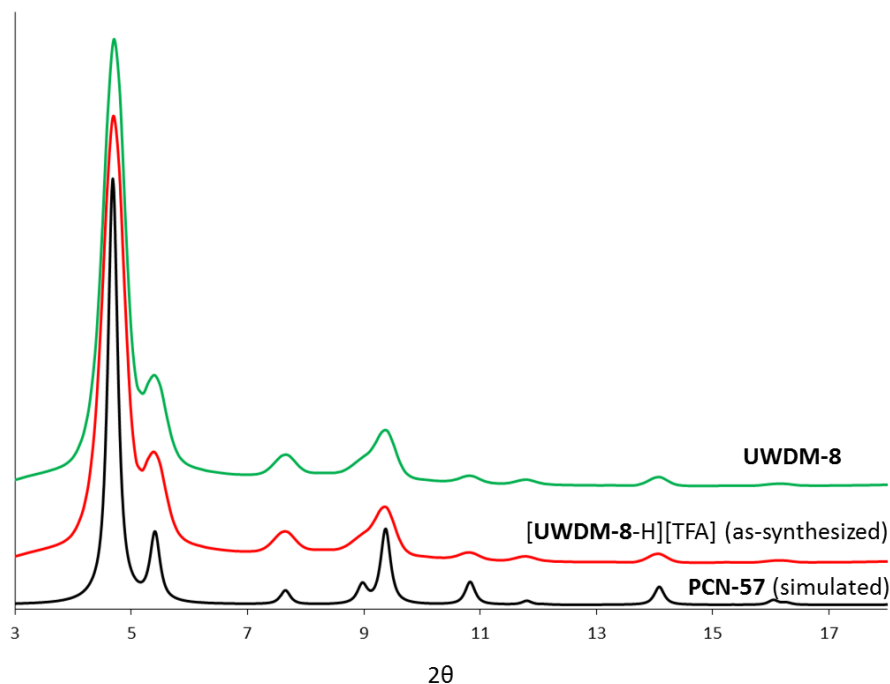


Fig 6.5 – PXRD (bottom to top) simulated from the single crystal X-ray structure of **PCN-57**, as-synthesized **[UWDM-8-H][TFA]** and **UWDM-8**.

6.1.3 Conclusions

The novel bistable [2]rotaxane molecular switch with two different recognition sites was successfully synthesized. The solution studies showed, addition of a chemical perturbation caused the macrocycle to translocate to new favorable recognition site. This bistable molecular switch was then incorporated into a Zr-based MOF in order to study the same switching process inside the MOF by ^1H - ^{15}N SSNMR spectroscopy. However, the ^1H - ^{15}N SSNMR did not prove the translational motion of the macrocycle between non-equivalent sites because of steric hindrance from the methyl groups of the **TTTP** linker.

6.2 Experimental

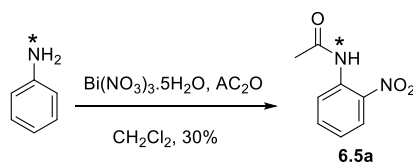
6.2.1 General comments

Aniline (^{15}N , 98%+) was purchased from Cambridge isotope laboratory. Bismuth(III) nitrate pentahydrate was purchased from Alpha Aesar. Compound **6.1** was prepared according to the literature method.^[14] **6a** was prepared according to the literature method.^[17,18] Deuterated solvents were obtained from Cambridge Isotope Laboratories and used as received. Solvents were dried using an Innovative Technologies Solvent Purification System. ^1H and ^{13}C NMR solution experiments were performed on a Bruker Avance 500 instruments at 298 K unless otherwise indicated and chemical shifts are quoted in ppm relative to tetramethylsilane using the residual solvent peak as a reference standard. ^{15}N - ^1D -cpd NMR solution experiments were performed on a Bruker Avance 500 instruments at 298 K. ^{19}F NMR solution experiments were performed on a Bruker Avance 500 instruments at 298 K. Powder XRD measurements were recorded on a Bruker D8 Discover diffractometer equipped with a GADDS 2D-detector and operated at 40 kV and 40 mA. $\text{CuK}\alpha$ radiation was used and the initial beam diameter was 0.5 mm. Melting points were recorded on a Stanford Research Systems, Opti Melt MPA100 instrument. High resolution mass spectrometry (HR-MS) experiments were performed on a Waters Xevo G2-XS time-of-flight (ToF) instrument using lock spray for accurate mass determinations.

6.2.2 Synthesis of 6.5a

Aniline (^{15}N , 98%+) (1 g, 10.6 mmol), bismuth(III) nitrate pentahydrate (5.1 g, 10.6 mmol) and acetic anhydride (7.5 mL, 74.3 mmol) were dissolved in CH_2Cl_2 and stirred at RT for 4 h. The mixture was then poured into a saturated solution of NaHCO_3 and extracted with ethyl acetate. The organic phase was dried with anhydrous Na_2SO_4 and then concentrated under vacuum. Evaporation of the solvent gave crude a product which was

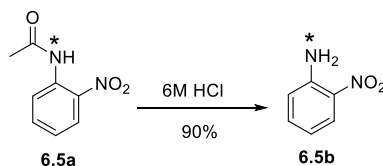
purified by column chromatography (SiO₂, petroleum ether/EtOAc (4:1)) R_f: 0.3. Yield: 30% (600 mg). Mp: 90-93 °C. ¹H NMR (500 MHz, CDCl₃, 298 K): δ = 2.29 (s, 3H), 7.14 (t, 1H, *J* = 7.2 Hz), 7.64 (t, 2H, *J* = 7.2 Hz), 8.2 (d, 1H, *J* = 7.3 Hz), 8.76 (d, 1H, *J* = 7.3 Hz), 10.23 (d, 1H, **H**-¹⁵N, *J* = 45.2 Hz). ¹³C NMR (126 MHz, CDCl₃, 298 K): δ = 168.97, 136.32, 136.00, 134.94, 125.74, 123.22, 122.19, 25.60. ¹⁵N NMR (51 MHz, CDCl₃, 298 K): δ = 124.90. HR-MS (ESI): calculated for [M+H]⁺, [C₈H₉N¹⁵NO₃]⁺, *m/z* = 182.0535, found *m/z* = 182.0583.



Scheme 6.2 – synthesis of 6.5a.

6.2.3 Synthesis of 6.5b

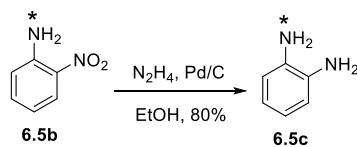
6.5a (500 mg, 2.77 mmol) was refluxed for 2 h in 6 M HCl (8 mL). The mixture was cooled to RT, neutralized with saturated NaHCO₃ solution and extracted with EtOAc. The organic phase was then dried with anhydrous Na₂SO₄ and concentrated under vacuum. The residue was crystallized from hexane. Yield: 90% (340 mg). Mp: 68-71 °C. ¹H NMR (500 MHz, CDCl₃, 298 K): δ = 5.96 (d, 2H, **H**-¹⁵N, *J* = 43.9 Hz), 6.70 (t, 1H, *J* = 7.7 Hz), 6.79 (d, 1H, *J* = 7.7 Hz), 7.35 (t, 1H, *J* = 7.6 Hz), 8.12 (d, 1H, *J* = 7.7 Hz). ¹³C NMR (126 MHz, CDCl₃, 298 K): δ = 144.66, 144.53, 135.65, 126.26, 118.72, 117.00. ¹⁵N NMR (51 MHz, CDCl₃, 298 K): δ = 68.02. HR-MS (ESI): calculated for [M+H]⁺, [C₆H₇N¹⁵NO₂]⁺, *m/z* = 140.0429, found *m/z* = 140.0475.



Scheme 6.3 – synthesis of 6.5b.

6.2.4 Synthesis of 6.5c

6.5b (300 mg, 2.15 mmol), Pd/C 10% (20 mg, 0.19 mmol) were added to a 250 mL Schlenk flask, degassed and backfilled with N₂. After adding anhydrous ethanol (40 mL), N₂H₄ (700 μL, 15.05 mmol) was added slowly to the mixture. The solution was refluxed (80 °C) for 24 h. The mixture was then cooled to room temperature, filtered and the solvent removed. The residue was extracted with brine/CH₂Cl₂ (2 x 50 mL), the solution was dried over anhydrous Na₂SO₄ and solvent removed. Yield: 80% (190 mg). Mp: 101-104 °C. ¹H NMR (500 MHz, DMSO-d₆, 298K): δ = 4.37 (m, 4H), 6.39 (m, 4H), 6.52 (m, 4H). ¹³C NMR (126 MHz, CDCl₃, 298 K): δ = 116.90, 120.86, 117.28. H-MS (ESI): calcd for [M+H]⁺, [C₆H₉N¹⁵N]⁺, *m/z* = 110.0687, found *m/z* = 110.0734.

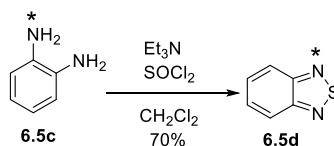


Scheme 6.4 – synthesis of 6.5c.

6.2.5 Synthesis of 6.5d

To a 100 mL Schlenk flask containing **6.5c** (160 mg, 1.45 mmol) which was backfilled with N₂, CH₂Cl₂ (40 mL) and Et₃N (304 μL, 2.17 mmol) were added. Then SOCl₂ (235 μL, 3.19 mmol) in CH₂Cl₂ (10 mL) was added dropwise to the mixture and refluxed for 4 h. After 4 h, solvent was removed and water (20 mL) was added. 0.1 N HCl was added to the mixture to give a pH value of about 2. The mixture was extracted with CH₂Cl₂, the organic phase was dried with anhydrous MgSO₄ and then the solvent was removed. Yield: 70% (140 mg). Mp: 41-44 °C. ¹H NMR (500 MHz, CDCl₃, 298 K): δ = 7.44 (m, 2H), 8.15 (m, 2H). ¹³C NMR (126

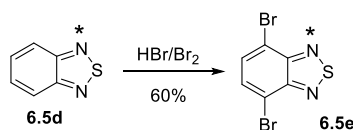
MHz, CDCl₃, 298 K): δ = 156.23, 128.92, 121.56. ¹⁵N NMR (51 MHz, CDCl₃, 298 K): δ = 99.98, HR-MS (ESI): calculated for [M+H]⁺, [C₆H₅¹⁵NNS]⁺, m/z = 138.0095, found m/z = 138.0105.



Scheme 6.5 – synthesis of 6.5d.

6.2.6 Synthesis of 6.5e

6.5d (120 mg, 0.875 mmol) was dissolved in HBr (850 μ L, 15.7 mmol) in a 250 mL round bottom flask. Br₂ (50 μ L, 2.62 mmol) was dissolved in HBr (570 μ L, 10.4 mmol) and added slowly to the reaction. The mixture was refluxed for 12 h. The mixture was then cooled to RT and saturated Na₂S₂O₃ solution was added until the color of the reaction did not change. The mixture was then filtered and washed with 20 mL water followed by diethyl ether. The residue was recrystallized from ethanol. Yield: 60% (155 mg). Mp: 182-185 °C. ¹H NMR (500 MHz, CDCl₃, 298 K): δ = 7.73 (s, 2H). ¹³C NMR (126 MHz, CDCl₃, 298 K): δ = 152.86, 132.39, 113.94. ¹⁵N NMR (51 MHz, CDCl₃, 298 K): δ = 100.04, HR-MS (ESI): calculated for [M+H]⁺, [C₆H₃Br₂N¹⁵NS]⁺, m/z = 295.8285, found m/z = 295.8255.

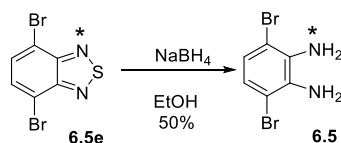


Scheme 6.6 – synthesis of 6.5e.

6.2.7 Synthesis of 6.5

6.5e (150 mg, 0.508 mmol) was dissolved in EtOH (30 mL) at 0 °C under N₂ and NaBH₄ (193 mg, 5.08 mmol) was added in portions. The mixture then warmed to RT and

stirred for 2 h. After stirring for 2 h, the mixture was filtered and the solvent was removed. The residue was extracted two times with CH₂Cl₂/brine (50:25 mL), the solution was dried over anhydrous Na₂SO₄ and solvent was removed. Yield: 50% (70 mg). Mp: 85-89 °C. ¹H NMR (300 MHz, CDCl₃, 298K): δ = 3.85 (s br, 4H), 6.85 (s, 2H). ¹³C NMR (126 MHz, CD₃CN, 298K): δ = 133.66, 123.20, 109.63. ¹⁵N NMR (51 MHz, CDCl₃, 298 K): δ = 53.40, HR-MS (ESI): calcd for [M+H]⁺, [C₆H₇Br₂N¹⁵N]⁺, m/z = 267.8877, found m/z = 267.8924.

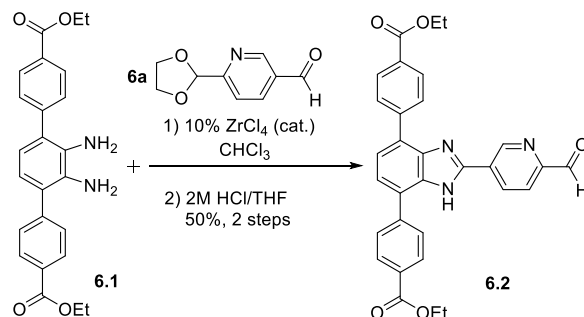


Scheme 6.7 – synthesis of 6.5.

6.2.8 Synthesis of 6.2

6.1 (195 mg, 0.482 mmol) and 6-(1,3-dioxolan-2-yl)pyridine-3-carbaldehyde (90 mg, 0.502 mmol) were dissolved in CHCl₃ in a small flask and then ZrCl₄ (12 mg, 0.051 mmol) was added. The solution was stirred for 24 h at room temperature. Et₃N (0.1 mL) was then added, the solution filtered and the solvent of the filtrate removed. The residue was recrystallized from CH₃CN. Mp: 165-170 °C. ¹H NMR (500 MHz, CDCl₃, 298 K): δ = 1.42 (t, 6H), 4.16 (m, 4H), 4.40, (q, 4H), 5.90 (s, 1H), 7.50 (s, 2H), 7.67 (d, 1H), 7.96 (s, 4H), 8.12 (m, 4H), 8.62 (d, 1H), 9.37 (s, 1H). ¹³CNMR (126 MHz, CDCl₃, 298 K): δ = 166.75, 158.21, 152.64, 149.50, 147.26, 142.66, 136.04, 130.13, 129.59, 129.55, 128.77, 126.55, 121.01, 103.00, 65.76, 61.19, 14.46. HR-MS (ESI): calc for [M+H]⁺, [C₃₃H₃₀N₃O₆]⁺, m/z = 564.2090, found m/z = 564.2131. The intermediate was dissolved in a mixture of 1M HCl (20 mL) and THF (20 mL), and then refluxed for 2 h. The solution cooled to RT and saturated NaHCO₃ was added. The mixture was extracted with EtOAc, the organic phase dried with anhydrous Na₂SO₄ and the solvent removed. The residue was crystallized from CH₃CN. Yield for two steps: 50%

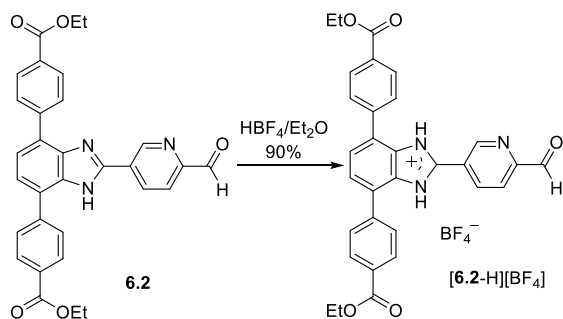
(140 mg). Mp: 175-180 °C. ^1H NMR (500 MHz, CDCl_3 , 298 K): δ = 1.46 (t, 6H), 4.43 (q, 4H), 7.54, (s, 2H), 7.96 (s br, 4H), 8.06 (d, 1H), 8.17 (m, 4H), 8.65 (d, 1H), 9.51 (s, 1H), 10.12 (s, 1H). ^{13}C NMR (126 MHz, CDCl_3 , 298 K): δ = 192.66, 166.72, 153.05, 148.56, 148.29, 142.43, 135.36, 130.09, 130.09, 130.06, 129.57, 129.57, 128.76, 128.62, 121.83, 61.38, 61.31, 14.37, 14.37. HR-MS (ESI): calc for $[\text{M}+\text{H}]^+$, $[\text{C}_{31}\text{H}_{26}\text{N}_3\text{O}_5]^+$, m/z = 520.1794, found m/z = 520.1873.



Scheme 6.8 – synthesis of **6.2**.

6.2.9 Synthesis of **[6.2-H][BF₄]**

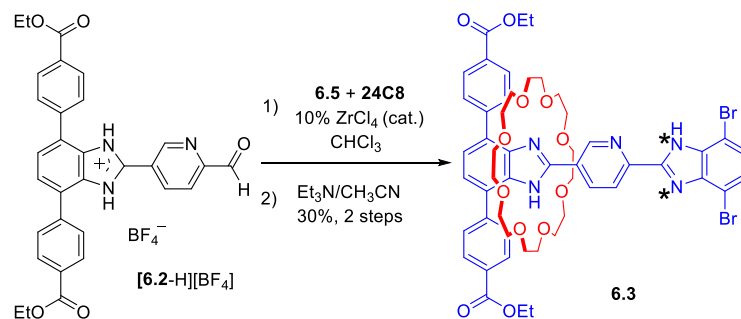
6.2 (140 mg, 0.27 mmol) was dissolved in a mixture of Et_2O (70 mL) and CH_2Cl_2 (60 mL). Tetrafluoroboric acid diethyl ether complex (40 μL , 0.29 mmol) was added and the mixture stirred for 1 h. The reaction was then concentrated to about 50 mL and hexane was added. The yellow product was filtered. Yield: 90% (127 mg). Mp: 230-235 °C. ^1H NMR (300 MHz, CD_3CN , 298 K): δ = 1.40 (t, 6H), 4.40 (q, 4H), 6.27 (s, 1H), 7.86 (m, 6H), 8.2 (m, 5H), 8.56 (d, 1H), 9.34 (d, 1H), 10.11 (s, 1H). ^{13}C NMR (126 MHz, CD_3CN , 298 K): δ = 193.00, 166.79, 155.53, 151.08, 149.20, 140.35, 132.08, 131.26, 131.16, 131.12, 130.14, 130.09, 128.70, 122.67, 118.26, 70.98, 62.17, 14.30. HR-MS (ESI): Calculated for $[\text{M}-\text{BF}_4]^+$, $[\text{C}_{31}\text{H}_{27}\text{N}_3\text{O}_5]^+$, m/z = 521.1946; found m/z = 520.1913.



Scheme 6.9 – synthesis of [6.2-H][BF₄].

6.2.10 Synthesis of 6.3

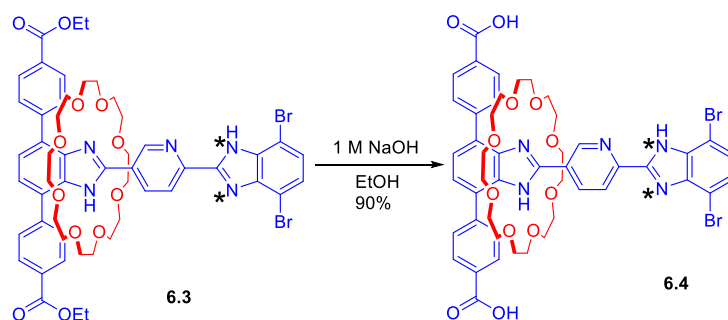
24C8 (138 mg, 0.39 mmol) was added to [6.2-H][BF₄] (120 mg, 0.19 mmol) in a round bottom flask. CHCl₃ (25 mL) was added and the reaction stirred at room temperature until a clear solution formed. **6.5** (51 mg, 0.19 mmol) was added, followed by ZrCl₄ (4.4 mg, 0.02 mmol) and the solution was stirred at room temperature for 24 h. The solution was filtered and the solvent removed. The residue was washed with diethyl ether to remove excess crown ether then dissolved in CH₃CN and filtered. Et₃N (0.3 mL) was added to the filtrate. The resulting solid was filtered and air dried producing a yellow product. Yield: 30% (65 mg). Mp: >255 °C. ¹H NMR (500 MHz, CD₂Cl₂, 298 K): δ = 1.44 (m, 6H), 3.22 (m, 32H), 4.44 (m, 4H), 7.30 (d, 1H, *J* = 8 Hz), 7.37 (t, 2H, *J* = 8.2 Hz), 7.58 (d, 1H, *J* = 7.6 Hz), 7.79 (d, 2H, *J* = 8 Hz), 8.18 (m, 4H, *J* = 8.3 Hz), 8.37 (d, 1H, *J* = 8.2 Hz), 8.63 (d, 1H, *J* = 8.3 Hz), 9.31 (d, 2H, *J* = 8.3 Hz), 9.98 (s, 1H), 11.85 (d, 1H). ¹³C NMR (126 MHz, CDCl₃, 298 K): δ = 166.88, 152.22, 143.39, 140.16, 130.90, 130.48, 129.84, 129.72, 129.48, 129.06, 126.95, 126.91, 121.59, 112.59, 70.81, 70.08, 69.93, 29.70, 14.38. ¹⁵N NMR (51 MHz, CDCl₃, 298 K): δ = 241.79, 141.81. HR-MS (ESI): calculated for [M+H]⁺, [C₅₃H₆₀Br₂¹⁵NN₄O₁₂]⁺, *m/z* = 1119.2507, found *m/z* = 1119.2561.



Scheme 6.10 – synthesis of **6.3**.

6.2.11 Synthesis of 6.4

To **6.3** (60 mg, 0.05 mmol) in tetrahydrofuran (10 mL) and ethanol (20 mL), 1M NaOH (20 mL) was added. After the reaction mixture was stirred at 80 °C for 24 h, the solvent was removed on a rotary evaporator. Then 0.1 N HCl was added to give a pH value of about 5. The precipitate was collected by vacuum filtration and air dried. Yield: 90%. (50 mg). Mp: >300 °C. ¹H NMR (500 MHz, DMSO-d₆, 298 K): δ = 2.98 (m, 16H), 3.15 (m, 16H), 7.51 (s, 1H), 7.93 (d, 4H), 8.00 (s, 2H), 8.18 (d, 2H), 8.22 (d, 4H), 8.68 (d, 1H), 8.79 (d, 1H), 9.44 (s, 1H), 12.98 (s, 2H), 13.26 (s br, 2H), 14.15 (s br, 1H). ¹³C NMR (126 MHz, DMSO-d₆, 298 K): δ = 166.89, 150.85, 148.74, 139.32, 131.00, 130.28, 129.74, 129.71, 129.69, 128.99, 128.94, 128.89, 128.79, 127.08, 126.96, 126.91, 121.65, 121.57, 69.56. HR-MS (ESI): [M+H]⁺, [C₄₉H₅₂Br₂¹⁵NN₄O₁₂]⁺, m/z = 1063.1882, found m/z = 1063.1930.



Scheme 6.11 – synthesis of **6.4**.

6.2.12 Analysis of UWDM-8 by ^1H NMR Spectroscopy

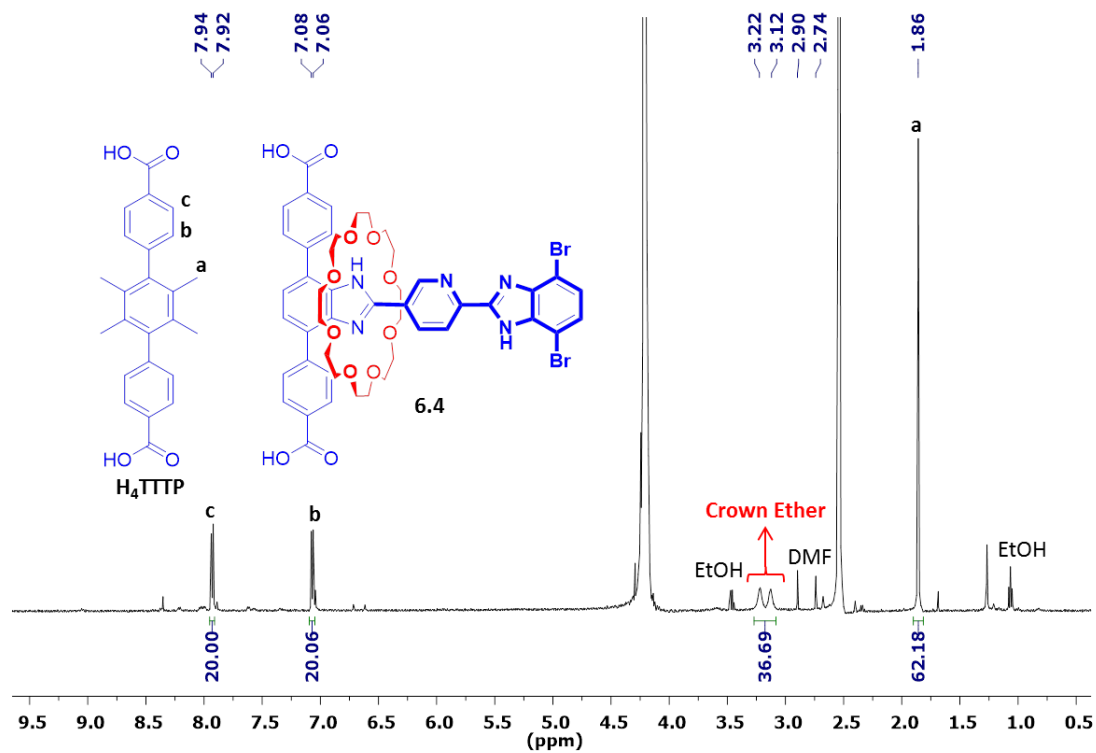


Fig 6.6 – ^1H NMR spectrum of UWDM-8 after digestion (500 MHz, DMSO-d_6), the integration shows the ratio of H_4TTTP to **6.4** is approximately 5:1.

6.2.13 ^1H - ^{15}N SSNMR of UWDM-8 and [UWDM-8-H][TFA]

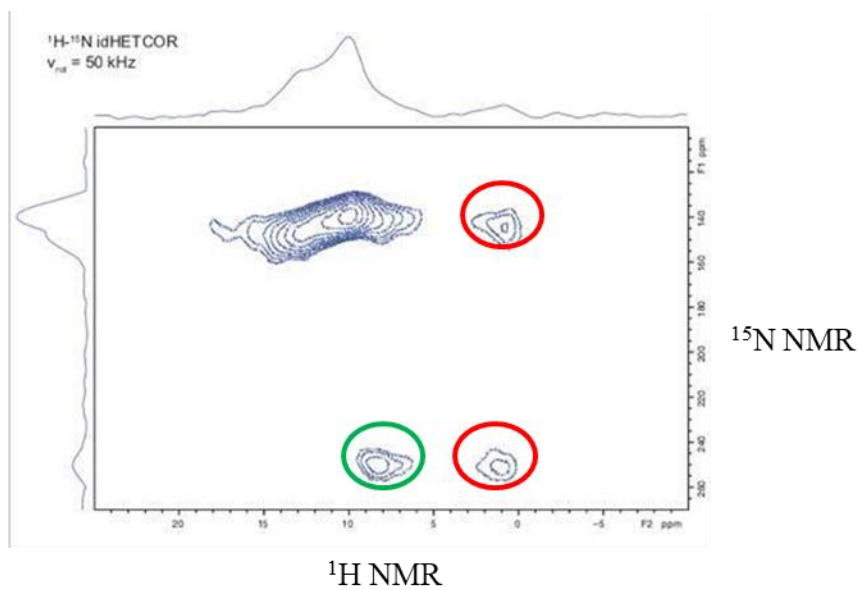


Fig 6.7 – ^1H - ^{15}N SSNMR spectrum of **UWDM-8**.

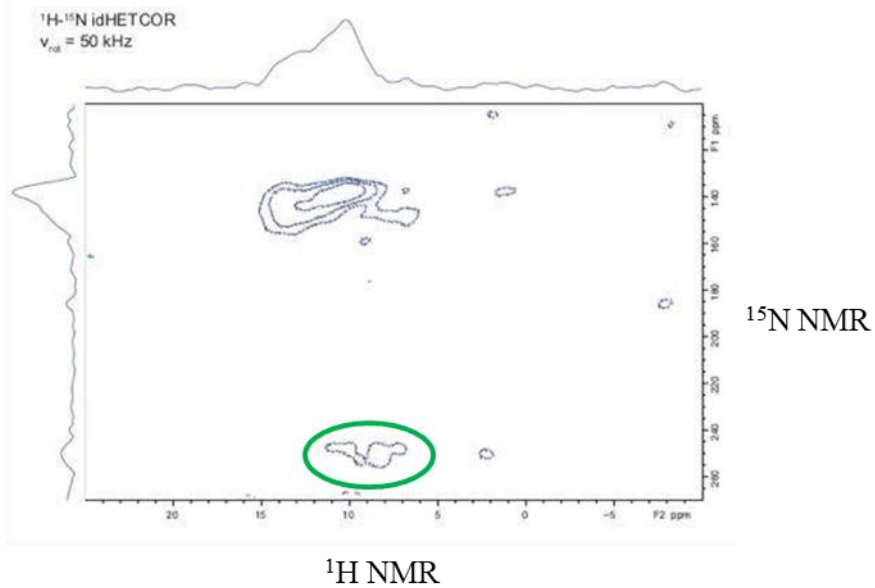


Fig 6.8 – ^1H - ^{15}N SSNMR spectrum of **[UWDM-8-H][TFA]**.

6.3. References

1. B. R. D. À. Acceptor, A. C. Fahrenbach, C. J. Bruns, D. Cao and J. F. Stoddart, *Acc.Chem. Res.*, **2014**, 47, 482–493.
2. R. Barat, T. Legigan, I. Tranoy-Opalinski, B. Renoux, E. Péraudeau, J. Clarhaut, P. Poinot, A. E. Fernandes, V. Aucagne, D. A. Leigh and S. Papot, *Chem. Sci.*, **2015**, 6, 2608-2613.
3. N. Farahani, K. Zhu and S. J. Loeb, *ChemPhysChem*, **2016**, 17, 1875-1880.
4. R. A. Bissell, E. Cordova, A. E. Kaifer, and J. F. Stoddart, *Nature*, **1994**, 369, 133-137.
5. A. Altieri, G. Bottari, F. Dehez, D. A. Leigh, J. K. Y. Wong, F. Zerbetto, *Angew. Chem. Int. Ed.* **2003**, 42, 2296-2300.
6. G. Ragazzon, M. Baroncini, S. Silvi, M. Venturi, and A. Credi, *Nat. Nanotechnol.* **2015**, 10, 70-75.
7. G. Bottari, D. A. Leigh and E. M. Perez, *J. Am. Chem. Soc.*, **2003**, 125, 13360–13361.
8. A. Coskun, M. Banaszak, R. D. Astumian, J. F. Stoddart and B. A. Grzybowski, *Chem. Soc. Rev.*, **2012**, 41, 19–30.
9. H. Li, C. Cheng, P. R. McGonigal, A. C. Fahrenbach, M. Frasconi, W. G. Liu, Z. Zhu, Y. Zhao, C. Ke, J. Lei, R. M. Young, S. M. Dyar, D. T. Co, Y. W. Yang, Y. Y. Botros, W. A. Goddard, M. R. Wasielewski, R. D. Astumian and J. F. Stoddart, *J. Am. Chem. Soc.*, **2013**, 135, 18609–18620.

10. J. W. Choi, A. H. Flood, D. W. Steurman, S. Nygaard, A. B. Braunschweig, N. N. P. Moonen, B. W. Laursen, Y. Luo, E. Delonno, A. J. Peters, J. O. Jeppesen, K. Xu, J. F. Stoddart and J. R. Heath, *Chem. Eur. J.*, **2006**, 12, 261–279.
11. E. R. Kay, D. A. Leigh and F. Zerbetto, *Angew. Chem. Int. Ed.*, **2007**, 46, 72-191.
12. H-C. Zhou, J. R. Long and O. M. Yaghi, *Chem. Rev.*, **2012**, 112, 673–674.
13. H. Li, M. Eddaoudi, M. O’Keeffe, and O. M. Yaghi, *Nature*, **1999**, 402, 276–279.
14. K. Zhu, C. O’Keefe, V. N. Vukotic, R. W. Schurko, S. J. Loeb, *Nat. Chem.* **2015**, 7, 514-519.
15. H. L. Jiang, D. Feng, T. F. Liu, J. R. Li and H. C. Zhou, *J. Am. Chem. Soc.*, **2012**, 134, 14690–14693.
16. K. Zhu, V. N. Vukotic and S. J. Loeb, *Angew. Chem. Int. Ed.*, **2012**, 51, 2168–2172.
17. E.-C. Yang, W. Wernsdorfer, S. Hill, R. S. Edwards, M. Nakano, S. Maccagnano, L. N. Zakharov, A. L. Rheingold, G. Christou and D. N. Hendrickson, *Polyhedron*, **2003**, 22, 1727–1733.
18. M. Van Den Heuvel, T. A. Van Den Berg, R. M. Kellogg, C. T. Choma and B. L. Feringa, *J. Org. Chem.*, **2004**, 69, 250–262.

CHAPTER 7

7.1 Summary and Future Work

In this dissertation, we studied the incorporation of [2]rotaxane linkers into metal-organic framework (MOF) materials. Since, [2]rotaxanes have demonstrated translational motion (shuttling), this feature was considered in both solution and solid state materials. **Chapter 1** provides an introduction to MIMs, rotaxanes as linkers, MOFs and all previous works on dynamic motion (rotation and translation) of rotaxanes in MOFs.

Incorporating rotaxanes into crystalline MOF materials provides a way to organize MIMs in the solid state^[1-3]. To this end, in **Chapter 2**, a [2]rotaxane linker with donor carboxylate groups (six) attached to both the axle and the wheel was successfully incorporated into a Zn-based MOF. This newly designed [2]rotaxane linker allows both the axle and wheel to be involved in independent frameworks that are interpenetrated through the mechanically interlocked nature of the ligand. The overall framework consisted of threefold interpenetration made from alternating axles and wheels that fill the void space. Usually an interpenetrated lattice would undergo phase changes or rapid loss of crystallinity at high temperature; however, variable-temperature powder X-ray diffraction (VT-PXRD) showed no loss of crystallinity over the temperature range of 25 to 200 °C.

This work was followed up in **Chapter 3**, by synthesizing a rotaxane linker that contained four carboxylic acid donors on the axle and two pyridine donors on the wheel. This idea came from the reported Zn(II) and Cu(II) MOFs which have 2D layers supported by carboxylate ligands pillared in the 3rd dimension by a bipyridine ligand^[4-8]. By incorporating our rotaxane linker into Zn and Cu-based MOFs, it was demonstrated that two independent lattices could be threaded together by interlocking of the linker components.

Future work for these two chapters could be to incorporate these linkers into MOF materials using two different types of metals to distinguish the different coordination environments of the axle and wheel.

A number of studies have been published which attempted to correlate the rate of molecular shuttling of a rotaxane with the molecular path along which the ring must travel. Hence, in **Chapter 4**, a series of [2]rotaxane molecular shuttles were prepared containing a dibenzo[24]crown-8 (**DB24C8**) macrocycle and a rigid H-shaped axle with varying track lengths between recognition sites; from 7.4 to 20.3 Å as defined by 1-4 phenyl rings or a naphthyl group. The rate of shuttling of **DB24C8** along the rigid track was measured by variable temperature ¹H NMR spectroscopy for the neutral compounds and EXSY experiments for the dicationic species. It was determined that the rate of shuttling was independent of the length of the axle. The only deviation from this observation occurred when the distance between the two recognition sites was short enough to allow the crown ether to simultaneously interact with both recognition sites; providing a short-cut mechanism which lowered the barrier to translocation.

Future work for this chapter would be converting these series of [2]rotaxanes to linkers and incorporating them into MOFs. In this manner, the rate of molecular shuttling inside the MOF would be studied.

Almost all studies on molecular shuttles have been in solution where the motion is incoherent and random. As a way to impose higher order on molecular shuttles, the Loeb group pioneered their incorporation into solid-state metal-organic framework (MOF) materials. In 2015, they reported the translational motion of a molecular shuttle inside Zn-based MOF^[10]. However, for acid/base control over the molecular shuttling process inside MOFs, a highly stable framework is required and Zn-based MOFs are not suitable.

This brought our focus to Zr-based MOFs which are well known for their exceptional stability under acidic and basic conditions. Therefore, in **Chapter 5**, molecular shuttling inside Zr-based MOFs under acid-base condition was studied. The two prepared MOFs, **UWDM-6** and **UWDM-7** (University of Windsor Dynamic Material) consisted of the same [2]rotaxanes **5.5**, but different linear linkers (with and without methyl groups). Both were stable under acid/base and high temperature conditions. ¹³C solid-state NMR (SSNMR) of **UWDM-6** containing **5.5** and 2',3',5',6'-tetramethylterphenyl-4,4'' dicarboxylate (**TTTP**) demonstrated no shuttling because of steric hindrance of methyl groups of the linear linker. This limitation for shuttling was fixed by changing to the linear linker (terphenyl dicarboxylate (**TPDC**)) in **UWDM-7**; however, the poor crystallinity of this MOF did not allow us to estimate the rate of shuttling inside the Zr-based MOF. Future work will focus on improving the crystallinity of **UWDM-7**. One alternative would be to change the linear linker to 2',5'-dimethyl-[1,1':4',1''-terphenyl]-4,4''-dicarboxylic acid (**TPDC-2CH₃**). The other alternative should be changing the conditions for making Zr-MOF; for example i) changing the modulator to benzoic acid or acetic acid, ii) changing the Zr starting material to ZrOCl₂ or iii) modifying the solvent-DEF, mixtures.

A bistable [2]rotaxane molecular shuttle that switches inside Zr-based MOF was studied in **Chapter 6**. A new non-degenerate [2]rotaxane was designed in which the crown ether initially prefers one recognition site over the other; therefore, the thermodynamic preference for the binding of crown ether can be reversed by using an external perturbation such as Li⁺ ion or H⁺. To impose higher order on this molecular switching, a mixture of the new non-degenerate [2]rotaxane molecular shuttle, **6.4**, and 2',3',5',6'-tetramethylterphenyl-4,4'' dicarboxylate (**TTTP**) with the ratio of 1:5 was incorporated into Zr-based MOF (**UWDM-8**). Reversible translational motion of the crown ether between the

two non-equivalent sites was performed by changing the pH. To monitor the reversible molecular switching in the MOF, ^{15}N SSNMR experiments will be done.

When a non-degenerate [2]rotaxane ligand is incorporated into the Zr-based MOF, It is possible for it to be present in either of the octahedral or tetrahedral cavities. As a result, different environments for the ^{15}N atoms of the benzimidazole recognition site may complicate the ^{15}N SSNMR experiments. To solve this problem, in future work the bistable [2]rotaxane will be redesigned to one (see Fig 7.1) that can only fit in the tetrahedral cavity— analogous to linker **5.5** used to create **UWDM-6** and **UWDM-7** in chapter 6. Moreover, 2',3',5',6'-tetramethylterphenyl-4,4'' dicarboxylate (**TTTP**) linear linker will be changed to (terphenyl dicarboxylate (**TPDC**)) in making new Zr-based MOF (**UWDM-9**) in order to eliminate the hindrance steric methyl group problem.

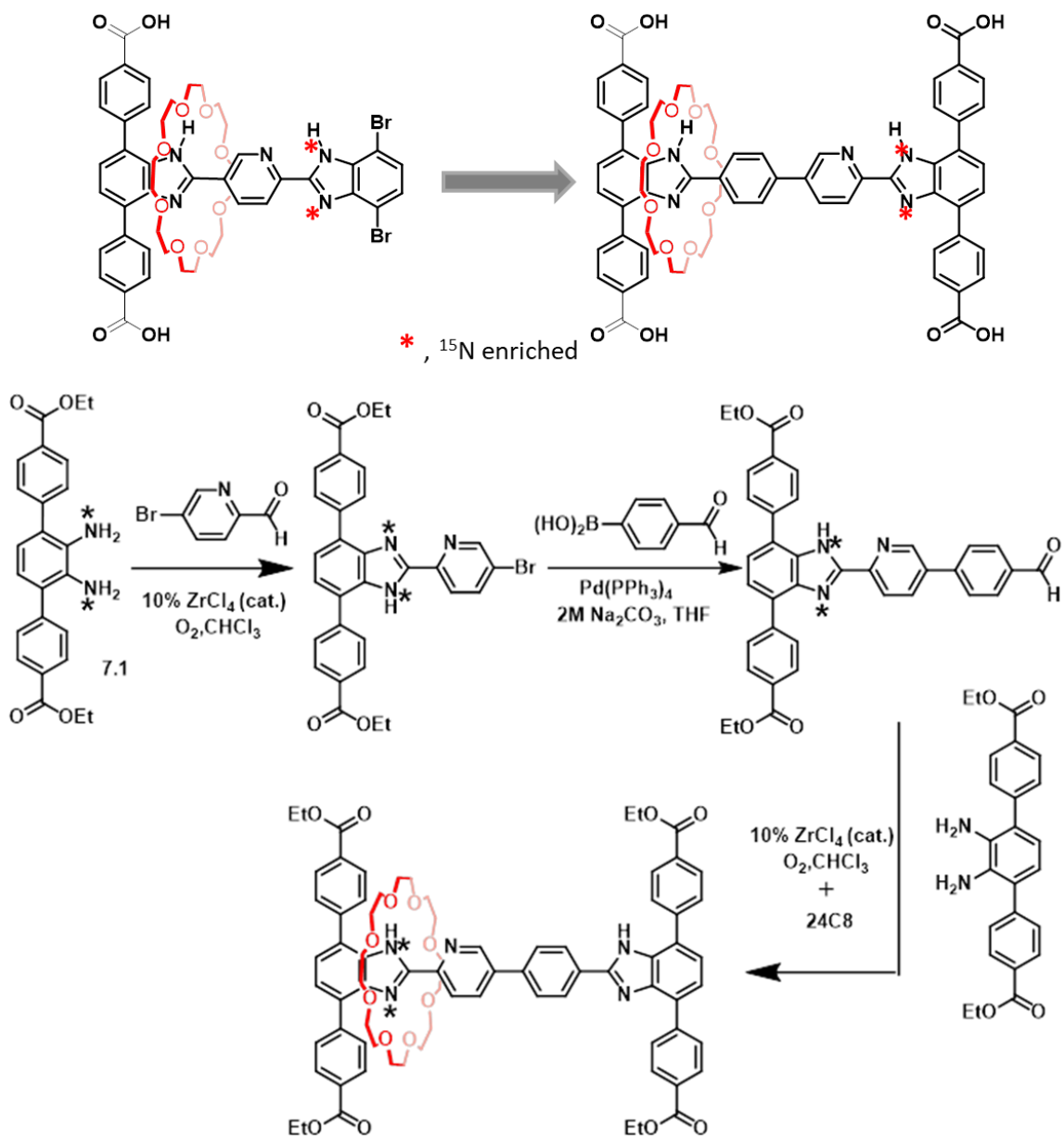


Fig 7.1 – redesigning the non_degenerate [2]rotaxane (on the top) and the proposed synthesis procedure (on the bottom), (the synthesis method for making 7.1 is outlined in Chapter 6, experimental 6.2).

7.2 References

1. H. X. Deng, M. A. Olson, J. F. Stoddart, O. M. Yaghi, *Nat. Chem.* **2010**, 2, 439–447.
2. A. Coskun, M. Banaszak, R. D. Astumian, J. F. Stoddart, B. A. Grzybowski, *Chem. Soc. Rev.* **2012**, 41, 19–35.
3. P. R. McGonigal, P. Deria, I. Hod, P. Z. Moghadam, A.-J. Avestro, N. E. Horwitz, I. C. Gibbs-Hall, A. K. Blackburn, D. Chen, Y. Y. Botros, W. R. Wasielewski, R. Q. Snurr, J. T. Hupp, O. K. Farha, J. F. Stoddart, *Proc. Natl. Acad. Sci. USA*, **2015**, 112, 11161–11168.
4. D. N. Dybtsev, H. Chun and K. Kim, *Angew. Chem., Int. Ed.*, **2004**, 43, 5033-5036.
5. B. Q. Ma, K. L. Mulfort and J. T. Hupp, *Inorg. Chem.*, **2005**, 44, 4912-4914.
6. O. K. Farha and J. T. Hupp, *Acc. Chem. Res.*, **2010**, 43, 1166-1175.
7. B. L. Chen, C. D. Liang, J. Yang, D. S. Contreras, Y. L. Clancy, E. B. Lobkovsky, O. M. Yaghi and S. Dai, *Angew. Chem., Int. Ed.*, **2006**, 45, 1390-1393.
8. I. H. Park, K. Kim, S. S. Lee and J. J. Vittal, *Cryst. Growth Des.*, **2012**, 12, 3397-3401.
9. E. R. Kay, D. A. Leigh and F. Zerbetto, *Angew. Chem. Int. Ed.*, **2007**, 46, 72-191.
10. K. Zhu, C. a O’Keefe, V. N. Vukotic, R. W. Schurko and S. J. Loeb, *Nat. Chem.*, **2015**, 7, 514–519.

APPENDIX

A1: Copyright Permissions

JOHN WILEY AND SONS LICENSE TERMS AND CONDITIONS

Jun 12, 2017

This Agreement between Ms. Ghazale Gholami ("You") and John Wiley and Sons ("John Wiley and Sons") consists of your license details and the terms and conditions provided by John Wiley and Sons and Copyright Clearance Center.

License Number	4126650051959
License date	Jun 12, 2017
Licensed Content Publisher	John Wiley and Sons
Licensed Content Publication	European Journal of Inorganic Chemistry
Licensed Content Title	Formation of a Polythreaded, Metal–Organic Framework Utilizing an Interlocked Hexadentate, Carboxylate Linker
Licensed Content Author	Ghazale Gholami, Kelong Zhu, Jas S. Ward, Paul E. Kruger, Stephen J. Loeb
Licensed Content Date	Jul 18, 2016
Licensed Content Pages	6
Type of use	Dissertation/Thesis
Requestor type	Author of this Wiley article
Format	Print and electronic
Portion	Full article
Will you be translating?	No
Title of your thesis / dissertation	Rotaxane Ligands for Incorporation into Metal–Organic Framework Materials
Expected completion date	Aug 2017
Expected size (number of pages)	250

Metal-organic frameworks utilising an interlocked, hexadentate linker containing a tetra-carboxylate axle and a bis(pyridine) wheel

G. Gholami, G. Baggi, K. Zhu and S. J. Loeb, *Dalton Trans.*, 2017, **46**, 2462

DOI: 10.1039/C6DT04596K

If you are not the author of this article and you wish to reproduce material from it in a third party non-RSC publication you must [formally request permission](#) using RightsLink. Go to our [Instructions for using RightsLink page](#) for details.

Authors contributing to RSC publications (journal articles, books or book chapters) do not need to formally request permission to reproduce material contained in this article provided that the correct acknowledgement is given with the reproduced material.

Georgio Baggi, Kelong Zhu and Stephen J. Loeb are aware of using this article in my thesis.

Ghazale gholami

**JOHN WILEY AND SONS LICENSE
TERMS AND CONDITIONS**

Jul 24, 2017

This Agreement between Ms. Ghazale Gholami ("You") and John Wiley and Sons ("John Wiley and Sons") consists of your license details and the terms and conditions provided by John Wiley and Sons and Copyright Clearance Center.

License Number	4155591126264
License date	Jul 24, 2017
Licensed Content Publisher	John Wiley and Sons
Licensed Content Publication	ChemPhysChem
Licensed Content Title	Wholly Synthetic Molecular Machines
Licensed Content Author	Chuyang Cheng, J. Fraser Stoddart
Licensed Content Date	Mar 1, 2016
Licensed Content Pages	14
Type of use	Dissertation/Thesis
Requestor type	University/Academic
Format	Print
Portion	Figure/table
Number of figures/tables	1
Original Wiley figure/table number(s)	Figure 2.
Will you be translating?	No
Title of your thesis / dissertation	Rotaxane Ligands for Incorporation into Metal-Organic Framework Materials
Expected completion date	Aug 2017
Expected size (number of pages)	250

**NATURE PUBLISHING GROUP LICENSE
TERMS AND CONDITIONS**

Jul 24, 2017

This Agreement between Ms. Ghazale Gholami ("You") and Nature Publishing Group ("Nature Publishing Group") consists of your license details and the terms and conditions provided by Nature Publishing Group and Copyright Clearance Center.

All payments must be made in full to CCC. For payment instructions, please see information listed at the bottom of this form.

License Number	4155601188425
License date	Jul 24, 2017
Licensed Content Publisher	Nature Publishing Group
Licensed Content Publication	Nature Materials
Licensed Content Title	Macroscopic transport by synthetic molecular machines
Licensed Content Author	José Berná, David A. Leigh, Monika Lubomska, Sandra M. Mendoza, Emilio M. Pérez et al.
Licensed Content Date	Aug 28, 2005
Licensed Content Volume	4
Licensed Content Issue	9
Type of Use	reuse in a dissertation / thesis
Requestor type	academic/educational
Format	print
Portion	figures/tables/illustrations
Number of figures/tables/illustrations	2
High-res required	yes
Figures	Figure 4 Figure 5
Author of this NPG article	no
Your reference number	
Title of your thesis / dissertation	Rotaxane Ligands for Incorporation into Metal-Organic Framework Materials
Expected completion date	Aug 2017
Estimated size (number of pages)	250



Title: Degenerate Molecular Shuttles with Flexible and Rigid Spacers
Author: D. Deniz Günbaş, Albert M. Brouwer
Publication: The Journal of Organic Chemistry
Publisher: American Chemical Society
Date: Jul 1, 2012
Copyright © 2012, American Chemical Society

Logged in as:
Ghazale Gholami
Account #:
3001161896

[LOGOUT](#)

PERMISSION/LICENSE IS GRANTED FOR YOUR ORDER AT NO CHARGE

This type of permission/license, instead of the standard Terms & Conditions, is sent to you because no fee is being charged for your order. Please note the following:

- Permission is granted for your request in both print and electronic formats, and translations.
- If figures and/or tables were requested, they may be adapted or used in part.
- Please print this page for your records and send a copy of it to your publisher/graduate school.
- Appropriate credit for the requested material should be given as follows: "Reprinted (adapted) with permission from (COMPLETE REFERENCE CITATION). Copyright (YEAR) American Chemical Society." Insert appropriate information in place of the capitalized words.
- One-time permission is granted only for the use specified in your request. No additional uses are granted (such as derivative works or other editions). For any other uses, please submit a new request.

If credit is given to another source for the material you requested, permission must be obtained from that source.

[BACK](#)[CLOSE WINDOW](#)



RightsLink®

Home

Account Info

Help



ACS Publications
Most Trusted. Most Cited. Most Read.

Title: Axle Length Does Not Affect Switching Dynamics in Degenerate Molecular Shuttles with Rigid Spacers

Author: Philip G. Young, Keiji Hirose, Yoshito Tobe

Publication: Journal of the American Chemical Society

Publisher: American Chemical Society

Date: Jun 1, 2014

Copyright © 2014, American Chemical Society

Logged in as:
Ghazale Gholami
Account #:
3001161896

LOGOUT

PERMISSION/LICENSE IS GRANTED FOR YOUR ORDER AT NO CHARGE

This type of permission/license, instead of the standard Terms & Conditions, is sent to you because no fee is being charged for your order. Please note the following:

- Permission is granted for your request in both print and electronic formats, and translations.
- If figures and/or tables were requested, they may be adapted or used in part.
- Please print this page for your records and send a copy of it to your publisher/graduate school.
- Appropriate credit for the requested material should be given as follows: "Reprinted (adapted) with permission from (COMPLETE REFERENCE CITATION). Copyright (YEAR) American Chemical Society." Insert appropriate information in place of the capitalized words.
- One-time permission is granted only for the use specified in your request. No additional uses are granted (such as derivative works or other editions). For any other uses, please submit a new request.

If credit is given to another source for the material you requested, permission must be obtained from that source.

BACK

CLOSE WINDOW

Copyright © 2017 [Copyright Clearance Center, Inc.](#) All Rights Reserved. [Privacy statement](#). [Terms and Conditions](#).
Comments? We would like to hear from you. E-mail us at customer@copyright.com



RightsLink®

Home

Account
Info

Help



ACS Publications
Most Trusted. Most Cited. Most Read.

Title: [2]Pseudorotaxanes from T-Shaped Benzimidazolium Axles and [24]Crown-8 Wheels
Author: Nadim Noujeim, Kelong Zhu, V. Nicholas Vukotic, et al

Publication: Organic Letters

Publisher: American Chemical Society

Date: May 1, 2012

Copyright © 2012, American Chemical Society

Logged in as:
Ghazale Gholami
Account #:
3001161896

LOGOUT

A

PERMISSION/LICENSE IS GRANTED FOR YOUR ORDER AT NO CHARGE

This type of permission/license, instead of the standard Terms & Conditions, is sent to you because no fee is being charged for your order. Please note the following:

- Permission is granted for your request in both print and electronic formats, and translations.
- If figures and/or tables were requested, they may be adapted or used in part.
- Please print this page for your records and send a copy of it to your publisher/graduate school.
- Appropriate credit for the requested material should be given as follows: "Reprinted (adapted) with permission from (COMPLETE REFERENCE CITATION). Copyright (YEAR) American Chemical Society." Insert appropriate information in place of the capitalized words.
- One-time permission is granted only for the use specified in your request. No additional uses are granted (such as derivative works or other editions). For any other uses, please submit a new request.

If credit is given to another source for the material you requested, permission must be obtained from that source.

BACK

CLOSE WINDOW

Copyright © 2017 [Copyright Clearance Center, Inc.](#) All Rights Reserved. [Privacy statement.](#) [Terms and Conditions.](#) Comments? We would like to hear from you. E-mail us at customercare@copyright.com



Title: Bis(benzimidazolium) axles and crown ether wheels: a versatile templating pair for the formation of [2]rotaxane molecular shuttles

Author: Kelong Zhu,V. Nicholas Vukotic,Nadim Noujeim,Stephen J. Loeb

Publication: Chemical Science

Publisher: Royal Society of Chemistry

Date: Aug 9, 2012

Copyright © 2012, Royal Society of Chemistry

Logged in as:
Ghazale Gholami
Account #:
3001161896

LOGOUT

Order Completed

Thank you for your order.

This Agreement between Ms. Ghazale Gholami ("You") and Royal Society of Chemistry ("Royal Society of Chemistry") consists of your license details and the terms and conditions provided by Royal Society of Chemistry and Copyright Clearance Center.

Your confirmation email will contain your order number for future reference.

[Printable details.](#)

License Number	4155960417163
License date	Jul 25, 2017
Licensed Content Publisher	Royal Society of Chemistry
Licensed Content Publication	Chemical Science
Licensed Content Title	Bis(benzimidazolium) axles and crown ether wheels: a versatile templating pair for the formation of [2]rotaxane molecular shuttles
Licensed Content Author	Kelong Zhu,V. Nicholas Vukotic,Nadim Noujeim,Stephen J. Loeb
Licensed Content Date	Aug 9, 2012
Licensed Content Volume	3
Licensed Content Issue	11
Type of Use	Thesis/Dissertation
Requestor type	academic/educational
Portion	figures/tables/images
Number of figures/tables/images	1
Distribution quantity	1
Format	print
Will you be translating?	no
Order reference number	
Title of the thesis/dissertation	Rotaxane Ligands for Incorporation into Metal-Organic Framework Materials
Expected completion date	Aug 2017
Estimated size	250
Requestor Location	Ms. Ghazale Gholami



Title: Molecular Shuttling of a Compact and Rigid H-Shaped [2]Rotaxane
Author: Kelong Zhu, V. Nicholas Vukotic, Stephen J. Loeb
Publication: Angewandte Chemie
Publisher: John Wiley and Sons
Date: Jan 19, 2012

Copyright © 2012 WILEY-VCH Verlag GmbH & Co. KGaA, Weinheim

Logged in as:
Ghazale Gholami
Account #:
3001161896

LOGOUT

Order Completed

Thank you for your order.

This Agreement between Ms. Ghazale Gholami ("You") and John Wiley and Sons ("John Wiley and Sons") consists of your license details and the terms and conditions provided by John Wiley and Sons and Copyright Clearance Center.

Your confirmation email will contain your order number for future reference.

[Printable details.](#)

License Number	4155961218587
License date	Jul 25, 2017
Licensed Content Publisher	John Wiley and Sons
Licensed Content Publication	Angewandte Chemie
Licensed Content Title	Molecular Shuttling of a Compact and Rigid H-Shaped [2]Rotaxane
Licensed Content Author	Kelong Zhu, V. Nicholas Vukotic, Stephen J. Loeb
Licensed Content Date	Jan 19, 2012
Licensed Content Pages	5
Type of use	Dissertation/Thesis
Requestor type	University/Academic
Format	Print
Portion	Figure/table
Number of figures/tables	1
Original Wiley figure/table number(s)	figure 5 figure 3
Will you be translating?	No
Title of your thesis / dissertation	Rotaxane Ligands for Incorporation into Metal-Organic Framework Materials
Expected completion date	Aug 2017
Expected size (number of pages)	250



Title: Acid-Base Switchable [2]- and [3]Rotaxane Molecular Shuttles with Benzimidazolium and Bis(pyridinium) Recognition Sites

Author: Kelong Zhu, V. Nicholas Vukotic, Stephen J. Loeb

Publication: Chemistry - An Asian Journal

Publisher: John Wiley and Sons

Date: Oct 13, 2016

© 2016 Wiley-VCH Verlag GmbH & Co. KGaA, Weinheim

Logged in as:
Ghazale Gholami
Account #:
3001161896

LOGOUT

Order Completed

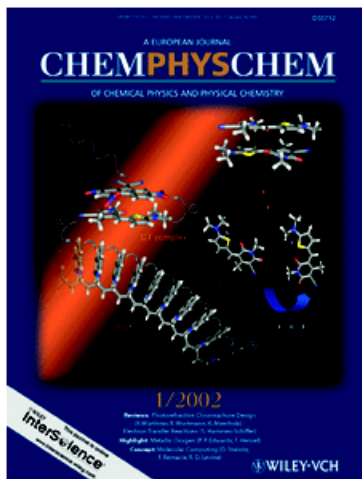
Thank you for your order.

This Agreement between Ms. Ghazale Gholami ("You") and John Wiley and Sons ("John Wiley and Sons") consists of your license details and the terms and conditions provided by John Wiley and Sons and Copyright Clearance Center.

Your confirmation email will contain your order number for future reference.

[Printable details.](#)

License Number	4155970225954
License date	Jul 25, 2017
Licensed Content Publisher	John Wiley and Sons
Licensed Content Publication	Chemistry - An Asian Journal
Licensed Content Title	Acid-Base Switchable [2]- and [3]Rotaxane Molecular Shuttles with Benzimidazolium and Bis(pyridinium) Recognition Sites
Licensed Content Author	Kelong Zhu, V. Nicholas Vukotic, Stephen J. Loeb
Licensed Content Date	Oct 13, 2016
Licensed Content Pages	9
Type of use	Dissertation/Thesis
Requestor type	University/Academic
Format	Print
Portion	Figure/table
Number of figures/tables	2
Original Wiley figure/table number(s)	Figure 5 Figure 7
Will you be translating?	No
Title of your thesis / dissertation	Rotaxane Ligands for Incorporation into Metal-Organic Framework Materials
Expected completion date	Aug 2017
Expected size (number of pages)	250



Title: Rigid, Bistable Molecular Shuttles Combining T-shaped Benzimidazolium and Y-shaped Imidazolium Recognition Sites

Author: Nasim Farahani, Kelong Zhu, Stephen J. Loeb

Publication: ChemPhysChem

Publisher: John Wiley and Sons

Date: Mar 22, 2016

© 2016 WILEY-VCH Verlag GmbH & Co. KGaA, Weinheim

Logged in as:
Ghazale Gholami
Account #:
3001161896

LOGOUT

Order Completed

Thank you for your order.

This Agreement between Ms. Ghazale Gholami ("You") and John Wiley and Sons ("John Wiley and Sons") consists of your license details and the terms and conditions provided by John Wiley and Sons and Copyright Clearance Center.

Your confirmation email will contain your order number for future reference.

[Printable details.](#)

License Number	4155970487808
License date	Jul 25, 2017
Licensed Content Publisher	John Wiley and Sons
Licensed Content Publication	ChemPhysChem
Licensed Content Title	Rigid, Bistable Molecular Shuttles Combining T-shaped Benzimidazolium and Y-shaped Imidazolium Recognition Sites
Licensed Content Author	Nasim Farahani, Kelong Zhu, Stephen J. Loeb
Licensed Content Date	Mar 22, 2016
Licensed Content Pages	6
Type of use	Dissertation/Thesis
Requestor type	University/Academic
Format	Print
Portion	Figure/table
Number of figures/tables	1
Original Wiley figure/table number(s)	Figure 4 Figure 5
Will you be translating?	No



Title: Coordination polymers containing rotaxane linkers
Author: V. Nicholas Vukotic, Stephen J. Loeb
Publication: Chemical Society Reviews
Publisher: Royal Society of Chemistry
Date: Jun 20, 2012
Copyright © 2012, Royal Society of Chemistry

Logged in as:
Ghazale Gholami
Account #:
3001161896

LOGOUT

Order Completed

Thank you for your order.

This Agreement between Ms. Ghazale Gholami ("You") and Royal Society of Chemistry ("Royal Society of Chemistry") consists of your license details and the terms and conditions provided by Royal Society of Chemistry and Copyright Clearance Center.

Your confirmation email will contain your order number for future reference.

[Printable details.](#)

License Number	4155971127174
License date	Jul 25, 2017
Licensed Content Publisher	Royal Society of Chemistry
Licensed Content Publication	Chemical Society Reviews
Licensed Content Title	Coordination polymers containing rotaxane linkers
Licensed Content Author	V. Nicholas Vukotic, Stephen J. Loeb
Licensed Content Date	Jun 20, 2012
Licensed Content Volume	41
Licensed Content Issue	18
Type of Use	Thesis/Dissertation
Requestor type	academic/educational
Portion	figures/tables/images
Number of figures/tables/images	5
Distribution quantity	1
Format	print
Will you be translating?	no
Order reference number	
Title of the thesis/dissertation	Rotaxane Ligands for Incorporation into Metal-Organic Framework Materials
Expected completion date	Aug 2017
Estimated size	250



Title: An Interwoven Metal-Organic Framework Combining Mechanically Interlocked Linkers and Interpenetrated Networks

Author: Nissa C. Frank, Darren J. Mercer, Stephen J. Loeb

Publication: Chemistry - A European Journal

Publisher: John Wiley and Sons

Date: Sep 9, 2013

Copyright © 2013 WILEY-VCH Verlag GmbH & Co. KGaA, Weinheim

Logged in as:
Ghazale Gholami
Account #:
3001161896

LOGOUT

Order Completed

Thank you for your order.

This Agreement between Ms. Ghazale Gholami ("You") and John Wiley and Sons ("John Wiley and Sons") consists of your license details and the terms and conditions provided by John Wiley and Sons and Copyright Clearance Center.

Your confirmation email will contain your order number for future reference.

[Printable details.](#)

License Number	4155971466747
License date	Jul 25, 2017
Licensed Content Publisher	John Wiley and Sons
Licensed Content Publication	Chemistry - A European Journal
Licensed Content Title	An Interwoven Metal-Organic Framework Combining Mechanically Interlocked Linkers and Interpenetrated Networks
Licensed Content Author	Nissa C. Frank, Darren J. Mercer, Stephen J. Loeb
Licensed Content Date	Sep 9, 2013
Licensed Content Pages	5
Type of use	Dissertation/Thesis
Requestor type	University/Academic
Format	Print
Portion	Figure/table
Number of figures/tables	2
Original Wiley figure/table number(s)	Figure 4 Scheme 1
Will you be translating?	No
Title of your thesis / dissertation	Rotaxane Ligands for Incorporation into Metal-Organic Framework Materials
Expected completion date	Aug 2017
Expected size (number of pages)	250



Title: Metal-organic frameworks with dynamic interlocked components
Author: V. Nicholas Vukotic, Kristopher J. Harris, Kelong Zhu, Robert W. Schurko, Stephen J. Loeb
Publication: Nature Chemistry
Publisher: Nature Publishing Group
Date: May 13, 2012
Copyright © 2012, Rights Managed by Nature Publishing Group

Logged in as:
Ghazale Gholami
Account #:
3001161896

[LOGOUT](#)

Order Completed

Thank you for your order.

This Agreement between Ms. Ghazale Gholami ("You") and Nature Publishing Group ("Nature Publishing Group") consists of your license details and the terms and conditions provided by Nature Publishing Group and Copyright Clearance Center.

Your confirmation email will contain your order number for future reference.

[Printable details.](#)

License Number	4155980292294
License date	Jul 25, 2017
Licensed Content Publisher	Nature Publishing Group
Licensed Content Publication	Nature Chemistry
Licensed Content Title	Metal-organic frameworks with dynamic interlocked components
Licensed Content Author	V. Nicholas Vukotic, Kristopher J. Harris, Kelong Zhu, Robert W. Schurko, Stephen J. Loeb
Licensed Content Date	May 13, 2012
Licensed Content Volume	4
Licensed Content Issue	6
Type of Use	reuse in a dissertation / thesis
Requestor type	academic/educational
Format	print
Portion	figures/tables/illustrations
Number of figures/tables/illustrations	2
High-res required	no
Figures	Figure 3 Figure 5
Author of this NPG article	no
Your reference number	
Title of your thesis / dissertation	Rotaxane Ligands for Incorporation into Metal-Organic Framework Materials
Expected completion date	Aug 2017
Estimated size (number of pages)	250



Title: Thermally Driven Dynamics of a Rotaxane Wheel about an Imidazolium Axle inside a Metal-Organic Framework

Author: Nasim Farahani, Kelong Zhu, Christopher A. O'Keefe, Robert W. Schurko, Stephen J. Loeb

Publication: CHEMPLUSCHEM

Publisher: John Wiley and Sons

Date: May 25, 2016

© 2016 WILEY-VCH Verlag GmbH & Co. KGaA, Weinheim

Logged in as:
Ghazale Gholami
Account #:
3001161896

LOGOUT

Order Completed

Thank you for your order.

This Agreement between Ms. Ghazale Gholami ("You") and John Wiley and Sons ("John Wiley and Sons") consists of your license details and the terms and conditions provided by John Wiley and Sons and Copyright Clearance Center.

Your confirmation email will contain your order number for future reference.

[Printable details.](#)

License Number	4155980933829
License date	Jul 25, 2017
Licensed Content Publisher	John Wiley and Sons
Licensed Content Publication	CHEMPLUSCHEM
Licensed Content Title	Thermally Driven Dynamics of a Rotaxane Wheel about an Imidazolium Axle inside a Metal-Organic Framework
Licensed Content Author	Nasim Farahani, Kelong Zhu, Christopher A. O'Keefe, Robert W. Schurko, Stephen J. Loeb
Licensed Content Date	May 25, 2016
Licensed Content Pages	6
Type of use	Dissertation/Thesis
Requestor type	University/Academic
Format	Print
Portion	Figure/table
Number of figures/tables	2
Original Wiley figure/table number(s)	Scheme 1 figure 1
Will you be translating?	No
Title of your thesis / dissertation	Rotaxane Ligands for Incorporation into Metal-Organic Framework Materials
Expected completion date	Aug 2017
Expected size (number of pages)	250



Title: A molecular shuttle that operates inside a metal-organic framework

Author: Kelong Zhu, Christopher A. O'Keefe, V. Nicholas Vukotic, Robert W. Schurko, Stephen J. Loeb

Publication: Nature Chemistry

Publisher: Nature Publishing Group

Date: May 4, 2015

Copyright © 2015, Rights Managed by Nature Publishing Group

Logged in as:

Ghazale Gholami

Account #:

3001161896

LOGOUT

Order Completed

Thank you for your order.

This Agreement between Ms. Ghazale Gholami ("You") and Nature Publishing Group ("Nature Publishing Group") consists of your license details and the terms and conditions provided by Nature Publishing Group and Copyright Clearance Center.

Your confirmation email will contain your order number for future reference.

[Printable details.](#)

License Number	4155981151004
License date	Jul 25, 2017
Licensed Content Publisher	Nature Publishing Group
Licensed Content Publication	Nature Chemistry
Licensed Content Title	A molecular shuttle that operates inside a metal-organic framework
Licensed Content Author	Kelong Zhu, Christopher A. O'Keefe, V. Nicholas Vukotic, Robert W. Schurko, Stephen J. Loeb
Licensed Content Date	May 4, 2015
Licensed Content Volume	7
Licensed Content Issue	6
Type of Use	reuse in a dissertation / thesis
Requestor type	academic/educational
Format	print
Portion	figures/tables/illustrations
Number of figures/tables/illustrations	2
High-res required	no
Figures	Figure 3 Figure 4 Figure 6
Author of this NPG article	no
Your reference number	
Title of your thesis / dissertation	Rotaxane Ligands for Incorporation into Metal-Organic Framework Materials
Expected completion date	Aug 2017
Estimated size (number of pages)	250

VITA AUCTORIS

Name: Ghazale Gholami

Year of Birth: 1985

Place of Birth: Tehran, Iran

Education: Ph.D Chemistry, University of Windsor, Windsor, Ontario, Canada, 2017

M. Sc.-Organic Chemistry, Tarbiat Moallem University (Kharazmi University), Tehran, Iran, 2010

B.Sc.-Applied Chemistry, Islamic Azad University, Tehran, Iran, 2007